

FLUID MECHANICS AND HEAT TRANSFER

Advances in Nonlinear Dynamics Modeling

FLUID MECHANICS AND HEAT TRANSFER

Advances in Nonlinear Dynamics Modeling

Kaveh Hariri Asli, PhD, and Soltan Ali Ogli Aliyev, DSc



CRC Press
Taylor & Francis Group
6000 Broken Sound Parkway NW, Suite 300
Boca Raton, FL 33487-2742

Apple Academic Press, Inc
3333 Mistwell Crescent
Oakville, ON L6L 0A2
Canada

© 2015 by Apple Academic Press, Inc.

Exclusive worldwide distribution by CRC Press an imprint of Taylor & Francis Group, an Informa business

No claim to original U.S. Government works
Version Date: 20150519

International Standard Book Number-13: 978-1-4987-0769-5 (eBook - PDF)

This book contains information obtained from authentic and highly regarded sources. Reasonable efforts have been made to publish reliable data and information, but the author and publisher cannot assume responsibility for the validity of all materials or the consequences of their use. The authors and publishers have attempted to trace the copyright holders of all material reproduced in this publication and apologize to copyright holders if permission to publish in this form has not been obtained. If any copyright material has not been acknowledged please write and let us know so we may rectify in any future reprint.

Except as permitted under U.S. Copyright Law, no part of this book may be reprinted, reproduced, transmitted, or utilized in any form by any electronic, mechanical, or other means, now known or hereafter invented, including photocopying, microfilming, and recording, or in any information storage or retrieval system, without written permission from the publishers.

For permission to photocopy or use material electronically from this work, please access www.copyright.com (<http://www.copyright.com/>) or contact the Copyright Clearance Center, Inc. (CCC), 222 Rosewood Drive, Danvers, MA 01923, 978-750-8400. CCC is a not-for-profit organization that provides licenses and registration for a variety of users. For organizations that have been granted a photocopy license by the CCC, a separate system of payment has been arranged.

Trademark Notice: Product or corporate names may be trademarks or registered trademarks, and are used only for identification and explanation without intent to infringe.

Visit the Taylor & Francis Web site at
<http://www.taylorandfrancis.com>

and the CRC Press Web site at
<http://www.crcpress.com>

For information about Apple Academic Press product
<http://www.appleacademicpress.com>

ABOUT THE AUTHORS

Kaveh Hariri Asli, PhD

Kaveh Hariri Asli, PhD, is a professional mechanical engineer with over 30 years of experience in practicing mechanical engineering design and teaching. He is the author and editor of several books as well as over 100 articles and reports in the fields of fluid mechanics, hydraulics, automation and control systems. Dr. Hariri has consulted for a number of major corporations.

Soltan Ali Oglı Aliyev, DSc

Soltan Ali Oglı Aliyev, DSc, is Deputy Director of the Department of Mathematics and Mechanics at the National Academy of Science of Azerbaijan (AMEA) in Baku, Azerbaijan. He served as a professor at several universities. He is the author and editor of several books as well as of a number of papers published in various journals and conference proceedings.

CONTENTS

| | |
|---|------------|
| <i>List of Abbreviations</i> | <i>ix</i> |
| <i>List of Symbols</i> | <i>xi</i> |
| <i>Preface</i> | <i>xv</i> |
| 1. Nonlinear Problems of Transitional Flow | 1 |
| 2. Fluid Mechanics and Nonlinear Dynamic Modeling | 15 |
| 3. Simulation and Modeling of Two Phases Flow | 49 |
| 4. Heat and Mass Transfer Modeling | 75 |
| 5. Liquid Water in Non Homogeneous Material | 105 |
| 6. Three Dimensional Heat Transfer Characteristics | 137 |
| 7. Computational Model for Heat Flow Process | 159 |
| 8. Simulation of Thermal Process | 185 |
| Index | 229 |

LIST OF ABBREVIATIONS

| | |
|-------|---------------------------------|
| ACQ | Ammonium Copper Quat |
| CCA | Chromated Copper Arsenate |
| CFD | Computational Fluid Dynamics |
| CV | Control Volumes |
| DNS | Direct Numerical Simulation |
| EDL | Electric Double Layer |
| FD | Finite Differences |
| FE | Finite Elements |
| FEM | Finite Element Method |
| FSP | Fiber Saturation Point |
| FV | Finite Volume |
| FVM | Finite Volume Method |
| GIS | Geography Information Systems |
| LES | Large Eddy Simulation |
| MC | Moisture Content |
| MR | Moisture Ratio |
| MOC | Method of Characteristics |
| PDE | Partial Differential Equation |
| PLC | Program Logic Control |
| RANS | Reynolds-Averaged Navier-Stokes |
| RE NO | Reynolds Number Magnitude |
| RMS | Root-Mean-Square |
| RTC | Real-Time Control |
| SGS | Sub Grid-Scale |
| VCF | Velocity Correction Factor |
| WCM | Wave Characteristic Method |

LIST OF SYMBOLS

| | |
|----------|---|
| A | cross-sectional area |
| a_1 | thermal diffusivity |
| B | universal gas constant |
| C | velocity of Surge wave |
| C_1 | pipe support coefficient |
| C^- | characteristic lines with negative slope |
| C^+ | characteristic lines with positive slope |
| D | diameter of pipe |
| D_b | bound water diffusion coefficient |
| D_v | water vapor diffusion coefficient |
| Dh | hydraulic diameter |
| D_{bt} | wood and the vapor diffusion coefficient |
| d | outer diameter of pipe |
| dp | static pressure rise |
| dV | incremental change in liquid volume with respect to initial volume |
| (dp/ρ) | incremental change in liquid density with respect to initial density |
| E | modulus of elasticity for pipeline material Steel |
| E_p | pipe module of elasticity |
| E_w | module of elasticity of water |
| f | angular frequency |
| g | acceleration of gravity |
| h_p | head gain from a pump |
| h_L | combined head loss |
| h_0 | ordinate denotes the free surface of liquid |
| H_p | surge wave head at intersection points of characteristic lines |
| H_{ri} | surge wave head at right hand side of intersection points of characteristic lines |
| H_{le} | surge wave head at left hand side of intersection points of characteristic lines |
| H_1 | channel height |
| H_2 | total height |

| | |
|------------------|--|
| J_{vf} | water vapor flow flux |
| J_f | liquid free water flow flux |
| K_l | specific permeability of liquid water |
| K | wave number |
| K_g | superficial gas permeability |
| K_r | relative permeability |
| K_w | conductivity of water |
| K_{cw} | conductivity of cell wall substance |
| k | volumetric coefficient |
| $k_{**}(\omega)$ | damping vibrations in length |
| L | length of specimen parallel to the direction of flow |
| L_h | heated length |
| M_w | molecular weight |
| M_{Cr1} | first critical moisture content |
| M_{Cr2} | second critical moisture content |
| N_v | moisture flux |
| n_i | number of moles |
| n_{param} | number of parameters |
| P | average pressure across the specimen |
| P_{sat} | saturated vapor pressure |
| P | surge pressure |
| p_c | capillary pressure |
| q | heat flux |
| R | radius |
| R_0 | radiuses of bubble |
| SG | specific gravity |
| T | period of motion |
| T_k | kelvin temperature |
| T_p | pipe thickness |
| T_v | temperature of mixture |
| T_{in} | inlet temperature |
| T_{max} | maximum temperature |
| t | time |
| u | fluid velocity |
| V | volume |
| V_p | surge wave velocity at pipeline points-intersection points of characteristic lines |

| | |
|-----------|---|
| V_{ri} | Surge wave velocity at right hand side of intersection points of characteristic lines |
| V_{le} | Surge wave velocity at left hand side of intersection points of characteristic lines |
| V_0 | liquid with an average speed |
| ν | fluid dynamic viscosity |
| W_2 | substrate width |
| x | water transfer distance |
| Y_{max} | Max. Fluctuation |
| Z | elevation |

GREEK SYMBOLS

| | |
|--------------------------------|---|
| ΔH_{wv} | water evaporation |
| ΔT | overheating of the liquid |
| ΔP | pressure difference between ends of specimen |
| δ | wall thickness |
| χ | water transfer distance |
| λ | wavelength |
| λ_1 | coefficient of thermal conductivity |
| ρ_i | density component of mix of steam in a bubble |
| ρ_s | basic density of wood |
| ρ_s | density of wood |
| ρ_v | vapor density |
| $\partial p_c / \chi$ | capillary pressure gradient |
| ρ_v, μ_v | density and viscosity of water vapor respectively |
| $\partial p_v / \partial \chi$ | vapor partial pressure gradient |
| Φ | function of frequency and wave vector |
| μ_i | molecular weight |
| μ_l | viscosity of liquid water |
| ω | wave number |
| σ | surface tension coefficient of liquid |
| ψ | relative humidity |

PREFACE

It is with great sense of gratitude and humility that we take this blessed moment to offer this edition of *Fluid Mechanics and Heat Transfer: Advances in Nonlinear Dynamics Modeling*. The challenge presented for the success of this volume, coupled with our objective to enhance its reference value and widen its scope, motivated us to reach out and draw upon the recognized expertise on fluid mechanics and heat transfer. In addition, we directed our synergetic efforts to enhance the contents of the volume to include the latest advances and developments in the field of fluid mechanics and heat transfer and related technologies.

Fluid Mechanics and Heat Transfer is unique because it covers topics related to the subject that are not covered in any other book. The inclusion of metric and/or SI units along with US customary units is intended to accommodate the growing needs of the shrinking world and the realities of the international market. The book includes the research of the authors as well as the development of optimal mathematical models.

The authors present the subject means of theoretical and experimental research and use modern computer technology and mathematical methods for analysis of nonlinear dynamic processes. The book attempts to provide as wide coverage as possible on those technologies applicable to both fluid mechanics and heat transfer problems. The methods and technologies discussed are a combination of physical, mechanical, and thermal techniques. This research collection develops a new method for the calculation of mathematical models by computer technology. The process of entering input for the calculation of mathematical models was simplified for the user through the use of mechanical systems. The authors used parametric modeling techniques and multiple analyzes for mechanical systems.

Incorporated into each chapter are sidebar discussions. These highlighted boxes contain information and facts about each subject area that will help to emphasize important points to remember and will assist plant managers in training technical staff, especially in training operators on the specific technologies relied upon in their operations. In addition there is a glossary of several hundred terms at the end of the book. This will prove

useful to you not only when reading through the chapters but as a general resource reference.

The authors believe that the results of this handbook of research can lead to new ideas and can help to reduce the risk of system damage or failure of mechanical systems. It is the authors' experience in teaching that the subject matter as presented in this volume is best suited for students with at least three years of engineering education under their belts, and the book will also serve as a valuable reference for plant managers and training technical staff in the field of fluid mechanics and heat transfer and related technologies.

— **Kaveh Hariri Asli**
Soltan Ali Oglı Aliyev

CHAPTER 1

NONLINEAR PROBLEMS OF TRANSITIONAL FLOW

CONTENTS

| | | |
|-----|----------------------------|----|
| 1.1 | Introduction..... | 2 |
| 1.2 | Materials and Methods..... | 4 |
| 1.3 | Results..... | 9 |
| 1.4 | Conclusion | 9 |
| | Keywords | 10 |
| | References..... | 10 |

1.1 INTRODUCTION

The starting point of any numerical method is the mathematical model, the set of partial differential equations and boundary conditions. After selecting the mathematical model, one has to choose a suitable discretization method. The most important are: finite differences (FD), finite volume (FV) and finite element (FE) methods. The discrete locations at which the variables are to be calculated are defined by the numerical grid, which is essentially a discrete representation of the geometric domain on which the problem is to be solved. It divides the solution domain into a finite number of sub domains. Different types of grids are:

- **Structured grid:** A structured mesh is defined as a mesh where all the nodes have the same number of elements around it. This makes that the matrix of algebraic equation system has a regular structure. There is large number of efficient solvers applicable only to structured grids. Disadvantages are only for geometrically simple domains.
- **Unstructured grid:** For very complex geometries, can fit arbitrary boundaries. Grids made of triangles or quadrilaterals in 2D and tetrahedral or hexahedra in 3D are the most often used. Such grids can be generated automatically by existing algorithms. Disadvantage: irregularity of the data structure. The solvers for the algebraic equation system are usually slower than those for structured grids.
- **Block-structured grid:** Structured grid inside each block, but the order of blocks is irregular. Consistency The discretization should become exact, as the grid spacing tends to zero. The difference between the discretized equation and the exact one is called truncation error. For a method to be consistent, the truncation error must become zero when the mesh spacing. If the most important term of the truncation error is proportional to n the method is of n -th order. $n > 0$ is required for consistency. Even if the approximations are consistent, it does not necessarily mean that the approximated solution will become the exact solution in the limit of small step size. For this to happen, the method has to be stable also. **Stability** A numerical method is stable if does not magnify the errors that appear during the process. For temporal problems, stability guarantees that the method produces a bounded solution whenever the exact solution is also bounded. A numerical method is convergent if the discrete solution tends to the

exact one as the grid spacing tends to zero. For linear initial value problems, the Lax Equivalence theorem states:

Consistency, Stability, and Convergence for nonlinear problems the stability and convergence of a method are difficult to demonstrate. Therefore, convergence is usually checked using a numerical experiment, which is, repeating the calculation on a series of successively refined grids. If the method is stable and if all approximations used in the discretization process are consistent, we usually find that the solution does converge to a grid-independent solution. Since the equations to be solved are conservation laws, the numerical scheme should also respect these laws. This means that, at steady state and in the absence of sources, the amount of a conserved quantity leaving a closed volume is equal to the amount entering that volume. If the strong conservation form of equations and a FV method are used, this is guaranteed for each individual control volume and for the domain as a whole. Accuracy numerical solutions of fluid flow are only approximate solutions. In addition to the errors that might be introduced in the development of the solution algorithm, in programming or setting up the boundary conditions, numerical solutions always include three kinds of systematic errors:

- Modeling errors: Difference between the actual flow and the exact solution of the mathematical model.
- Discretization errors: Difference between the exact solution of the conservation equations and the exact solution of the algebraic system of equations obtained by discretizing these equations.
- Iteration errors: Difference between the iterative and exact solutions of the algebraic equation systems.
- The governing equations of fluid flow represent mathematical statements of the conservation laws of physics:
 - the mass of fluid is conserved.
 - the rate of change of momentum equals the sum of the forces applied on a fluid particle (Newton's second law).
 - the rate of change of energy is equal to the sum of the rate of heat addition and to the rate of work done on a fluid particle (first law of thermodynamics).

This book discusses on Lagrangian and Eulerian based model for water hammer. This model was defined by the method of characteristics "MOC," finite difference form. The method was encoded into an existing hydraulic simulation model. The surge wave was assumed as a failure factor in an

elastic case of water pipeline with free water bubble. The results were compared by regression analysis. It indicated that the accuracy of the Eulerian based model for the process of interpenetration of two fluids into water transmission line.

These ranges of methods are included by approximate equations to numerical solutions of the nonlinear Navier–Stokes equations.

Various methods have been developed to solve transient flow in pipes. These ranges have been formed from approximate equations to numerical solutions of the nonlinear Navier–Stokes equations. Elastic theory describes the unsteady flow of a compressible liquid in an elastic system. Transient theory stem from the two governing equations. The continuity equation and the momentum equation are needed to determine velocity and surge pressure in a one-dimensional flow system. Solving these two equations produces a theoretical result that usually corresponds quite closely to actual system measurements, if the data and assumptions used to build the numerical model are valid. Among the approaches proposed to solve.

The single-phase (pure liquid) transient equations are the MOC (FD), wave characteristic method (WCM), FEs, and FV. One difficulty that commonly arises relates to the selection of an appropriate level of time step to use for the analysis. The obvious trade off is between computational speed and accuracy. In general, for the smaller the time step, there is the longer the run time but the greater the numerical accuracy [1–22].

1.2 MATERIALS AND METHODS

This chapter is started with the solving of approximate equations by numerical solutions of the nonlinear Navier-Stokes equations based on the MOC. Then it derived the Joukowski formula and velocity of surge or pressure wave in an elastic case with the high value of free water bubble. So the numerical modeling and simulation, which was defined by “MOC” provided a set of results. Basically the “MOC” approach transforms the water hammer partial differential equations into the ordinary differential equations along the characteristic lines.

1.2.1 FINITE ELEMENT METHOD (FEM)

This is a short introduction to the FEM, which is, besides others like the FD approximation, a technique to solve partial differential equations (PDE's) numerically.

There is a systematic account of changes in the mass, momentum and energy of the fluid element due to flow across the boundaries and the sources inside the element. Infinitesimal fluid element has six faces: North, South, East, West, Top, and Bottom.

Types of time integration methods for unsteady flows, initial value problem:

Explicit, values at time $n+1$ computed from values at time n .

Advantages:

- Direct computation without solving system of equation.
- Few number of operations per time step.

Disadvantage:

- Strong conditions on time step for stability.

Implicit, values at time $n+1$ computed from the unknown values at time $n+1$.

Advantage:

- Larger time steps possible, always stable.

Disadvantages:

- Every time step requires solution of system.
- More number of operations.

1.2.2 FINITE VOLUME METHOD (FVM)

- FVM uses integral form of conservation (transport) equation.
- Domain subdivided in control volumes (CV).
- Surface and volume integrals approximated by numerical quadrature.
- Interpolation used to express variable values at CV faces in terms of nodal values.
- It results in an algebraic equation per CV.
- Suitable for any type of grid.
- Conservative by construction.
- Commercial codes: CFX, Fluent, Phoenix, Flow3D.

1.2.3. TURBULENT FLOWS

- Most flows in practice are turbulent.
- With increasing Re , smaller eddies.
- Very fine grid necessary to describe all length scales.
- Even the largest supercomputer does not have (yet) enough speed and memory to simulate turbulent flows of high Re -computational methods for turbulent flows:
 - Direct Numerical Simulation (DNS)
 - § Large Eddy Simulation (LES)
 - § Reynolds-Averaged Navier-Stokes (RANS)

The FEM was mainly developed for equations of elasticity and structural mechanics. In these fields problems have to be solved in complicated and irregular geometries. So one of the main advantages of the FEM, in comparison to the FD approximation, lies in the flexibility concerning the geometry of the domain where the PDE is to be solved.

Moreover, the FEM is perfectly suitable as adaptive method, because it makes local refinements of the solution easily possible. The method does not operate on the PDE itself; instead the PDE is transformed to a equivalent variational or weak form. This will be the topic of the second part: the variational principle.

For transient analysis by FE, first we choose a geometric shape and divide the domain into a finite number of regions. In one dimension the domain is split into intervals. In two dimensions the elements are usually of triangular or quadrilateral shape. And in three dimensions tetrahedral or hexahedral forms are most common. Most elements used in practice have fairly simple geometries, because this result in very easy computation, since integrating over these shapes is quite basic.

The basic functions are usually not defined directly. Instead a function types, the so-called ansatz function, (e.g., linear or quadratic polynomial) is selected which our approximation should adopt on each of these elements. Most commonly a linear function is chosen, which means that it will be a linear function on each element and continuous over (but not continuously differentiable).

Each element possesses a set of distinguishing points called nodal points or nodes. Nodes define the element geometry, and are the degrees of freedom of the ansatz function. So the number of nodes in an element depends on the ansatz function as well as the geometry. They are usually

located at the corners or end points of elements. For higher-order (higher than linear) ansatz functions, nodes are also placed on sides or faces, as well as perhaps the interior of the element.

The combination of the geometric shape of the FE and their associated ansatz function on this region is referred as FE type.

The basis arises from the choice of the FE type for water hammer analysis. Water hammer is the result of sharp changes of fluid pressure by the instantaneous changes in the rate of flow in the pipeline [23–41]. This phenomena occurs during transient are explained on the basis of compressibility of liquid drops. After closing the valves on the horizontal pipe of constant diameter, which moves the liquid with an average speed V_0 , a liquid layer, located directly at the gate, immediately stops [42–44]. Then successively terminate movement of the liquid layers (turbulence, counter flows) to increase with time away from the gate. It is compacted before stopping the mass of liquid. As a result of increasing pressure somewhat expanded pipe. In the tube includes an additional volume of liquid. Since the fluid is compressible, the whole of its mass in the pipeline does not stop immediately. It moves from the gate along the pipeline with some velocity C , called the speed of propagation of the pressure wave.

A first approach to solve the variational or weak form was made by Ritz (1908). A discussion of this method is the subject in the third section: the Ritz method. Considering the disadvantages of the Ritz method will lead to the FE method and to the fourth and last part: the FE method. PDE are separated into different types, which behave very differently and demand an entirely own treatment. In the field of second-order linear differential equations three types are of fundamental interest, these are the hyperbolic, parabolic and elliptic equations. Depending on the type of the PDE boundary or initial conditions have to be given. The main focus of the FE method is elliptic PDE's so we will concentrate on this type. The correct side conditions for elliptic PDE's are boundary conditions. In this book, an experimental and computational method was used. It applied for prediction of surge tank effects on pressure and flow variation in the following case.

Direct Numerical Simulation (DNS) applies for analysis of pressure and flow variation at surge tank location due to transient flow.

- Fluid transient flow in practice was turbulent.
- Fluid transient flow with smaller eddies was lead to increasing Re.
- Very fine grid described by all length scales.

- The main problem was the supercomputer, which has not enough speed and memory to simulate turbulent flows of high Re.

Navier-Stokes equations:

$$(\partial\rho/\partial t) + \text{div}(\rho\bar{u}) = 0, \text{ Mass (Continuity equation),} \quad (1)$$

$$(\partial\rho u/\partial t) + \text{div}(\rho u\bar{u}) = -(\partial\rho/\partial x) + \text{div}(\mu\text{grad}u) + q_x, \text{ X (momentum equation),} \quad (2)$$

$$(\partial\rho v/\partial t) + \text{div}(\rho v\bar{u}) = -(\partial\rho/\partial y) + \text{div}(\mu\text{grad}v) + q_y, \text{ Y (momentum equation),} \quad (3)$$

$$(\partial\rho w/\partial t) + \text{div}(\rho w\bar{u}) = -(\partial\rho/\partial z) + \text{div}(\mu\text{grad}w) + q_z, \text{ Z (momentum equation),} \quad (4)$$

$$(\partial\rho i/\partial t) + \text{div}(\rho i\bar{u}) = -p\text{div}\bar{u} + \text{div}(k\text{grad}T) + \phi, \text{ Z (internal energy equation),} \quad (5)$$

1.2.3.1 DIRECT NUMERICAL SIMULATION (DNS)

- Discretize Navier-Stokes equation on a sufficiently fine grid for resolving all motions occurring in turbulent flow.
- No uses any models.
- Equivalent to laboratory experiment.
- Relationship between length η of smallest eddies and the length L of largest eddies.

$$\frac{L}{\eta} \approx (\text{Re}_L)^{\frac{3}{4}}, \quad (6)$$

Number of elements necessary to discretize the flow field in industrial applications,

$$\text{Re} > 10^6, n_{elem} > 10^{13}, u = \bar{u} + u', \quad (7)$$

1.2.3.2 LARGE EDDY SIMULATION (LES)

- Only large eddies are computed.
- Small eddies are modeled, sub grid-scale (SGS) models.

1.2.3.3 REYNOLDS-AVERAGED NAVIER-STOKES (RANS)

- Variables decomposed in a mean part and a fluctuating part.
- Navier-Stokes equations averaged over time.
- Turbulence models are necessary.

1.3 RESULTS

In this book, numerical analysis and simulation processes applied for water hammer nonlinear heterogeneous model.

Generally, water hammer is manifested as a hydro-machines phenomenon, which can lead to the destruction of pipelines. The cycles of increased and decreased in pressure iterates at intervals equal to time for dual-path shock wave length of the pipeline from the valve prior to the pipeline. Thus, the hydraulic impact of the liquid in the pipeline performed oscillatory motion. The cause of oscillatory motion was the hydraulic resistance and viscosity. It absorbed the initial energy of the liquid for overcoming the friction [45–80].

1.4 CONCLUSION

The effects of the penetrated air on the surge wave velocity in water pipeline. It showed that Eulerian based computational model is more accurate than the regression model. Hence in order to presentation for importance of penetrated air on water hammer phenomenon, it was compared the models for laboratory; computational and field tests experiments. As long as these procedures, it was showed that the Eulerian based model for water

transmission line in comparison with the regression model. On the other hand, this idea were included the proper analysis to provide a dynamic response to the shortcomings of the system. It also performed the design protection equipments to manage the transition energy and determine the operational procedures to avoid transients. Consequently, the results will help to reduce the risk of system damage or failure at the water pipeline.

KEYWORDS

- **Eulerian based model**
- **Method of characteristics**
- **Navier-Stokes equations**
- **Surge wave**
- **Water transmission**

REFERENCES

1. Harms, T. M., Kazmierczak, M. J., Cerner, F. M., Holke A., Henderson, H. T., Pilchowski, H. T., & Baker, K. (1997). Experimental Investigation of Heat Transfer and Pressure Drop through Deep Micro channels in a 100 Silicon Substrate, in: Proceedings of the ASME. Heat Transfer Division, HTD, 351, 347–357.
2. Holland, F. A., & Bragg, R. (1995). Fluid Flow for Chemical Engineers, Edward Arnold Publishers, London, 1–3.
3. George, E., & Glimm, J. (2005). “Self-similarity of Rayleigh-Taylor Mixing Rates,” *Phys. Fluids*, 17, 054101, 1–3.
4. Goncharov, V. N. (2002). “Analytical Model of Nonlinear, Single-Mode, Classical Rayleigh-Taylor Instability at Arbitrary Atwood Numbers,” *Phys., Rev. Letters*, 88, 134502, 10–15.
5. Ishii, M. (1975). Thermo-Fluid Dynamic Theory of Two-Phase Flow, Collection de D. R. Liles and Reed, W. H. “A Sern-Implicit Method for Two-Phase Fluid la Direction des Etudes et al. Recherché D’ Electricite de France, 22, Dynamics,” *Journal of Computational Physics*, 26, Paris, 390–407.
6. JaimeSuárez, A. (2005). “Generalized Water Hammer Algorithm For Piping Systems with Unsteady Friction,” 72–77.
7. Jaeger, C. (1977). “Fluid Transients in Hydro-Electric Engineering Practice,” Blackie & Son Ltd, 87–88.
8. Joukowski, N. (1904). Paper to Polytechnic Soc., Moscow Spring of 1898, English Translation by Miss Simin, O., *Proc. AWWA*, 57–58.

9. Kodura, A., & Weinerowska, K. (2005). The Influence of the Local Pipeline Leak on Water Hammer Properties, Materials of the II Polish Congress of Environmental Engineering, Lublin, 125–133.
10. Kane, J., Arnett, D., Remington, B. A., Glendinning, S. G., & Baz'an, G. (2000). "Two-Dimensional Versus Three-Dimensional Supernova Hydrodynamic Instability Growth," *J. Astrophys.*, 528–989.
11. Karassik, I. J. (2001). "Pump Handbook Third Edition," McGraw-Hill, 19–22.
12. Koelle, E., Jr. Luvizotto, E., & Andrade, J. P. G. (1996). "Personality Investigation of Hydraulic Networks using MOC–Method of Characteristics" Proceedings of the 7th International Conference on Pressure Surges and Fluid Transients, Harrogate Durham, United Kingdom, 1–8.
13. Kerr, S. L. (1949). "Minimizing Service Interruptions due to Transmission Line failures Discussion," *Journal of the American Water Works Association*, 41(634), July, 266–268.
14. Kerr, S. L. (1951). "Water Hammer Control," *Journal of the American Water works Association*, 43, December, 985–999.
15. Kraichnan, R. H., & Montgomery, D. (1967). "Two-Dimensional Turbulence," *Rep. Prog., Phys.*, 43, 547, 1417–1423.
16. Leon Arturo, S. (2007). "An Efficient Second-Order Accurate Shock-Capturing Scheme for Modeling One and Two-Phase Water Hammer Flows" PhD Thesis, March 29, 4–44.
17. Lee, T. S., & Pejovic, S. (1996) Air Influence on Similarity of Hydraulic Transients and Vibrations, *ASME J. Fluid Eng.*, 118(4), 706–709.
18. Li, J., & McCorquodale, A. (1999). "Modeling Mixed Flow in Storm Sewers," *Journal of Hydraulic Engineering, ASCE*, 125(11), 1170–1180.
19. Mala, G., Li, D., & Dale, J. D. (1997). Heat Transfer and Fluid Flow in Micro Channels, *J. Heat Transfer*, 40, 3079–3088.
20. Miller, P. L., Cabot, W. H., & Cook, A. W. (2005). "Which Way is up? A Fluid Dynamics Riddle," *Physics Fluids*, 17, 091110, 1–26.
21. Minnaert, M. (1933). On Musical Air Bubbles and the Sounds of Running Water, *Phil. Mag.*, 16(7), 235–248.
22. Moeng, C. H., McWilliams, J. C., Rotunno, R., Sullivan, P. P., & Weil, J. (2004). "Investigating 2D Modeling of Atmospheric Convection in the PBL," *J. Atm. Sci.* 61, 889–903.
23. Moody, L. F. (1944). "Friction Factors for Pipe Flow," *Trans. ASME*, 66, 671–684.
24. Nagiyev, F. B. (1993). Dynamics, Heat and Mass Transfer of Vapor-Gas Bubbles in a Two-Component Liquid, Turkey-Azerbaijan Petrol Semin., Ankara, Turkey, 32–40.
25. Nagiyev, F. B. (1995). The Method of Creation Effective Coolness Liquids, Third Baku International Congress, Baku, Azerbaijan Republic, 19–22.
26. Neshan, H. (1985). Water Hammer, Pumps Iran Co. Tehran, Iran, 1–60.
27. Nigmatulin, R. I., Khabeev, N. S., & Nagiyev, F. B. (1981). Dynamics, Heat and Mass Transfer of Vapor-Gas Bubbles in a Liquid, *Int. J. Heat Mass Transfer*, 24, N6, Printed in Great Britain, 1033–1044.
28. Oron, D., Arazi, L., Kartoon, D., Rikanati, A., Alon, U., & Shvarts, D. (2001). "Dimensionality Dependence of the Rayleigh-Taylor & Richtmyer-Meshkov instability, late-time scaling laws," *Physics Plasmas*, 8, 2883p.

29. Parmakian, J. (1957). "Water hammer Design Criteria," J. Power Div., ASCE, Sept., 456–460.
30. Parmakian, J. (1963). "Water Hammer Analysis," Dover Publications, Inc., New York, New York, 51–58.
31. Perry, R. H., Green, D. W., & Maloney, J. O. (1997). Perry's Chemical Engineers Handbook, 7th Edition, McGraw-Hill, New York, 1–61.
32. Peng, X. F., & Peterson, G. P. (1996). Convective Heat Transfer and Flow Friction for Water Flow in Micro channel Structure, Int. J. Heat Mass Transfer, 36, 2599–2608.
33. Pickford, J. (1969). "Analysis of Surge," MacMillan, London, 153–156.
34. Pipeline Design for Water and Wastewater, American Society of Civil Engineers (1975), New York, 54p.
35. Qu, W., Mala, G. M., & Li, D. (1993). Heat Transfer for Water Flow in Trapezoidal Silicon Micro channels, 399–404.
36. Quick, R. S. (1933). "Comparison and Limitations of Various Water hammer Theories," J. Hyd. Div., ASME, May, 43–45.
37. Rayleigh, (1917). On the Pressure developed in a Liquid during the Collapse of a Spherical Cavity, Philos. Mag. Ser. 6, 34(N200), 94–98.
38. Ramaprabhu, P., & Andrews, M. J. (2004). "Experimental Investigation of Rayleigh-Taylor mixing at small Atwood numbers" J. Fluid Mech., 502, 233.
39. Rich, G. R. (1963). "Hydraulic Transients," Dover, USA, 148–154.
40. Savić, D. A., & Walters, G. A. (1995). "Genetic Algorithms Techniques for Calibrating Network Models," Report No. 95/12, Centre for Systems and Control Engineering, 137–146.
41. Savić, D. A., & Walters, G. A. (1995). Genetic algorithms Techniques for Calibrating Network Models, University of Exeter, Exeter, United Kingdom, 41–77.
42. Shvarts, D., Oron, D., Kartoon, D., Rikanati, A., & Sadot, O. (2000). "Scaling Laws of Nonlinear Rayleigh-Taylor and Richtmyer-Meshkov instabilities in Two and Three Dimensions," C. R. Acad. Sci. Paris IV, 719, 312p.
43. Sharp, B. (1981). "Water Hammer Problems and Solutions," Edward Arnold Ltd., London, 43–55.
44. Skousen, P. (1998). "Valve Handbook," McGraw Hill, New York, Hammer Theory and Practice, 687–721.
45. Song, C. C. et al. (1983). "Transient Mixed-Flow Models for Storm Sewers," J. Hyd. Div., Nov., 109, 458–530.
46. Stephenson, D. (1984). "Pipe Flow Analysis," Elsevier, 19, S.A., 670–788.
47. Streeter, V. L., & Lai, C. (1962). "Water hammer Analysis Including Fluid Friction," Journal of Hydraulics Division, ASCE, 88, 79p.
48. Streeter, V. L., & Wylie, E. B. (1979). "Fluid Mechanics," McGraw-Hill Ltd., USA, 492–505.
49. Streeter, V. L., & Wylie, E. B. (1981), "Fluid Mechanics," McGraw-Hill Ltd., USA, 398–420.
50. Tijsseling, "Alan, E. Vardy, (1993). Time Scales and FSI in Unsteady Liquid-Filled Pipe Flow," 5–12.
51. Tuckerman, D. B., & Pease, R. F. W. (1981). High Performance Heat Sinking for VLSI, IEEE Electron Device letter, DEL-2, 126–129.

52. Tennekes, H., & Lumley, J. L. (1972). *A First Course in Turbulence*, the MIT Press, 410–466.
53. Thorley, A. R. D. (1991). “Fluid Transients in Pipeline Systems,” D&L George, Herts, England, 231–242.
54. Tullis, J. P. (1971). “Control of Flow in Closed Conduits,” Fort Collins, Colorado, 315–340.
55. Tuckerman, D. B. (1984). *Heat Transfer Microstructures for Integrated Circuits*, PhD. Thesis, Stanford University, 10–120.
56. Vallentine, H. R. (1965). “Rigid Water Column Theory for Uniform Gate Closure,” *J. Hyd. Div. ASCE*, July, 55–243.
57. Waddell, J. T., Niederhaus, C. E., & Jacobs, J. W. (2001). “Experimental Study of Rayleigh-Taylor Instability: Low Atwood Number Liquid Systems with Single-Mode Initial Perturbations,” *Phys. Fluids*, *13*, 1263–1273.
58. Waters, G. Z. (1984). “Modern Analysis and Control of Unsteady Flow in Pipelines,” *Ann Arbor Sci.*, 2nd Ed., 1098–1104.
59. Walski, T. M., & Lutes, T. L. (1994). “Hydraulic Transients Cause Low-Pressure Problems,” *Journal of the American Water Works Association*, *75*(2), 58.
60. Weber, S. V., Dimonte, G., & Marinak, M. M. (2003). “Arbitrary Lagrange-Eulerian Code Simulations of Turbulent Rayleigh-Taylor Instability in Two and Three Dimensions,” *Laser and Particle Beams*, *21*, 455p.
61. Wood, D. J., Dorsch, R. G., & Lightener, C. (1966). “Wave-Plan Analysis of Unsteady Flow in Closed Conduits,” *Journal of Hydraulics Division, ASCE*, *92*, 83–110.
62. Wood, D. J., & Jones, S. E. (1973). “Water Hammer Charts for Various Types of Valves,” *Journal of the Hydraulics Division, Proceedings of the American Society of Civil Engineers*, January, 167–178.
63. Wood, F. M. (1970). “History of Water Hammer,” *Civil Engineering Research Report #65*, Queens University, Canada, 66–70.
64. Wu, Z. Y., & Simpson, A. R. (2001). Competent Genetic-Evolutionary Optimization of Water Distribution Systems, *J. Computer Civ. Eng.*, *15*(2), 89–101.
65. Wylie, E. B., & Talpin, L. B. (1983). Matched Impedance to controls fluid transients, *Trans.*, *ASME*, *105*(2), 219–224.
66. Wylie, E. B., & Streeter, V. L. (1993). *Fluid Transients in systems*, Prentice-Hall, Engle wood Cliffs, New Jersey, 4.
67. Wylie, E. B., & Streeter, V. L. (1982). *Fluid Transients*, Feb Press, Ann Arbor, MI, Corrected Copy, (1983), 158p.
68. Wu, P. Y., & Little, W. A. (1983). Measurement of Friction Factor for Flow of Gases in very Fine Channels Used For Micro Miniature, Joule Thompson Refrigerators, *Cryogenics*, *24*(8), 273–277.
69. Xu, B., Ooi, K. T., Mavriplis, C., & Zaghoul, M. E. (2002). Viscous Dissipation Effects for Liquid Flow in Micro channels, *Microsystems*, 53–57.
70. Young, Y. N., Tufò, H., Dubey, A., & Rosner, R. (2001). “On the Miscible Rayleigh-Taylor Instability Two and Three Dimensions,” *J. Fluid Mech.*, *447*(377), 2003–2500.
71. Wood, D. J., Dorsch, R. G., & Lightener, C. (1966). “Wave-Plan Analysis of Unsteady Flow in Closed Conduits,” *Journal of Hydraulics Division, ASCE*, *92*, 83–110.
72. Wylie, E. B., & Streeter, V. L. (1993). *Fluid Transients in system*, Prentice-Hall, Engle wood Cliffs, New Jersey, 4.

73. Brunone, B., Karney, B. W., Mecarelli, M., & Ferrante, M. (2000 July). "Velocity Profiles and unsteady pipe frictions in Transient Flow," *Journal of Water Resources Planning and Management ASCE*, *126(4)*, 236–244.
74. Koelle, E., Jr. Luvizotto, E., & Andrade, J. P. G. (1996). "Personality Investigation of Hydraulic Networks using MOC Method of Characteristics" *Proceedings of the 7th International Conference on Pressure Surges and Fluid Transients*, Harrogate Durham, United Kingdom, 1–8.
75. Filion, Y., & Karney, B. W. (2002). "A Numerical Exploration of Transient Decay Mechanisms in Water Distribution Systems," *Proceedings of the ASCE Environmental Water Resources Institute Conference*, American Society of Civil Engineers, Roanoke, Virginia, 30.
76. Hamam, M. A., & Mc Corquodale, J. A. (1982). "Transient Conditions in the Transition from Gravity to Surcharged Sewer Flow," *Canadian J. Civil Eng.*, Canada, Sep 65–98.
77. Savic, D. A., & Walters, G. A. (1995). "Genetic Algorithms Techniques for Calibrating Network Models," Report No. 95/12, Centre for Systems and Control Engineering, 137–146.
78. Walski, T. M., & Lutes, T. L. (1994). "Hydraulic Transients Cause Low-Pressure Problems," *Journal of the American Water Works Association*, *75(2)*, 58.
79. Lee, T. S., & Pejovic, S. (1996). Air Influence on Similarity of Hydraulic Transients and Vibrations, *ASME J. Fluid Eng.*, *118(4)*, 706–709.
80. Till Mathis Wagner, (2004). A very short introduction to the Finite Element Method, Technical University of Munich, JASS, St Petersburg, May 4, 2004.

CHAPTER 2

FLUID MECHANICS AND NONLINEAR DYNAMIC MODELING

CONTENTS

| | | |
|-----|----------------------------|----|
| 2.1 | Introduction..... | 16 |
| 2.2 | Materials and Methods..... | 16 |
| 2.3 | Conclusion | 42 |
| | Keywords | 43 |
| | References..... | 43 |

2.1 INTRODUCTION

In this book, miscible liquids condition, for example, velocity, pressure, temperature and the other properties are as similar and the main approach is the changes study on behavior of the fluids flow state. According to Reynolds number magnitude (RE. NO.), separation of fluid direction happened. For fluid motion modeling, 2D-component disperses fluid motion used. Modeling of two-phase liquid–liquid flows through a Kinetics static mixer by means of computational fluid dynamics (CFD) has been presented. The two-modeled phases were assumed viscous and Newtonian with the physical properties mimicking an aqueous solution in the continuous and oil in the dispersed (secondary) phase. Differential equations included in the proposed model describe the unsteady motion of a real fluid through the channels and pipes. These differential equations are derived from the following assumptions. It was assumed that the pipe is cylindrical with a constant cross-sectional area with the initial pressure. The fluid flow through the pipe is the one-dimensional. It is assumed that the characteristics of resistors, fixed for steady flows and unsteady flows are equivalent.

One of the problems in the study of fluid flow in plumbing systems is the behavior of stratified fluid in the channels. Mostly steady flows initially are ideal, then the viscous and turbulent fluid in the pipes [1–9].

2.2 MATERIALS AND METHODS

A fluid flow is compressible if its density ρ changes appreciably within the domain of interest. Typically, this will occur when the fluid velocity exceeds Mach 0.3. Hence, low velocity flows (both gas and liquids) behave incompressibly. An incompressible fluid is one whose density is constant everywhere. All fluids behave incompressibly (to within 5%) when their maximum velocities are below Mach 0.3. Mach number is the relative velocity of a fluid compared to its sonic velocity. Mach numbers less than 1 correspond to subsonic velocities, and Mach numbers > 1 corresponds to super-sonic velocities. A Newtonian fluid (1–34) is a viscous fluid whose shear stress is a linear function of the fluid strain rate. Mathematically, this can be expressed as: $\tau_{ij} = K_{ijqp} \times D_{pq}$, where τ_{ij} is the shear stress component, and D_{pq} are fluid strain rate components [10–12].

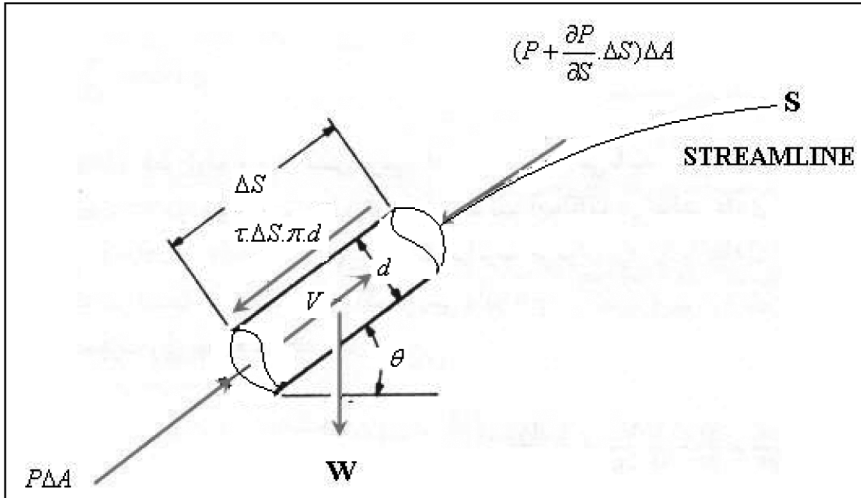


FIGURE 2.1 Newton Second Law (conservation of momentum equation) for fluid element.

It is defined as the combination of momentum equation (Fig. 2.1) and continuity equation (Fig. 2.2) for determining the velocity and pressure in a one-dimensional flow system. The solving of these equations produces a theoretical result that usually corresponds quite closely to actual system measurements.

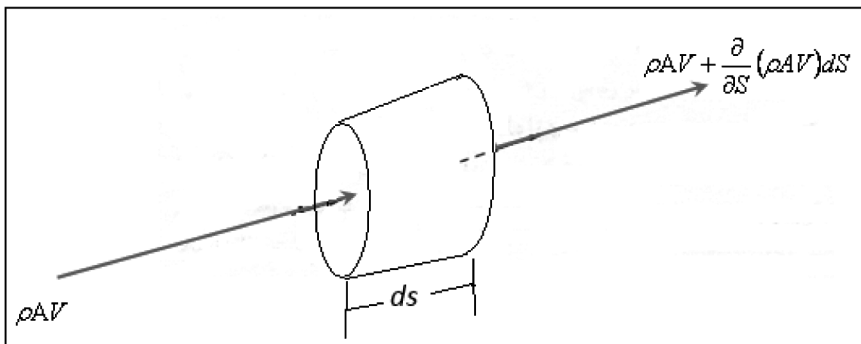


FIGURE 2.2 Continuity equation (Conservation of Mass) for fluid element.

$$P\Delta A - \left(P + \frac{\partial P}{\partial S}\Delta S\right)\Delta A - W \cdot \sin \theta - \tau \Delta S \cdot \pi \cdot d = \frac{W}{g} \cdot \frac{dV}{dt}, \quad (1)$$

Both sides are divided by m and with assumption:

$$\frac{\partial Z}{\partial S} = +\sin \theta, \quad (2)$$

$$-\frac{1}{\partial} \cdot \frac{\partial P}{\partial S} - \frac{\partial Z}{\partial S} - \frac{4\tau}{\gamma D} = \frac{1}{g} \cdot \frac{dV}{dt}, \quad (3)$$

$$\Delta A = \frac{\Pi \cdot D^2}{4}, \quad (4)$$

If, fluid diameter assumed equal to pipe diameter then:

$$\frac{-1}{\gamma} \cdot \frac{\partial P}{\partial S} - \frac{\partial Z}{\partial S} - \frac{4\tau}{\gamma D}, \quad (5)$$

$$\tau = \frac{1}{8} \rho \cdot f \cdot V^2, \quad (6)$$

$$\frac{1}{\gamma} \cdot \frac{\partial P}{\partial S} - \frac{\partial Z}{\partial S} - \frac{f}{D} \cdot \frac{V^2}{2g} = \frac{1}{g} \cdot \frac{dV}{dt}, \quad (7)$$

$$V^2 = V |V|, \quad \frac{dV}{dt} + \frac{1}{\rho} \cdot \frac{\partial P}{\partial S} + g \frac{dZ}{dS} + \frac{f}{2D} V |V| = 0, \quad (8)$$

(Euler equation)

For finding (V) and (P) we need to “conservation of mass law” (Fig. 2.2):

$$\rho AV - \left[\rho AV - \frac{\partial}{\partial S}(\rho AV) dS \right] = \frac{\partial}{\partial t}(\rho A dS) - \frac{\partial}{\partial S}(\rho AV) dS = \frac{\partial}{\partial t}(\rho A dS) \quad (9)$$

$$-\left(\rho A \frac{\partial V}{\partial S} dS + \rho V \frac{\partial A}{\partial S} dS + AV \frac{\partial \rho}{\partial S} dS \right) = \rho A \frac{\partial}{\partial t}(dS) + \rho dS \frac{\partial A}{\partial t} + A dS \frac{\partial \rho}{\partial t}, \quad (10)$$

$$\frac{1}{\rho} \left(\frac{\partial \rho}{\partial t} + V \frac{\partial \rho}{\partial S} \right) + \frac{1}{A} \left(\frac{\partial A}{\partial t} + V \frac{\partial A}{\partial S} \right) + \frac{1}{dS} \cdot \frac{\partial}{\partial t} (dS) + \frac{\partial V}{\partial S} = 0$$

With $\frac{\partial \rho}{\partial t} + V \frac{\partial \rho}{\partial S} = \frac{d\rho}{dt}$ and $\frac{\partial A}{\partial t} + V \frac{\partial A}{\partial S} = \frac{dA}{dt}$, (11)

$$\frac{1}{\rho} \cdot \frac{d\rho}{dt} + \frac{1}{A} \cdot \frac{dA}{dt} + \frac{\partial V}{\partial S} + \frac{1}{dS} \cdot \frac{1}{dt} (dS) = 0, \tag{12}$$

$$K = \left(\frac{d\rho}{\left(\frac{d\rho}{\rho} \right)} \right)$$

(Fluid module of elasticity) then:

$$\frac{1}{\rho} \cdot \frac{d\rho}{dt} = \frac{1}{k} \cdot \frac{d\rho}{dt}, \tag{13}$$

Put Eq. (7) into Eq. (8) Then:

$$\frac{\partial V}{\partial S} + \frac{1}{k} \cdot \frac{d\rho}{dt} + \frac{1}{A} \cdot \frac{dA}{dt} + \frac{1}{dS} \cdot \frac{d}{dt} (dS) = 0, \tag{14}$$

$$\rho \frac{\partial V}{\partial S} + \frac{d\rho}{dt} \rho \left[\frac{1}{k} + \frac{1}{A} \cdot \frac{dA}{d\rho} + \frac{1}{dS} \cdot \frac{d}{d\rho} (dS) \right] = 0, \tag{15}$$

$$\rho \left[\frac{1}{k} + \frac{1}{A} \cdot \frac{dA}{dt} + \frac{1}{dS} \cdot \frac{d}{d\rho} (dS) \right] = \frac{1}{C^2}, \tag{16}$$

Then $C^2 \frac{\partial V}{\partial S} + \frac{1}{\rho} \cdot \frac{d\rho}{dt} = 0,$ (17)

(Continuity equation)

Partial differential Eqs. (4) and (10) are solved by method of characteristics “MOC”:

$$\frac{dp}{dt} = \frac{\partial p}{\partial t} + \frac{\partial p}{\partial S} \cdot \frac{dS}{dt}, \quad (18)$$

$$\frac{dV}{dt} = \frac{\partial V}{\partial t} + \frac{\partial V}{\partial S} \cdot \frac{dS}{dt}, \quad (19)$$

Then:

$$\begin{cases} \left| \frac{\partial V}{\partial t} + \frac{1}{\rho} \frac{\partial p}{\partial S} + g \frac{dz}{dS} + \frac{f}{2D} V|V| \right| = 0, \\ \left| C^2 \frac{\partial V}{\partial S} + \frac{1}{\rho} \frac{\partial P}{\partial t} \right| = 0, \end{cases}, \quad (20)$$

By Linear combination of Eqs. (13) and (14)

$$\lambda \left(\frac{\partial V}{\partial t} + \frac{1}{\rho} \frac{\partial p}{\partial S} + g \cdot \frac{dz}{dS} + \frac{f}{2D} V|V| \right) + C^2 \frac{\partial V}{\partial S} + \frac{1}{\rho} \frac{\partial p}{\partial t} = 0, \quad (21)$$

$$\left(\lambda \frac{\partial V}{\partial t} + C^2 \frac{\partial V}{\partial S} \right) + \left(\frac{1}{\rho} \cdot \frac{\partial p}{\partial t} + \frac{\lambda}{\rho} \cdot \frac{\partial P}{\partial S} \right) + \lambda \cdot g \cdot \frac{dz}{dS} + \frac{\lambda \cdot f}{2D} V|V| = 0, \quad (22)$$

$$\lambda \frac{\partial V}{\partial t} + C^2 \frac{\partial V}{\partial S} = \lambda \frac{dV}{dt} \Rightarrow \lambda \frac{dS}{dt} = C^2, \quad (23)$$

$$\begin{aligned} \frac{1}{\rho} \cdot \frac{\partial p}{\partial t} + \frac{\lambda}{\rho} \cdot \frac{\partial p}{\partial S} &= \frac{1}{\rho} \cdot \frac{dp}{dt} \Rightarrow \\ \frac{\lambda}{\rho} &= \frac{1}{\rho} \cdot \frac{dS}{dt} \end{aligned}, \quad (24)$$

$$\left| \frac{C^2}{\lambda} = \lambda \text{ (By removing } \frac{dS}{dt} \text{)}, \lambda = \pm C \right.$$

For $\lambda = \pm C$ from Eq. (18) we have:

$$\frac{dV}{dt} + \frac{1}{\rho} \cdot \frac{dp}{dt} + C \cdot g \cdot \frac{dz}{dS} + C \cdot \frac{f}{2D} V|V| = 0, \tag{25}$$

With dividing both sides by “C”:

$$\frac{dV}{dt} + \frac{1}{c \cdot \rho} \frac{dP}{dt} + g \cdot \frac{dz}{dS} + \frac{f}{2D} V|V| = 0, \tag{26}$$

For $\lambda = -C$ by Eq. (16):

$$\frac{dV}{dt} - \frac{1}{c \cdot \rho} \frac{dp}{dt} + g \cdot \frac{dZ}{dS} + \frac{f}{2D} V|V| = 0, \tag{27}$$

$$\text{If } \rho = \rho \cdot g(H - Z) \text{ I,} \tag{28}$$

From Eqs. (9) and (10):

$$\left\{ \begin{array}{l} \frac{dV}{dt} + \frac{g}{c} \cdot \frac{dH}{dt} + \frac{f}{2D} V|V| = 0 \\ \text{if: } \frac{dS}{dt} = C, \end{array} \right. , \tag{29}$$

$$\left\{ \begin{array}{l} \frac{dV}{dt} + \frac{g}{c} \cdot \frac{dH}{dt} + \frac{f}{2D} V|V| = 0, \\ \text{if: } \frac{dS}{dt} = -C, \end{array} \right. \tag{30}$$

The method of characteristics is a finite difference technique which pressures (Figs. 2.3 and 2.4) were computed along the pipe for each time step (1)–(35).

Calculation automatically subdivided the pipe into sections (intervals) and selected a time interval for computations Eqs. (22) and (24) are the characteristic equation of Eqs. (21) and (23).

If: $f = 0$, Then Eq. (23) will be (Figs. 2.3 and 2.4):

$$\frac{dV}{dt} - \frac{g}{c} \cdot \frac{dH}{dt} = 0 \text{ or}$$

$$dH = \left(\frac{C}{g}\right) dV, (\text{Zhukousky}), \tag{31}$$

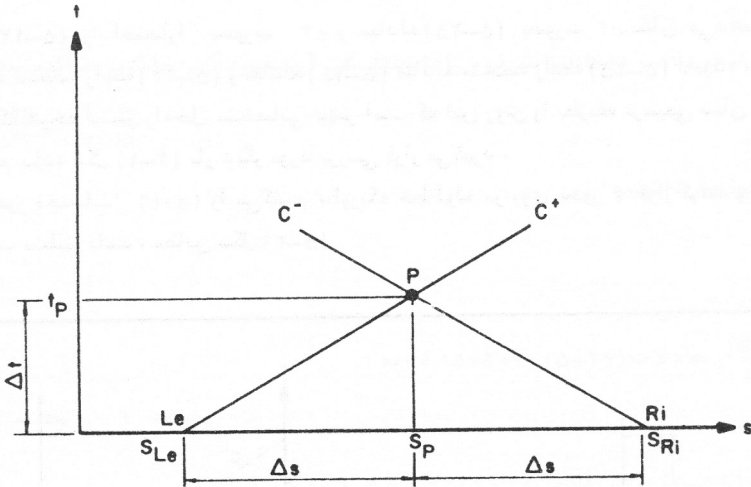


FIGURE 2.3 Intersection of characteristics lines with positive and negative slope.

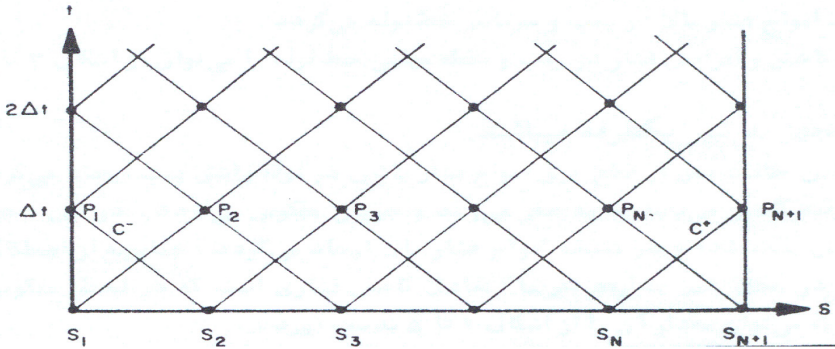


FIGURE 2.4 Set of characteristic lines intersection for assumed pipe.

If the pressure at the inlet of the pipe and along its length is equal to p_0 , then slugging pressure undergoes a sharp increase:

$$\Delta p : p = p_0 + \Delta p, \tag{32}$$

The Zhukousky formula is as flowing:

$$\Delta p = \left(\frac{C \cdot \Delta V}{g} \right), \tag{33}$$

The speed of the shock wave is calculated by the formula:

$$C = \sqrt{\frac{g \cdot \frac{E_w}{\rho}}{1 + \frac{d}{t_w} \cdot \frac{E_w}{E}}}, \tag{34}$$

By finite difference method of water hammer:

$$T_p - 0 = \Delta t$$

$$c^+ : (V_p - V_{Le}) / (TP - 0) + \left(\frac{g}{c}\right)(H_p - H_{Le}) / (TP - 0) + fV_{Le} |V_{Le}| / 2D = 0, \tag{35}$$

$$c^- : (V_p - V_{Ri}) / (TP - 0) + \left(\frac{g}{c}\right)(H_p - H_{Ri}) / (TP - 0) + fV_{Ri} |V_{Ri}| / 2D = 0, \tag{36}$$

$$c^+ : (V_p - V_{Le}) + \left(\frac{g}{c}\right)(H_p - H_{Le}) + (f \cdot \Delta t)(fV_{Le} |V_{Le}| / 2D) = 0, \tag{37}$$

$$c^- : (V_p - V_{Ri}) + \left(\frac{g}{c}\right)(H_p - H_{Ri}) + (f \cdot \Delta t)(fV_{Ri} |V_{Ri}| / 2D) = 0, \tag{38}$$

$$V_p = \frac{1}{2} \left[(V_{Le} + V_{Ri}) + \frac{g}{c} (H_{Le} - H_{Ri}) - (f \cdot \Delta t / 2D)(V_{Le} |V_{Le}| - V_{Ri} |V_{Ri}|) \right], \tag{39}$$

$$H_p = \frac{1}{2} \left[\frac{c}{g} (V_{Le} + V_{Ri}) + (H_{Le} - H_{Ri}) - \frac{c}{g} (f \cdot \Delta t / 2D)(V_{Le} |V_{Le}| - V_{Ri} |V_{Ri}|) \right], \tag{40}$$

$VLe, V Ri, HLe, H Ri, f, D$ are initial conditions parameters.

They are applied for solution at steady state condition. Water hammer equations calculation starts with pipe length “ L ” divided by “ N ” parts:

$$\Delta S = \frac{L}{N} \ \& \ \Delta t = \frac{\Delta S}{C}, \tag{41}$$

Equations (28) and (29) are solved for the range P_2 through P_N , therefore H and V are found for internal points. Hence:

At P_1 there is only one characteristic Line (c^-).

At P_{N+1} there is only one characteristic Line (c^+).

For finding H and V at P_1 and P_{N+1} the boundary conditions are used.

The Lagrangian approach was used to track the trajectory of dispersed fluid elements (drops) in the simulated static mixer [10–29]. The particle history was analyzed in terms of the residence time in the mixer. Although two relaxing miscible fluids (35–50) are mixed together, their appearances in terms of colors and shapes will change due to their mixing interpenetration (Fig. 2.5).

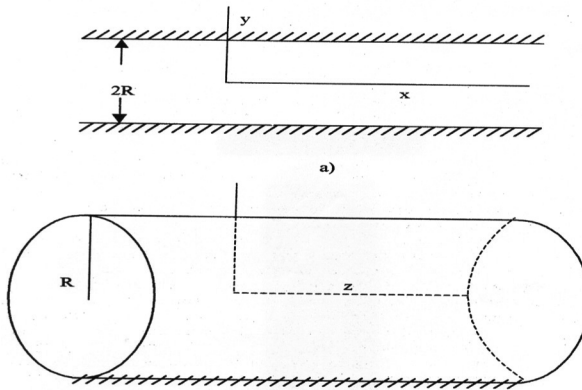


FIGURE 2.5 Two Dimensional fluids flow.

Use equations of motion of two relaxing fluids in pipe are as flowing:

$$u_1 = u_1(y, t) , \quad u_2 = u_2(y, t)$$

$$\left. \begin{aligned} \rho_1 \frac{\partial u_1}{\partial t} &= f_1 \mu_1 \frac{\partial^2 u_1}{\partial y^2} + k(u_2 - u_1) - f_1 \frac{\partial p}{\partial x}, \\ \rho_2 \frac{\partial u_2}{\partial t} &= f_2 \mu_2 \frac{\partial^2 u_2}{\partial y^2} + k(u_1 - u_2) - f_2 \frac{\partial p}{\partial x}, \\ \frac{\partial p}{\partial y} &= 0, \quad \frac{\partial p}{\partial z} = 0, \quad f_1 + f_2 = 0 \end{aligned} \right\} \quad (42)$$

where \bar{u} – Velocity (m/s), p – pressure, k – module of elasticity of water (kg/m²), f – Darcy-Weisbach friction factor (obtained from Moody diagram) for each pipe, μ –fluid dynamic, viscosity (kg/m.s), ρ – density (kg/m³).

Calculation for equation of motion for relaxing fluids:

$$\left. \begin{aligned} \theta_1 \frac{\partial \tau_1}{\partial t} + \tau_1 &= \mu_1 \frac{\partial u_1}{\partial y}, \\ \theta_2 \frac{\partial \tau_2}{\partial t} + \tau_2 &= \mu_2 \frac{\partial u_2}{\partial y} \end{aligned} \right\}, \quad (43)$$

where θ_1, θ_2 – relaxing time of fluids, define equation of motion for Interpenetration of two 2D pressurized relaxing fluids at parallel between plates and turbulent moving in pipe as flowing [30–39]:

$$\left. \begin{aligned} \rho_1 \frac{\partial u_1}{\partial t} + \rho_1 \theta_1 \frac{\partial^2 u_1}{\partial t^2} &= f_1 \mu_1 \frac{\partial^2 u_1}{\partial y^2} + \theta_1 k \frac{\partial(u_1 - u_2)}{\partial t} + k(u_2 - u_1) - f_1 \left[\theta_1 \frac{\partial^2 p}{\partial t \partial x} + \frac{\partial p}{\partial x} \right] \\ \rho_2 \frac{\partial u_2}{\partial t} + \rho_2 \theta_2 \frac{\partial^2 u_2}{\partial t^2} &= f_2 \mu_2 \frac{\partial^2 u_2}{\partial y^2} + \theta_2 k \frac{\partial(u_1 - u_2)}{\partial t} + k(u_1 - u_2) - f_2 \left[\theta_2 \frac{\partial^2 p}{\partial t \partial x} + \frac{\partial p}{\partial x} \right] \\ \frac{\partial p}{\partial y} &= 0, \quad \frac{\partial p}{\partial z} = 0, \\ f_1 + f_2 &= 0 \end{aligned} \right\} \quad (43a)$$

From Eq. (3) derived that pressure drop $\partial p / \partial x$ it is not effective but time is effective.

Assumed that at first time both plan are stopped and pressure at coordination for this time is low.

$$\left. \begin{aligned}
 t = 0 & \left\{ \begin{aligned} u_1 = 0, u_2 = 0 \\ \partial u_1 / \partial t = 0, \partial u_2 / \partial t = 0 \end{aligned} \right. \\
 y = h \quad (t > 0) & \left\{ \begin{aligned} u_1 = 0 \quad u_2 = 0 \\ y = -h \quad (t > 0) \quad u_1 = 0 \quad u_2 = 0 \end{aligned} \right.
 \end{aligned} \right\}, \quad (44)$$

At time t condition with Laplace rule we have:

$$\left. \begin{aligned}
 \frac{d^2 \bar{u}_1}{dy^2} - \alpha_1 \bar{u}_1 + \beta_1 \bar{u}_2 &= \frac{1}{\mu_1} \frac{\partial P}{\partial x} \\
 \frac{d^2 \bar{u}_2}{dy^2} - \alpha_2 \bar{u}_2 + \beta_2 \bar{u}_1 &= \frac{1}{\mu_2} \frac{\partial P}{\partial x}
 \end{aligned} \right\}, \quad (45)$$

With:

$$\left. \begin{aligned}
 y = h \quad \bar{u}_1 = 0, \quad \bar{u}_2 = 0 \\
 y = -h \quad \bar{u}_1 = 0, \quad \bar{u}_2 = 0
 \end{aligned} \right\}, \quad (46)$$

where:

$$\left. \begin{aligned}
 \alpha_1 &= \frac{\rho_1(\theta_1 s^2 + s) + k(\theta_1 s + 1)}{f_1 \mu_1}, \\
 \beta_1 &= \frac{k(\theta_1 s + 1)}{f_1 \mu_1}, \\
 \alpha_2 &= \frac{\rho_2(\theta_2 s^2 + s) + k(\theta_2 s + 1)}{f_2 \mu_2}, \\
 \beta_2 &= \frac{k(\theta_2 s + 1)}{f_2 \mu_2}
 \end{aligned} \right\}, \quad (47)$$

Calculation $\partial p / \partial x = A = \text{const}$

$$\frac{d^2}{dy^2} (N \bar{u}_1 + \bar{u}_2) - (\alpha_2 - N \beta_1)(N \bar{u}_1 + \bar{u}_2) = \left[\frac{N(1 + \theta_1 s)}{\mu_1} + \frac{1 + \theta_2 s}{\mu_2} \right] A, \quad (48)$$

$$N_{1,2} = \frac{-(\alpha_1 - \alpha_2) \pm \sqrt{(\alpha_1 - \alpha_2)^2 + 4\beta_1\beta_2}}{2\beta_1}, \quad (49)$$

$$A\bar{u}_1 + \bar{u}_2 = -A \left[\frac{N}{\mu_1} + \frac{1}{\mu_2} \right] \left[1 - \frac{ch\sqrt{\alpha_2 - N\beta_1 y}}{ch\sqrt{\alpha_2 - N\beta_1 h}} \right], \quad (50)$$

N calculation with two meaning:

$$N_1\bar{u}_1 + \bar{u}_2 = -A \left[\frac{N_1}{\mu_1} + \frac{1}{\mu_2} \right] \left[1 - \frac{ch\sqrt{\alpha_2 - N_1\beta_1 y}}{ch\sqrt{\alpha_2 - N_1\beta_1 h}} \right], \quad (51)$$

$$N_2\bar{u}_1 + \bar{u}_2 = -A \left[\frac{N_2}{\mu_1} + \frac{1}{\mu_2} \right] \left[1 - \frac{ch\sqrt{\alpha_2 - N_2\beta_1 y}}{ch\sqrt{\alpha_2 - N_2\beta_1 h}} \right], \quad (52)$$

where for equation velocity find:

$$\bar{u}_1 = \frac{A}{N_2 - N_1} \left\{ \frac{N_1 + 1}{\mu_1 \mu_2} \left[1 - \frac{ch\sqrt{\alpha_2 - N_1\beta_1 y}}{ch\sqrt{\alpha_2 - N_1\beta_1 h}} \right] - \frac{N_2 + 1}{\mu_1 \mu_2} \left[1 - \frac{ch\sqrt{\alpha_2 - N_2\beta_1 y}}{ch\sqrt{\alpha_2 - N_2\beta_1 h}} \right] \right\},$$

$$\bar{u}_2 = \frac{A}{N_1 - N_2} \left\{ \frac{N_2 - \beta_2}{\mu_1 \beta_1 \mu_2} \left[1 - \frac{ch\sqrt{\alpha_2 - N_1\beta_1 y}}{ch\sqrt{\alpha_2 - N_1\beta_1 h}} \right] - \frac{N_1 - \beta_2}{\mu_2 \beta_1 \mu_1} \left[1 - \frac{ch\sqrt{\alpha_2 - N_2\beta_1 y}}{ch\sqrt{\alpha_2 - N_2\beta_1 h}} \right] \right\}.$$

$$\bar{u}_i = \frac{1}{2\pi} \int_{\sigma - i\infty}^{\sigma + i\infty} \frac{A}{N_2 - N_1} \left\{ \frac{N_1 - 1}{\mu_1 \mu_2} \left[1 - \frac{ch\sqrt{\alpha_2 - N_1\beta_1 y}}{ch\sqrt{\alpha_2 - N_1\beta_1 h}} \right] - \frac{N_2 - 1}{\mu_1 \mu_2} \left[1 - \frac{ch\sqrt{\alpha_2 - N_2\beta_1 y}}{ch\sqrt{\alpha_2 - N_2\beta_1 h}} \right] \right\} e^{st} \frac{ds}{s}, \quad (53)$$

In this calculation we have:

$$S = S_1, \quad S = S_2, \quad S = S_3, \quad S = S_4 \quad \therefore S_1, S_2, S_3, S_4,$$

Proportional to forth procedure:

$$\alpha_2 - N_1\beta_1 = -\frac{\pi^2}{h^2} \left(n + \frac{1}{2} \right)^2, \quad (54)$$

$$\alpha_2 - N_2\beta_1 = -\frac{\pi^2}{h^2} \left(n + \frac{1}{2} \right)^2, \quad (55)$$

In this state for velocity we have:

$$u_1 = -\frac{\frac{1}{f_1\mu_1 f_2\mu_2}}{\frac{1}{f_1\mu_1} + \frac{1}{f_2\mu_2}} A \left\{ -\frac{1}{2}(y^2 - h^2) + \frac{\left(\frac{1}{\mu_1} - \frac{1}{\mu_2} \right) f_2\mu_2}{\left(\frac{1}{f_1\mu_1} + \frac{1}{f_2\mu_2} \right) k} \times \right.$$

$$\left. \times \left[1 - \frac{ch \sqrt{\left(\frac{1}{f_1\mu_1} + \frac{1}{f_2\mu_2} \right) ky}}{ch \sqrt{\left(\frac{1}{f_1\mu_1} + \frac{1}{f_2\mu_2} \right) kh}} \right] + \frac{4A}{\pi} \sum_{i=1}^4 \sum_{n=1}^{\infty} \frac{(-1)^{n+1}}{\left(n + \frac{1}{2} \right)} \cos \left[\pi \left(n + \frac{1}{2} \right) \frac{y}{h} \right] \right\} \times$$

$$\left. \left\{ \frac{\left[\frac{\pi^2}{h^2} \left(n + \frac{1}{2} \right) + \frac{(\theta_2^{\gamma_{in}} + 1)(\rho_2^{\gamma_{in}} + k)}{f_2 \mu_2} \right] \frac{1}{\mu_1} + \frac{k(\theta_1^{\gamma_{in}} + 1)}{f_1 \mu_1} \frac{1}{\mu_2}}{\frac{(\theta_1^{\gamma_{in}} + 1)(\rho_1^{\gamma_{in}} + k)}{f_1 \mu_1} + \frac{(\theta_2^{\gamma_{in}} + 1)(\rho_2^{\gamma_{in}} + k)}{f_2 \mu_2}} - 2 \frac{\pi^2}{h^2} \left(n + \frac{1}{2} \right)^2} \cdot \frac{1}{\gamma_{in}} \right. \right.$$

$$\left. \left. \frac{2\gamma_{in} \left(\frac{\theta_1 \rho_1}{f_1 \mu_1} + \frac{\theta_2 \rho_2}{f_2 \mu_2} \right) + \frac{\theta_1 k + \rho_1}{f_1 \mu_1} + \frac{\theta_2 k + \rho_2}{f_2 \mu_2} + \frac{f_1 \mu_1}{2 \frac{\pi^2}{h^2} \left(n + \frac{1}{2} \right)^2 + \frac{(\theta_1^{\gamma_{in}} + 1)(\rho_1^{\gamma_{in}} + k)}}{f_1 \mu_1}}{\frac{(\theta_1^{\gamma_{in}} + 1)(\rho_1^{\gamma_{in}} + k)}}{f_1 \mu_1}} \right\} \right.$$

$$\left. \left. \frac{e^{-\gamma_{in} t}}{\frac{(\theta_2^{\gamma_{in}} + 1)(\rho_2^{\gamma_{in}} + k)}{f_2 \mu_2}} \left(2\gamma_{in} \left(\frac{\theta_1 \rho_1}{f_1 \mu_1} + \frac{\theta_2 \rho_2}{f_2 \mu_2} \right) - \frac{\theta_2 k + \rho_2}{f_2 \mu_2} - \frac{\theta_1 k + \rho_1}{f_1 \mu_1} \right) \right) \right\} , \tag{56}$$

$$u_2 = - \frac{1}{\frac{1}{f_1 \mu_1} + \frac{1}{f_2 \mu_2}} A \left[- \frac{1}{2} (y^2 + h^2) + \frac{\left(\frac{1}{\mu_1} - \frac{1}{\mu_2} \right) f_1 \mu_1}{\left(\frac{1}{f_1 \mu_1} - \frac{1}{f_2 \mu_2} \right) k} \times \right.$$

$$\left. \times \left[1 - \frac{ch \sqrt{\left(\frac{1}{f_1 \mu_1} + \frac{1}{f_2 \mu_2} \right) ky}}{ch \sqrt{\left(\frac{1}{f_1 \mu_1} + \frac{1}{f_2 \mu_2} \right) kh}} \right] \right] + \frac{4A}{\pi} \sum_{i=1}^4 \sum_{n=1}^{\infty} \frac{(-1)^{n+1}}{\left(n + \frac{1}{2} \right)} \cos \left[\pi \left(n + \frac{1}{2} \right) \frac{y}{h} \right] \times$$

$$\left[\frac{\left[\frac{\pi^2}{h^2} \left(n + \frac{1}{2} \right) + \frac{(\theta_1^2 \gamma_{in} + 1)(\rho_1 \gamma_{in} + k)}{f_1 \mu_1} \right] \frac{1}{\mu_2} + \frac{k(\theta_1 \gamma_{in} + 1)}{f_2 \mu_2} \frac{1}{\mu_1}}{\frac{(\theta_1 \gamma_{in} + 1)(\rho_1 \gamma_{in} + k)}{f_1 \mu_1} + \frac{(\theta_2 \gamma_{in} + 1)(\rho_2 \gamma_{in} + k)}{f_2 \mu_2} - 2 \frac{\pi^2}{h^2} \left(n + \frac{1}{2} \right)^2 \gamma_{in}} \right] \frac{1}{2^{\gamma_{in}}} \left(\frac{(\theta_1 \gamma_{in} + 1)(\rho_1 \gamma_{in} + k)}{f_1 \mu_1} \right) \right. \\
 \left. + \frac{(\theta_1 \rho_1}{f_1 \mu_1} + \frac{\theta_2 \rho_2}{f_2 \mu_2})}{f_1 \mu_1} + \frac{\theta_1 k + \rho_1}{f_1 \mu_1} + \frac{\theta_2 k + \rho_2}{f_2 \mu_2} + \frac{2^{\gamma_{in}} \left(\frac{(\theta_1 \gamma_{in} + 1)(\rho_1 \gamma_{in} + k)}{f_1 \mu_1} \right)}{2 \frac{\pi^2}{h^2} \left(n + \frac{1}{2} \right)^2 + \frac{(\theta_1 \gamma_{in} + 1)(\rho_1 \gamma_{in} + k)}{f_1 \mu_1}} \right] \\
 \left. \frac{e^{-\gamma_{in} t}}{\frac{(\theta_2 \gamma_{in} + 1)(\rho_2 \gamma_{in} + k)}{f_2 \mu_2}} \left[\frac{2^{\gamma_{in}} \left(\frac{\theta_1 \rho_1}{f_1 \mu_1} + \frac{\theta_2 \rho_2}{f_2 \mu_2} \right)}{f_2 \mu_2} - \frac{\theta_2 k + \rho_2}{f_2 \mu_2} - \frac{\theta_1 k + \rho_1}{f_1 \mu_1} + \frac{4k^2(\theta_1 \theta_2 \gamma_{in} + \theta_1 + \theta_2)}{f_1 \mu_1 f_2 \mu_2} \right] \right. \\
 \left. + \frac{(\theta_1 \gamma_{in} + 1)(\rho_1 \gamma_{in} + k)}{f_1 \mu_1} - \frac{(\theta_2 \gamma_{in} + 1)(\rho_2 \gamma_{in} + k)}{f_2 \mu_2} \right] \quad (57)$$

When $\theta_1 = \theta_2 = 0$ from Eqs. (9) and (10) we have:

$$\theta_1 = \theta_2 = 0$$

$$\mu_1 = \mu_2 \quad , \quad \rho_{1i} = \rho_{2i} \quad ,$$

$$u = u_1 = u_2 = \frac{A}{2\mu} (h^2 - y^2) - \frac{16h^2 A}{\pi\mu} \sum_{n=1}^{\infty} \frac{(-1)^n}{(2n+1)^3} \cos \left(\frac{2n+1}{2h} y \right) e^{-\frac{\pi^2}{h^2} \left(n + \frac{1}{2} \right)^2 \frac{\mu t}{\rho}}$$

At condition $t \rightarrow \infty$ for unsteady motion of fluid, it is easy for calculation table procedure.

$$\left. \begin{aligned} \rho_1 \frac{\partial u_1}{\partial t} &= f_1 \mu_1 \left(\frac{\partial^2 u_1}{\partial r^2} + \frac{1}{r} \frac{\partial u_1}{\partial r} \right) + k(u_2 - u_1) - f_1 \frac{\partial P}{\partial z} \\ \rho_2 \frac{\partial u_2}{\partial t} &= f_2 \mu_2 \left(\frac{\partial^2 u_2}{\partial r^2} + \frac{1}{r} \frac{\partial u_2}{\partial r} \right) + k(u_1 - u_2) - f_2 \frac{\partial P}{\partial z} \end{aligned} \right\}, \quad (58)$$

For every relaxing phase we have:

$$\left. \begin{aligned} \theta_1 \frac{\partial \tau_1}{\partial t} + \tau_1 &= \mu_1 \frac{\partial u_1}{\partial r}, \\ \theta_2 \frac{\partial \tau_2}{\partial t} + \tau_2 &= \mu_2 \frac{\partial u_2}{\partial r}, \end{aligned} \right\}, \quad (59)$$

Start and limiting conditions:

$$\left. \begin{aligned} t = 0 \quad u_1 = 0, u_2 = 0, \\ r = R(t > 0) \quad u_1 = 0, u_2 = 0. \end{aligned} \right\} \quad (60)$$

$$\left. \begin{aligned} \rho_1 \left(\frac{\partial u_1}{\partial t} + \theta_1 \frac{\partial^2 u_1}{\partial t^2} \right) &= f_1 \mu_1 \left(\frac{\partial^2 u_1}{\partial r^2} + \frac{1}{r} \frac{\partial u_1}{\partial r} \right) + k \left[\theta_1 \frac{\partial}{\partial t} (u_2 - u_1) + (u_2 - u_1) \right] - \\ &- f_1 \left[\theta_1 \frac{\partial^2 p}{\partial t \partial z} + \frac{\partial p}{\partial z} \right], \\ \rho_2 \left(\frac{\partial u_2}{\partial t} + \theta_2 \frac{\partial^2 u_2}{\partial t^2} \right) &= f_2 \mu_2 \left(\frac{\partial^2 u_2}{\partial r^2} + \frac{1}{r} \frac{\partial u_2}{\partial r} \right) + k \left[\theta_2 \frac{\partial}{\partial t} (u_1 - u_2) + (u_1 - u_2) \right] - \\ &- f_2 \left[\theta_2 \frac{\partial^2 p}{\partial t \partial z} + \frac{\partial p}{\partial z} \right]. \end{aligned} \right\} \quad (61)$$

Then solution finds in the form of velocity equation, *ID* fluid viscosity in round pipe is:

$$u_1 = - \frac{A}{f_1 \mu_1 \left(\frac{1}{f_1 \mu_1} + \frac{1}{f_2 \mu_2} \right)} \left\{ \frac{1}{4} (r^2 - R^2) \frac{1}{f_2 \mu_2} + \frac{\left(\frac{1}{\mu_2} - \frac{1}{\mu_1} \right) f_2 \mu_2}{k \left(\frac{1}{f_1 \mu_1} + \frac{1}{f_2 \mu_2} \right)} \right\} \times$$

$$\begin{aligned}
& \times \left[1 - \frac{I_0 \sqrt{\left(\frac{1}{f_1 \mu_1} + \frac{1}{f_2 \mu_2}\right) k r}}{I_0 \sqrt{\left(\frac{1}{f_1 \mu_1} + \frac{1}{f_2 \mu_2}\right) k R}} \right] + \sum_{i=1}^4 \sum_{n=1}^{\infty} \frac{4A}{\alpha_n} \frac{J_0\left(\alpha_n \frac{r}{R}\right)}{J_1(\alpha_n)} \times \\
& \times \left\{ \frac{\frac{\alpha_n^2}{R^2} + \frac{(\theta_2 \gamma_{in} + 1)(-\rho_2 \gamma_{in} + k)}{f_1 \mu_1} \frac{1}{\mu_1} + \frac{k(\theta_1 \gamma_{in} + 1)}{f_1 \mu_1} \frac{1}{\mu_2}}{(\theta_1 \gamma_{in} + 1)(-\rho_1 \gamma_{in} + k) \frac{1}{f_1 \mu_1} + (\theta_2 \gamma_{in} + 1)(-\rho_2 \gamma_{in} + k) \frac{1}{f_2 \mu_2}} \pm 2 \frac{\alpha_n^2}{R^2} \right\} \times \\
& \times e^{\frac{-\gamma}{\bar{a}_{in}} \int_0^r \gamma_{in} \left(\frac{\theta_1 \rho_1}{f_1 \mu_1} + \frac{\theta_2 \rho_2}{f_2 \mu_2} \right) \pm \frac{\theta_1 k + \rho_1}{f_1 \mu_1} + \frac{\theta_2 k + \rho_2}{f_2 \mu_2}} \\
& + \left[\left(\frac{(\theta_1 \gamma_{in} + 1)(\rho_1 \gamma_{in} + k)}{f_1 \mu_1} - \frac{(\theta_2 \gamma_{in} + 1)(\rho_2 \gamma_{in} + k)}{f_2 \mu_2} \right) \left(2 \gamma_{in} \left(\frac{\theta_1 \rho_1}{f_1 \mu_1} + \frac{\theta_2 \rho_2}{f_2 \mu_2} \right) \right) - \right. \\
& \left. - \frac{\theta_2 k + \rho_2}{f_2 \mu_2} - \frac{\theta_1 k + \rho_1}{f_1 \mu_1} + 4k^2 \frac{\theta_1 \theta_2 \gamma_{in} + \theta_1 + \theta_2}{f_1 \mu_1 f_2 \mu_2} \right] \left/ \left[2 \frac{\alpha_n^2}{R^2} + \right. \right. \\
& \left. \left. + \frac{(\theta_1 \gamma_{in} + 1)(-\rho_1 \gamma_{in} + k)}{f_1 \mu_1} + \frac{(\theta_2 \gamma_{in} + 1)(-\rho_2 \gamma_{in} + k)}{f_2 \mu_2} \right] \right\}, \tag{62}
\end{aligned}$$

$$u_2 = -\frac{A}{f_1 \mu_1 \left(\frac{1}{f_1 \mu_1} + \frac{1}{f_2 \mu_2} \right)} \left\{ \frac{1}{4} (r^2 - R^2) \frac{1}{f_2 \mu_2} + \frac{\left(\frac{1}{\mu_2} - \frac{1}{\mu_1} \right) f_2 \mu_2}{k \left(\frac{1}{f_1 \mu_1} + \frac{1}{f_2 \mu_2} \right)} \right\} \times$$

$$\begin{aligned}
 & \times \left[1 - \frac{I_0 \sqrt{\left(\frac{1}{f_1 \mu_1} + \frac{1}{f_2 \mu_2}\right) kr}}{I_0 \sqrt{\left(\frac{1}{f_1 \mu_1} + \frac{1}{f_2 \mu_2}\right) kR}} \right] + \sum_{i=1}^4 \sum_{n=1}^{\infty} \frac{4A}{\alpha_n} \frac{J_0\left(\alpha_n \frac{r}{R}\right)}{J_1(\alpha_n)} \times \\
 & \times \left[\frac{\alpha_n^2}{R^2} + \frac{(\theta_2 \gamma_{in} + 1)(\rho_1 \gamma_{in} + k)}{f_1 \mu_1} \frac{1}{\mu_2} + \frac{k(\theta_2 \gamma_{in} + 1)}{f_2 \mu_2} \frac{1}{\mu_1} \right. \\
 & \times \left. \frac{(\theta_1 \gamma_{in} + 1)(-\rho_1 \gamma_{in} + k)}{f_1 \mu_1} + \frac{(\theta_2 \gamma_{in} + 1)(-\rho_2 \gamma_{in} + k)}{f_2 \mu_2} \pm 2 \frac{\alpha_n^2}{R^2} \right] \times \\
 & \times \frac{e^{-\gamma_{in} t}}{\gamma_{in}} \left/ \left\{ 2 \gamma_{in} \left(\frac{\theta_1 \rho_1}{f_1 \mu_1} + \frac{\theta_2 \rho_2}{f_2 \mu_2} \right) + \frac{\theta_1 k + \rho_1}{f_1 \mu_1} + \frac{\theta_2 k - \rho_2}{f_2 \mu_2} \pm \right. \right. \\
 & \pm \left[\left(\frac{(\theta_1 \gamma_{in} + 1)(\rho_1 \gamma_{in} + k)}{f_1 \mu_1} - \frac{(\theta_2 \gamma_{in} + 1)}{f_2 \mu_2} \right) \left(2 \gamma_{in} \left(\frac{\theta_1 \rho_1}{f_1 \mu_1} + \frac{\theta_2 \rho_2}{f_2 \mu_2} \right) + \right. \right. \\
 & \left. \left. + \frac{\theta_2 k + \rho_2}{f_2 \mu_2} - \frac{\theta_1 k + \rho_1}{f_1 \mu_1} + 4k^2 \frac{\theta_1 \theta_2 \gamma_{in} + \theta_1 + \theta_2}{f_1 \mu_1 f_2 \mu_2} \right) \right] \left/ \left[-2 \frac{\alpha_n^2}{R} + \right. \right. \\
 & \left. \left. + \frac{(\theta_1 \gamma_{in} + 1)(\rho_1 \gamma_{in} + k)}{f_1 \mu_1} - \frac{(\theta_2 \gamma_{in} + 1)(\rho_2 \gamma_{in} + k)}{f_2 \mu_2} \right] \right\}, \tag{63}
 \end{aligned}$$

$$\begin{cases} \theta_1 = \theta_2 = 0 \\ \mu_1 = \mu_2 = \mu \\ \rho_{1i} = \rho_{2i} = \rho \end{cases}$$

One of the problems in the study of fluid flow in plumbing systems is the behavior of stratified fluid in the channels. Mostly steady flows initially are ideal, then the viscous and turbulent fluid in the pipes.

At the deep pool filled with water, and on its surface to create a disturbance, then the surface of the water will begin to propagate. Their origin is explained by the fact that the fluid particles are located near the cavity.

The fluid particles create disturbance, which will seek to fill the cavity under the influence of gravity. The development of this phenomenon is led to the spread of waves on the water. The fluid particles in such a wave do not move up and down around in circles. The waves of water are neither longitudinal nor transverse. They seem to be a mixture of both. The radius of the circles varies with depth of moving fluid particles. They reduce to as long as they do not become equal to zero.

If we analyze the propagation velocity of waves on water, it will be revealed that the velocity of waves depends on length of waves. The speed of long waves is proportional to the square root of the acceleration of gravity multiplied by the wavelength [40–59]:

$$v_{\Phi} = \sqrt{g\lambda}$$

The cause of these waves is the force of gravity.

For short waves the restoring force due to surface tension force, and therefore, the speed of these waves is proportional to the square root of the private. The numerator of which is the surface tension, and in the denominator—the product of the wavelength to the density of water:

$$v_{\Phi} = \sqrt{\sigma / \lambda \rho}, \quad (64)$$

Suppose there is a channel with a constant slope bottom, extending to infinity along the axis Ox .

And let the feed in a field of gravity flows, incompressible fluid. It is assumed that the fluid is devoid of internal friction. Friction neglects on the sides and bottom of the channel. The liquid level is above the bottom of the channel h . A small quantity compared with the characteristic dimensions of the flow, the size of the bottom roughness, etc.

Free liquid surface h_0 (Fig. 2.5), which is in equilibrium in the gravity field is flat. As a result of any external influence, liquid surface in a location removed from its equilibrium position. There is a movement spread-

ing across the entire surface of the liquid in the form of waves, called gravity.

They are caused by the action of gravity field. This type of waves occurs mainly on the liquid surface. They capture the inner layers, the deeper for the smaller liquid surface.

Let
$$h = \xi + h_0, \tag{65}$$

where h_0 – ordinate denotes the free surface of the liquid; ξ – a deviation from the level of the liquid free surface; h – depth of the fluid; and z – vertical coordination of any point in the water column. We assume that the fluid flow is characterized by a spatial variable x and time dependent t .

Thus, it is believed that the fluid velocity u has a nonzero component u_x , which will be denoted by u (other components can be neglected). In addition, the level of h depends only on x and t .

Let us consider such gravitational waves, in which the speed of moving particles are so small that for the Euler equation, it can be neglected the $(u\nabla)u$ compared with $\partial u / \partial t$.

During the time period τ , committed by the fluid particles in the wave, these particles pass the distance of the order of the amplitude a .

Therefore, the speed of their movement will be $u \sim a / \tau$.

Rate u varies considerably over time intervals of the order τ and for distances of the order λ along the direction of wave propagation, λ – Wavelength.

Therefore, the derivatives of the velocity time-order u/τ and the coordinate-order u/λ .

Thus, the condition:

$$(u\nabla)u < \partial u / \partial t$$

Equivalent to the requirement.

$$\frac{1}{\lambda} \left(\frac{a}{\lambda} \right)^2 \ll \frac{a}{\tau} \frac{1}{\tau} \quad a < \lambda, \text{ or,} \tag{66}$$

That is, amplitude of the wave must be small compared with the wavelength. Consider the propagation of waves in the channel Ox directed along the axis for fluid flow along the channel.

Channel cross section can be of any shape and change along its length with changes in liquid level, cross-sectional area of the liquid in the channel denoted by: $h = h(x, t)$.

The depth of the channel and basin are assumed to be small compared with the wavelength. We write the Euler equation in the form of [60–70]:

$$\frac{\partial u}{\partial t} = -\frac{1}{\rho} \frac{\partial p}{\partial x}, \quad (67)$$

$$\frac{1}{\rho} \frac{\partial p}{\partial z} = -g, \quad (68)$$

where ρ – density, p – pressure, and g – acceleration of free fall.

Quadratic in velocity members omitted, since the amplitude of the waves is still considered low. From the second equation we have that at the free surface:

$$z = h(x, t)$$

where $p = p_0$ should be satisfied:

$$p = p_0 + \rho g(h - z), \quad (69)$$

Substituting this expression in Eq. (67), we obtain:

$$\frac{\partial u}{\partial t} = -g \frac{\partial h}{\partial x}, \quad (70)$$

In order to determine u and h we use the continuity equation for the case under consideration.

Consider the volume of fluid contained between two planes of the cross-section of the canal at a distance dx from each other per unit time through a cross-section x enter the amount of fluid, equal to $(hu)_x$.

At the same time through the section:

$$x + dx$$

There is forth coming $(hu)_{x+dx}$.

Therefore, the volume of fluid between the planes is changed to

$$(hu)_{x+dx} - (hu)_x = \frac{\partial(hu)}{\partial x} dx, \tag{71}$$

By virtue of incompressibility of the liquid is a change could occur only due to changes in its level. Changing the volume of fluid between these planes in a unit time is equal

$$\frac{\partial h}{\partial t} dx$$

Consequently, we can write:

$$\frac{\partial(hu)}{\partial x} dx = -\frac{\partial h}{\partial t} dx \text{ and } \frac{\partial(hu)}{\partial x} + \frac{\partial h}{\partial t} = 0, t > 0, -\infty < x < \infty \text{ or,} \tag{72}$$

Since $h = h_0 + \xi$ where h_0 denotes the ordinate of the free liquid surface, in a state of relative equilibrium and evolving the influence of gravity is:

$$\frac{\partial \xi}{\partial t} + h_0 \frac{\partial u}{\partial x} = 0 \tag{73}$$

Thus, we obtain the following system of equations describing the fluid flow in the channel:

$$\frac{\partial \xi}{\partial t} + h_0 \frac{\partial u}{\partial x} = 0, \frac{\partial u}{\partial t} + g \frac{\partial \xi}{\partial x} = 0, t > 0, -\infty < x < \infty, \tag{74}$$

2.2.1 VELOCITY PHASE OF THE HARMONIC WAVE

The phase velocity h_0 expressed in terms of frequency ν_Φ and wavelength f (or the angular frequency) λ and wave number $\omega = 2\pi f$ formula $k = 2\pi / \lambda$.

The concept of phase velocity can be used if the harmonic wave propagates without changing shape.

This condition is always performed in linear environments. When the phase velocity depends on the frequency, it is equivalent to talk about the velocity dispersion. In the absence of any dispersion the waves assumed with a rate equal to the phase velocity.

Experimentally, the phase velocity at a given frequency can be obtained by determining the wavelength of the interference experiments. The

ratio of phase velocities in the two media can be found on the refraction of a plane wave at the plane boundary of these environments. This is because the refractive index is the ratio of phase velocities.

It is known that the wave number k satisfies the wave equation is not any values ω but only if their relationship. To establish this connection is sufficient to substitute the solution of the form:

$$\exp[i(\omega t - kx)], \quad (75)$$

in the wave equation.

The complex form is the most convenient and compact. We can show that any other representation of harmonic solutions, including in the form of a standing wave leads to the same connection between ω and k .

Substituting the wave solution into the equation for a string, we can see that the equation becomes an identity for:

$$\omega^2 = k^2 v_{\Phi}^2, \quad (76)$$

Exactly the same relation follows from the equations for waves in the gas, the equations for elastic waves in solids and the equation for electromagnetic waves in vacuum.

The presence of energy dissipation leads to the appearance of the first derivatives (forces of friction) in the wave equation. The relationship between frequency and wave number becomes the domain of complex numbers.

For example, the telegraph equation (for electric waves in a conductive line) yields:

$$\omega^2 = k^2 v_{\Phi}^2 + i \cdot \omega R / L, \quad (77)$$

The relation connecting between a frequency and wave number (wave vector), in which the wave equation has a wave solution is called a dispersion relation, the dispersion equation or dispersion.

This type of dispersion relation determines the nature of the wave. Since the wave equations are partial differential equations of second order in time and coordinates, the dispersion is usually a quadratic equation in the frequency or wave number.

The simplest dispersion equations presented above for the canonical wave equation are also two very simple solutions:

$$\omega = +kv_\phi \text{ and } \omega = -kv_\phi \quad (78)$$

We know that these two solutions represent two waves traveling in opposite directions. By its physical meaning the frequency is a positive value so that the two solutions must define two values of the wave number, which differ in sign. The Act permits the dispersion, generally speaking, the existence of waves with all wave numbers that is of any length, and, consequently, any frequencies. The phase velocity of these waves:

$$v_\phi = \omega / k, \quad (79)$$

Coincides with the most velocity, which appear in the wave equation and is a constant, which depends only on the properties of the medium.

The phase velocity depends on the wave number, and, consequently, on the frequency. The dispersion equation for the telegraph equation is an algebraic quadratic equation has complex roots. By analogy with the theory of oscillations, the presence of imaginary part of the frequency means the damping or growth of waves. It can be noted that the form of the dispersion law determines the presence of damping or growth.

In general terms, the dispersion can be represented by the equation: $\Phi(\omega, k) = 0$, where Φ – a function of frequency and wave vector.

By solving this equation for ω you can obtain an expression for the phase velocity):

$$v_\phi = \omega / k = f(\omega, \vec{k}), \quad (80)$$

By definition, the phase velocity is a vector directed normal to phase surface.

Then, more correctly write the last expression in the following form:

$$\vec{v}_\phi = \frac{\lambda}{T} = \frac{\omega}{k^2} \cdot \vec{k} = f(\omega, \vec{k}), \quad (81)$$

2.2.2 DISPERSIVE PROPERTIES OF MEDIA

The most important subject of research in wave physics, which has the primary practical significance.

If we refer to dimensionless parameters and variables:

$$\tau = t \sqrt{\frac{g}{h_0}}, \quad X = \frac{x}{h_0}, \quad U = u \frac{1}{\sqrt{gh_0}}, \quad \delta = \frac{\xi}{h_0}, \quad (82)$$

$$\frac{\partial \delta}{\partial \tau} + \frac{\partial U}{\partial X} = 0, \quad \frac{\partial U}{\partial \tau} + \frac{\partial \delta}{\partial X} = 0, \quad t > 0, \quad -\infty < X < \infty, \quad (83)$$

Consider a plane harmonic longitudinal wave, that is, we seek the solution of Eq. (83) as the real part of the following complex expressions:

$$\Psi = \Psi^0 \exp[i(k_* X + \omega_* \tau)], \quad \Psi^0 = \Psi_*^0 + i\Psi_{**}^0, \quad k_* = k + ik_{**}, \quad \omega_* = \omega + i\omega_{**}, \quad (84)$$

where:

$$\Psi = \delta, U, \text{ a } \Psi^0 = \delta^0, U^0$$

It determines the amplitude of the perturbations of displacement and velocity. There are two types of solutions.

Type I. Solution or wave of the first type, when:

$k_* = k$ – a real positive number ($k > 0, k_{**} = 0$).

In this case we have:

$$\Psi = (\Psi_*^0 + i\Psi_{**}^0) \exp[i(kX + \omega\tau + i\omega_{**}\tau)] = (\Psi_*^0 + i\Psi_{**}^0) \exp(-\omega_{**}\tau) \times [\cos(kX + \omega\tau) + i \sin(kX + \omega\tau)] \quad (85)$$

$$\operatorname{Re}\{\Psi\} = \exp(-\omega_{**}\tau) |\Psi^0| \sin[\phi + (kX + \omega\tau)], \quad (86)$$

$$|\Psi^0| = \sqrt{\Psi_*^{02} + \Psi_{**}^{02}}, \quad \phi = \operatorname{arctg}(-\Psi_*^0 / \Psi_{**}^0)$$

Thus, the decision of the first type is a sinusoidal coordinate and $\omega_{**} > 0$ decaying exponentially in time perturbation, which is called k wave:

$$\Psi(k) = |\Psi^0| \exp[-\omega_{**}(k)\tau] \sin\left\{\phi + \frac{2\pi[X + v_\phi(k)\tau]}{\lambda(k)}\right\}, \quad (87)$$

where:

$$v_{\phi}(k) = \omega(k) / k, \lambda(k) = 2\pi / k, \tag{88}$$

where, ϕ – initial phase; $v_{\phi}(k)$ – phase velocity or the velocity of phase fluctuations; $\lambda(k)$ – wavelength, $\omega_{**}(k)$ – damping the oscillations in time.

In other words, k is the waves that have uniform length, but time-varying amplitude. These waves are analog of free oscillations.

Type II. Decisions, or wave, the second type, where: $\omega_* = \omega$ – a real positive number ($\omega > 0, \omega_{**} = 0$).

In this case we have:

$$\begin{aligned} \psi = (\psi_*^0 + i\psi_{**}^0) \exp[i(kX + \omega\tau + ik_{**}z)] = (\Psi_*^0 + i\Psi_{**}^0) \exp(-k_{**}X) \times \\ [\cos(kX + \omega\tau) + i \sin(kX + \omega\tau)], \end{aligned} \tag{89}$$

$$\text{Re}\{\Psi\} = \exp(-k_{**}X) |\Psi^0| \sin[\phi + (kX + \omega\tau)], \tag{90}$$

Thus, the solution of the second type is a sinusoidal oscillation in time (excited, for example, any stationary source of external monochromatic vibrations at) $X = 0$, decaying exponentially along the length of the amplitude.

Such disturbances, which are analogous to a wave of forced oscillations, called ω – waves:

$$\Psi(\omega) = |\Psi^0(\omega)| \exp(-k_{**}(\omega)X) \sin\left\{\phi + \frac{2\pi[X + v_{\phi}(\omega)\tau]}{\lambda(\omega)}\right\}, \tag{91}$$

$$v_{\phi}(\omega) = \omega / k(\omega), \tag{92}$$

$$\lambda(\omega) = 2\pi / k(\omega)$$

where, $k_{**}(\omega)$ – damping vibrations in length.

In other words, ω – waves with stationary in time and varying in length amplitudes.

Cases $k < 0, k_{**} > 0$ and $k > 0, k_{**} < 0$ consistent with attenuation of amplitude of the disturbance regime in the direction of phase fluctuations or phase velocity.

Let us obtain the characteristic equation, linking k_* and ω_* . After substituting Eq. (92) in the system of Eq. (91) we obtain:

$$\delta^0 \frac{\omega_*}{k_*} + U^0 = 0 \quad U^0 \frac{\omega_*}{k_*} + \delta^0 = 0 \quad (93)$$

From the condition of the existence of a system of linear homogeneous algebraic Eq. (93) with respect to perturbations of a nontrivial solution implies the desired characteristic, or dispersion, which has one solution:

$$v_\Phi = \sqrt{gh_0}, \quad (94)$$

Thus, we obtain a solution representing a sinusoidal in time and coordinate free undammed oscillations [12–14].

Such behaviors of the waves are due to the absence of any dissipation in the fluid. The fluid is incompressible and ideal. There is no heat-mass transfer. Equation (94) with respect to perturbations takes the form of wave equations:

$$\frac{\partial^2 \xi}{\partial t^2} = gh_0 \frac{\partial^2 \xi}{\partial x^2} \quad \text{and} \quad \frac{\partial^2 u}{\partial t^2} = gh_0 \frac{\partial^2 u}{\partial x^2}, \quad (95)$$

Note that in gas dynamics $v_\Phi = \sqrt{gh_0}$ equivalent to the speed of sound [71–75].

2.3 CONCLUSION

Thus, we obtain a solution representing a sinusoidal in time and coordinate free undammed oscillations. Such behaviors of the waves are due to the absence of any dissipation in the fluid. The fluid is incompressible and ideal. There is no heat mass transfer.

KEYWORDS

- **Dispersed fluid**
- **Hydraulic system**
- **Ideal fluid**
- **Incompressible fluid**
- **Pipe wall**

REFERENCES

1. Chaudhry, M. H. (1979). "Applied Hydraulic Transients," Van Nostrand Reinhold Co., N.Y., 1322–1324.
2. Parmakian, J. (1963). "Water Hammer Analysis," Dover Publications, Inc., New York, New York, 51–58.
3. Streeter, V. L., & Wylie, E. B. (1979). "Fluid Mechanics," McGraw-Hill Ltd., USA, 492–505.
4. Leon Arturo, S. (2007). "An Efficient Second-Order Accurate Shock-Capturing Scheme for Modeling One and Two-Phase Water Hammer Flows," PhD Thesis, March 29, 4–44.
5. Wu, P. Y., & Little, W. A. (1983). Measurement of Friction Factor for Flow of Gases in Very Fine Channels used For Micro Miniature, Joule Thompson Refrigerators, *Cryogenics*, 24(8), 273–277.
6. Harms, T. M., Kazmierczak, M. J., Cerner, F. M., Holke, A., Henderson, H. T., Pilchowski, H. T., & Baker, K. (1997). Experimental Investigation of Heat Transfer and Pressure Drop through Deep Micro channels in a (100) Silicon Substrate, in: Proceedings of the ASME. Heat Transfer Division, HTD, 351, 347–357.
7. Fedorov, A. G., & Viskanta, R. (2000). Three-Dimensional Conjugate Heat Transfer into Micro channel Heat Sink for Electronic Packaging, *Int. J. Heat Mass Transfer*, 43, 399–415.
8. Qu, W., Mala, G. M., & Li, D. (1993). Heat Transfer for Water Flow in Trapezoidal Silicon Micro Channels, 399–404.
9. Choi, S. B., Barren, R. R., & Warrington, R. O. (1991). Fluid Flow and Heat Transfer in Micro Tubes, *ASME DSC*, 40, 89–93.
10. Adams, T. M., Abdel-Khalik, S. I., Jeter, S. M., & Qureshi, Z. H. (1998). AN Experimental Investigation of Single-Phase Forced Convection in Micro Channels, *Int. J. Heat Mass Transfer*, 41, 851–857.
11. Peng, X. F., & Peterson, G. P. (1996). Convective Heat Transfer and Flow Friction for Water Flow in Micro channel Structure, *Int. J. Heat Mass Transfer*, 36, 2599–2608.
12. Mala, G., Li, D., & Dale, J. D. (1997). Heat Transfer and Fluid Flow in Micro channels, *J. Heat Transfer*, 40, 3079–3088.

13. Xu, B., Ooi, K. T., Mavriplis, C., & Zaghoul, M. E. (2002). Viscous Dissipation Effects for Liquid Flow in Micro Channels, *Microsystems*, 53–57.
14. Tuckerman, D. B., & Pease, R. F. W. (1981). High Performance Heat Sinking for VLSI, *IEEE Electron device Letter*, DEL-2, 126–129.
15. Kraichnan, R. H., & Montgomery, D. (1967). “Two-Dimensional Turbulence,” *Rep. Prog., Physics*, 43(547), 1417–1423.
16. Leon Arturo, S. (2007). “An Efficient Second-Order Accurate Shock-Capturing Scheme for Modeling One and Two-Phase Water Hammer Flows” PhD Thesis, March 29, 4–44.
17. Lee, T. S., & Pejovic, S. (1996) Air Influence on Similarity of Hydraulic Transients and Vibrations, *ASME J. Fluid Eng.*, 118(4), 706–709.
18. Li, J., & Mc Corquodale A. (1999). “Modeling Mixed Flow in Storm Sewers,” *Journal of Hydraulic Engineering*, ASCE, 125(11), 1170–1180.
19. Mala, G., Li, D., & Dale, J. D. (1997). Heat Transfer and Fluid Flow in Micro channels, *J. Heat Transfer*, 40, 3079–3088.
20. Miller, P. L., Cabot, W. H., & Cook, A. W. (2005). “Which Way Is Up? A Fluid Dynamics Riddle,” *Phys., Fluids*, 17, 091110, 1–26.
21. Minnaert, M. (1933). On Musical Air Bubbles and the Sounds of Running Water *Phil. Mag.*, 16(7), 235–248.
22. Moeng, C. H., McWilliams, J. C., Rotunno, R., Sullivan, P. P., & Weil, J. (2004). “Investigating 2D Modeling of Atmospheric Convection in the PBL,” *J. Atm. Sci.*, 61, 889–903.
23. Moody, L. F. (1944). “Friction Factors for Pipe Flow,” *Trans., ASME*, 66, 671–684.
24. Nagiyev, F. B. (1993). Dynamics, Heat and Mass Transfer of Vapor-Gas Bubbles in a Two-Component Liquid, Turkey-Azerbaijan Petrol Semin., Ankara, Turkey, 32–40.
25. Nagiyev, F. B. (1995). The Method of Creation Effective Coolness Liquids, Third Baku international Congress, Baku, Azerbaijan Republic, 19–22.
26. Neshan, H. (1985). Water Hammer, pumps Iran Co. Tehran, Iran, 1–60.
27. Nigmatulin, R. I., Khabeev, N. S., & Nagiyev, F. B. (1981). Dynamics, Heat and Mass Transfer of Vapor-Gas Bubbles in a Liquid, *Int. J. Heat Mass Transfer*, 24(N6), Printed in Great Britain, 1033–1044.
28. Oron, D., Arazi, L., Kartoon, D., Rikanati, A., Alon, U., & Shvarts, D. (2001). “Dimensionality Dependence of the Rayleigh-Taylor & Richtmyer-Meshkov instability, late-time scaling laws,” *Phys., Plasmas*, 8, 2883p.
29. Parmakian, J. (1957). “Water hammer Design Criteria,” *J. Power Div. ASCE*, Sept., 456–460.
30. Hamam, M. A., & Mc Corquodale, J. A. (1982). “Transient Conditions in the Transition from Gravity to Surcharged Sewer Flow,” *Canadian J. Civil Eng.*, Canada, Sep., 65–98.
31. Perry, R. H., Green, D. W., & Maloney, J. O. (1997). *Perry’s Chemical Engineers Handbook*, 7th Edition, McGraw-Hill, New York, 1–61.
32. Peng, X. F., & Peterson, G. P. (1996). Convective Heat Transfer and Flow Friction for Water Flow in Micro channel Structure, *Int. J. Heat Mass Transfer*, 36, 2599–2608.
33. Pickford, J. (1969). “Analysis of Surge,” *Macmillan*, London, 153–156.

34. Pipeline Design for Water and Wastewater, American Society of Civil Engineers (1975), New York, 54p.
35. Qu, W., Mala, G. M., & Li, D. (1993). Heat Transfer for Water Flow in Trapezoidal Silicon Micro channels, 399–404.
36. Quick, R. S. (1933). “Comparison and Limitations of Various Water hammer Theories,” J. Hyd. Div., ASME, May, 43–45.
37. Rayleigh, (1917). On the Pressure Developed in a Liquid During The Collapse of a Spherical Cavity. Philos Mag. Ser. 6, 34(200), 94–98.
38. Ramaprabhu, P., & Andrews, M. J. (2004). “Experimental Investigation of Rayleigh-Taylor mixing at small Atwood numbers” J. Fluid Mech., 502, 233p.
39. Rich, G. R. (1963). “Hydraulic Transients,” Dover, USA, 148–154.
40. Savic, D. A., & Walters, G. A. (1995). “Genetic Algorithms Techniques for Calibrating Network Models,” Report No. 95/12, Centre for Systems and Control Engineering, 137–146.
41. Savic, D. A., & Walters, G. A. (1995). Genetic Algorithms Techniques for Calibrating network Models, University of Exeter, Exeter, United Kingdom, 41–77.
42. Shvarts, D., Oron, D., Kartoon, D., Rikanati, A., & Sadot, O. (2000). “Scaling Laws of Nonlinear Rayleigh-Taylor and Richtmyer-Meshkov Instabilities in Two and Three Dimensions,” C. R. Acad. Sci. Paris IV, 719, 312 p.
43. Sharp, B. (1981). “Water Hammer Problems and Solutions,” Edward Arnold Ltd., London, 43–55.
44. Skousen, P. (1998). “Valve Handbook,” McGraw Hill, New York, Hammer Theory and Practice, 687–721.
45. Song, C. C. et al. (1983). “Transient Mixed-Flow Models for Storm Sewers,” J. Hyd. Div., Nov. 109, 458–530.
46. Stephenson, D. (1984). “Pipe Flow Analysis,” Elsevier, 19, S.A., 670–788.
47. Streeter, V. L., & Lai, C. (1962). “Water hammers Analysis including Fluid Friction,” Journal of Hydraulics Division, ASCE, 88, 79p.
48. Streeter, V. L., & Wylie, E. B. (1979). “Fluid Mechanics,” McGraw-Hill Ltd., USA, 492–505.
49. Streeter, V. L., & Wylie, E. B. (1981). “Fluid Mechanics,” McGraw-Hill Ltd., USA, 398–420.
50. Tijsseling, (1993). “Alan E Vardy Time Scales and FSI in Unsteady Liquid Filled Pipe Flow,” 5–12.
51. Tuckerman, D. B., & Pease, R. F. W. (1981). High Performance Heat Sinking for VLSI, IEEE Electron device Letter, DEL-2, 126–129.
52. Tennekes, H., & Lumley, J. L. (1972). A First Course in Turbulence, the MIT Press, 410–466.
53. Thorley, A. R. D. (1991). “Fluid Transients in Pipeline Systems,” D. & George, L., Herts, England, 231–242.
54. Tullis, J. P. (1971). “Control of Flow in Closed Conduits,” Fort Collins, Colorado, 315–340.
55. Tuckerman, D. B. (1984). Heat Transfer Microstructures for Integrated Circuits, PhD. Thesis, Stanford University, 10–120.

56. Vallentine, H. R. (1965). "Rigid Water Column Theory for Uniform Gate Closure," *J. Hyd. Div. ASCE*, July, 55–243.
57. Waddell, J. T., Niederhaus, C. E., & Jacobs, J. W. (2001). "Experimental Study of Rayleigh-Taylor Instability Low Atwood Number Liquid Systems with Single-Mode Initial Perturbations," *Phys. Fluids*, 13, 1263–1273.
58. Watters, G. Z. (1984). "Modern Analysis and Control of Unsteady Flow in Pipelines," *Ann Arbor Sci.*, 2nd Ed., 1098–1104.
59. Walski, T. M., & Lutes, T. L. (1994). "Hydraulic Transients Cause Low-Pressure Problems," *Journal of the American Water Works Association*, 75(2), 58.
60. Weber, S. V., Dimonte, G., & Marinak, M. M. (2003). "Arbitrary Lagrange-Eulerian Code Simulations of Turbulent Rayleigh-Taylor instability in Two and Three Dimensions," *Laser and Particle beams*, 21, 455p.
61. Wood, D. J., Dorsch, R. G., & Lightener, C. (1966). "Wave-Plan Analysis of Unsteady Flow in Closed Conduits," *Journal of Hydraulics Division, ASCE*, 92, 83–110.
62. Wood, D. J., & Jones, S. E. (1973). "Water hammer Charts for various types of Valves," *Journal of the Hydraulics Division, Proceedings of the American Society of Civil Engineers*, January, 167–178.
63. Wood, F. M. (1970). "History of Water hammers" *Civil Engineering Research Report #65*, Queens University, Canada, 66–70.
64. Wu, Z. Y., & Simpson, A. R. (2001). Competent Genetic-Evolutionary Optimization of Water Distribution Systems, *J. Comput., Civ. Eng.* 15(2), 89–101.
65. Wylie, E. B., & Talpin, L. B. (1983). Matched Impedance to controls fluid transients, *Trans., ASME*, 105(2), 219–224.
66. Wylie, E. B., & Streeter, V. L. (1993). *Fluid Transients in system*, Prentice-Hall Englewood Cliffs, New Jersey, 4.
67. Wylie, E. B., & Streeter, V. L. (1982). *Fluid Transients*, Feb Press, Ann Arbor, MI, Corrected Copy, 1983, 158p.
68. Wu, P. Y., & Little, W. A. (1983). Measurement of Friction Factor For Flow of Gases in Very Fine Channels Used For Micro Miniature, Joule Thompson refrigerators, *Cryogenics*, 24(8), 273–277.
69. Xu, B., Ooi, K. T., Mavriplis, C., & Zaghoul, M. E. (2002). Viscous dissipation effects for liquid flow in Micro channels, *Microsystems*, 53–57.
70. Young, Y. N., Tufo, H., Dubey, A., & Rosner, R. (2001). "On the Miscible Rayleigh-Taylor Instability: Two and Three Dimensions," *J. Fluid Mech*, 447, 377, 2003–2500.
71. Wood, D. J., Dorsch, R. G., & Lightener, C. (1966). "Wave-Plan Analysis of Unsteady Flow in Closed Conduits," *Journal of Hydraulics Division, ASCE*, 92, 83–110.
72. Wylie, E. B., & Streeter, V. L. (1993). *Fluid Transients in systems*, Prentice-Hall, Englewood Cliffs, New Jersey, 4.
73. Brunone, B., Karney, B. W., Mecarelli, M., & Ferrante, M. (2000). "Velocity Profiles and unsteady pipe frictions in Transient Flow" *Journal of Water Resources Planning and Management, ASCE*, 126(4), July, 236–244.
74. Koelle, E., Jr. Luvizotto, E., & Andrade, J. P. G. (1996). "Personality Investigation of Hydraulic Networks using MOC–Method of Characteristics" *Proceedings of the 7th*

International Conference on Pressure Surges and Fluid Transients, Harrogate Durham, United Kingdom, 1–8.

75. Fillion, Y., & Karney B. W. (2002). “A Numerical Exploration of Transient Decay Mechanisms in Water Distribution Systems,” Proceedings of the ASCE Environmental Water Resources Institute Conference, American Society of Civil Engineers, Roanoke, Virginia, 30.

CHAPTER 3

SIMULATION AND MODELING OF TWO PHASES FLOW

CONTENTS

| | | |
|-----|---|----|
| 3.1 | Introduction..... | 50 |
| 3.2 | Materials and Methods..... | 50 |
| 3.3 | Results..... | 54 |
| 3.4 | Basic Equations Describing the Spherically Symmetric Motion of a Bubble Binary Solution..... | 56 |
| 3.5 | The Braking Effect of the Intensity of Phase Transformations in Boiling Binary Solutions | 60 |
| 3.5 | Conclusion | 69 |
| | Keywords | 69 |
| | References..... | 69 |

3.1 INTRODUCTION

In the two phases flow is extremely important to the concept of volume concentration. This is the relative volume fraction of one phase in the volume of the pipe [1]. Such an environment typical fluid is a high density and little compressibility. This property contributes to the creation of various forms of transient conditions [2, 3]. Figure 3.1 shows an experimental setup, which investigated the formation of different modes of fluid flow with gas bubbles and steam.

3.2 MATERIALS AND METHODS

The experimental results show that the bubble flow usually occurs at low concentrations of vapor. It includes three main types of flow regimes in microgravity bubble, slug and an annular.

TABLE 3.1 Simulators, Models and Problems

| Cases | Range of problems |
|--|---|
| Steady or gradually varying turbulent flow | Rapidly varying or transient flow |
| Incompressible, Newtonian, single-phase fluids | Slightly compressible, two-phase fluids (vapor and liquid) and two-fluid systems (air and liquid) |
| Full pipes | Closed-conduit pressurized systems with air intake and release at discrete points |

Figure 3.2 shows snapshots of the flow pattern for various configurations of the tube [4, 5]. The flow enters the tee at the bottom of the picture, and then is divided at the entrance to the tube. The inner diameter of the tee is 1.27 cm (Figs. 3.1–3.3). The narrowing of the flow is achieved by reducing the diameter of the hose.

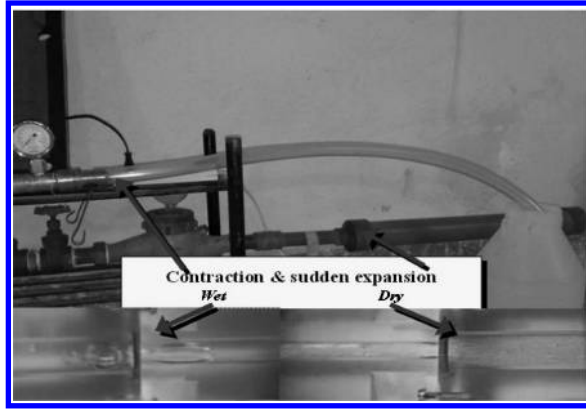


FIGURE 3.1 Snapshot laboratory set up for studying the structure of flow in different configurations tube.

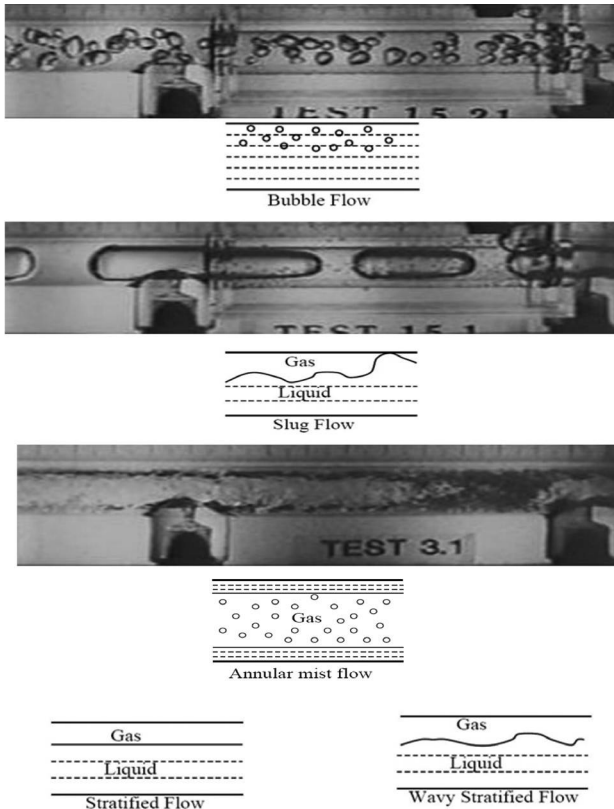


FIGURE 3.2 Types of flows.

Within the reduction is a liquid recirculation zone, called the “vena contraction” Wet picture that, when the liquid is recirculated to the “vena contraction.” However, there are conditions, whereby the gas phase of the contract is caught vena. Figure 3.3 shows the different flow regimes observed in the experimental setup [6].

Increased flow is achieved by increasing the size of the pipe. Again, there is an area of the liquid recirculation near the “corner” a sudden expansion. Depending on the level of consumption of bubbly liquid or gas, it falls into the trap in this area.

In the inlet fluid moves out of the pipe diameter of 12.7 mm in the pipe diameter of 25 mm.

Normal extension occurs at the beginning of the flow. Soon comes the expansion section, and the flow rate continues to increase. Two-phase jet stream created, ultimately, with areas of air flowing above and below the bubble region [6]. The behavior of gas-liquid mixture in the expansion is proportional to increasing the diameter of the pipe [7, 8].

It is shown Figs. 3.1–3.3 that in place of the sudden expansion of a transition flow regime of the turbulent flow. Depending on the flow or gas bubble mixture it falls into the trap in this area.

Experiments were conducted on the pipe, whose diameter is suddenly doubled [9]. In this case the region of turbulence of fluid are observed around the “corner” a sudden expansion. The expansion is observed at the beginning of the flow. As a result of turbulence flow gap expansion increases and the flow rate continues to increase. In the end, creates a stream of two-phase flow, with airfields, the current above and below the bubble area [10, 11].

With this experimental setup is shown that the formation of different modes of two-phase flow depends on the relative concentration of these phases and the flow rate. Figures 3.1 and 3.2 shows a diagram of core flows of vapor-liquid flow regimes, in particular, the bubble, stratified, slug, stratified, and the wave dispersion circular flow.

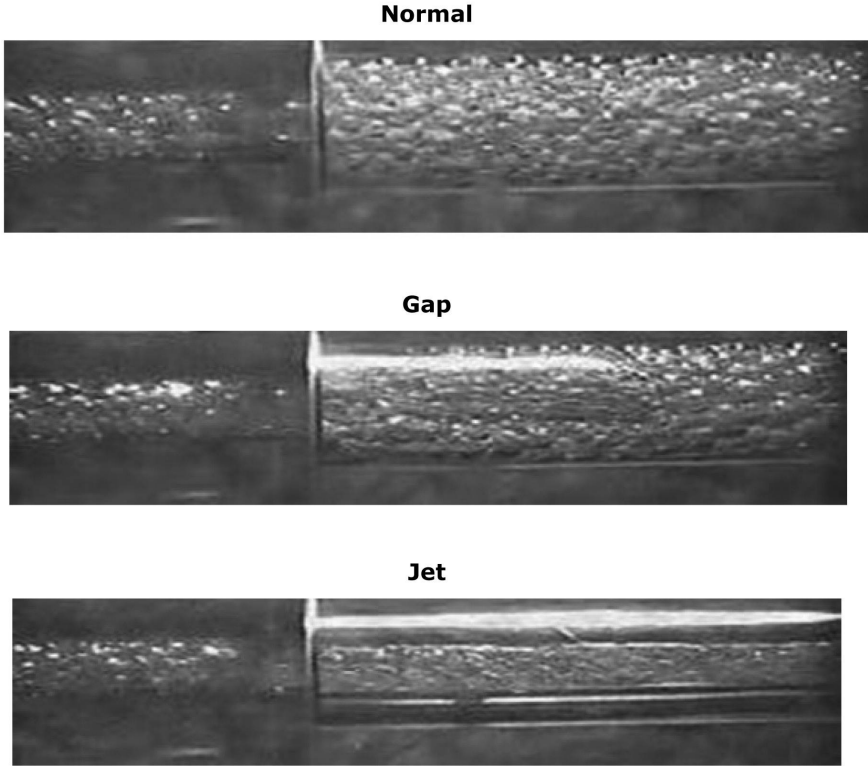


FIGURE 3.3 Narrowing and sudden expansions flow level.

In these experiments (Figs. 3.1–3.3) the mode of vapor-liquid flow in a pipe, when the bubbles are connected in long steam field, whose dimensions are commensurate with the diameter of the pipe [12, 13]. This flow is called the flow of air from the tube. In the transition from moderate to high-speed flow, when the concentration of vapor and liquid are approximately equal, the flow regime is often irregular and even chaotic [14, 15]. By the simulated conditions, It is assumed that the electricity suddenly power off without warning (i.e., no time to turn the diesel generators or pumps) [15, 16].

3.3 RESULTS

Such situations are the strong reason of the installation of pressure sensors, equipped with high-speed data loggers. Therefore, the following items are consequences, which may result in these situations.

3.3.1 EFFECTS OF TRANSIENTS

Hydraulic transients can lead to the following physical phenomena. The high or low transient pressures may arise in the piping and connections in the share of second. They often alternate from highest to lowest levels and vice versa. High pressures are a consequence of the collapse of steam bubbles or cavities is similar to steam pump cavitations. It can yield the tensile strength of the pipes. It can also penetrate the groundwater into the pipeline [17, 18].

3.3.2 HIGH TRANSIENT FLOWS

High-speed flows are also very fast pulse pressure. It leads to temporary but very significant transient forces in the bends and other devices that can make a connection to deform. Even strain buried pipes under the influence of cyclical pressures may lead to deterioration of joints and lead to leakage. In the low-pressure pumping stations at downstream a very rapid closing of the valve, known as shut off valve, may lead to high pressure transient flows.

3.3.3 WATER COLUMN SEPARATION

Water column, usually are separated with sharp changes in the profile or the local high points. It is because of the excess of atmospheric pressure. The spaces between the columns are filled with water or the formation of steam (e.g., steam at ambient temperature) or air, if allowed admission into the pipe through the valve. Collapse of cavitations bubbles or steam can cause the dramatic impact of rising pressure on the transition process.

If the water column is divided very quickly, it could in turn lead to rupture of the pipeline. Vapors cavitations may also lead to curvature of

the pipe. High-pressure wave can also be caused by the rapid removal of air from the pipeline.

Steam bubbles or cavities are generated during the hydraulic transition. The level of hydraulic pressure (EGD) or pressure in some areas could fall low enough to reach the top of the pipe. It leads to subatmospheric pressure or even full-vacuum pressures. Part of the water may undergo a phase transition, changing from liquid to steam, while maintaining the vacuum pressure.

This leads to a temporary separation of the water column. When the system pressure increases, the columns of water rapidly approach to each other. The pair reverts to the liquid until vapor cavity completely dissolved. This is the most powerful and destructive power of water hammer phenomenon.

3.3.4 GLOBAL REGULATION OF STEAM PRESSURE

If system pressure drops to vapor pressure of the liquid, the fluid passes into the vapor, leading to the separation of liquid columns. Consequently, the vapor pressure is a fundamental parameter for hydraulic transient modeling. The vapor pressure varies considerably at high temperature or altitude.

Fortunately, for typical water pipelines and networks, the pressure does not reach such values. If the system is at high altitude or if it is the industrial system, operating at high temperatures or pressures, it should be guided by a table or a state of vapor pressure curve vapor liquid.

3.3.5 VIBRATION

Pressure fluctuations associated with the peculiarities of the system, as well as the peculiarities of its design. The pump must be assumed just as one of the promoters of the system. Effect of pressure relief valve on the fluctuations of the liquid often turned out three times more damaging than the effect of the pump. Such monitoring fluid flow controlling means usually has more negative impact than the influence of the pump.

Rapid changes in the transition pressures can lead to fluctuations or resonance. It can damage the pipe, resulting in leakage or rupture. Experi-

ments show that the flows in the pipe will very small, say, located at 24 km/h.

This corresponds to about 0.45% of the velocity of pressure. In this case, the flow fluctuations can be easily accumulated and redeemed until the next perturbation. Fluctuations of the flow are no fluctuations of pressure.

In the case when the source of the pressure fluctuations is the so-called, “Acceleration factor,” one can say that in order to accelerate the mass of fluid in the system until the new rate of additional efforts.

3.4 BASIC EQUATIONS DESCRIBING THE SPHERICALLY SYMMETRIC MOTION OF A BUBBLE BINARY SOLUTION

The dynamics and heat and mass transfer (the Eqs. (1)–(20)) of vapor bubble in a binary solution of liquids, in Ref. [8], was studied for significant thermal, diffusion and inertial effect.

It was assumed that binary mixture with a density ρ_p , consisting of components 1 and 2, respectively, the density ρ_1 and ρ_2 .

Moreover:

$$\rho_1 + \rho_2 = \rho_l,$$

Where the mass concentration of component 1 of the mixture also [8] consider a two-temperature model of interphase heat exchange for the bubble liquid. This model assumes homogeneity of the temperature in phases [25, 26].

The intensity of heat transfer for one of the dispersed particles with an endless stream of carrier phase will be set by the dimensionless parameter of Nusselt (Nu_l).

Bubble dynamics described by the Rayleigh equation:

$$R \dot{w}_l + \frac{3}{2} w_l^2 = \frac{p_1 + p_2 - p_\infty - 2\sigma / R}{\rho_l} - 4\nu_l \frac{w_l}{R} \quad (1)$$

where p_1 and p_2 – the pressure component of vapor in the bubble; p_∞ – the pressure of the liquid away from the bubble; σ and ν_l – surface tension coefficient of kinematic viscosity for the liquid.

Consider the condition of mass conservation at the interface.

Mass flow j_i^{TH} component ($i = 1, 2$) of the interface $r = R(t)$ in j_i^{TH} phase per unit area and per unit of time and characterizes the intensity of the phase transition is given by:

$$j_i = \rho_i \left(\dot{R} - w_i - w_i \right), \quad (i = 1, 2), \quad (2)$$

where w_i – the diffusion velocity component on the surface of the bubble.

The relative motion of the components of the solution near the interface is determined by Fick's law [30, 31].

$$\rho_1 w_1 = -\rho_2 w_2 = -\rho_l D \left. \frac{\partial k}{\partial r} \right|_R \quad (3)$$

If we add Eq. (3), while considering that:

$\rho_1 + \rho_2 = \rho_l$ and draw the Eq. (3), we obtain

$$\dot{R} = w_i + \frac{j_1 + j_2}{\rho_l} \quad (4)$$

Multiplying the first Eq. (3) on ρ_2 , the second in ρ_1 and subtract the second equation from the first. In view of Eq. (3) we obtain

$$k_R j_2 - (1 - k_R) j_1 = -\rho_l D \left. \frac{\partial k}{\partial r} \right|_R$$

where k_R – the concentration of the first component at the interface. With the assumption of homogeneity of parameters inside the bubble changes in the mass of each component due to phase transformations can be written

as $\frac{d}{dt} \left(\frac{4}{3} \pi R^3 \rho_i' \right) = 4 \pi R^2 j_i$ or

$$\frac{R}{3} \dot{\rho}_i' + \dot{R} \rho_i' = j_i, \quad (i = 1, 2), \quad (5)$$

Express the composition of a binary mixture in mole fractions of the component relative to the total amount of substance in liquid phase,

$$N = \frac{n_1}{n_1 + n_2} \quad (6)$$

The number of moles i^{TH} component n_i , which occupies the volume v_i , expressed in terms of its density:

$$n_i = \frac{\rho_i V}{\mu_i} \quad (7)$$

Substituting Eq. (7) in Eq. (6), we obtain

$$N_1(k) = \frac{\mu_2 k}{\mu_2 k + \mu_1 (1-k)} \quad (8)$$

By law, Raul partial pressure of the component above the solution is proportional to its molar fraction in the liquid phase, i.e.,

$$p_1 = p_{s1}(T_v) N_1(k_R), \quad p_2 = p_{s2}(T_v) [1 - N_1(k_R)] \quad (9)$$

Equations of state phases have the form:

$$p_i = B T_v \rho_i' / \mu_i, \quad (i = 1, 2), \quad (10)$$

where: B – Gas constant, T_v – the temperature of steam, ρ_i' – the density of the mixture components in the vapor bubble, μ_i – molecular weight, p_{Si} – saturation pressure.

The boundary conditions $r = \infty$ and on a moving boundary can be written as:

$$k|_{r=\infty} = k_0, \quad k|_{r=R} = k_R, \quad T_l|_{r=\infty} = T_0, \quad T_l|_{r=R} = T_v, \quad (11)$$

$$j_1 l_1 + j_2 l_2 = \lambda_l D \left. \frac{\partial T_l}{\partial r} \right|_{r=R}, \quad (12)$$

where l_i – specific heat of vaporization.

By the definition of Nusselt parameter-the dimensionless parameter characterizing the ratio of particle size and the thickness of thermal boundary layer in the phase around the phase boundary and determined from additional considerations or from experience.

The heat of the bubble's intensity with the flow of the carrier phase will be further specified as:

$$\left(\lambda_l \frac{\partial T_l}{\partial r} \right)_{r=R} = Nu_l \cdot \frac{\lambda_l (T_0 - T_v)}{2R} \quad (13)$$

In [16] obtained an analytical expression for the Nusselt parameter:

$$Nu_l = 2\sqrt{\frac{\omega R_0^2}{a_l}} = 2\sqrt{\frac{R_0}{a_l} \sqrt{\frac{3\gamma P_0}{\rho_l}}} = 2\sqrt{\sqrt{3\gamma} \cdot Pe_l}, \quad (14)$$

where: $a_l = \frac{\lambda_l}{\rho_l c_l}$ – thermal diffusivity of fluid,

$$Pe_l = \frac{R_0}{a_l} \sqrt{\frac{P_0}{\rho_l}} \text{ – Peclet number}$$

The intensity of mass transfer of the bubble with the flow of the carrier phase will continue to ask by using the dimensionless parameter Sherwood (Sh):

$$\left(D \frac{\partial k}{\partial r} \right)_{r=R} = Sh \cdot \frac{D(k_0 - k_R)}{2R}$$

where: D – diffusion coefficient; k – the concentration of dissolved gas in liquid; the subscripts 0 and R refer to the parameters in an undisturbed state and at the interface.

We define a parameter in the form of Sherwood [16]

$$Sh = 2\sqrt{\frac{\omega R_0^2}{D}} = 2\sqrt{\frac{R_0}{D} \sqrt{\frac{3\gamma P_0}{\rho_l}}} = 2\sqrt{\sqrt{3\gamma} \cdot Pe_D} \quad (15)$$

where $Pe_D = \frac{R_0}{D} \sqrt{\frac{P_0}{\rho_l}}$ – diffusion Peclet number.

The system of Eqs. (1)–(15) is a closed system of equations describing the dynamics and heat transfer of insoluble gas bubbles with liquid.

3.5 THE BRAKING EFFECT OF THE INTENSITY OF PHASE TRANSFORMATIONS IN BOILING BINARY SOLUTIONS

If we use Eqs. (7)–(9), we obtain relations for the initial concentration of component 1:

$$k_0 = \frac{1 - \chi_2^0}{1 - \chi_2^0 + \mu(\chi_1^0 - 1)}, \mu = \mu_2 / \mu_1, \chi_i^0 = p_{si0} / p_0, i = 1, 2 \quad (16)$$

where: μ_2, μ_1 – Molecular weight of the liquid components of the mixture; p_{si0} – saturated vapor pressure of the components of the mixture at an initial temperature of the mixture T_0 , which were determined by integrating the Clausius-Clapeyron relation. The parameter χ_i^0 is equal to

$$\chi_i^0 = \exp \left[\frac{l_i \mu_i}{B} \left(\frac{1}{T_{ki}} - \frac{1}{T_0} \right) \right], \quad (17)$$

Gas-phase liquid components in the derivation of Eq. (17) seemed perfect gas equations of state:

$$p_i = \rho_i B T_i / \mu_i.$$

where B – universal gas constant; p_i – the vapor pressure inside the bubble T_i to the temperature in the ratio of Eq. (17); T_{ki} – temperature evaporating the liquid components of binary solution at an initial pressure p_0 ; l_i – specific heat of vaporization.

The initial concentration of the vapor pressure of component p_0 is determined from the relation:

$$c_0 = \frac{k_0 \chi_1^0}{k_0 \chi_1^0 + (1 - k_0) \chi_2^0} \quad (18)$$

In this chapter [8], the problem of radial motions of a vapor bubble in binary solution [8] was solved. It was investigated at various pressure drops in the liquid for different initial radii R_0 for a bubble. It is of great practical interest of aqueous solutions of ethanol and ethylene glycol.

It was revealed an interesting effect. The parameters characterized the dynamics of bubbles in aqueous ethyl alcohol. It was studied in the field

of variable pressure lie between the limiting values of the parameter p_0 for pure components.

The pressure drops and consequently the role of diffusion are assumed unimportant. The pressure drop along with the heat dissipation is included diffusion dissipation. The rate of growth and collapse of the bubble is much higher than in the corresponding pure components of the solution under the same conditions. A completely different situation existed during the growth and collapse of vapor bubble in aqueous solutions of ethylene glycol.

In this case, the effect of diffusion resistance, led to inhibition of the rate of phase transformations. The growth rate and the collapse of the bubble is much smaller than the corresponding values, but for the pure components of the solution. Further research and calculations have to give a physical explanation for the observed effect. In studied the influence of heat transfer and diffusion on damping of free oscillations of a vapor bubble binary solution.

It was found that the dependence of the damping rate of oscillations of a bubble of water solutions of ethanol, methanol, and toluene monotonic on k_0 .

It was mentioned for the aqueous solution of ethylene glycol similar dependence with a characteristic minimum at:

$$k_0 \approx 0,02$$

Moreover, for:

$$0,01 \leq k_0 \leq 0,3$$

decrement, binary solution has less damping rates for pulsations of a bubble in pure (one-component) water and ethylene glycol.

This means that in the range of concentrations of water:

$$0,01 \leq k_0 \leq 0,3$$

Pulsations of the bubble (for water solution of ethylene glycol) decay much more slowly and there are inhibition of the process of phase transformations. A similar process was revealed and forced oscillations of bubbles in an acoustic field [10].

In this chapter the influence of non-stationary heat and mass transfer processes was investigated in the propagation of waves in a binary solution of liquids with bubbles. The influence of component composition and concentration of binary solution was investigated on the dispersion, dissipation and attenuation of monochromatic waves in two-phase, two-component media.

The aqueous solution of ethyl alcohol in aqueous ethylene glycol decrements showed perturbations less relevant characteristics of pure components of the solution.

Unsteady interphase heat transfer revealed in calculation, the structure of stationary shock waves in bubbly binary solutions. The problem signifies on effect a violation of monotonicity behavior of the calculated curves for concentration, indicating the presence of diffusion resistance.

In some of binary mixtures, it is seen the effect of diffusion resistance. It is led to inhibition of the intensity of phase transformations.

The physical explanation revealed the reason for an aqueous solution of ethylene glycol. Pronounced effect of diffusion resistance is related to the solution with limited ability. It diffuses through the components of $D = 10^{-9} (m^2 / sec)$, where D – diffusion coefficient volatility of the components is very different, and thus greatly different concentrations of the components in the solution and vapor phase.

In the case of aqueous solution of ethanol volatility component are roughly the same $\chi_1^0 \approx \chi_2^0$.

In accordance with $c_0 \approx k_0$, so the finiteness of the diffusion coefficient does not lead to significant effects in violation of the thermal and mechanical equilibrium phases.

Figures 3.4 and 3.5 shows the dependence $k_0(c_0)$ of ethyl alcohol and ethylene glycol's aqueous solutions. From Fig. 3.5, it is clear that almost the entire range of k_0 , $k_0 \approx c_0$.

At the same time for an aqueous solution of ethylene glycol, by the calculations and Fig. 3.2 $0,01 \leq k_0 \leq 0,3$ $k_0 \leq c_0$, and when $k_0 > 0,3$ $k_0 \sim c_0$.

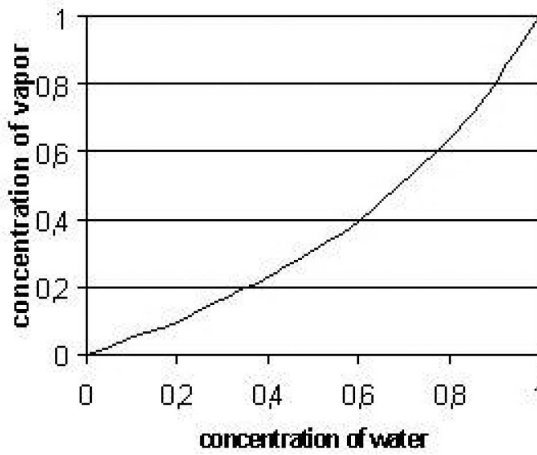


FIGURE 3.4 The dependence $(k_0(c_0))$ for an aqueous solution of ethanol.

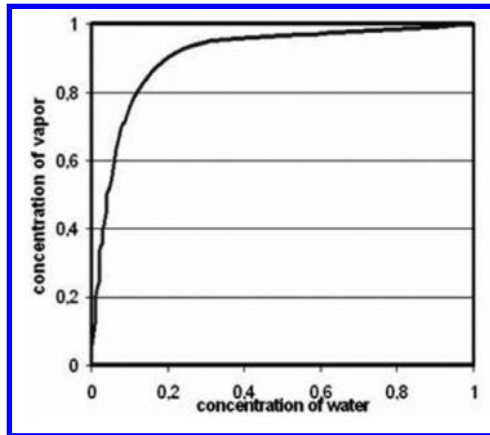


FIGURE 3.5 Dependence of $(k_0(c_0))$ for an aqueous solution of ethylene glycol.

In Figs. 3.6 and 3.7 show the boiling point of the concentration for the solution of two systems.

When $k_0 = 1$, $c_0 = 1$ and get clean water to steam bubbles. It is for boiling of a liquid at $T_0 = 373^\circ\text{K}$.

If $k_0=0$, $c_0=0$ and have correspondingly pure bubble ethanol ($T_0=350^\circ\text{K}$) and ethylene glycol ($T_0=470^\circ\text{K}$).

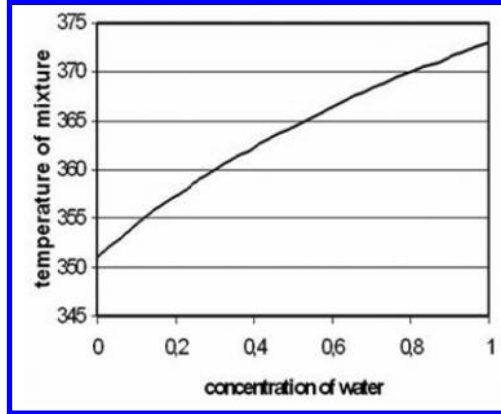


FIGURE 3.6 The dependence of the boiling temperature of the concentration of the solution to an aqueous solution of ethanol.

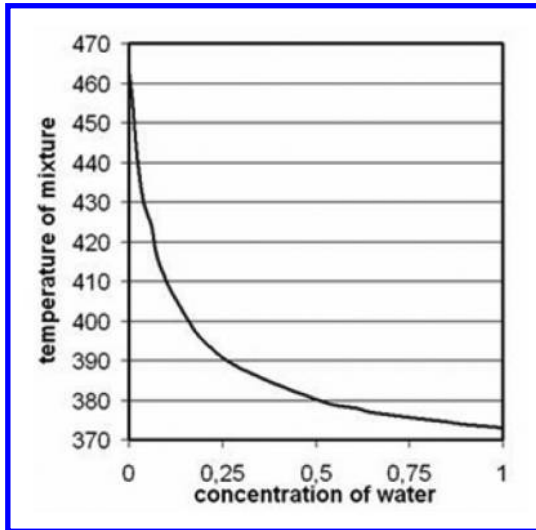


FIGURE 3.7 The dependence of the boiling point of the concentration of the solution to an aqueous solution of ethylene glycol.

It should be noted that in all the above works regardless of the above problems in the mathematical description of the cardinal effects of component composition of the solution shows the value of the parameter β equal:

$$\beta = \left(1 - \frac{1}{\gamma}\right) \frac{(c_0 - k_0)(N_{c_0} - N_{k_0})}{k_0(1 - k_0)} \frac{c_l}{c_{pv}} \left(\frac{c_{pv} T_0}{L}\right)^2 \sqrt{\frac{a_l}{D}} \quad (19)$$

where N_{k_0}, N_{c_0} – molar concentration of 1-th component in the liquid and steam:

$$N_{k_0} = \frac{\mu k_0}{\mu k_0 + 1 - k_0},$$

$$N_{c_0} = \frac{\mu c_0}{\mu c_0 + 1 - c_0}$$

where γ – adiabatic index; c_l and c_{pv} , respectively the specific heats of liquid and vapor at constant pressure; a_l – thermal diffusivity; $L = l_1 c_0 + l_2 (1 - c_0)$.

We also note that option is a self-similar solution describing the growth of a bubble in a superheated solution. This solution has the form:

$$R = 2\sqrt{\frac{3}{\pi}} \frac{\lambda_l \Delta T \sqrt{t}}{L \rho_v \sqrt{a_l (1 + \beta)}} \quad (20)$$

where ρ_v – vapor density; t – time; R – radius of the bubble; λ_l is the coefficient of thermal conductivity; ΔT – overheating of the liquid.

Figures 3.8 and 3.9 shows the dependence $\beta(k_0)$ for the above binary solutions. For aqueous ethanol β is negative for any value of concentration and dependence on k_0 is monotonic.

For an aqueous solution of ethylene glycol β – is positive and has a pronounced maximum at $k_0 = 0.02$.

As a result of present work at low-pressure drops (superheating and super cooling of the liquid, respectively), diffusion does not occur in aqueous solutions of ethyl alcohol. By approximate equality of k_0 and c_0 all calculated dependence lie between the limiting curves for the case of one-component constituents of the solution.

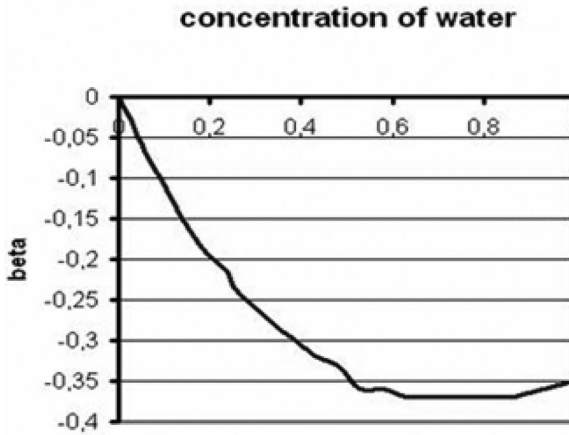


FIGURE 3.8 The dependence $\beta(k_0)$ for an aqueous solution of ethanol.

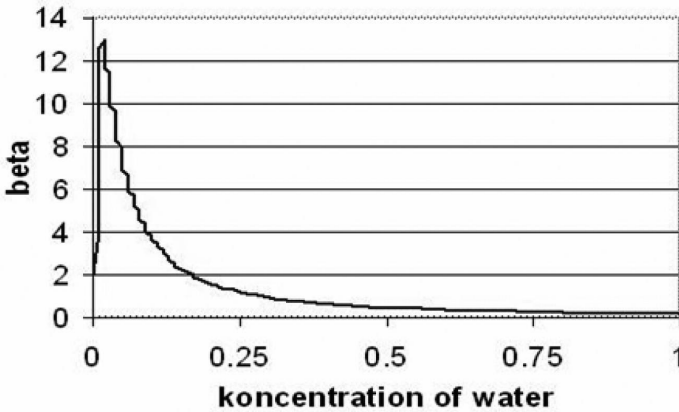


FIGURE 3.9 Dependence of $\beta(k_0)$ for an aqueous solution of ethylene glycol.

They are included dependence of pressure, temperature, vapor bubble radius, the intensity of phase transformations, and so from time to time).

The pressure difference becomes important diffusion processes. Mass transfer between bubble and liquid is in a more intensive mode than in single-component constituents of the solution.

In particular, the growth rate of the bubble in a superheated solution is higher than in pure water and ethyl alcohol. It is because of the negative β according to Ref. [19].

In an aqueous solution of ethylene glycol, there are the same perturbations due to significant differences between k_0 and c_0 . It is especially when $0,01 \leq k_0 \leq 0,3$, the effect of diffusion inhibition contributes to a significant intensity of mass transfer. In particular, during the growth of the bubble, the rate of growth in solution is much lower than in pure water and ethylene glycol. It is because of the positive β by Ref. [19].

Moreover, the maximum braking effect is achieved at the maximum value of β , when $k_0 = 0.02$.

A similar pattern is observed at the pulsations and the collapse of the bubble. Dependence of the damping rate of fluctuations in an aqueous solution of ethyl alcohol from the water concentration is monotonic. Aqueous solution of ethylene glycol dependence of the damping rate has a minimum at $k_0 = 0.02$, $0,01 \leq k_0 \leq 0,3$.

The function decrement is small respectively large difference between k_0 and c_0 and β takes a large value. These ranges of concentrations in the solution have significant effect of diffusion inhibition.

For aqueous solutions of glycerin, methanol, toluene, etc., calculations are performed. Comparison with experimental data confirms the possibility of theoretical prediction of the braking of Heat and Mass Transfer.

It was analyzed the dependence of the parameter β , decrement of oscillations of a bubble from the equilibrium concentration of the mixture components. Therefore, in every solutions, it was determined the concentration of the components of a binary mixture [11–26].

Figures 3.10 and 3.11 are illustrated by theoretical calculations. These figures defined on the example of aqueous solutions of ethyl alcohol and ethylene glycol (antifreeze used in car radiators). It is evident that the first solution is not suitable to the task.

The aqueous solution of ethylene glycol with a certain concentration is theoretically much more slowly boils over with clean water and ethylene glycol. This confirms the reliability of the method.

Calculations show that such a solution is almost never freezes. The same method can offer concrete solutions for cooling of hot parts and components of various machines and mechanisms.

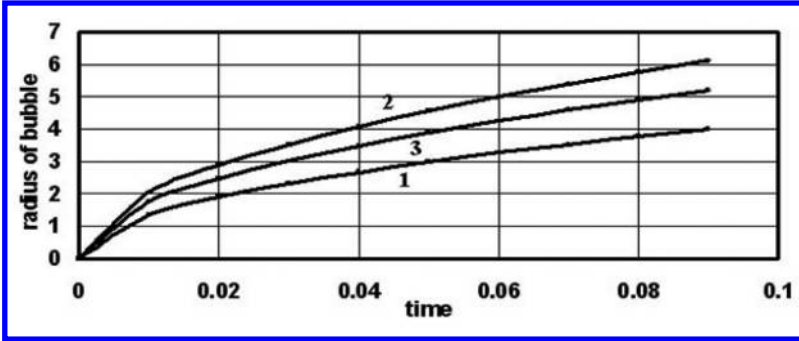


FIGURE 3.10 Dependence from time of vapor bubble radius. 1 – water, 2 – ethyl spirit, 3 – water mixtures of ethyl spirit.

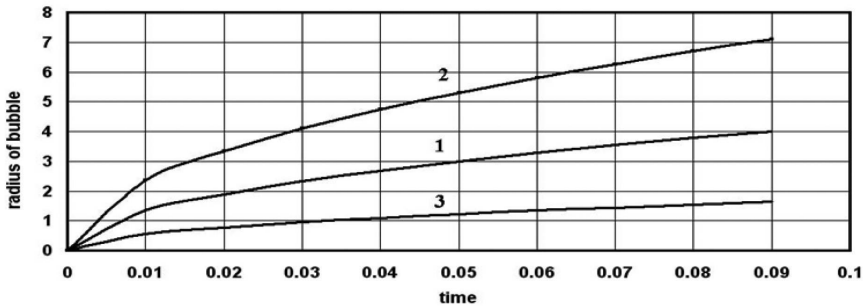


FIGURE 3.11 Dependence from time of vapor bubble radius. 1 – water, 2 – ethylene glycol, 3 – water mixtures of ethylene glycol.

solution of the reduced system of equations revealed an interesting effect. The parameters were characterized the dynamics of bubbles in aqueous ethyl alcohol in the field of variable pressure.

They lied between the limiting values of relevant parameters for the pure components. It was for the case, which pressure drops and consequently the role of diffusion was unimportant.

A completely different situation is observed during the growth and collapse of vapor bubble in aqueous solutions of ethylene glycol. The effect of diffusion resistance, leads to inhibition of the rate of phase transformations. For pure components of the solution, the growth and the collapse rate of the bubble is much smaller than the corresponding values [27–62].

3.5 CONCLUSION

It was confirmed the two temperature model theoretically on anomalous braking speed of phase transformations in boiling of binary mixtures.

It was investigated a comparison on accuracy of the numerical methods, regression model and the method of characteristics for the analysis of transient flows. It was shown that the method of characteristics is computationally more efficient for the analysis of large water pipelines.

KEYWORDS

- **Bubble binary solution**
- **Hydraulic transition**
- **Nusselt parameter**
- **Vapor bubble**
- **Vena contraction**

REFERENCES

1. Streeter, V. L., & Wylie, E. B. (1979). "Fluid Mechanics," McGraw-Hill Ltd., USA, 492–505.
2. Leon Arturo, S. (2007). "An Efficient Second-Order Accurate Shock-Capturing Scheme for Modeling One and Two-Phase Water Hammer Flows" PhD Thesis, March 29, 4–44.
3. Adams, T. M., Abdel-Khalik, S. I., Jeter, S. M., & Qureshi, Z. H. (1998). AN Experimental Investigation of Single-Phase Forced Convection in Micro channels, *Int. J. Heat Mass Transfer*, *41*, 851–857.
4. Peng, X. F., & Peterson, G. P. (1996). Convective Heat Transfer and Flow Friction for Water Flow in Micro channel Structure, *Int. J. Heat Mass Transfer*, *36*, 2599–2608.
5. Mala, G., Li, D., & Dale, J. D. (1997). Heat Transfer and Fluid Flow in Micro channels, *J. Heat Transfer*, *40*, 3079–3088.
6. Xu, B., Ooi, K.T., Mavriplis, C., & Zaghoul, M. E. (2002). Viscous dissipation effects for Liquid Flow in Micro channels, *Micro systems*, 53–57.
7. Pickford, J. (1969). "Analysis of Surge," Macmillan, London, 153–156.
8. Pipeline Design for Water and Wastewater, American Society of Civil Engineers, New York, (1975), 54p.
9. Xu, B., Ooi, K. T., Mavriplis, C., & Zaghoul, M. E. (2002). Viscous dissipation effects for Liquid Flow in Micro channels, *Microsystems*, 53–57.

10. Fedorov, A. G., & Viskanta, R. (2000). Three-dimensional Conjugate Heat Transfer into Micro channel Heat Sink for Electronic Packaging, *Int. J. Heat Mass Transfer*, *43*, 399–415.
11. Tuckerman, D. B. (1984). Heat Transfer Microstructures for Integrated Circuits, Ph.D. Thesis, Stanford University, 10–120.
12. Harms, T. M., Kazmierczak, M. J., Cerner, F. M., Holke, A., Henderson, H. T., Pilchowski, H. T., & Baker, K. (1997). Experimental Investigation of Heat Transfer and Pressure Drop through Deep Micro channels in a 100 Silicon Substrate, in: *Proceedings of the ASME. Heat Transfer Division, HTD*, *351*, 347–357.
13. Holland, F.A., & Bragg, R. (1995). *Fluid Flow for Chemical Engineers*, Edward Arnold Publishers, London, 1–3.
14. Lee, T. S., & Pejovic, S. (1996) Air Influence on Similarity of Hydraulic Transients and Vibrations, *ASME J. Fluid Eng.*, *118(4)*, 706–709.
15. Li, J., & McCorquodale, A. (1999). “Modeling Mixed Flow in Storm Sewers,” *Journal of Hydraulic Engineering, ASCE*, *125(11)*, 1170–1180.
16. Minnaert, M. (1933). On Musical Air Bubbles and the Sounds of Running Water, *Phil. Mag.*, *16(7)*, 235–248.
17. Moeng, C. H., McWilliams, J. C., Rotunno, R., Sullivan, P. P., & Weil, J. (2004). “Investigating 2D Modeling of Atmospheric Convection in the PBL,” *J. Atm. Sci.*, *61*, 889–903.
18. Tuckerman, D. B., Pease, R. F.W. (1981). High performance Heat Sinking for VLSI, *IEEE Electron device letter, DEL-2*, 126–129.
19. Nagiyev, F. B., & Khabeev, N. S. (1988). Bubble Dynamics of Binary Solutions, *High Temperature*, *27(3)*, 528–533.
20. Shvarts, D., Oron, D., Kartoon, D., Rikanati, A., & Sadot, O. (2000). “Scaling Laws of Nonlinear Rayleigh-Taylor and Richtmyer-Meshkov Instabilities in Two and Three Dimensions,” *C. R. Acad. Sci. Paris IV*, *719*, 312p.
21. Cabot, W. H., Cook, A. W., Miller, P. L., Laney, D. E., Miller, M. C., & Childs, H. R. (2005). “Large Eddy Simulation of Rayleigh-Taylor Instability,” *Phys. Fluids*, September, *17*, 91–106.
22. Cabot, W. (2006). University of California, Lawrence Livermore National Laboratory, Livermore, CA, *Physics of Fluids*, 94–550.
23. Goncharov, V. N. (2002). “Analytical Model of Nonlinear, Single-Mode, Classical Rayleigh-Taylor Instability at Arbitrary Atwood Numbers,” *Phys. Rev. Letters*, *88*, 134502, 10–15.
24. Ramaprabhu, P., & Andrews, M. J. (2004). “Experimental Investigation of Rayleigh-Taylor mixing at small Atwood numbers” *J. Fluid Mech.*, *502*, 233.
25. Clark, T. T. (2003). “A Numerical Study of the Statistics of a Two-Dimensional Rayleigh-Taylor Mixing Layer,” *Phys., Fluids*, *15*, 2413.
26. Cook, A. W., Cabot, W., & Miller, P. L. (2004). “The Mixing Transitions in Rayleigh-Taylor Instability” *J. Fluid Mech.*, *511*, 333.

27. Waddell, J. T., Niederhaus, C. E., & Jacobs, J. W. (2001). "Experimental study of Rayleigh-Taylor Instability, Low Atwood number liquid systems with single-mode initial perturbations," *Phys., Fluids*, *13*, 1263–1273.
28. Weber, S.V., Dimonte, G., & Marinak, M. M. (2003). "Arbitrary Lagrange-Eulerian Code Simulations of Turbulent Rayleigh-Taylor Instability in Two and Three Dimensions," *Laser and Particle Beams*, *21*, 455 p.
29. Dimonte, G., Youngs, D., Dimits, A., Weber, S., & Marinak, M. (2004). "A Comparative Study of the Rayleigh-Taylor Instability using High-Resolution Three-Dimensional Numerical Simulations, the Alpha Group Collaboration," *Phys., Fluids*, *16*, 1668.
30. Young, Y. N., Tufo, H., Dubey, A., & Rosner, R. (2001). "On the Miscible Rayleigh-Taylor Instability Two and Three Dimensions," *J. Fluid Mech.*, *447*, 377, 2003–2500.
31. George, E., & Glimm, J. (2005). "Self-Similarity of Rayleigh-Taylor Mixing Rates," *Phys., Fluids*, *17*, 054101, 1–3.
32. Oron, D., Arazi, L., Kartoon, D., Rikanati, A., Alon, U., & Shvarts, D. (2001). "Dimensionality dependence of the Rayleigh-Taylor and Richtmyer-Meshkov instability, late-time scaling laws," *Phys., Plasmas*, *8*, 2883p.
33. Nigmatulin, R. I., Nagiyev, F. B., & Khabeev, N. S. (1980). Effective Heat Transfer Coefficients of the Bubbles in the Liquid Radial Pulse, Mater, Second-Union, Conf. Heat Mass Transfer, "Heat Mass Transfer in the Biphasic with Minsk, 5, 111–115.
34. Nagiyev, F. B., & Khabeev, N. S. (1988). Bubble dynamics of binary solutions, *High Temperature*, *27(3)*, 528–533.
35. Nagiyev, F. B. (1988). Damping of the Oscillations of Bubbles boiling Binary solutions, Mater, VIII, Resp, Conf., Mathematics and Mechanics, Baku, October 26–29, 177–178.
36. Nagiyev, F. B., & Kadyrov, B. A. (1986). Small Oscillations of the Bubbles in a Binary Mixture in the Acoustic Field, *Math., AN Az.SSR Ser. Physicotech and mate, Science*, *(1)*, 23–26.
37. Nagiyev, F. B. (1993). Dynamics, Heat and Mass Transfer of Vapor-Gas Bubbles in a two-component Liquid, Turkey-Azerbaijan Petrol Semin., Ankara, Turkey, 32–40.
38. Nagiyev, F. B. (1995). The Method of Creation effective Coolness Liquids, Third Baku international Congress, Baku, Azerbaijan Republic, 19–22.
39. Nagiyev, F. B. (1986). The Linear Theory of Disturbances in Binary Liquids Bubble Solution, *Dep.*, In *VINITI*, *405*, 86, 76–79.
40. Nagiyev, F. B. (1989). Structure of Stationary Shock Waves in Boiling Binary Solutions, *Math., USSR, Fluid Dynamics*, *1*, 81–87.
41. Rayleigh, (1917). On the Pressure developed in a Liquid during the collapse of a Spherical Cavity, *Philos., Mag. Ser. 6*, *34(N200)*, 94–98.
42. Perry, R. H., Green, D. W., & Maloney, J. O. (1997). *Perry's Chemical Engineers Handbook*, 7th Edition, McGraw-Hill, New York, 1–61.
43. Nigmatulin, R. I. (1987). Dynamics of Multiphase Media, Moscow, "Nauka," *1(2)*, 12–14.

44. Kodura, A., & Weinerowska, K. (2005). The Influence of the Local Pipeline Leak on Water Hammer Properties, Materials of the II Polish Congress of Environmental Engineering, Lublin, 125–133.
45. Kane, J., Arnett, D., Remington, B. A., Glendinning, S. G., & Baz'an, G. (2000). "Two-Dimensional Versus Three-Dimensional Supernova Hydrodynamic Instability Growth," *J. Astrophys.*, 528–989.
46. Quick, R. S. (1933). "Comparison and Limitations of Various Water hammer Theories," *J. Hyd. Div., ASME*, May, 43–45.
47. Jaeger, C. (1977). "Fluid Transients in Hydro-Electric Engineering Practice," Blackie and Son Ltd, 87–88.
48. Jaime Suárez, A. (2005). "Generalized Water Hammer Algorithm for piping systems with unsteady friction," 72–77.
49. Fok, A., Ashamalla, A., & Aldworth, G. (1978). "Considerations in Optimizing Air Chamber for Pumping Plants," Symposium on Fluid Transients and Acoustics in the Power Industry, San Francisco, USA, Dec., 112–114.
50. Fok, A. (1980). "Design Charts for Surge Tanks on Pump Discharge Lines," BHRA 3rd Int. Conference on Pressure Surges, Bedford, England, Mar., 23–34.
51. Fok, A. (1982). "Water Hammer and its Protection in Pumping Systems," Hydro Technical Conference, CSCE, Edmonton, May, 45–55.
52. Fok, A. (1987). "A Contribution to the Analysis of Energy Losses in Transient Pipe Flow," PhD. Thesis, University of Ottawa, 176–182.
53. Brunone, B., Karney, B. W., Mecarelli, M., & Ferrante, M. (2000). "Velocity Profiles and unsteady pipe frictions in Transient Flow," *Journal of Water Resources Planning and Management ASCE*, 126(4), Jul., 236–244.
54. Koelle, E., & Jr. Luvizotto, E., & Andrade, J. P. G. (1996). "Personality Investigation of Hydraulic Networks using MOC Method of Characteristics" Proceedings of the 7th International Conference on Pressure Surges and Fluid Transients, Harrogate Durham, United Kingdom, 1–8.
55. Fillion, Y., & Karney, B. W. (2002). "A Numerical Exploration of Transient Decay Mechanisms in Water Distribution Systems," Proceedings of the ASCE Environmental Water Resources Institute Conference, American Society of Civil Engineers, Roanoke, Virginia, 30.
56. Hamam, M. A., & Mc Corquodale, J. A. (1982). "Transient Conditions in the Transition from Gravity to Surcharged Sewer Flow," *Canadian, J. Civil Eng., Canada*, Sep., 65–98.
57. Savic, D. A., & Walters, G. A. (1995). "Genetic Algorithms Techniques for Calibrating Network Models," Report No. 95/12, Centre for Systems and Control Engineering, 137–146.
58. Walski, T. M., & Lutes, T. L. (1994). "Hydraulic Transients Cause Low-Pressure Problems," *Journal of the American Water Works Association*, 75(2), 58.
59. Lee, T. S., & Pejovic, S. (1996). Air Influence on Similarity of Hydraulic Transients and Vibrations, *ASME J. Fluid Eng.*, 118(4), 706–709.

60. Chaudhry, M. H. (1979). "Applied Hydraulic Transients," Van Nostrand Reinhold Co., N.Y., 1322–1324.
61. Parmakian, J. (1963). "Water hammer Analysis," Dover Publications, Inc., New York, New York, 51–58.
62. Tuckerman, D. B., & Pease, R. F. W. (1981). High performance Heat Sinking for VLSI, IEEE Electron device letter, DEL-2, 126–129.

CHAPTER 4

HEAT AND MASS TRANSFER MODELING

CONTENTS

| | | |
|-----|------------------------------|-----|
| 4.1 | Introduction..... | 76 |
| 4.2 | Materials and Methods..... | 76 |
| 4.3 | Results..... | 80 |
| 4.4 | Results and Discussion | 97 |
| 4.5 | Conclusion | 99 |
| | Keywords | 100 |
| | References..... | 100 |

4.1 INTRODUCTION

Heat flow in porous media is the study of energy movement in the form of heat, which occurs in many types of processes. The transfer of heat in porous media occurs from the high to the low temperature regions. Therefore, a temperature gradient has to exist between the two regions for heat transfer to happen. It can be done by conduction (within one porous solid or between two porous solids in contact), by convection (between two fluids or a fluid and a porous solid in direct contact with the fluid), by radiation (transmission by electromagnetic waves through space) or by combination of the above three methods [1–12].

4.2 MATERIALS AND METHODS

The general equation for heat transfer in porous media is (Eqs. (1)–(20)):

$$\left(\begin{array}{c} \text{rate of} \\ \text{heat in} \end{array} \right) + \left(\begin{array}{c} \text{rate of generation} \\ \text{of heat} \end{array} \right) = \left(\begin{array}{c} \text{rate of} \\ \text{heat out} \end{array} \right) + \left(\begin{array}{c} \text{rate of accumulation} \\ \text{of heat} \end{array} \right) \quad (1)$$

When a wet porous material is subjected to thermal drying two processes occur simultaneously, namely:

1. transfer of heat to raise the wet porous media temperature and to evaporate the moisture content.
2. transfer of mass in the form of internal moisture to the surface of the porous material and its subsequent evaporation.

The rate at which drying is accomplished is governed by the rate at which these two processes proceed. Heat is a form of energy that can cross the boundary of a system. Heat can, therefore, be defined as “the form of energy that is transferred between a system and its surroundings as a result of a temperature difference.” There can only be a transfer of energy across the boundary in the form of heat if there is a temperature difference between the system and its surroundings. Conversely, if the system and surroundings are at the same temperature there is no heat transfer across the boundary.

Strictly speaking, the term “heat” is a name given to the particular form of energy crossing the boundary. However, heat is more usually referred to in thermodynamics through the term “heat transfer,” which is consistent with the ability of heat to raise or lower the energy within a system.

There are three modes of heat flow in porous media:

1. convection,
2. conduction, and
3. radiation.

All three are different. Convection relies on movement of a fluid in porous material. Conduction relies on transfer of energy between molecules within a porous solid or fluid. Radiation is a form of electromagnetic energy transmission and is independent of any substance between the emitter and receiver of such energy. However, all three modes of heat flow rely on a temperature difference for the transfer of energy to take place.

The greater the temperature difference the more rapidly will the heat be transferred. Conversely, the lower the temperature difference, the slower will be the rate at which heat is transferred. When discussing the modes of heat transfer it is the rate of heat transfer Q that defines the characteristics rather than the quantity of heat.

As it was mentioned earlier, there are three modes of heat flow in porous structures, convection, conduction and radiation. Although two, or even all three, modes of heat flow may be combined in any particular thermodynamic situation, the three are quite different and will be introduced separately.

The coupled heat and liquid moisture transport of porous material has wide industrial applications. Heat transfer mechanisms in porous textiles include conduction by the solid material of fibers, conduction by intervening air, radiation, and convection. Meanwhile, liquid and moisture transfer mechanisms include vapor diffusion in the void space and moisture sorption by the fiber, evaporation, and capillary effects. Water vapor moves through porous textiles as a result of water vapor concentration differences. Fibers absorb water vapor due to their internal chemical compositions and structures. The flow of liquid moisture through the textiles is caused by fiber-liquid molecular attraction at the surface of fiber materials, which is determined mainly by surface tension and effective capillary pore distribution and pathways. Evaporation and/or condensation take place, depending on the temperature and moisture distributions. The heat transfer process is coupled with the moisture transfer processes with phase changes such as moisture sorption/desorption and evaporation/condensation.

All three of the mechanisms by which heat is transferred- conduction, radiation and convection, may enter into drying. The relative importance of the mechanisms varies from one drying process to another and very of-

ten one mode of heat transfer predominates to such extent that it governs the overall process.

As an example, in air-drying the rate of heat transfer is given by:

$$q = h_s A (T_a - T_s) \quad (2)$$

Where q is the heat transfer rate in Js^{-1} , h_s is the surface heat-transfer coefficient in $\text{Jm}^{-2} \text{s}^{-1} \text{ } ^\circ\text{C}^{-1}$, A is the area through which heat flow is taking place, m^2 . T_a is the air temperature and T_s is the temperature of the surface which is drying, $^\circ\text{C}$.

To take another example, in a cylindrical dryer where moist material is spread over the surface of a heated cylinder, heat transfer occurs by conduction from the cylinder to the porous media, so that the equation is

$$q = UA(T_i - T_s) \quad (3)$$

where U is the overall heat-transfer coefficient, T_i is the cylinder temperature (usually very close to that of the steam), T_s is the surface temperature of textile and A is the area of the drying surface on the cylinder. The value of U can be estimated from the conductivity of the cylinder material and of the layer of porous solid.

Mass transfer in the drying of a wet porous material will depend on two mechanisms: movement of moisture within the porous material which will be a function of the internal physical nature of the solid and its moisture content; and the movement of water vapor from the material surface as a result of water vapor from the material surface as a result of external conditions of temperature, air humidity and flow, area of exposed surface and supernatant pressure.

Some porous materials such as textiles exposed to a hot air stream may be cooled evaporatively by bleeding water through its surface. Water-vapor may condense out of damp air onto cool surfaces. Heat will flow through an air-water mixture in these situations, but water-vapor will diffuse or convect through air as well. This sort of transport of one substance relative to another called mass transfer. The moisture content, X , is described as the ratio of the amount of water in the materials, m_{H_2O} to the dry weight of material, $m_{material}$:

$$X = \frac{m_{H_2O}}{m_{material}} \quad (4)$$

There are large differences in quality between different porous materials depending on structure and type of material. A porous material such as textiles can be hydrophilic or hydrophobic. The hydrophilic fibers can absorb water, while hydrophobic fibers do not. A textile that transports water through its porous structures without absorbing moisture is preferable to use as a first layer. Mass transfer during drying depends on the transport within the fiber and from the textile surface, as well as on how the textile absorbs water, all of which will affect the drying process.

As the critical moisture content or the falling drying rate period is reached, the drying rate is less affected by external factors such as air velocity. Instead, the internal factors due to moisture transport in the material will have a larger impact. Moisture is transported in porous media during drying through:

- capillary flow of unbound water,
- movement of bound water, and
- vapor transfer.

Unbound water in a porous media will be transported primarily by capillary flow. As water is transported out of the porous material, air will be replacing the water in the pores. This will leave isolated areas of moisture where the capillary flow continues.

Moisture in a porous structure can be transferred in liquid and gaseous phases. Several modes of moisture transport can be distinguished:

- transport by liquid diffusion;
- transport by vapor diffusion;
- transport by effusion (Knudsen-type diffusion);
- transport by thermo diffusion;
- transport by capillary forces;
- transport by osmotic pressure; and
- transport due to pressure gradient.

A very common method of removing water from porous structures is convective drying. Convection is a mode of heat transfer that takes place as a result of motion within a fluid. If the fluid, starts at a constant temperature and the surface is suddenly increased in temperature to above that of the fluid, there will be convective heat transfer from the surface to the fluid as a result of the temperature difference. Under these conditions the temperature difference causing the heat transfer can be defined as:

$$\Delta T = \text{surface temperature} - \text{mean fluid temperature.}$$

Using this definition of the temperature difference, the rate of heat transfer due to convection can be evaluated using Newton's law of cooling:

$$Q = h_c A \Delta T, \quad (5)$$

where A is the heat transfer surface area and h_c is the coefficient of heat transfer from the surface to the fluid, referred to as the "convective heat transfer coefficient."

The units of the convective heat transfer coefficient can be determined from the units of other variables [13–22].

$$\begin{aligned} Q &= h_c A \Delta T \\ W &= (h_c) m^2 K \end{aligned} \quad (6)$$

so the units of h_c are $W / m^2 K$.

The relationships given in equations (0.4 and 0.5) are also true for the situation where a surface is being heated due to the fluid having higher temperature than the surface. However, in this case the direction of heat transfer is from the fluid to the surface and the temperature difference will now be $\Delta T = \text{mean fluid temperature} - \text{surface temperature}$.

The relative temperatures of the surface and fluid determine the direction of heat transfer and the rate at which heat transfer take place.

As given in previous equations, the rate of heat transfer is not only determined by the temperature difference but also by the convective heat transfer coefficient h_c . This is not a constant but varies quite widely depending on the properties of the fluid and the behavior of the flow. The value of h_c must depend on the thermal capacity of the fluid particle considered, that is, mC_p for the particle. So the higher the density and C_p of the fluid the better the convective heat transfer.

4.3 RESULTS

Two common heat transfer fluids are air and water, due to their widespread availability. Water is approximately 800 times more dense than air and also has a higher value of C_p . If the argument given above is valid then water has a higher thermal capacity than air and should have a better convective

heat transfer performance. This is borne out in practice because typical values of convective heat transfer coefficients are as follows (Table 4.1):

TABLE 4.1 Heat Transfer Coefficients

| Fluid | h_c ($W / m^2 K$) |
|-------|-----------------------|
| Water | 500–10,000 |
| Air | 5–100 |

The variation in the values reflects the variation in the behavior of the flow, particularly the flow velocity, with the higher values of h_c resulting from higher flow velocities over the surface.

When a fluid is in forced or natural convective motion along a surface, the rate of heat transfer between the solid and the fluid is expressed by the following equation:

$$q = h.A(T_w - T_f), \quad (7)$$

The coefficient h is dependent on the system geometry, the fluid properties and velocity and the temperature gradient. Most of the resistance to heat transfer happens in the stationary layer of fluid present at the surface of the solid, therefore the coefficient h is often called film coefficient.

Correlations for predicting film coefficient h are semi empirical and use dimensionless numbers, which describe the physical properties of the fluid, the type of flow, the temperature difference and the geometry of the system.

The Reynolds Number characterizes the flow properties (laminar or turbulent). L is the characteristic length: length for a plate, diameter for cylinder or sphere [23–42].

$$N_{Re} = \frac{\rho L v}{\mu}, \quad (8)$$

The Prandtl Number characterizes the physical properties of the fluid for the viscous layer near the wall.

$$N_{Pr} = \frac{\mu c_p}{k}$$

The Nusselt Number relates the heat transfer coefficient h to the thermal conductivity k of the fluid.

$$N_{Nu} = \frac{hL}{k}, \quad (9)$$

The Grashof Number characterizes the physical properties of the fluid for natural convection.

$$N_{Gr} = \frac{L^3 \Delta \rho g}{\rho \gamma^2} = \frac{L^3 \rho^2 g \beta \Delta T}{\mu^2}, \quad (10)$$

In capillary porous materials, moisture migrates through the body as a result of capillary forces and gradients of moisture content, temperature and pressure. This movement contributes to other heat transfer mechanisms while eventual phase change occurring within the material act as heat sources or sinks.

Drying is fundamentally a problem of simultaneous heat and mass transfer under transient conditions resulting in a system of coupled nonlinear partial differential equations.

Scientists defined a coupled system of partial differential equations for heat and mass transfer in porous bodies. Although they used different approaches to obtain equations, their formulations don't differ substantially from each other. Many numerical works have been executed in this field, on basis of these two theories.

Researchers have developed a one-dimensional model for simultaneous heat and moisture transfer in porous materials. Also many scientists have used one-dimensional in studying heat and mass transfer during convective drying of porous media.

Researchers studied drying problem of timber, with a two-dimensional model. Many scientists used finite element method for solution of two-dimensional heat and mass transfer in porous media.

All of above listed studies have estimated heat and mass transfer between porous materials and drying fluid, by coefficients obtained from standard correlations based on boundary layer equations, and more of them assumed analogy between heat and mass transfer coefficients. However, since the actual process of drying is a conjugate problem, the heat and mass transfer, to and from the porous solid have to be studied along with the flow field.

Scientists in a conjugate study of paper drying have shown that results of solution by conjugate view differ considerably from those of decoupled system. Also the analogy between heat and mass transfer coefficient may not exist in reality, even in drying of one-dimensional objects.

Researchers found that the mentioned analogy holds good only for initial period of unsaturated sand drying, and for the later part of drying, the heat and mass transfer coefficients at the interface may doesn't satisfy the analogy, due to the non-uniformity of moisture and temperature distribution at the interface resulting from conjugate nature of transfers.

Scientists studied drying of wood as a conjugate problem. They have used boundary layer equations for flow field, and presented temperature and moisture contours during the process.

Researchers applied two-dimensional model for brick drying. They used Navier-Stokes equations for flow field including buoyancy terms in their conjugate analysis. They concluded that restricting heat and mass transfer to top surface of two-dimensional porous body will cause considerable errors into solution. They also have shown that neglecting buoyant forces in flow analysis, leads to considerable differences in heat and mass transfer values and lower drying rate, in Reynolds number of 200.

In the majority of the previous conjugate studies, the buoyancy effects have been simply ignored in flow field analysis except the study performed by some researchers. The solution method used is finite volume approach and is related to an unsteady problem. In this chapter we have tried to use a much conservative method for calculation of energy and momentum fluxes. Regarding the weak capability of the finite element methods (specially in their flux averaging steps), the motivation of the current work concerns on solving the same two dimensional conjugate problem with a finite volume approach which fundamentally guaranties the energy and the mass fluxes to be conserved during the solution and the discretization procedures. However, using the same mesh and consequently the same cells, entire the solution domain highlights the ability of finite volume approach on using unstructured grids. On the other hand, the solution is extended to a higher Reynolds numbers to give a wider range study of the buoyancy effects not only on temperature and the moisture content, but also on flow patterns during the drying process.

4.3.1 MODELING

The problem model, including corresponding boundary conditions is shown in (Figs. 4.1–4.16). The problem considers a sample of rectangular brick exposed to convective airflow. The brick is assumed to be saturated with water initially. The governing moisture removal from brick to air exceeds in cause of concentration gradient between air in vicinity of body and free stream air. Flow is incompressible and thermo physical properties are taken to be constant. The initial moisture content of the brick is 0.13 kg/kg of dry solid, and the solid temperature is set to 293K and the drying air has a 50% of relative humidity. At the Reynolds 200 the air velocity is 0.02 m/s. The thermal conductivity of the brick is 1.8 W/mK, and the thermal capacity is set to 1200 J/kg K. The brick density is set to 1800 kg/m³.

Non-isothermal diffusion coefficient of porous body in vapor phase,
 $D_{iv} = 1(10)^{-12}$.

Non-isothermal diffusion coefficient of porous body in liquid phase,
 $D_{il} = 1(10)^{-12}$.

Iso-thermal diffusion Coefficient of porous body in vapor phase,
 $D_{mv} = 1(10)^{-12}$.

Iso-thermal diffusion Coefficient of porous body in liquid phase,
 $D_{ml} = 1(10)^{-8}$.

Enthalpy of Evaporation (Initial value), $H_{fg} = 2454Kj / KgK$.

Mass diffusion coefficient of vapor in air, $D_{diff} = 0.256(10)^{-4}$.

Fluid thermal conductivity, $K_f = 0.02568$.

Porous body thermal conductivity, $K_s = 1.8$.

Bouyancy coefficient of temperature, $\beta = 3.4129(10)^{-3} 1 / K$.

Bouyancy coefficient of Concentration, $\beta' = 0.0173$.

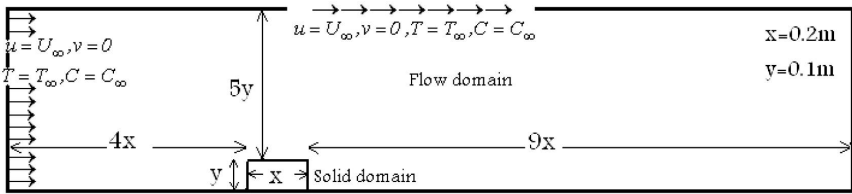


FIGURE 4.1 Geometry of computational field.

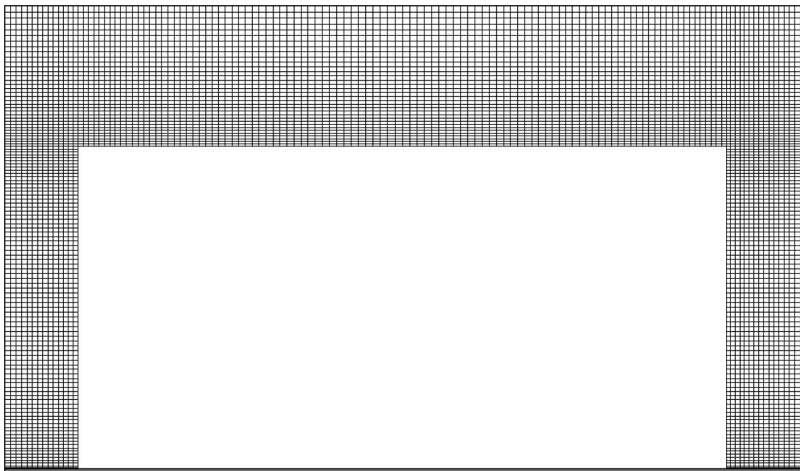


FIGURE 4.2 Mesh structure over the porous material.

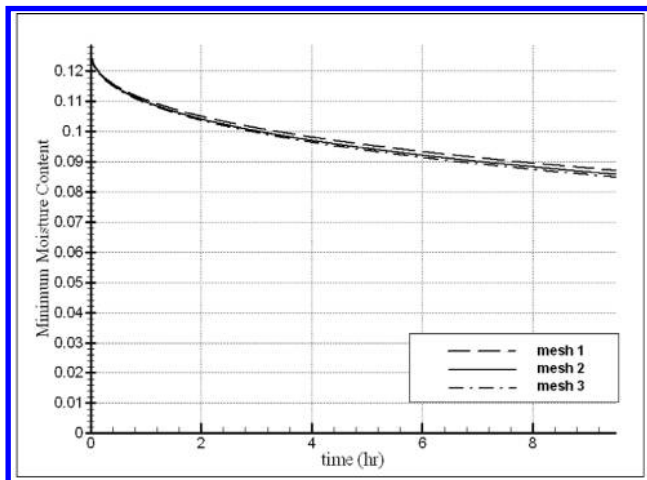


FIGURE 4.3 Value of moisture content in leading edge obtained with three different meshes.

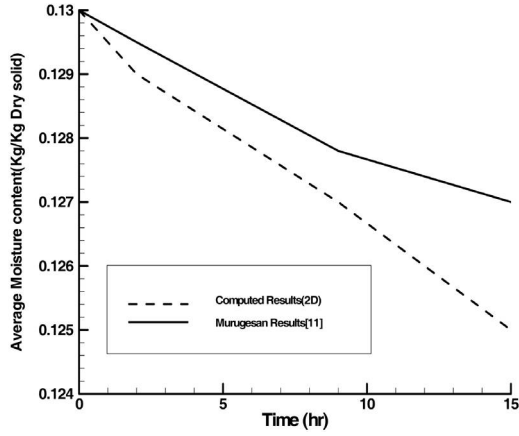


FIGURE 4.4 Drying curve.

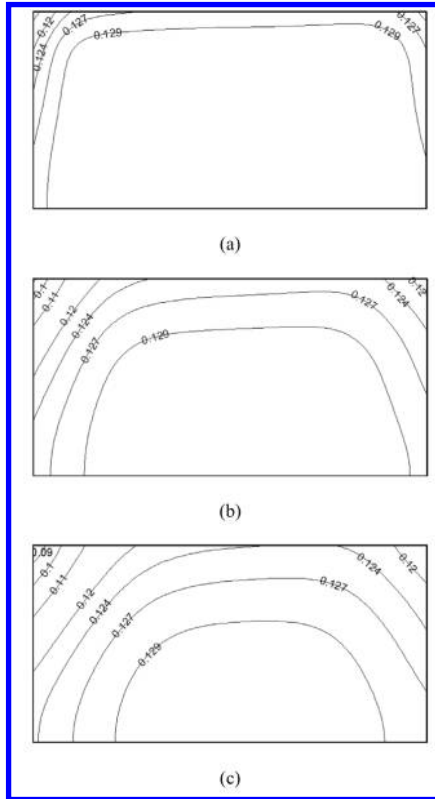


FIGURE 4.5 Moisture content distributions (kg moisture/kg dry) during drying (a) $t = 2\frac{1}{2}$ h (b) $t = 9$ h (c) $t = 15\frac{1}{2}$ h.

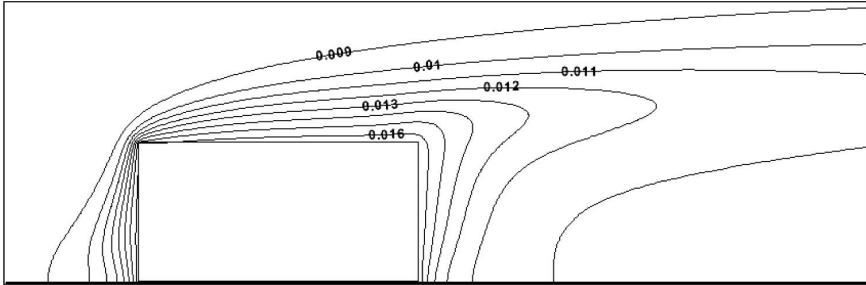


FIGURE 4.6 concentration contours in air around porous body.

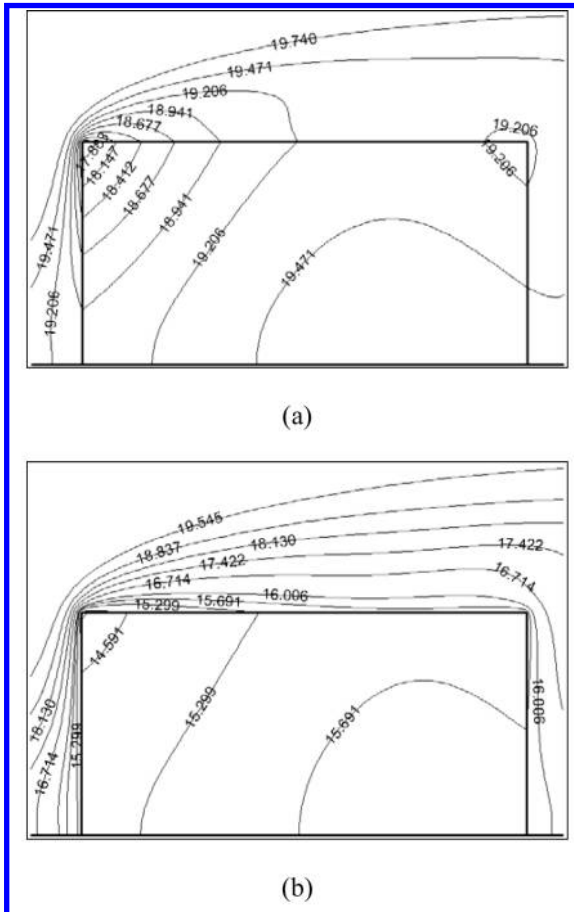


FIGURE 4.7 Temperature distributions in porous body and around (a) $t = 2\frac{1}{2}$ h (b) $t = 15\frac{1}{2}$ h.

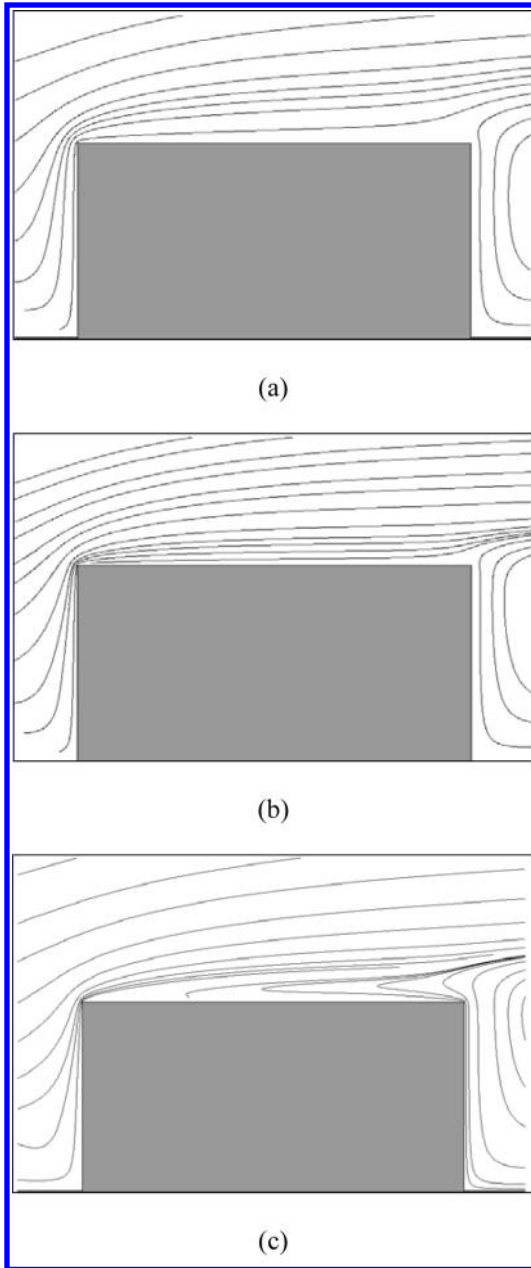


FIGURE 4.8 Streamlines for different value of Re (a) $Re_y=50$ (b) $Re_y=100$ (c) $Re_y=200$.

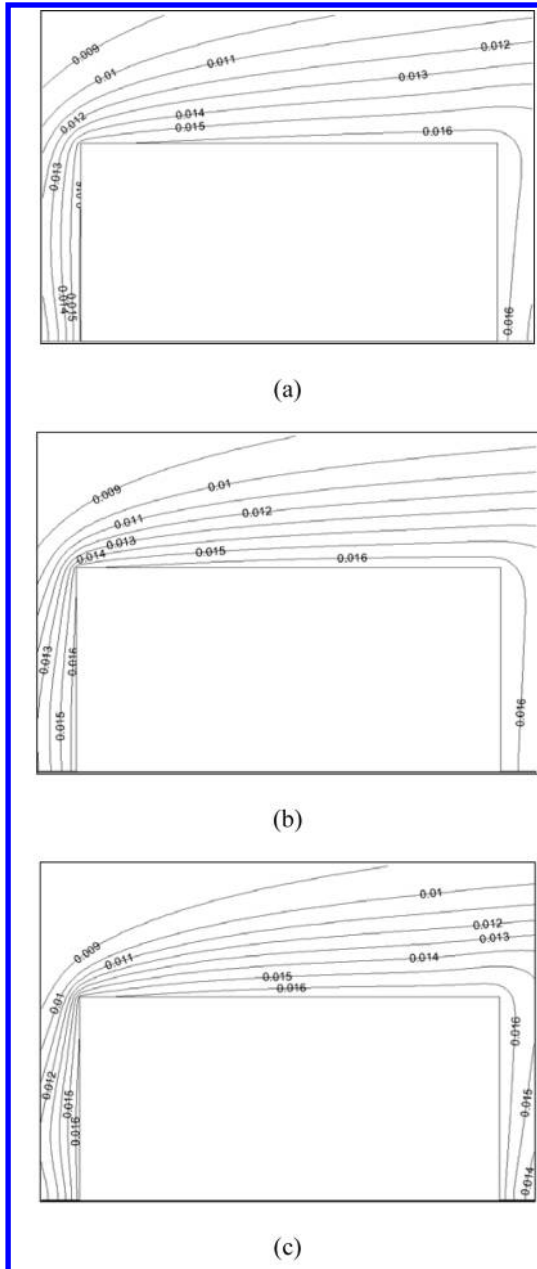


FIGURE 4.9 Concentration contours for different value of Re (a) $Re_y=50$ (b) $Re_y=100$ (c) $Re_y=200$.

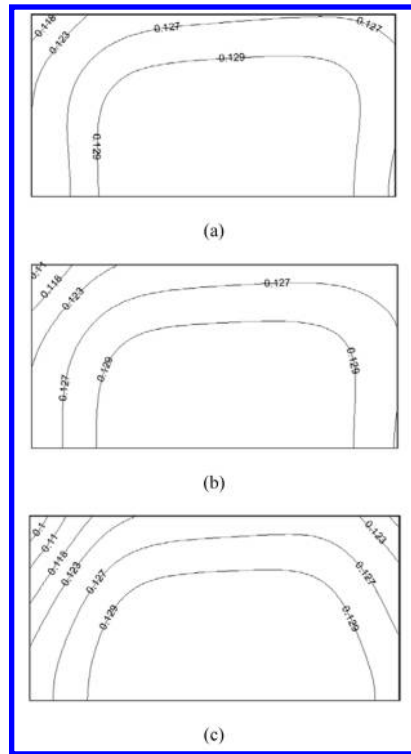


FIGURE 4.10 Moisture content contours (kg moisture/kg dry) for different value of Re (a) $Re_y=50$ (b) $Re_y=100$ (c) $Re_y=200$.

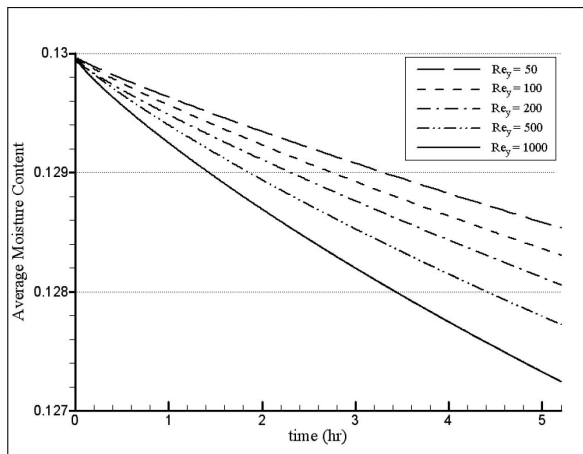


FIGURE 4.11 Drying curves for $Re=50$ to 100.

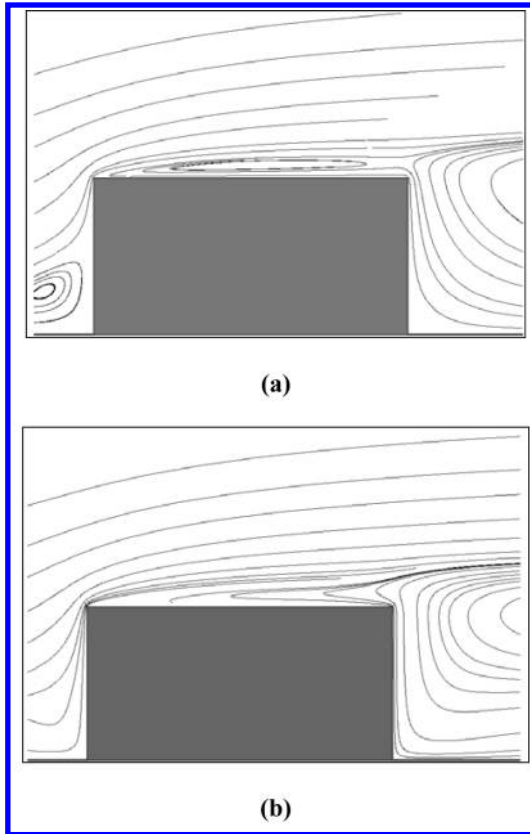


FIGURE 4.12 Effect of buoyancy forces on streamlines in $Re=200$ (a) forced convection (b) mixed convection.

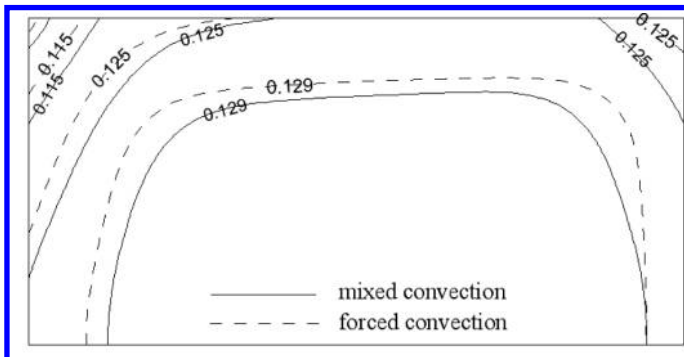


FIGURE 4.13 Moisture profiles obtained by mixed and forced convection models in $Re=200$ ($t = 8^{-1/4}$ h).

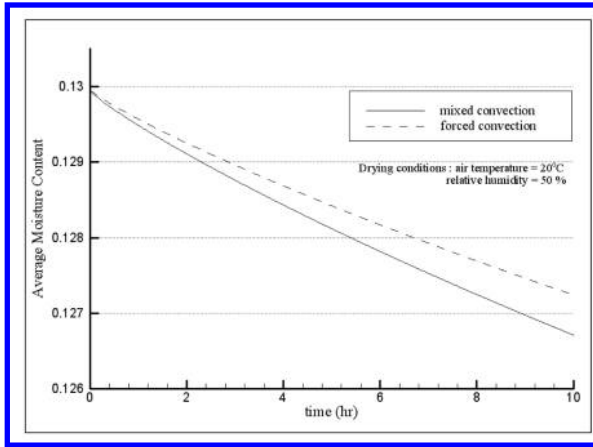


FIGURE 4.14 Drying curve for mixed and forced convection models in $Re=200$.

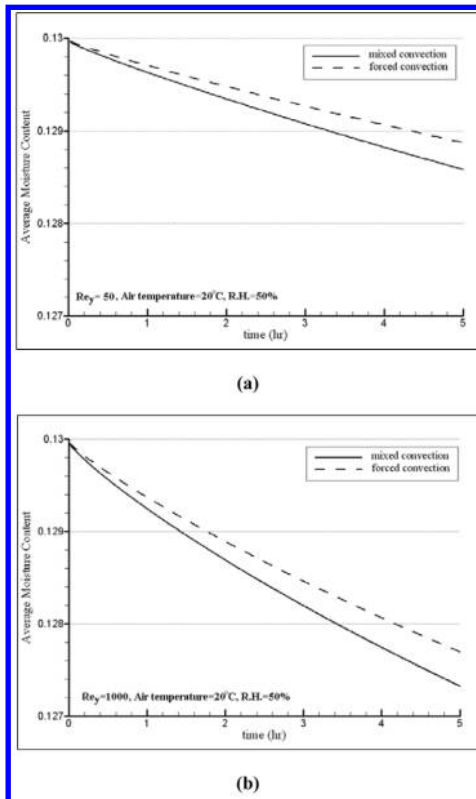


FIGURE 4.15 Drying curve for mixed and forced convection models Re (a) $Re = 50$ (b) $Re = 1000$.

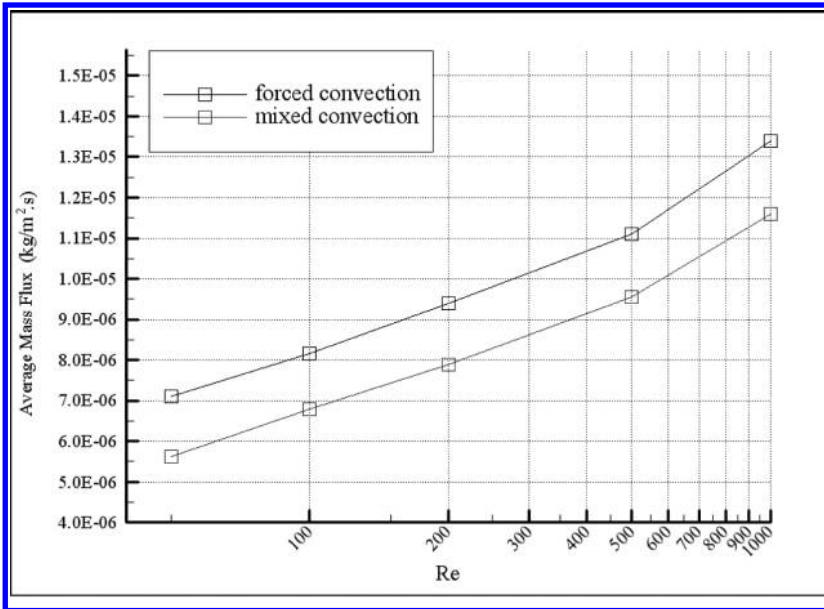


FIGURE 4.16 Average mass flux during initial 5 h of drying for mixed and forced convection models.

4.3.2 GOVERNING EQUATIONS FOR SOLID (BRICK)

The equations for porous solid phase as obtained by researchers on the basis of continuum approach, were applied for numerical solution

Energy equation

$$c^* \frac{\partial T}{\partial t} = \left(\frac{k}{\rho_0} + h_{fg} D_{iv} \right) \left(\frac{\partial^2 T}{\partial x^2} + \frac{\partial^2 T}{\partial y^2} \right) + h_{fg} D_{mv} \left(\frac{\partial^2 M}{\partial x^2} + \frac{\partial^2 M}{\partial y^2} \right), \quad (11)$$

where

$$c^* = c_0 + m_l c_l + m_v c_v$$

Moisture conservation equation

$$\frac{\partial M}{\partial t} = (D_{il} + D_{iv}) \left(\frac{\partial^2 T}{\partial x^2} + \frac{\partial^2 T}{\partial y^2} \right) + (D_{ml} + D_{mv}) \left(\frac{\partial^2 M}{\partial x^2} + \frac{\partial^2 M}{\partial y^2} \right) \quad (12)$$

Governing equations for flow field

o Continuity

$$\frac{\partial u}{\partial x} + \frac{\partial v}{\partial y} = 0, \quad (13)$$

Momentum equation (2D Navier-Stokes)

$$\frac{\partial u}{\partial t} + u \frac{\partial u}{\partial x} + v \frac{\partial u}{\partial y} = -\frac{1}{\rho} \frac{\partial P}{\partial x} + \nu \left(\frac{\partial^2 u}{\partial x^2} + \frac{\partial^2 u}{\partial y^2} \right), \quad (14)$$

$$\frac{\partial v}{\partial t} + u \frac{\partial v}{\partial x} + v \frac{\partial v}{\partial y} = -\frac{1}{\rho} \frac{\partial P}{\partial y} + \nu \left(\frac{\partial^2 v}{\partial x^2} + \frac{\partial^2 v}{\partial y^2} \right) + g\beta(T - T_\infty) + g\beta'(C - C_\infty) \quad (15)$$

Energy equation

$$\frac{\partial T}{\partial t} + u \frac{\partial T}{\partial x} + v \frac{\partial T}{\partial y} = \alpha \left(\frac{\partial^2 T}{\partial x^2} + \frac{\partial^2 T}{\partial y^2} \right) \quad (16)$$

Vapor concentration equation

$$\frac{\partial C}{\partial t} + u \frac{\partial C}{\partial x} + v \frac{\partial C}{\partial y} = D \left(\frac{\partial^2 C}{\partial x^2} + \frac{\partial^2 C}{\partial y^2} \right) \quad (17)$$

BOUNDARY AND INITIAL CONDITIONS

Initially the porous material is assumed to be at uniform moisture content (saturation value), and temperature (equal to air temperature).

$$T(x, y, 0) = T_0; M(x, y, 0) = M_0, \quad (18)$$

The boundary condition at interface of solid and fluid are:

No slip condition

$$u = 0; v = 0$$

Continuity of temperature

$$T_f = T_s$$

Continuity of concentration

$$C = C(T, M)_s$$

Heat balance

$$\left(k + \rho_0 h_{fg} D_{iv}\right) \frac{\partial T}{\partial n} + \rho_0 h_{fg} D_{mv} \frac{\partial M}{\partial n} = k_f \frac{\partial T_f}{\partial n} + h_{fg} D \frac{\partial C}{\partial n} \quad (19)$$

Species flux balance

$$\rho_0 \left(D_{iv} \frac{\partial T}{\partial n} + D_{mv} \frac{\partial M}{\partial n} \right) = D \frac{\partial C}{\partial n} \quad (20)$$

BOUNDARY CONDITIONS FOR FLOW FIELD ARE

Inlet boundary condition

$$u = U_\infty, v = 0, T = T_\infty, C = C_\infty$$

Far stream boundary condition (upper boundary)

$$u = U_\infty, T = T_\infty, C = C_\infty$$

Outflow boundary condition

$$\frac{\partial u}{\partial x} = 0$$

Also bottom surface of solid is taken adiabatic [43–52].

4.3.3 GRID DEPENDENCY

A structured mesh was used for computational work. Mesh clustering around body is illustrated in Fig. 4.2.

To clarify effect of mesh refinement on numerical solution, three meshes with different precision were used in numerical analysis:

Mesh.1, with 69,120 total nodes.

Mesh.2, with 108,000 total nodes.

Mesh.3, with 155,520 total nodes.

The value of moisture content in leading edge (minimum value of moisture content) obtained by numerical solution with mesh 1 and mesh 2 in 9 h have maximum difference of 1.28%, while for mesh 2 and mesh 3 the maximum difference is 0.66%. So mesh 2 seems to be optimum in accuracy and run-time, and therefore was decided to continue the computational work.

4.3.4 NUMERICAL SOLUTION

In each time-step, following items should be carried out:

1. Solving two-dimensional flow field equations (continuity + NS) by SIMPLE algorithm, with finite volume scheme.
2. Solution of energy equation for fluid by ADI technique with finite difference scheme. Neumann boundary condition was used for interface, which obtained from last time-step derivative value of solid temperature.
3. Then energy equation for porous field is solved by ADI technique with finite difference scheme. Boundary condition at interface is the known value of fluid temperature.
4. Determining concentration distribution for the flow field. The solution is similar with step 2, but boundary condition is obtained by explicit moisture content derivative at interface.
5. Calculation of moisture content distribution for porous body. The solution is similar with step 3, but boundary value of moisture is obtained by known fluid concentration (from previous step) value at interface.

Because of using explicit values in the solution procedure, we have to do internal repetition in each time-step, until internal conversion is reached for all four variables. After that, solution for next time step starts [53–62].

4.4 RESULTS AND DISCUSSION

4.4.1 VALIDATION AND GENERAL RESULTS

Drying curve of modeled brick in $Re=200$ is verified here. As illustrated, this comparison reveals that samples possessed almost the nearly same trend of moisture content reduction in the overall drying time of 15 h. Nevertheless, the accuracy of above mentioned curves are within 0.6%.

The computational results of moisture content profile for $Re=200$ illustrates that drying rate in region near leading edge (which corresponds to maximum concentration gradient in adjacent air) is more than other regions in porous body. Gradually, drying spreads from that region to centric regions of body.

Concentration values in air around porous body. Concluding from Fig. 4.6, gradient of concentration in the body surface has shown strong effect on moisture content distribution in body (as seen for leading edge).

Temperature distributes in porous body and around air in the course of drying. It's evident that, temperature value of porous body near leading edge decreases quickly as a result of higher moisture vaporization from surface there, and this temperature drop transfer to centric regions of porous body.

4.4.2 DIFFERENT AIR VELOCITIES

Numerical solution was executed for different velocities of drying fluid (different Reynolds number) to clarify the effect of this parameter. It shows streamlines around body for Reynolds number of 50, 100 and 200. As shown in Fig. 4.8, velocity increment in $Re=50$ to $Re=100$, results in more compactness of streamlines above body, and then in $Re=200$ separation occurs, while a vortex forms on upper surface.

In contours of concentration around body for denoted numbers of Reynolds are illustrated. It is obvious that Reynolds increment results a significant decrement in thickness of concentration boundary layer on the

upper side (especially for leading edge) due to changes in streamlines and velocity boundary layer.

For $Re=100$, moisture contents are less than those obtained for $Re=50$, especially for regions nearby leading edge. This is mainly due to thinner concentration boundary layer aforementioned. In transition to $Re=200$ from $Re=100$, this matter satisfies just for leading edge and left side of body (as a result of vortex formation above body in $Re=200$).

In curves are shown for various Reynolds number ranging from 50 to 1000. Effect of drying fluid velocity on process speed could be clearly analyzed. For example, removed moisture after 5 h of drying process for $Re=100$ is 15.4% more than corresponding value of $Re=50$. This difference is 17.5% for two Reynolds numbers of 500 and 200.

4.4.3 THE EFFECT OF BUOYANCY

To study the contribution of buoyancy on flow patterns and consequently on drying process, the computations were performed with and without buoyancy terms in flow equations (i.e., mixed and forced convection, respectively). It shows streamlines around porous body in $Re=200$ for both of forced and mixed convection assumptions. As shown, buoyancy forces clustered the streamlines near vertical walls. The moisture content (MC) distributions was shown for $8\frac{1}{4}$ duration for both cases ($Re=200$). Obviously, the mixed convection results show a higher drying performance [63–72].

The comparison between drying curves of mixed and forced assumptions. The decrease of (MC) has a lower rate in forced convection case for a 10 h period, (e.g., 19.7 percent after 10 h of drying). Consequently, the forced convection model underestimates drying rate noticeably in $Re=200$.

As stated above, the buoyancy forces has a great contribution in drying prediction in $Re=200$. To investigate effect intensity in various drying fluid velocities (different Reynolds numbers), drying curves resulted by mixed and forced convection models in Reynolds numbers 50 and 1000 (a practical range in drying) are illustrated. It Shows average moisture fluxes (during initial 5 h of process) obtained by each of two models, and so percentage increase in average moisture flux by taking buoyancy into account, are listed for different Reynolds numbers. These figs and table implies that despite relative decreasing in drying rate with increasing Reynolds, the effect of buoyancy on drying process in whole of Reynolds range of 50 to 1000, are considerable. So, in the

denoted range of Re , which include most practical velocities in porous bodies drying (especially clay products drying), ignoring buoyancy effects in flow analysis, will impose noticeable error into computations [73–78].

In other words, forced convection model hasn't enough accuracy for drying process analysis in governing range (Table 4.2):

TABLE 4.2 Effect of Buoyancy on Average Moisture Flux for Different Reynolds Numbers

| Re | Percentage increase in average moisture flux |
|------|--|
| 50 | 26% |
| 100 | 20% |
| 200 | 19% |
| 500 | 16% |
| 1000 | 15% |

4.5 CONCLUSION

Using a FV method, which employed in this article the pressure based conservative algorithms, performed a two dimensional conjugated solution that guaranties the conservation laws despite of the finite elements methods.

By studying drying process in a variety of flow velocity (various Reynolds number), It's observed that airflow velocity increment has proportional effect on drying rate, with a factor between $1/4$ and $1/5$.

Moisture profiles and drying rate are considerably affected by buoyancy forces. Moisture removal from porous body surface for mixed convection model is more than forced convection in whole of Reynolds range of 50 to 1000. So, it's suggested to taking into consideration buoyancy effects in analysis of flow around porous bodies in drying or other similar processes.

KEYWORDS

- Average mass flux
- Computational method
- Finite elements methods
- Porous bodies
- Reynolds numbers

REFERENCES

1. Harms, T. M., Kazmierczak, M. J., Cerner, F. M., Holke A., Henderson, H. T., Pilchowski, H. T., & Baker, K. (1997). Experimental Investigation of Heat Transfer and Pressure Drop through Deep Micro channels in a (100) Silicon Substrate, in: Proceedings of the ASME, Heat Transfer Division, HTD, 351, 347–357.
2. Holland, F. A., & Bragg, R. (1995). Fluid Flow for Chemical Engineers, Edward Arnold Publishers, London, 1–3.
3. George, E., & Glimm, J. (2005). “Self-Similarity of Rayleigh-Taylor Mixing Rates,” *Phys. Fluids*, 17, 054101, 1–3.
4. Goncharov, V. N. (2002). “Analytical Models of nonlinear single-mode classical Rayleigh-Taylor instability at Arbitrary Atwood numbers,” *Phys. Rev. Letters*, 88, 134502, 10–15.
5. Ishii, M. (1975). Thermo-Fluid Dynamic Theory of Two-Phase Flow, Collection de D. R. Liles and W. H. Reed, “A Sern-Implicit Method for Two-Phase Fluid la Direction des Etudes et Recherché d’Electricite de France, Vol. 22 Dynamics,” *Journal of Computational Physics*, 26, Paris, 390–407.
6. Chen, C. S., & Johnson, W. H. (1969). Kinetics of Moisture Movement in Hygroscopic Materials, In: Theoretical Considerations of Drying Phenomenon, *Trans. ASAE*, 12, 109–113.
7. Barnes, J., & Holcombe, B. (1996). Moisture Sorption and Transport in Clothing during Wear, *Textile Res. J.* 66(12), 777–786.
8. Chen, P., & Pei, D. (1988). A Mathematical Models of Drying Process Int., *J. Heat Mass Transfer*, 31 (12), 2517–2562.
9. Davis, A., & James, D. (1996). Slow Flow through a Model Fibrous Porous Medium, *Int. J. Multiphase Flow*, 22, 969–989.
10. Jirsak, O., Gok, T., Ozipek, B., & Pau, N. (1998). Comparing Dynamic and Static Methods for Measuring Thermal Conductive Properties of Textiles, *Textile Res. J.* 68(1), 47–56.
11. Kaviany, M., “Principle of Heat Transfer in Porous Media,” Springer, New York, 1991.
12. Jackson, J., & James, D. (1986). The Permeability of Fibrous Porous Media, *Can. J. Chem. Eng.* 64, 364–374.

13. Dietl, C., George, O. P., & Bansal, N. K. (1995). Modeling of Diffusion in Capillary Porous Materials During the Drying Process, *Drying Technol.*, *13 (1&2)*, 267–293.
14. Ea, J. Y. (1988). Water Vapour Transfer in Breathable Fabrics for Clothing, PhD thesis, University of Leeds.
15. Haghi, A. K. (2004). Moisture Permeation of Clothing, *JTAC* 76, 1035–1055.
16. Haghi, A. K. (2003). Thermal Analysis of Drying Process *JTAC*, 74, 827–842.
17. Haghi, A. K. (2000). Some Aspects of Microwave Drying, the *Annals of Stefancel Mare University*, Year VII, *14*, 22–25
18. Haghi, A. K. (2000). A Thermal Imaging Technique for Measuring Transient Temperature Field An Experimental Approach, *The Annals of Stefancel Mare University*, Year VI, *12*, 73–76.
19. Haghi, A. K. (2001). Experimental Investigations on Drying of Porous Media using Infrared Radiation, *Acta Polytechnica*, *41(1)*, 55–57.
20. Haghi, A. K. (2001). A Mathematical Model of the Drying Process, *Acta Polytechnical*, *41(3)*, 20–23.
21. Haghi, A. K. (2001). Simultaneous Moisture and Heat Transfer in Porous System, *Journal of Computational and Applied Mechanics*, *2(2)*, 195–204.
22. Haghi, A. K. (2002). A Detailed Study on Moisture Sorption of Hygroscopic Fiber, *Journal of Theoretical and Applied Mechanics*, *32(2)*, 47–62.
23. Dietl, C., George, O. P., & Bansal, N. K. (1995). Modeling of Diffusion in Capillary Porous Materials During the Drying Process, *Drying Technol.*, *13 (1&2)*, 267–293.
24. Ea, J. Y. (1988). Water Vapour Transfer in Breathable Fabrics for Clothing, PhD thesis, University of Leeds.
25. Flory, P. J. (1969). *Statistical Mechanics of Chain Molecules*, Interscience Pub., NY.
26. Walski, T. M., & Lutes, T. L. (1994). “Hydraulic Transients Cause Low-Pressure Problems,” *Journal of the American Water Works Association*, *75(2)*, 58.
27. Nigmatulin, R. I., Khabeev, N. S., & Nagiyev, F. B. (1981). Dynamics, Heat and Mass transfer of Vapor-Gas Bubbles in a Liquid Int., *J. Heat Mass Transfer*, *24(N6)*, Printed in Great Britain, 1033–1044.
28. Oron, D., Arazi, L., Kartoon, D., Rikanati, A., Alon, U., & Shvarts, D. (2001). “Dimensionality dependence of the Rayleigh-Taylor & Richtmyer-Meshkov instability, late-time scaling laws,” *Phys., Plasmas*, *8*, 2883p.
29. Parmakian, J. (1957). “Water hammer Design Criteria,” *J. Power Div., ASCE*, Sept., 456–460.
30. Parmakian, J. (1963). “Water hammer Analysis,” Dover Publications, Inc., New York, New York, 51–58.
31. Perry, R. H., Green, D. W., & Maloney, J. O. (1997). *Perry’s Chemical Engineers Handbook*, 7th Edition, McGraw-Hill, New York, 1–61.
32. Peng, X. F., & Peterson, G. P. (1996). Convective Heat Transfer and Flow Friction for Water Flow in Micro channel Structure, *Int. J. Heat Mass Transfer*, *36*, 2599–2608.
33. Pickford, J. (1969). “Analysis of Surge,” MacMillan, London, 153–156.
34. *Pipeline Design for Water and Wastewater*, American Society of Civil Engineers, New York, (1975), 54 p.
35. Qu, W., Mala, G. M., & Li, D. (1993). Heat Transfer for Water Flow in Trapezoidal Silicon Micro channels, 399–404.

36. Quick, R. S. (1933). "Comparison and Limitations of Various Water hammer Theories," J. Hyd. Div., ASME, May, 43–45.
37. Rayleigh, (1917). On the pressure developed in a liquid during the collapse of a spherical cavity. Philos. Mag. Ser. 6, 34(N200), 94–98.
38. Ramaprabhu, P., & Andrews, M. J. (2004). "Experimental Investigation of Rayleigh-Taylor Mixing at Small Atwood Numbers," J. Fluid Mech., 502, 233p
39. Rich, G. R. (1963). "Hydraulic Transients," Dover, USA, 148–154.
40. Savic, D. A., & Walters, G. A. (1995). "Genetic Algorithms Techniques for Calibrating Network Models," Report No. 95/12, Centre for Systems and Control Engineering, 137–146.
41. Savic, D. A., & Walters, G. A. (1995). Genetic algorithms Techniques for Calibrating Network Models, University of Exeter, Exeter, United Kingdom, 41–77.
42. Shvarts, D., Oron, D., Kartoon, D., Rikanati, A., & Sadot, O. (2000). "Scaling Laws of nonlinear Rayleigh-Taylor & Richtmyer-Meshkov instabilities in two and three dimensions," C. R. Acad. Sci. Paris IV, 719, 312p.
43. Sharp, B. (1981). "Water Hammer Problems and Solutions," Edward Arnold Ltd, London, 43–55.
44. Skousen, P. (1998). "Valve Handbook," McGraw Hill, New York, Hammer Theory and Practice, 687–721.
45. Song, C. C. et al. (1983). "Transient Mixed-Flow Models for Storm Sewers," J. Hyd. Div., Nov., 109, 458–530.
46. Stephenson, D. (1984). "Pipe Flow Analysis," Elsevier, 19, S.A., 670–788.
47. Streeter, V. L., & Lai, C. (1962). "Water hammers Analysis Including Fluid Friction," Journal of Hydraulics Division, ASCE, 88, 79p.
48. Streeter, V. L., & Wylie, E. B. (1979). "Fluid Mechanics," McGraw-Hill Ltd., USA, 492–505.
49. Streeter, V. L., & Wylie, E. B. (1981). "Fluid Mechanics," McGraw-Hill Ltd., USA, 398–420.
50. Tijsseling, (1993). "Alan E Vardy Time scales and FSI in unsteady Liquid-Filled Pipe Flow," 5–12.
51. Tuckerman, D. B., & Pease, R. F. W. (1981). High performance Heat Sinking for VLSI, IEEE Electron device letter, DEL-2, 126–129.
52. Tennekes, H., & Lumley, J. L. (1972). A First Course in Turbulence, the MIT Press, 410–466.
53. Thorley, A. R. D. (1991). "Fluid Transients in Pipeline Systems," D. and L. George, Herts, England, 231–242.
54. Tullis, J. P. (1971). "Control of Flow in Closed Conduits," Fort Collins, Colorado, 315–340.
55. Tuckerman, D. B. (1984). Heat Transfer Microstructures for Integrated Circuits, PhD. Thesis, Stanford University, 10–120.
56. Vallentine, H. R. (1965). "Rigid Water Column Theory for Uniform Gate Closure," J. Hyd. Div. ASCE, July, 55–243.
57. Waddell, J. T., Niederhaus, C. E., & Jacobs, J. W. (2001). "Experimental study of Rayleigh-Taylor Instability, Low Atwood number liquid systems with single-mode initial perturbations," Phys., Fluids, 13, 1263–1273.

58. Watters, G. Z. (1984). "Modern Analysis and Control of Unsteady Flow in Pipelines," Ann Arbor Sci., 2nd Ed., 1098–1104.
59. Walski, T. M., & Lutes, T. L. (1994). "Hydraulic Transients Cause Low-Pressure Problems," Journal of the American Water Works Association, 75(2), 58.
60. Weber, S. V., Dimonte, G., & Marinak, M. M. (2003). "Arbitrary Lagrange-Eulerian code simulations of turbulent Rayleigh-Taylor instability in two and three dimensions," Laser and Particle Beams, 21, 455 p.
61. Wood, D. J., Dorsch, R. G., & Lightener, C. (1966). "Wave-Plan Analysis of Unsteady Flow in Closed Conduits," Journal of Hydraulics Division, ASCE, 92, 83–110.
62. Wood, D. J., & Jones, S. E. (1973). "Water hammer charts for various types of valves," Journal of the Hydraulics Division, Proceedings of the American Society of Civil Engineers, January, 167–178.
63. Wood, F. M. (1970). "History of Water Hammers," Civil Engineering Research Report #65, Queens University, Canada, 66–70.
64. Wu, Z. Y., & Simpson, A. R. (2001). Competent Genetic-Evolutionary Optimization of water distribution systems, J. Comput. Civ. Eng., 15(2), 89–101.
65. Wylie, E. B., & Talpin, L. B. (1983). Matched Impedance to controls fluid transients, Trans., ASME, 105(2), 219–224.
66. Wylie E. B., & Streeter, V. L. (1993). Fluids Transients in systems, Prentice-Hall, Engle wood Cliffs, New Jersey, 4.
67. Wylie E. B., & Streeter, V. L. (1983). Fluid Transients, Feb Press, Ann Arbor, MI, 1982, corrected copy, 158p.
68. Wu, P. Y., & Little, W. A. (1983). Measurement of Friction Factor for Flow of Gases in Very Fine Channels used For Micro Miniature, Joule Thompson Refrigerators, Cryogenics, 24(8), 273–277.
69. Xu, B., Ooi, K. T., Mavriplis, C., & Zaghoul, M. E. (2002). Viscous dissipation effects for liquid flow in Micro channels, Microsystems, 53–57.
70. Young, Y. N., Tufo, H., Dubey, A., & Rosner, R. (2001). "On the Miscible Rayleigh-Taylor Instability Two and Three Dimensions," J. Fluid Mech., 447, 377, 2003–2500.
71. Wood, D. J., Dorsch, R. G., & Lightener C. (1966). "Wave-Plan Analysis of Unsteady Flow in Closed Conduits," Journal of Hydraulics Division, ASCE, 92, 83–110.
72. Wylie, E. B., & Streeter, V. L. (1993). Fluid Transients in systems, Prentice-Hall, Engle wood Cliffs, New Jersey, 4p.
73. Brunone, B., Karney, B. W., Mecarelli, M., & Ferrante, M. (2000). "Velocity Profiles and unsteady pipe friction in Transient Flow" Journal of Water Resources Planning and Management, ASCE, 126(4), Jul., 236–244.
74. Koelle, E., Jr. Luvizotto, E., & Andrade, J. P. G. (1996). "Personality Investigation of Hydraulic Networks using MOC–Method of Characteristics" Proceedings of the 7th International Conference on Pressure Surges and Fluid Transients, Harrogate Durham, United Kingdom, 1–8.
75. Fillion, Y., & Karney, B. W. (2002). "A Numerical Exploration of Transient Decay Mechanisms in Water Distribution Systems," Proceedings of the ASCE Environmental Water Resources Institute Conference, American Society of Civil Engineers, Roanoke, Virginia, 30.

76. Hamam, M. A., & Mc Corquodale, J. A. (1982). "Transient Conditions in the Transition from Gravity to Surcharged Sewer Flow," *Canadian J. Civil Eng.*, Canada, Sep., 65–98.
77. Savic, D. A., & Walters, G. A. (1995). "Genetic Algorithms Techniques for Calibrating Network Models," Report No. 95/12, Centre for Systems and Control Engineering, 137–146.
78. Till Mathis Wagner, (2004). A very short introduction to the Finite Element Method, Technical University of Munich, JASS, St Petersburg, May 4, 2004.

CHAPTER 5

LIQUID WATER IN NONHOMOGENEOUS MATERIAL

CONTENTS

| | | |
|-----|----------------------------|-----|
| 5.1 | Introduction..... | 106 |
| 5.2 | Materials and Methods..... | 106 |
| 5.3 | Results..... | 114 |
| 5.4 | Conclusion | 130 |
| | Keywords | 132 |
| | References..... | 132 |

5.1 INTRODUCTION

Wood is a hygroscopic, porous, anisotropic and non-homogeneous material. After log sawing, the lumber contains liquid water in fiber cavities (capillary water) and bound water inside the fiber wall (hygroscopic water). Porosity refers to volume fraction of void space. This void space can be actual space filled with air or space filled with both water and air. Capillary-porous materials are sometimes defined as those having pore diameter less than m . Capillary porous materials were defined as those having a clearly recognizable pore space. In capillary porous material, transport of water is a more complex phenomena. In addition to molecular diffusion, water transport can be due to vapor diffusion, surface diffusion, Knudsen diffusion, capillary flow, and purely hydrodynamic flow. In hygroscopic materials, there is large amount of physically bound water and the material often shrinks during heating.

5.2 MATERIALS AND METHODS

In hygroscopic materials there is a level of moisture saturation below which the internal vapor pressure is a function of saturation and temperature. These relationships are called equilibrium moisture isotherms. Above this moisture saturation, the vapor pressure is a function of temperature only (as expressed by the Clapeyron equation) and is independent of the moisture level. Thus, above certain moisture level, all materials behave non-hygroscopic [1].

5.2.1 COMPUTER MODELS FOR HEAT FLOW IN NON-HOMOGENEOUS MATERIAL

Green wood contains a lot of water. In the outer parts of the stem, in the sapwood, spruce and pine have average moisture content of about 130%, and in the inner parts, in the heartwood, the average moisture content is about 35%. Wood drying is the art of getting rid of that surplus water under controlled forms. It will dry to an equilibrium moisture content of 8–16% fluid content when left in air, which improves its stability, reduces its weight for transport, prepares it for chemical treatment or painting and improves its mechanical strength.

Water in wood is found in the cell cavities and cell walls. All void spaces in wood can be filled with liquid water called free water. Free water is held by adhesion and surface tension forces. Water in the cell walls is called bound water. Bound water is held by forces at the molecular level. Water molecules attach themselves to sites on the cellulose chain molecules. It is an intimate part of the cell wall but does not alter the chemical properties of wood. Hydrogen bonding is the predominant fixing mechanism. If wood is allowed to dry, the first water to be removed is free water. No bound water is evaporated until all free water has been removed. During removal of water, molecular energy is expended. Energy requirement for vaporization of bound water is higher than free water. Moisture content at which only the cell walls are completely saturated (all bound water) but no free water exists in all lumens is called the fiber saturation point (F.S.P). Typically the F.S.P of wood is within the range of 20–40% moisture content depending on temperature and wood species. Water in wood normally moves from high to low zones of moisture content. The surface of the wood must be drier than the interior if moisture is to be removed. Drying can be divided into two phases: movement of water from the interior to the surface of the wood, and removal of water from the surface. Water moves through the interior of the wood as a liquid or water vapor through various air passageways in the cellular structure of wood and through the cell walls [2].

Drying is a process of simultaneous heat and moisture transfer with a transient nature. The evolution process of the temperature and moisture with time must be predicted and actively controlled in order to ensure an effective and efficient drying operation. Lumber drying can be understood as the balance between heat transfer from airflow to wood surface and water transport from the wood surface to the airflow. Reduction in drying time and energy consumption offers the wood industries a great potential for economic benefit. In hygroscopic porous material like wood, mathematical models describing moisture and heat movements may be used to facilitate experimental testing and to explain the physical mechanisms underlying such mass transfer processes. The process of wood drying can be interpreted as simultaneous heat and moisture transfer with local thermodynamic equilibrium at each point within the timber. Drying of wood is in its nature an unsteady-state non-isothermal diffusion of heat and moisture, where temperature gradients may counteract with the moisture gradient [3].

5.2.2 SOME ASPECTS OF HEAT FLOW DURING DRYING PROCESS

5.2.2.1 STAGES OF DRYING

- *First stage:* When both surface and core MC are greater than the F.S.P. Moisture movement is by capillary flow. Drying rate is evaporation controlled.
- *Second stage:* When surface MC is less than the F.S.P. and core MC is greater than the F.S.P. Drying is by capillary flow in the core and by bound water diffusion near the surface as fiber saturation line recedes into wood, resistance to drying increases. Drying rate is controlled by bound water diffusion.
- *Third stage:* When both surface and core MC are less than the F.S.P. Drying is entirely by diffusion. As the MC gradient between surface and core becomes less, resistance to drying increases and drying rate decreases.

5.2.2.2 CAPILLARY

Capillary pressure is a driving force in convective wood drying at mild conditions. The temperature is higher outside than inside. The moisture profile during convective drying is in the opposite direction, namely, the drier part is toward the exposed surface of wood. This opposite pattern of moisture and temperature profiles lead to the concept of the wet front that separates the outer area, where the water is bound to the cell wall, from the inner area, where free water exists in liquid and vapor form. A wet front that moves slowly from the surface toward the center of a board during convective drying leads to subsequent enhancement of the capillary transportation. Capillary transportation can then be justified due to the moisture gradients developed around that area. When the drying conditions are mild, the drying period is longer so the relative portion of the total moisture removal, due to the capillary phenomena, is high, and it seems that this is the most important mass transfer mechanism [4].

5.2.2.3 BOUND WATER DIFFUSION

Credible data on the bound water diffusion coefficient in wood and the boundary condition for the interface between moist air and wood surface are very important for accurate description of timber drying as well as for the proper design and use of products, structures and buildings made of wood already dried below the fiber saturation point. During the last century, two groups of methods for measuring the bound water diffusion coefficient in wood were developed. The first one, traditionally called the cup method, uses data from the steady-state experiments of bound water transfer and is based on Fick's first law of diffusion. Unfortunately, the method is not valid for the bound water diffusion coefficient determination in wood because it cannot satisfy the requirements of the boundary condition of the first kind and the constant value of the diffusion coefficient. The second group of methods is based on the unsteady-state experiments and Fick's second law of diffusion. The common name of this group is the sorption method and it was developed to overcome the disadvantages of the cup technique [5].

5.2.2.4 DIFFUSION

In solving the diffusion equation for moisture variations in wood, some authors have assumed that the diffusion coefficient depends strongly on moisture content, while others have taken the diffusion coefficient as constant. It has been reported that the diffusion coefficient is influenced by the drying temperature, density and moisture content of timber. The diffusion coefficient of water in cellophane and wood substance was shown to increase with temperature in proportion to the increase in vapor pressure of water. It is also observed that the diffusion coefficient decreased with increasing wood density. Other factors affecting the diffusion coefficient that are yet to be quantified are the species (specific gravity) and the growth ring orientation. Literature has suggested that the ratios of radial and tangential diffusion coefficients vary for different tree species. The radial diffusion coefficient of New Zealand *Pinus radiata* has been estimated to be approximately 1.4 times the tangential diffusion coefficient. It is observed that for northern red oak, the diffusion coefficient is a function of moisture content only. It increases dramatically at low moisture content and tends to level off as the fiber saturation point is approached.

In a one-dimensional formulation with moisture moving in the direction normal to a specimen of a slice of wood of thickness $2a$, the diffusion equation can be written as:

$$\frac{\partial(MC)}{\partial t} = \frac{\partial}{\partial X} \left(D \frac{\partial(MC)}{\partial X} \right) \quad (0 < X < a, t > 0) \quad (1)$$

where MC is moisture content, t is time, D is diffusion coefficient, and X is space coordinate measured from the center of the specimen.

The moisture content influences on the coefficient D only if the moisture content is below the fiber saturation point (F.S.P) (typically 20%–30% for softwoods):

$$D(u) = \begin{cases} f_D(u) & , u < u_{fsp} \\ f_D(u_{fsp}) & , u \geq u_{fsp} \end{cases} \quad (2)$$

where u_{fsp} denotes the F.S.P. and $f_D(u)$ is a function which expresses diffusion coefficient in moisture content, temperature and may be some other parameters of ambient air climate. The expression of $f_D(u)$ depends on variety of wood.

It was assumed that the diffusion coefficient bellow F.S.P. can be represented by:

$$f_D(u) = A e^{-\frac{5280}{T}} e^{\frac{B \cdot u}{100}} \quad (3)$$

where T is the temperature in Kelvin, u is percent moisture content, A and B can be experimentally determined.

The regression equation of diffusion coefficient of *Pinus radiata* timber using the dry bulb temperature and the density is:

$$D(10^{-9}) = 1.89 + 0.127 \times T_{DB} - 0.00213 \times \rho_s \quad (R^2 = 0.499) \quad (4)$$

The regression equations of diffusion coefficients below of Masson's pine during high temperature drying are:

Tangential diffusion

$$D = 0.0046MC^2 + 0.1753MC + 4.2850 \quad (R^2 = 0.9391) \quad (5)$$

Radial diffusion

$$D = 0.0092MC^2 + 0.3065MC + 4.9243 \quad (R^2 = 0.9284) \quad (6)$$

The transverse diffusion coefficient D can be expressed by the porosity of wood ν , the transverse bound water diffusion coefficient D_{bt} of wood and the vapor diffusion coefficient D_ν in the lumens:

$$D = \frac{\sqrt{\nu}D_{bt}D_\nu}{(1-\nu)(\sqrt{\nu}D_{bt} + (1-\sqrt{\nu})D_\nu)} \quad (7)$$

The vapor diffusion coefficient D_ν in the lumens can be expressed as:

$$D_\nu = \frac{M_w D_a P_s}{SG_d \rho_w R T_k} \cdot \frac{d\phi}{du} \quad (8)$$

where M_w (kg/kmol) is the molecular weight of water.

$$D_a = \frac{9.2 \cdot 10^{-9} T_k^{2.5}}{(T_k + 245.18)} \quad (9)$$

is the inter diffusion coefficient of vapor in air,

$$SG_d = \frac{1.54}{(1+1.54u)} \quad (10)$$

where SG_d is the nominal specific gravity of wood substance at the given bound water content. $\rho_w = 103 \text{ kg/m}^3$ is the density of water, $R = 8314.3 \text{ kJ/kmol}\cdot\text{K}$ is the gas constant, T_k is the Kelvin temperature, ψ is the relative humidity (%/100), and P_{sat} is saturated vapor pressure given by:

$$P_{sat} = 3390 \exp(-1.74 + 0.0759T_C - 0.000424T_C^2 + 2.44 \cdot 10^{-6} T_C^3) \quad (11)$$

The derivative of air relative humidity ψ with respect to moisture content MC is given as:

$$MC = \frac{18}{w} \left(\frac{k_1 k_2 \psi}{1 + k_1 k_2 \psi} + \frac{k_2 \psi}{1 - k_2 \psi} \right) \quad (12)$$

where:

$$k_1 = 4.737 + 0.04773T_C - 0.00050012T_C^2 \quad (13)$$

$$k_2 = 0.7059 + 0.001695T_C + -0.000005638T_C^2 \quad (14)$$

$$W = 223.4 + .6942T_C + 0.01853T_C^2 \quad (15)$$

The diffusion coefficient D_{bt} of bound water in cell walls is defined according to the Arrhenius equation as:

$$D_{bt} = 7.10^{-6} \exp(-E_b / RT_k) \quad (16)$$

where:

$$E_b = (40.195 - 71.179Mc + 291Mc^2 - 669.92Mc^3) \cdot 10^6 \quad (17)$$

is the activation energy.

The porosity of wood is expressed as:

$$\nu = 1 - SG(0.667 + Mc) \quad (18)$$

where specific gravity of wood SG at the given moisture content u is defined as:

$$SG = \frac{\rho_s}{\rho_w (1 + Mc)} = \frac{\rho_0}{\rho_w + 0.883\rho_0 Mc} \quad (19)$$

where ρ_s is density of wood, ρ_0 is density of oven-dry wood (density of wood that has been dried in a ventilated oven at approximately 104 °C until there is no additional loss in weight).

Wood thermal conductivity (K_{wood}) is the ratio of the heat flux to the temperature gradient through a wood sample. Wood has a relatively low thermal conductivity due to its porous structure, and cell wall properties. The density, moisture content, and temperature dependence of thermal conductivity of wood and wood-based composites were demonstrated by several researchers. The transverse thermal conductivity can be expressed as:

$$K_{wood} = [SG \times (4.8 + 0.09 \times MC) + 0.57] \times 10^{-4} \frac{cal}{cm \cdot Cs} \quad (20)$$

When moisture content of wood is <40%.

$$K_{wood} = [SG \times (4.8 + 0.125 \times MC) + 0.57] \times 10^{-4} \frac{cal}{cm \cdot Cs} \quad (21)$$

When moisture content of wood is >40%.

The specific gravity and moisture content dependence of the solid wood thermal conductivity in the transverse (radial and tangential) direction is given by:

$$K_T = SG(K_{cw} + K_w \cdot Mc) + K_a \nu \quad (22)$$

where: SG = specific gravity of wood, K_{cw} = Conductivity of cell wall substance (0.217 J/m/s/K), K_w = conductivity of water (0.4 J/m/s/K), K_a = conductivity of air (0.024 J/m/s/K), Mc = moisture content of wood (fraction), ν = porosity of wood.

The thermal conductivity of wood is affected by a number of basic factors: density, moisture content, extractive content, grain direction, structural irregularities such as checks and knots, fibril angle, and temperature. Thermal conductivity increases as density, moisture content, temperature, or extractive content of the wood increases. Thermal conductivity is nearly the same in the radial and tangential directions with respect to the growth rings.

The longitudinal thermal conductivity of solid wood is approximately 2.5 times higher than the transverse conductivity:

$$K_L = 2.5K_T \quad (23)$$

For moisture content levels <25%, approximate thermal conductivity K across the grain can be calculated with a linear equation of the form:

$$K_{wood} = G(B + CM) + A \quad (24)$$

where: SG is specific gravity based on oven dry weight and volume at a given moisture content MC (%) and A , B , and C are constants. For specific gravity >0.3, temperatures around 24 °C, and moisture content values

<25%, $A = 0.01864$, $B = 0.1941$, and $C = 0.004064$ (with k in $W/(m \cdot K)$). The Eq. (24) was derived from measurements made by several researchers on a variety of species.

During the early stages of drying the material consists of so much water that liquid surfaces exist and drying proceeds at a constant rate. Constant drying rates are achieved when surface free water is maintained and the only resistance to mass transfer is external to the wood. The liquid water moves by capillary forces to the surface in same proportion of moisture evaporation. Moisture movement across the lumber will depend on the wood permeability and the drying rate itself is controlled by external conditions in this period. This part of energy was received by the surface increase temperature in this region. The heat transfer to the inner part of lumber was started. Since the moisture source for the surface is internal moisture, constant drying rates can only be maintained if there is sufficient moisture transport to keep the surface moisture content above the F.S.P. If this level is not maintained then some of the resistance to mass transfer becomes internal and neither the drying rate nor the surface temperature remains constant and drying proceeds to the falling rate period. As the lumber dries, the liquid water or wet line recedes into wood and the internal moisture movement involves the liquid flow and diffusion of water vapor and hygroscopic water. The effect of internal resistance on the drying rate increases. In the last phase (second falling rate period) there is no more liquid water in the lumber, and the drying rate is controlled only by internal resistance (material characteristics) until an equilibrium moisture content is reached [5–25].

5.3 RESULTS

A typical drying curve showing three stages of drying characteristic is illustrated in (Figs. 5.1–5.5).

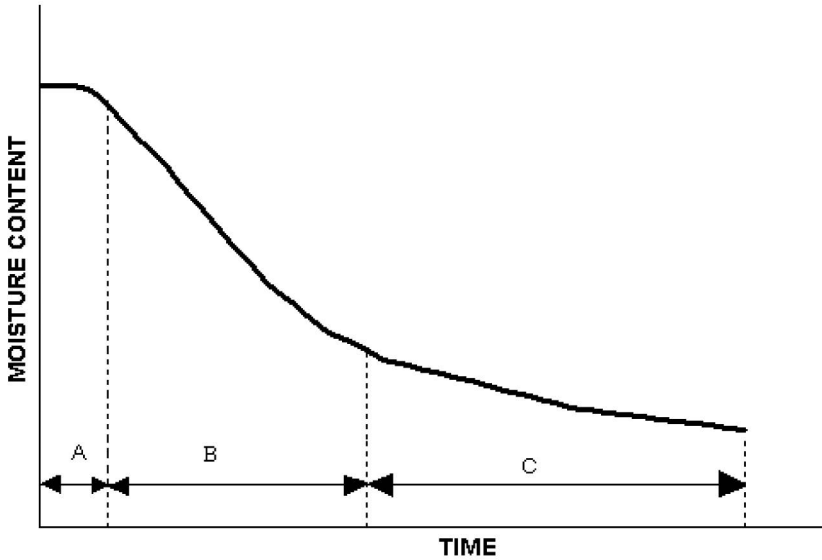


FIGURE 5.1 Drying characteristic of porous media: (a) constant rate region; (b) first falling rate region; (c) second falling rate region.

Pang et al. proposed that the three drying periods (constant rate, first falling rate and second falling rate) based on simulated drying of veneer be expressed by the following equations:

$$-\frac{d(MC)}{dt} = j_0 \text{ For } MC > M_{Cr1} \tag{25}$$

$$-\frac{d(MC)}{dt} = A + B * MC \text{ For } M_{Cr1} > MC > M_{Cr2} \tag{26}$$

$$-\frac{d(MC)}{dt} = \frac{A + B * M_{Cr2}}{M_{Cr2} - M_e} * (MC - M_e) \text{ For } MC < M_{Cr2} \tag{27}$$

where j_0 is constant drying rate, M_{Cr1} is the first critical moisture content, M_{Cr2} is the second critical moisture content, constants A and B also vary with wood thickness, wood density, and drying conditions.

Moisture content of wood is defined as the weight of water in wood expressed as a fraction, usually a percentage, of the weight of oven dry

wood. Moisture exists in wood as bound water within the cell wall, capillary water in liquid form and water vapor in gas form in the voids of wood. Capillary water bulk flow refers to the flow of liquid through the interconnected voids and over the surface of a solid due to molecular attraction between the liquid and the solid. Moisture content varies widely between species and within species of wood. It varies particularly between heartwood and sapwood. The amount of moisture in the cell wall may decrease as a result of extractive deposition when a tree undergoes change from sapwood to heartwood. The butt logs of trees may contain more water than the top logs. Variability of moisture content exists even within individual boards cut from the same tree. Green wood is often defined as freshly sawn wood in which the cell walls are completely saturated with water. Usually green wood contains additional water in the lumens. Moisture content at which both the cell lumens and cell walls are completely saturated with water is the maximum moisture content. An average green moisture content value taken from the Wood Handbook (Forest products society, 1999) of southern yellow pine (loblolly) is 33 and 110% for heartwood and sapwood, respectively. Sweet gum is 79 and 137% while yellow-poplar is 83 and 106% for heartwood and sapwood, respectively.

Permeability refers to the capability of a solid substance to allow the passage of gases or liquids under pressure. Permeability assumes the mass movement of molecules in which the pressure or driving force may be supplied by such sources as mechanically applied pressure, vacuum, thermal expansion, gravity, or surface tension. Under this condition, the permeability of wood is the dominant factor controlling moisture movement.

Fluid movement (Tables 5.1–5.3) in wood is a very important process in wood products industries. An understanding of wood permeability is essential for determining lumber drying schedules for treating lumber and for producing high-quality wood products. The flow of gas inside the wood particle is limited due to the fact that wood consists of a large number of clustered small pores. The pore walls act as barriers largely preventing convective flow between adjacent pores. The wood annular rings also act as barriers for flow in the radial direction which makes flow in the axial direction more favorable and giving a lower permeability in the radial direction than in the axial direction where the axial flow is regarded as flow parallel to the wood fiber grains and the radial flow as flow perpendicular to the wood grains. The permeability in the wood cylinder is therefore an important parameter for the velocity field in the wood. The dry wood

radial permeability is 10,000 times lower than the dry wood axial permeability. The chemical composition of the wood/char structure also affects the permeability, where the permeability in char is in order of 1,000 times larger than for wood.

Longitudinal flow becomes important, particularly in specimens having a low ratio of length to diameter, because of the high ratio of longitudinal to transverse permeability. Longitudinal permeability was found to be dependent upon specimen length in the flow direction, i.e., the decrease of specimen length appears result in greater permeability in less permeable species.

The effect of drying conditions on gas permeability and preservative treatability was assessed on western hemlock lumber. Although there were no differences in gas permeability between lumber dried at conventional and high temperatures, there were differences in preservative penetration. High temperature drying significantly reduced drying time, but did not appear to affect permeability or shell-to-core MC differences compared with drying at conventional temperature. Pits have a major influence on softwood permeability. Across pits can be impeded by aspiration or occlusion by deposition extractives on the membrane. Drying conditions can significantly affect pit condition, sometimes inducing aspiration that blocks both air and fluid flow. Pressure treatment is presumed to enhance preservative uptake and flow across pits, but the exact impact of pit condition (i.e., open or aspirated) is unknown. Drying conditions may also alter the state of materials deposited on pits, thereby altering the effects of pressure and perhaps the nature of preservative wood interactions. The latter effect may be especially important, since changes in wood chemistry could affect the rates of preservative fixation, which could produce more rapid preservative deposition on pit membranes that would slow further fluid ingress. The longitudinal permeability of the outer heartwood of each species also was determined to evaluate the effect of growth rate on the decrease in longitudinal permeability following sapwood conversion to heartwood. Faster diameter growth produced higher longitudinal permeability in the sapwood of yellow-polar, but not in the sapwood of northern red oak or black walnut. Growth rate had no effect on either vessel lumen area percentage or decrease in longitudinal permeability in newly formed heartwood for all three species. Table 5.1 represents typical values for gas permeability. Values are given in orders of magnitude.

TABLE 5.1 Typical Values for Gas Permeability

| Type of sample | Longitudinal gas permeability [cm ³ (gas)/(cm at sec)] |
|--|--|
| Red oak (R = 150 micrometers) | 10,000 |
| Basswood (R = 20 micrometers) | 1000 |
| Maple, Pine sapwood, Coast Douglas-fir sapwood | 100 |
| Yellow-poplar sapwood, Spruce sapwood, Cedar sapwood | 10 |
| Coast Douglas-fir heartwood | 1 |
| White oak heartwood, Beech heartwood | 0.1 |
| Yellow-poplar heartwood, Cedar heartwood, Inland Douglasfir heartwood | 0.01 |
| Transverse Permeabilities (In approx. same species order as longitudinal) | 0.001–0.0001 |

Darcy's law for liquid flow:

$$k = \frac{\text{flux}}{\text{gradient}} = \frac{V/(t \times A)}{\Delta P/L} = \frac{V \times L}{t \times A \times \Delta P} \quad (28)$$

where k = Permeability [$\text{cm}^3(\text{liquid})/(\text{cm atm sec})$], V = Volume of liquid flowing through the specimen (cm^3), t = Time of flow (sec), A = Cross-sectional area of the specimen perpendicular to the direction of flow (cm^2), ΔP = Pressure difference between ends of the specimen (atm), L = Length of specimen parallel to the direction of flow (cm).

Darcy's law for gaseous flow:

$$K_g = \frac{V \times L \times P}{t \times A \times \Delta P \times \bar{P}} \quad (29)$$

where: K_g = Superficial gas permeability [$\text{cm}^3(\text{gas})/(\text{cm atm sec})$], V = Volume of gas flowing through the specimen ($\text{cm}^3(\text{gas})$), P = Pressure at which V is measured (atm), t = Time of flow (sec), A = Cross-sectional area of the specimen perpendicular to the direction of flow (cm^2), ΔP =

Pressure difference between ends of the specimen (atm), L = Length of specimen parallel to the direction of flow (cm), \bar{P} = Average pressure across the specimen (atm).

To simulate the heat and mass transport in drying, conservation equations for general non-hygroscopic porous media have been developed by Whitaker based on averaging procedures of all of the variables. These equations were further employed and modified for wood drying. Mass conservation equations for the three phases of moisture in local form are summarized in Eqs. (30)–(32).

Water vapor:

$$\frac{\partial}{\partial t}(\phi_g \rho_v) = -\text{div}(\rho_v V_v) + \dot{m}_{wv} + \dot{m}_{bv} \quad (30)$$

Bound water:

$$\frac{\partial}{\partial t}(\phi_s \rho_b) = -\text{div}(\rho_b V_b) + \dot{m}_{bv} + \dot{m}_{wb} \quad (31)$$

Free water:

$$\frac{\partial}{\partial t}(\phi_w \rho_w) = -\text{div}(\rho_w V_w) - \dot{m}_{wv} - \dot{m}_{wb} \quad (32)$$

Where the velocity of the transported quantity is denoted by V_i , ρ_i is the density, and \dot{m}_{ij} denotes the transition from phases i and j . From here on, the subscripts w , b , v , and s refer, respectively, to free water, bound water, water vapor, and the solid skeleton of wood. Denoting the total volume by V and the volume of the phase i by V_i , the volumetric fraction of this phase is:

$$\phi_i = \frac{V_i}{V} \quad (33)$$

with the geometrical constraint:

$$\phi_g + \phi_s + \phi_w = 1 \quad (34)$$

Darcy's Law, by using relative permeabilities, provides expressions for the free liquid and gas phase velocities as follows:

$$v = -\frac{K_l K_{rl}}{\mu_l} \nabla P_l \quad (35)$$

and

$$v = -\frac{K_v K_{rv}}{\mu_v} \nabla P_v \quad (36)$$

where K is the intrinsic permeability (m^2), K_r is the relative permeability, P is the pressure (Pa), and μ is the viscosity (Pa.s).

The heat flux (q) and the moisture flux (N_v) are estimated by:

$$q = h(T_G - T_{surf}) \quad (37)$$

$$N_v = \psi K_0 (Y_{surf} - Y_G) = \beta (p_G^v - p_{ats}^v) \quad (38)$$

In which T_{surf} , Y_{surf} and p_s^v are the wood temperature, the air humidity and the vapor partial pressure, respectively, at the wood surface and, T_G , Y_G and p_G^v are the corresponding parameters in the air stream. The heat-transfer coefficient is represented by h . The mass-transfer coefficient is β when vapor partial pressure difference is taken as driving force and is k_0 when humidity difference is taken as the driving force with ψ being the humidity factor. The mass-transfer coefficient related to humidity difference is a function of distance along the airflow direction from the inlet side. The heat-transfer coefficient is correlated to the mass-transfer coefficient, as shown by and can be calculated from it. The humidity coefficient ϕ has been found to vary from 0.70 to 0.76, depending on the drying schedules and board thickness.

For the moisture mass transfer and balance, the moisture loss from wood equals the moisture gain by the hot air, and the moisture transfer rate from the board is described by mass transfer coefficient multiplied by driving force (humidity difference, for example). These considerations yield:

$$-\frac{\partial}{\partial \tau} [MC \cdot \rho_s \cdot (1 - \varepsilon)] = G \cdot \frac{\partial Y}{\partial X} = \begin{cases} -\psi K_0 \cdot a \cdot (Y_{surf} - Y_G) (\text{condensation}) \\ \psi K_0 \cdot a \cdot f \cdot (Y_{sat} - Y_G) (\text{evaporation}) \end{cases} \quad (39)$$

Where MC is the wood moisture content, ρ_s is the wood basic density, ϵ is the void fraction in the lumber stack, a is the exposed area per unit volume of the stack and G is the dry air mass flow rate. In order to solve the above equations, the relative drying rate (f) needs to be defined which is a function of moisture content.

For the heat transfer and balance, the energy loss from the hot air equals the heat gain by the moist wood. The convective heat transfer is described by product of heat transfer coefficient and the temperature difference between the hot air and the wood surface. The resultant relationships are as follows:

$$\frac{\partial T_{wood}}{\partial \tau} = \frac{(1 + \alpha_R - \alpha_{LS})}{\rho_s \cdot (1 - \epsilon) \cdot C_{Pwood}} \left[h \cdot a \cdot (T_G - T_{wood}) - G \cdot \Delta H_{wv} \cdot \frac{\partial Y_G}{\partial X} \right] \quad (40)$$

$$\frac{\partial T_G}{\partial X} = \frac{\left(h \cdot a + G \cdot C_{Pv} \frac{\partial Y_G}{\partial X} \right) \cdot (T_G - T_{wood})}{G \cdot (C_{Pv} + Y_G \cdot C_{Pv})}$$

In the above equations, T_{wood} is the wood temperature, α_R and α_{LS} are coefficients to reflect effects of heat radiation and heat loss, C_{Pwood} is the specific heat of wood, and ΔH_{wv} is the water evaporation. These equations have been solved to determine the changes of air temperature and wood temperature along the airflow direction and with time.

The energy rate balance (kW) of a drying air adjacent to the wood throughout the wood board can be represented as follows:

$$\frac{1}{2} V_a \rho_{a,mt} c_{p,a,mt} \frac{dT_a}{dt} = \frac{1}{2} v A_{cs} c_{p,a,mt} (T_{a,in} - T_{a,ex}) + \dot{Q}_{evap} - \dot{Q}_{conv} \quad (41)$$

Where \dot{Q}_{evap} and \dot{Q}_{conv} (kW) are the evaporation and convection heat transfer rates between the drying air and wood, which can be calculated as follows:

$$\dot{Q}_{evap} = r \dot{m}_{wv,s} A_{surf} \quad (42)$$

$$\dot{Q}_{conv} = hA(T_a - T_{SO}) \quad (43)$$

The specific water vapor mass flow rate ($\dot{m}_{wv,surf}$) ($\text{kg}/\text{m}^2 \text{ s}$) to the drying air can be calculated as follows:

$$\dot{m}_{wv,surf} = \frac{h_D}{R_{wv} T_{SO}} (P_{wv,surf} - P_{wv,a}) \quad (44)$$

The vapor pressure on the wood surface can be determined from the sorption isotherms of wood. The mass transfer coefficient (h_D) (m/s) can be calculated from the convection heat transfer coefficient (h) ($\text{kW}/\text{m}^2 \text{ K}$) as follows:

$$h_D = h \frac{1}{\rho_{a,m} c p_{a,m} L e^{0.58}} / \left(1 - \frac{\rho_{wv,m}}{P} \right) \quad (45)$$

Water transfer in wood involves liquid free water and water vapor flow while MC of lumber is above the F.S.P.

According to Darcy's law the liquid free water flux is in proportion to pressure gradient and permeability. So Darcy's law for liquid free water may be written as:

$$J_f = \frac{K_l \rho_l}{\mu_l} \cdot \frac{\partial P_c}{\partial \chi} \quad (46)$$

Where J_f = liquid free water flow flux, $\text{kg}/\text{m}^2 \cdot \text{s}$, K_l = specific permeability of liquid water, $\text{m}^3(\text{liquid})/\text{m}$, ρ_l = density of liquid water, kg/m^3 , μ_l = viscosity of liquid water, $P_a \cdot S$, P_c = capillary pressure, P_a , χ = water transfer distance, m, $\partial p_c / \partial \chi$ = capillary pressure gradient, P_a / m .

The water vapor flow flux is also proportional to pressure gradient and permeability as follows:

$$J_{vf} = \frac{K_v \rho_v}{\mu_v} \cdot \frac{\partial P_v}{\partial \chi} \quad (47)$$

where J_{vf} = water vapor flow flux, $\text{kg}/\text{m}^2 \cdot \text{s}$, K_v = specific permeability of water vapor, $\text{m}^3(\text{vapor})/\text{m}$, ρ_v, μ_v = density and viscosity of water vapor, respectively, kg/m^3 and $P_a \cdot S$, $\partial p_v / \partial \chi$ = vapor partial pressure gradient, P_a / m .

Therefore, the water transfer equation above F.S.P. during high temperature drying can be written as:

$$\rho_s \frac{\partial(MC)}{\partial t} = \frac{\partial}{\partial x} (J_f + J_v) \quad (48)$$

where ρ_s = basic density of wood, kg/m^3 , MC = moisture content of wood, %, t = time, s, $\partial(MC)/\partial t$ = the rate of moisture content change, %/s, x = water transfer distance, m.

5.3.1 WATER TRANSFER MODEL BELOW F.S.P.

Water transfer in wood below F.S.P. involves bound water diffusion and water vapor diffusion. The bound water diffusion in lumber usually is unsteady diffusion; the diffusion equation follows Fick's Second law as follows:

$$\frac{\partial(MC)}{\partial t} = \frac{\partial}{\partial x} \left(D_b \frac{\partial(MC)}{\partial x} \right) \quad (49)$$

where D_b is bound water diffusion coefficient, m^2/s , $\partial(MC)/\partial x$ is MC gradient of lumber, %/m. The bound water diffusion flux J_b can be expressed as:

$$J_b = D_b \rho_s \frac{\partial(MC)}{\partial x} \quad (50)$$

where ρ_s is basic density of wood, kg/m^3 .

The water vapor diffusion equation is similar to bound water diffusion equation as follows:

$$\frac{\partial(MC)}{\partial t} = \frac{\partial}{\partial x} \left(D_v \frac{\partial(MC)}{\partial x} \right) \quad (51)$$

where D_v is water vapor diffusion coefficient, m^2/s . The water vapor diffusion flux can be expressed as:

$$J_v = D_v \rho_s \frac{\partial(MC)}{\partial x} \quad (52)$$

Therefore, the water transfer equation below F.S.P. during high temperature drying can be expressed as:

$$\rho_s \frac{\partial(MC)}{\partial t} = \frac{\partial}{\partial x}(J_b + J_v) \quad (53)$$

Two types of wood samples (namely; spruce and pine) were selected for drying investigation. Natural defects such as knots, checks, splits, etc., which would reduce strength of wood are avoided. All wood samples were dried to a moisture content of approximately 30%. The effect of drying temperature and drying modes on the surface roughness, hardness and color development of wood samples are evaluated.

The average roughness is the area between the roughness profile and its mean line, or the integral of the absolute value of the roughness profile height over the evaluation length:

$$R_a = \frac{1}{L} \int_0^L |r(x)| dx \quad (54)$$

When evaluated from digital data, the integral is normally approximated by a trapezoidal rule:

$$R_a = \frac{1}{N} \sum_{n=1}^N |r_n| \quad (55)$$

The root-mean-square (RMS) average roughness of a surface is calculated from another integral of the roughness profile:

$$R_q = \sqrt{\frac{1}{L} \int_0^L r^2(x) dx} \quad (56)$$

The digital equivalent normally used is:

$$R_q = \sqrt{\frac{1}{N} \sum_{n=1}^N r_n^2} \quad (57)$$

R_z (ISO) is a parameter that averages the height of the five highest peaks plus the depth of the five deepest valleys over the evaluation length. These

parameters, which are characterized by ISO 4287, were employed to evaluate influence of drying methods on the surface roughness of the samples.

We investigated the influence of drying temperatures on the surface roughness characteristics of veneer samples as well. The results showed that the effect of drying temperatures used in practice is not remarkable on surface roughness of the sliced veneer and maximum drying temperature (130 °C) applied to sliced veneers did not affect significantly surface roughness of the veneers. Veneer sheets were classified into four groups and dried at 20, 110, 150, and 180 °C. According to the results, the smoothest surfaces were obtained for 20 °C drying temperature while the highest values of surface roughness were obtained for 180 °C. Because some surface checks may develop in the oven-drying process. It was also found in a study that the surface roughness values of beech veneers dried at 110 °C was higher than that of dried at 20 °C.

In another experimental study, veneer sheets were oven-dried in a veneer dryer at 110 °C (normal drying temperature) and 180°C (high drying temperature) after peeling process. The surfaces of some veneers were then exposed at indoor laboratory conditions to obtain inactive wood surfaces for glue bonds, and some veneers were treated with borax, boric acid and ammonium acetate solutions. After these treatments, surface roughness measurements were made on veneer surfaces. Alder veneers were found to be smoother than beech veneers. It was concluded that the values mean roughness profile (R_a) decreased slightly or no clear changes were obtained in R_a values after the natural inactivation process. However, little increases were obtained for surface roughness parameters, no clear changes were found especially for beech veneers.

The changes created by weathering on impregnated wood with several different wood preservatives were investigated. The study was performed on the accelerated weathering test cycle, using UV irradiation and water spray in order to simulate natural weathering. Wood samples were treated with ammonium copper quat (ACQ 1900 and ACQ 2200), chromated copper arsenate (CCA), Tanalith E 3491 and Wolmanit CX-8 in accelerated weathering experiment. The changes on the surface of the weathered samples were characterized by roughness measurements on the samples with 0, 200, 400 and 600 h of total weathering. Generally the surface values of alder wood treated with copper-containing preservatives decreased with over the irradiation time except for treated Wolmanit CX-82% when comparing un-weathered values. Surface values of pine treated samples

generally increased with increasing irradiation time except for ACQ-1900 groups.

Because the stylus of detector was so sensitive first each sample was smoothed with emery paper then measurement test was performed before and after drying. The Mitutoyo Surface roughness tester SJ-201P instrument was employed for surface roughness measurements. Cut-off length was 2.5 mm, sampling length was 12.5 mm and detector tip radius was $5\mu\text{m}$ in the surface roughness measurements. Tables 5.2 and 5.3 displays the changes in surface roughness parameters (R_a , R_z and R_q) of the Pine and spruce at varying drying methods. In both cases the surface roughness becomes higher during microwave and infrared heating while surface smoothness of both pine and spruce increased during convection and combined drying. However, the roughness of wood is a complex phenomenon because wood is an anisotropic and heterogeneous material. Several factors such as anatomical differences, growing characteristics, machining properties of wood, pretreatments (e.g., steaming, drying, etc.) applied to wood before machining should be considered for the evaluation of the surface roughness of wood.

TABLE 5.2 Surface Roughness (μm) for Pine

| Drying methods | Drying conditions | R_a | R_z | R_q |
|----------------|-------------------|-------|-------|-------|
| Microwave | Before drying | 4.52 | 24.68 | 5.39 |
| | After drying | 5.46 | 30.21 | 6.62 |
| Infrared | Before drying | 4.42 | 25.52 | 5.43 |
| | After drying | 4.87 | 26.55 | 5.69 |
| Convection | Before drying | 4.66 | 26.87 | 5.86 |
| | After drying | 4.08 | 24.64 | 5.12 |
| Combined | Before drying | 5.23 | 32.59 | 6.42 |
| | After drying | 3.41 | 21.7 | 4.27 |

TABLE 5.3 Surface Roughness (μm) for Guilan Spruce

| Drying methods | Drying conditions | R_a | R_z | R_q |
|----------------|-------------------|-------|-------|-------|
| Microwave | Before drying | 6.44 | 34.18 | 7.85 |
| | After drying | 7.77 | 44.3 | 9.82 |
| Infrared | Before drying | 4.92 | 30.61 | 6.30 |
| | After drying | 6.42 | 38.93 | 8.17 |
| Convection | Before drying | 4.97 | 32.41 | 6.5 |
| | After drying | 4.78 | 32.27 | 6.34 |
| Combined | Before drying | 10.41 | 59.5 | 13.37 |
| | After drying | 9.11 | 54.31 | 11.5 |

Hardness represents the resistance of wood to indentation and marring. In order to measure the hardness of wood samples, the Brinell hardness method was applied. In this method a steel hemisphere of diameter 10 mm was forced into the surface under test. The Brinell method measures the diameter of the mark caused by the steel ball in the specimens. The specimens were loaded parallel and perpendicular to the direction of wood grains. After applying the force the steel ball was kept on the surface for about 30 seconds. The values of hardness are shown in Figs. 5.2 and 5.3, respectively. In both type of samples the hardness measured in longitudinal direction is reported to be higher than tangential. The amount of fibers and its stiffness carrying the load are expected to be lower when the load direction is angled to the grain. Results showed that hardness of wood increased in combined drying. The hardness of wood is proportional to its density. The hardness of wood varies, depending on the position of the measurement. Latewood is harder than early wood and the lower part of a stem is harder than the upper part. Increase in moisture content decreases the hardness of wood. It was observed the effect of different drying temperatures during air circulation drying. The result indicates no significant influence of temperature on hardness; still the specimens dried at higher temperature gave a hard and brittle impression. It was also investigated whether wood hardness is affected by temperature level during microwave drying and whether the response is different from that of conventionally

dried wood. It was concluded that there is a significant difference in wood hardness parallel to the grain between methods when drying progresses to relatively lower level of moisture content, that is, wood hardness becomes higher during microwave drying. Variables such as density and moisture content have a greater influence on wood hardness than does the drying method or the drying temperature.

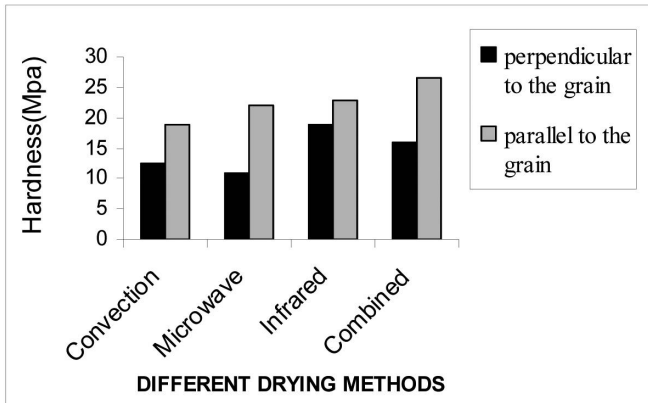


FIGURE 5.2 Brinell hardness for spruce.

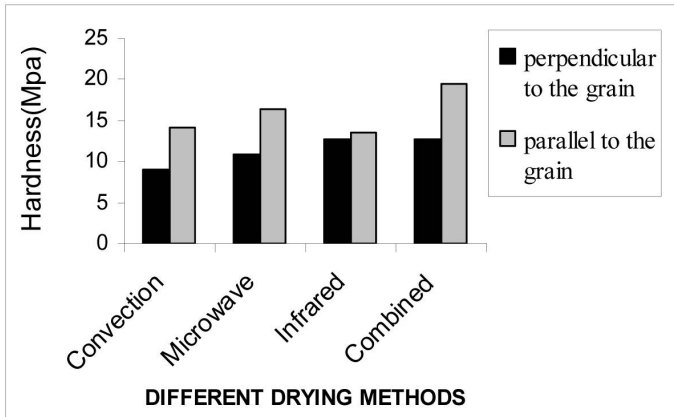


FIGURE 5.3 Brinell hardness for pine.

Color development of wood surfaces can be measured by using optical devices such as spectrophotometers. With optical measurement methods, the uniformity of color can be objectively evaluated and presented as L^* ,

a^* and b^* coordinates named by CIEL*a*b* color space values. Measurements were made both on fresh and dried boards and always from the freshly planted surface. Three measurements in each sample board were made avoiding knots and other defects and averaged to one recording. The spectrum of reflected light in the visible region (400–750 nm) was measured and transformed to the CIEL*a*b* color scale using a 10° standard observer and D65 standard illuminant.

These color space values were used to calculate the total color change (ΔE^*) applied to samples according to the following equations:

$$\begin{aligned}\Delta L^* &= L_f^* - L_i^* \\ \Delta a^* &= a_f^* - a_i^* \\ \Delta b^* &= b_f^* - b_i^* \\ \Delta E^* &= \sqrt{(\Delta L^*)^2 + (\Delta a^*)^2 + (\Delta b^*)^2}\end{aligned}\quad (58)$$

f and i are subscripts after and before drying, respectively.

In this three-dimensional coordinates, L^* axis represents non-chromatic changes in lightness from an L^* value of 0 (black) to an L^* value of 100 (white), $+a^*$ represents red, $-a^*$ represents green, $+b^*$ represents yellow and $-b^*$ represents blue.

As can be seen from (Figs. 5.4 and 5.5) color space values of both pine and Guilan spruce changed after drying [20–77].

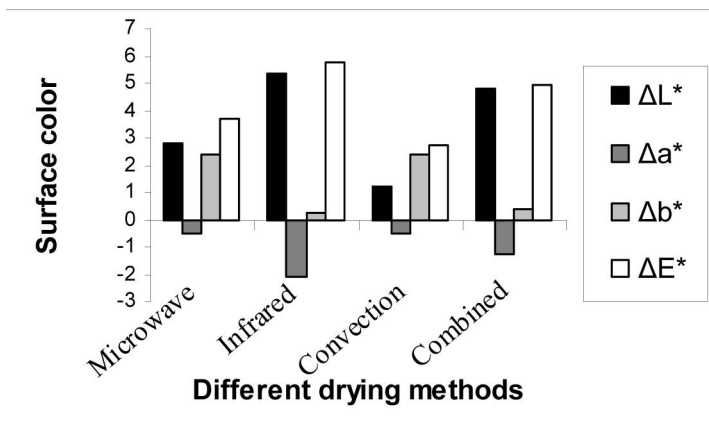


FIGURE 5.4 Surface color of Pine.

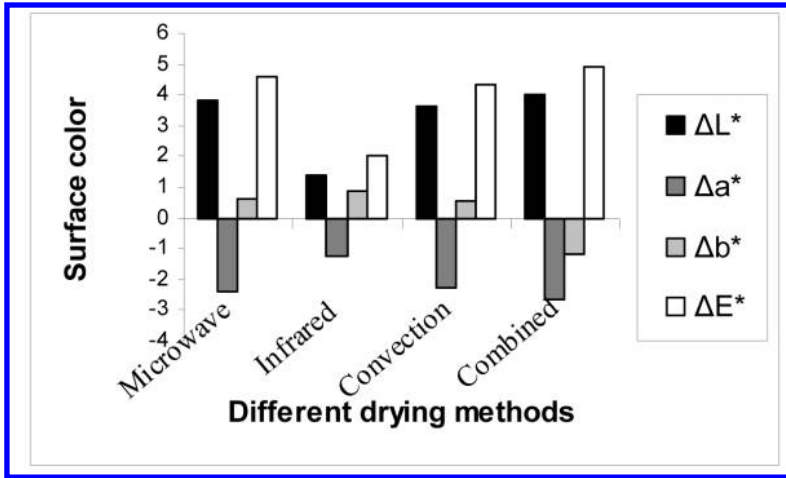


FIGURE 5.5 Surface color of spruce.

5.4 CONCLUSION

Results shows that Δa^* generally decreased but Δb^* increased for both pine and spruce wood samples except for spruce during combined heating. The lightness values ΔL^* increased during drying. The L^* of wood species such as tropical woods, which originally have dark color increases by exposure to light. This is due to the special species and climate condition of spruce and pines wood. Positive values of Δb^* indicate an increment of yellow color and negative values an increase of blue color. Negative values of Δa^* indicate a tendency of wood surface to greenish. A low ΔE^* corresponds to a low color change or a stable color. The biggest changes in color appeared in ΔE^* values of pine samples during infrared drying while for spruce it was reversed. Due to differences in composition of wood components, the color of fresh, untreated wood varies between different species, between different trees of the same species and even within a tree. Within a species wood color can vary due to the genetic factors and environmental conditions. In discoloration, chemical reactions take place in wood, changing the number and type of chromophores.

Discolorations caused by the drying process are those that actually occur during drying and are mainly caused by non-microbial factors. Many environmental factors such as solar radiation, moisture and temperature cause weathering or oxidative degradation of wooden products during

their normal use; these ambient phenomena can eventually change the chemical, physical, optical and mechanical properties of wood surfaces.

A number of studies have been conducted that have attempted to find a solution to kiln brown stain, the majority of them being pretreatment processes. Biological treatment, compression rolling, sap displacement and chemical inhibitors have all been used as pretreatments. In all cases these processes were successful in reducing or eliminating stain but were not considered economically viable. Vacuum drying and modified schedules have been tried as modified drying processes with only limited success. Within industry various schedules have been developed, though these are generally kept secret and it is difficult to gauge their success. Generally it seems that industry has adopted a post-drying process involving the mechanical removal of the kiln brown stain layer.

Microwave processing of materials is a relatively new technology that provides new approaches to improve the physical properties of materials. Microwave drying generate heat from within the grains by rapid movement of polar molecules causing molecular friction and help in faster and more uniform heating than does conventional heating. If wood is exposed to an electromagnetic field with such high frequency as is characteristic for microwaves, the water molecules, which are dipoles, begin to turn at the same frequency as the electromagnetic field. Wood is a complex composite material, which consists mainly of cellulose (40–45%), hemicelluloses (20–30%) and lignin (20–30%). These polymers are also polar molecules, and therefore even they are likely to be affected by the electromagnetic field. This could possibly cause degradation in terms wood hardness. For spruce the average of hardness is shown to be much higher than pine. From the experimental results it can be observed that in combined microwave dryer, the hardness was relatively improved in comparison to the other drying methods. Microwave and infrared drying can increase wood surface roughness while the smoothness of wood increases during convection and combined drying. The effect varies with the wood species. Thus this work suggests keeping the core temperature below the critical value until the wood has dried below fiber saturation as one way of ensuring that the dried wood is acceptably bright and light in color.

KEYWORDS

- **Electromagnetic field**
- **Eulerian based model**
- **High frequency**
- **Microwave**

REFERENCES

1. Incropera, F. P., & Dewitt, D. P. (1985). *Fundamentals of Heat and Mass Transfer*, second Ed., Wiley, New York.
2. Ghali, K., Jones, B., & Tracy, E. (1995). Modeling Heat and Mass Transfer in Fabrics, *Int. J. Heat Mass Transfer*, *38(1)*, 13–21.
3. Flory, P. J. (1969). *Statistical Mechanics of Chain Molecules*, Inter Science Pub., NY.
4. Hadley, G. R. (1984). Numerical Modeling of the Drying of Porous Materials, in *Proceedings of the Fourth International Drying Symposium, 1*, 151–158
5. Hong, K., Hollies, N. R. S., & Spivak, S. M. (1988). Dynamic Moisture Vapour Transfer through Textiles, Part I: Clothing Hygrometry and the Influence of Fiber Type, *Textile Res. J.* *58(12)*, 697–706.
6. Chen, C. S., & Johnson, W. H. (1969). Kinetics of Moisture Movement in Hygroscopic Materials, In: *Theoretical Considerations of Drying Phenomenon*, *Trans. ASAE, 12*, 109–113.
7. Barnes, J., & Holcombe, B. (1996). Moisture Sorption and Transport in Clothing during Wear, *Textile Res. J.* *66 (12)*, 777–786.
8. Chen, P., & Pei, D. A. (1988). Mathematical Models of Drying Process, *Int. J. Heat Mass Transfer* *31 (12)*, 2517–2562.
9. Davis, A., & James, D. (1996). Slow Flow through a Model Fibrous Porous Medium, *Int. J. Multiphase Flow*, *22*, 969–989.
10. Jirsak, O., Gok, T., Ozipek, B., & Pau, N. (1998). Comparing Dynamic and Static Methods for Measuring Thermal Conductive Properties of Textiles, *Textile Res. J.* *68(1)*, 47–56.
11. Kaviany, M. (1991). “Principles of Heat transfer in Porous Media,” Springer, New York.
12. Jackson, J., & James, D. (1986). The Permeability of Fibrous Porous Media, *Can. J. Chem. Eng.* *64*, 364–374.
13. Dietl, C., George, O. P., & Bansal, N. K. (1995). Modeling of Diffusion in Capillary Porous Materials During the Drying Process, *Drying Technol.*, *13 (1&2)*, 267–293.
14. Ea, J. Y. (1988). *Water Vapour Transfer in Breathable Fabrics for Clothing*, PhD thesis, University of Leeds.
15. Haghi, A. K. (2004). Moisture Permeation of Clothing, *JTAC*, *76*, 1035–1055.
16. Haghi, A. K. (2003). Thermal Analysis of Drying Process *JTAC*, *74*, 827–842.

17. Haghi, A. K. (2000). Some Aspects of Microwave Drying, The Annals of Stefan Cel Mare University, Year VII, (14), 22–25.
18. Haghi, A. K. (2000). A Thermal Imaging Technique for Measuring Transient Temperature Field an Experimental Approach, The Annals of Stefan Cel Mare University, Year VI, (12), 73–76.
19. Haghi, A. K. (2001). Experimental Investigations on Drying of Porous Media using Infrared Radiation, Acta Polytechnica, 41(1), 55–57.
20. Haghi, A. K. (2001). A Mathematical Model of the Drying Process, Acta Polytechnica, 41(3), 20–23.
21. Haghi, A. K. (2001). Simultaneous Moisture and Heat Transfer in Porous System, Journal of Computational and Applied Mechanics, 2(2), 195–204.
22. Haghi, A. K. (2002). A Detailed Study on Moisture Sorption of Hygroscopic Fiber, Journal of Theoretical and Applied Mechanics, 32(2) 47–62.
23. Dietl, C., George, O. P., & Bansal, N. K. (1995). Modeling of Diffusion in Capillary Porous Materials During the Drying Process, Drying Technol., 13 (1&2), 267–293.
24. Ea, J. Y. (1988). Water Vapour Transfer in Breathable Fabrics for Clothing, PhD thesis, University of Leeds.
25. Flory, P. J. (1969). Statistical Mechanics of Chain Molecules, Inter Science Pub., NY.
26. Walski, T. M., & Lutes, T. L. (1994). “Hydraulic Transients Cause Low-Pressure Problems,” Journal of the American Water Works Association, 75(2), 58.
27. Nigmatulin, R. I., Khabeev, N. S., & Nagiyev, F. B. (1981). Dynamics, Heat and Mass transfer of Vapor-Gas Bubbles in a liquid, Int. J. Heat Mass Transfer, 24(N6), Printed in Great Britain, 1033–1044.
28. Oron, D., Arazi, L., Kartoon, D., Rikanati, A., Alon, U., & Shvarts, D. (2001). “Dimensionality Dependences of the Rayleigh-Taylor & Richtmyer-Meshkov instability, late-time scaling laws,” Phys., Plasmas, 8, 2883p.
29. Parmakian, J. (1957). “Water hammer Design Criteria,” J. Power Div., ASCE, Sept., 456–460.
30. Parmakian, J. (1963). “Water hammer Analysis,” Dover Publications, Inc., New York, New York, 51–58.
31. Perry. R. H., Green, D. W., & Maloney, J. O. (1997). Perry’s Chemical Engineers Handbook, 7th Edition, McGraw-Hill, New York, 1–61.
32. Peng, X. F., & Peterson, G. P. (1996). Convective Heat Transfer and Flow Friction for Water Flow in Micro channel Structure, Int. J. Heat Mass Transfer, 36, 2599–2608.
33. Pickford, J. (1969). “Analysis of Surge,” MacMillan, London, 153–156.
34. Pipeline Design for Water and Wastewater, American Society of Civil Engineers, New York, (1975), 54p.
35. Qu, W., Mala, G. M., & Li, D. (1993). Heat Transfer for Water Flow in Trapezoidal Silicon Microchannels, 399–404.
36. Quick, R. S. (1933). “Comparison and Limitations of Various Water hammer Theories,” J. Hyd. Div., ASME, May, 43–45.
37. Rayleigh, (1917). On the Pressure developed in a Liquid during the collapse of a Spherical Cavity, Philos., Mag. Ser. 6, 34(N200), 94–98.
38. Ramaprabhu, P., & Andrews, M. J. (2004). “Experimental Investigation of Rayleigh-Taylor mixing at small Atwood numbers” J. Fluid Mech., 502, 233.
39. Rich, G. R. (1963). “Hydraulic Transients,” Dover, USA, 148–154.

40. Savic, D. A., & Walters, G. A. (1995). "Genetic Algorithms Techniques for Calibrating Network Models," Report No. 95/12, Centre for Systems and Control Engineering, 137–146.
41. Savic, D. A., & Walters, G. A. (1995). Genetic algorithms Techniques for Calibrating Network Models, University of Exeter, Exeter, United Kingdom, 41–77.
42. Shvarts, D., Oron, D., Kartoon, D., Rikanati, A., & Sadot O. (2000). "Scaling Laws of nonlinear Rayleigh-Taylor and Richtmyer-Meshkov instabilities in two and three dimensions," *C. R. Acad. Sci., Paris IV*, 719, 312p.
43. Sharp, B. (1981). "Water Hammer Problems and Solutions," Edward Arnold Ltd, London, 43–55.
44. Skousen, P. (1998). "Valve Handbook," McGraw Hill, New York, Hammer Theory and Practice, 687–721.
45. Song, C. C. et al. (1983). "Transient Mixed-Flow Models for Storm Sewers," *J. Hyd., Div. Nov.*, 109, 458–530.
46. Stephenson, D. (1984). "Pipe Flow Analysis," Elsevier, 19, S.A., 670–788.
47. Streeter, V. L., & Lai, C. (1962). "Water hammer Analysis Including Fluid Friction," *Journal of Hydraulics Division, ASCE*, 88, 79p.
48. Streeter, V. L., & Wylie, E. B. (1979). "Fluid Mechanics," McGraw-Hill Ltd., USA, 492–505.
49. Streeter, V. L., & Wylie, E. B. (1981). "Fluid Mechanics," McGraw-Hill Ltd., USA, 398–420.
50. Tijsseling, (1993). "Alan, E. Vardy, Time Scales and FSI in Unsteady Liquid-Filled Pipe Flow," 5–12.
51. Tuckerman, D. B., Pease, R. F. W. (1981). High Performance Heat Sinking for VLSI, *IEEE Electron device letter, DEL-2*, 126–129.
52. Tennekes, H., & Lumley, J. L. (1972). *A First Course in Turbulence*, the MIT Press, 410–466.
53. Thorley, A. R. D. (1991). "Fluid Transients in Pipeline Systems," D. and L. George, Herts, England, 231–242.
54. Tullis, J. P. (1971). "Control of Flow in Closed Conduits," Fort Collins, Colorado, 315–340.
55. Tuckerman, D. B. (1984). *Heat Transfer Microstructures for Integrated Circuits*, Ph.D. Thesis, Stanford University, 10–120.
56. Vallentine, H. R. (1965). "Rigid Water Column Theory for Uniform Gate Closure," *J. Hyd. Div. ASCE*, July, 55–243.
57. Waddell, J. T., Niederhaus, C. E., & Jacobs, J. W. (2001). "Experimental study of Rayleigh-Taylor instability: Low Atwood number Liquid Systems with single-mode initial perturbations," *Phys., Fluids 13*, 1263–1273.
58. Watters, G. Z. (1984). "Modern Analysis and Control of Unsteady Flow in Pipelines," *Ann Arbor Sci.*, 2nd Ed., 1098–1104.
59. Walski, T. M., & Lutes, T. L. (1994). "Hydraulic Transients Cause Low-Pressure Problems," *Journal of the American Water Works Association*, 75(2), 58.
60. Weber, S. V., Dimonte, G., & Marinak, M. M. (2003). "Arbitrary Lagrange-Eulerian code simulations of turbulent Rayleigh-Taylor instability in two and three dimensions," *Laser and Particle Beams*, 21, 455p.

61. Wood, D. J., Dorsch, R. G., & Lightener, C. (1966). "Wave-Plan Analysis of Unsteady Flow in Closed Conduits," *Journal of Hydraulics Division, ASCE*, 92, 83–110.
62. Wood, D. J., & Jones, S. E. (1973). "Water Hammer Charts For Various Types of Valves," *Journal of the Hydraulics Division, Proceedings of the American Society of Civil Engineers*, January, 167–178.
63. Wood, F. M. (1970). "History of Water Hammers," *Civil Engineering Research Report #65, Queens University, Canada*, 66–70.
64. Wu, Z. Y., & Simpson, A. R. (2001). Competent Genetic-Evolutionary Optimization of water Distribution Systems, *J. Comput., Civ. Eng.*, 15(2), 89–101.
65. Wylie, E. B., & Talpin, L. B. (1983). Matched Impedance to controls fluid transients, *Trans., ASME*, 105(2), 219–224.
66. Wylie, E. B., & Streeter, V. L. (1993). *Fluid Transients in systems*, Prentice-Hall, Engle wood Cliffs, New Jersey, 4.
67. Wylie, E. B., & Streeter, V. L. (1983). *Fluid Transients*, Feb Press, Ann Arbor, MI, 1982, corrected copy, 158p.
68. Wu, P. Y., & Little, W. A. (1983). Measurement of Friction Factor for flow of Gases in very Fine Channels used for Micro Miniature, Joule Thompson Refrigerators, *Cryogenics*, 24 (8), 273–277.
69. Xu, B., Ooi, K. T., Mavriplis, C., & Zaghoul, M. E., (2002). Viscous Dissipation Effects for Liquid Flow in Micro Channels, *Microsystems*, 53–57.
70. Young, Y. N., Tufo, H., Dubey, A., & Rosner, R. (2001). "On the Miscible Rayleigh-Taylor Instability Two and Three Dimensions," *J. Fluid Mech.*, 447, 377, 2003–2500.
71. Wood, D. J., Dorsch, R. G., & Lightener, C. (1966). "Wave-Plan Analysis of Unsteady Flow in Closed Conduits," *Journal of Hydraulics Division, ASCE*, 92, 83–110.
72. Wylie, E. B., & Streeter, V. L. (1993). *Fluid Transients in systems*, Prentice-Hall, Engle wood Cliffs, New Jersey, 4.
73. Brunone, B., Karney, B. W., Mecarelli, M., & Ferrante, M. (2000). "Velocity Profiles and unsteady pipe friction in Transient Flow," *Journal of Water Resources Planning and Management ASCE*, 126(4), July, 236–244.
74. Koelle, E., Jr. Luvizotto, E., & Andrade, J. P. G. (1996). "Personality Investigation of Hydraulic Networks using MOC–Method of Characteristics," *Proceedings of the 7th International Conference on Pressure Surges and Fluid Transients, Harrogate Durham, United Kingdom*, 1–8.
75. Filion, Y., & Karney, B. W. (2002). "A Numerical Exploration of Transient Decay Mechanisms in Water Distribution Systems," *Proceedings of the ASCE Environmental Water Resources Institute Conference, American Society of Civil Engineers, Roanoke, Virginia*, 30.
76. Hamam, M. A., & Mc Corquodale, J. A. (1982). "Transient Conditions in the Transition from Gravity to Surcharged Sewer Flow," *Canadian J. Civil Eng.*, Canada, Sep., 65–98.
77. Savic, D. A., & Walters, G. A. (1995). "Genetic Algorithms Techniques for Calibrating Network Models," *Report No. 95/12, Centre for Systems and Control Engineering*, 137–146.

CHAPTER 6

THREE DIMENSIONAL HEAT TRANSFER CHARACTERISTICS

CONTENTS

| | | |
|-----|----------------------------|-----|
| 6.1 | Introduction..... | 138 |
| 6.2 | Materials and Methods..... | 138 |
| 6.3 | Results..... | 145 |
| 6.4 | Conclusion | 152 |
| | Keywords | 152 |
| | References..... | 152 |

6.1 INTRODUCTION

Three dimensional heat transfer characteristics and pressure drop of water flow in a set of rectangular micro tubes were numerically investigated. A FV solver was employed to predict the temperature field for the conjugate heat transfer problem in both the solid and liquid regions in the micro channels. The full Navier-Stoke's approach was examined for this kind of narrow tubes for the pressure drop evaluations. The complete form of the energy equation with the dissipation terms was also linked to the momentum equations. The computed thermal characteristics and pressure drop showed good agreements with the experimental data. The effects of flow rate and channel geometry on the heat transfer capability and pressure drop of the system were also predicted.

6.2 MATERIALS AND METHODS

To design an effective micro tubes heat sink, fundamental understanding of the characteristics of heat transfer and fluid flow in micro channels are necessary. At the early stages, the designs and relations of macro scale fluid flow and heat transfer were employed. However, many experimental observations in micro channels deviate significantly from those in macro scale channels.

These disagreements were first observed by Tuckerman and Pease [18]. They demonstrated that micro rectangular passages have a higher heat transfer coefficient in laminar regimes in comparison with turbulent flow through macro scale channels. Therefore, they are capable of dissipating significant high heat fluxes.

Since, the regime of the flow has a noticeable influence on studying determination of heat dissipation rate; several researches have been conducted in this field. Wu and Little [19] measured the heat transfer characteristics for gas flows in miniature channels with inner diameter ranging from 134 μm to 164 μm . The tests involved both laminar and turbulent flow regimes. Their results showed that the turbulent convection occurs at Reynolds number of approximately 1000.

They also found that the convective heat transfer characteristics depart from the predictions of the established empirical correlations for the macro scale tubes. They attributed these deviations to the large asymmetric relative roughness of the micro channel walls. Harms et al. [20] tested a 2.5

cm long, 2.5 cm wide silicon heat sink having 251 μm wide and 1030 μm deep micro channels. A relatively low Reynolds number of 1500 marked transitions from laminar to turbulent flow which was attributed to a sharp inlet, relatively long entrance region, and channel surface roughness. They concluded the classical relation for Nusselt number was fairly accurate for modeling micro channel flows.

Fedrov and Viskanta [21] reported that the thermal resistance decreases with Reynolds number and reaches an asymptote at high Reynolds numbers.

Qu et al. [22] investigated heat transfer and flow characteristics in trapezoidal silicon micro tubes. In comparison, the measured friction factors were found to be higher than the numerical predictions. The difference was attributed to the wall roughness. Based on a roughness-viscosity model, they explained that the numerically predicted Nusselt numbers are smaller than the experimentally determined ones.

Choi et al. [23] measured the convective heat transfer coefficients for flow of nitrogen gas in micro tubes for both laminar and turbulent regimes. They found that the measured Nusselt number in laminar flow exhibits a Reynolds number dependence in contrast with the conventional prediction for the fully developed laminar flow, in which Nusselt number is constant.

Adam et al. [24] conducted single-phase flow studies in micro tubes using water as the working fluid. Two diameters of the circular micro tubes, namely 0.76 mm and 1.09 mm, were used in the investigation. It was found that the Nusselt numbers are larger than those encountered in microtubes. Peng and Peterson [25] investigated water flows in rectangular micro tubes with hydraulic diameters ranging from 0.133 to 0.336 mm. In laminar flows, it was found that the heat transfer depends on the aspect ratio and the ratio of the hydraulic diameter to the center-to-center distance of the micro channel.

Mala et al. [26] considered the electrical body forces resulting from the double layer field in the equations of motion. These effects are negligible in the macro scale as the dimensions of the electric double layer, EDL, is very small with respect to tube dimensions. They solved the Poisson-Boltzmann equation for the steady state flow. It was found that without the double layer a higher heat transfer rate is obtained. They proposed to consider the effects of the EDL on liquid flows and heat transfer in micro tubes to prevent the overestimation of the heat transfer capacity of the system. Xu et al. [27] investigated the effects of viscous dissipation on

the micro scale dimensions. They used a 2D micro tube and considered the viscous dissipation term in energy equation. The results show that this term plays a significant role in temperature, pressure and velocity distributions. Therefore, the relationships between the friction factor and the Reynolds number change when the hydraulic diameter of the micro tube is very small. The viscous dissipation effects are brought about by rises in the velocity gradient as hydraulic diameter reduces for a constant Reynolds number, a numerical study is conducted based on the experimental results of Tuckerman [28]. A FV method is used to solve the conjugate heat transfer through the heat sinks. The flow and heat transfer development regions inside the tubes are considered. The numerical results are then compared with the available experimental data. The effects of liquid velocity through channels and their effects on heat transfer and pressure drop along micro channels are investigated. Finally, the effects of aspect ratio on heat dissipation and pressure drop in micro tubes are predicted.

The characteristics of the model are depicted in Fig. 6.1. The width and thickness of micro channels are W_j and H_j , respectively. The thickness of the silicon substrate is H_2-H_1 ; and the total length of the micro channels is L . The heat supplies by a 1×1 cm heat source located at the entrance of the channels and were centered across the whole channel heat sink. A uniform heat flux of q is provided to heat the micro channels. The heat is removed by flowing water through channels. The inlet temperature of the cooling water is 20°C . The analysis is performed for five different cases in Figs. 6.1–6.9.

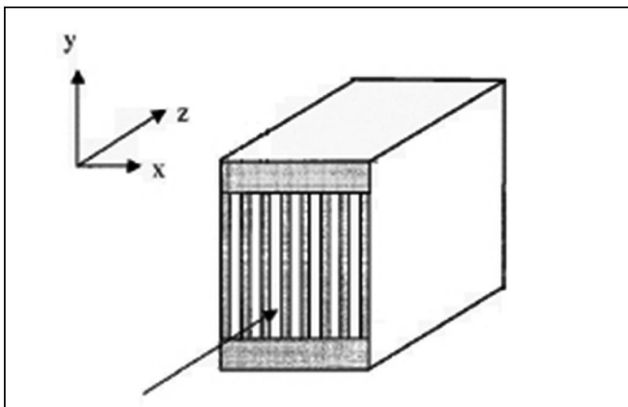


FIGURE 6.1 A sample micro tubes.

The dimensions related to each case are given in Table 6.1. By these dimensions; there will be 150 micro channels for cases 0 and 1 and 200 micro channels for cases 2, 3, and 4.

For the second section, case 2 was considered as the base geometry. The water velocity changed from 50 (cm/s) to 400 (cm/s).

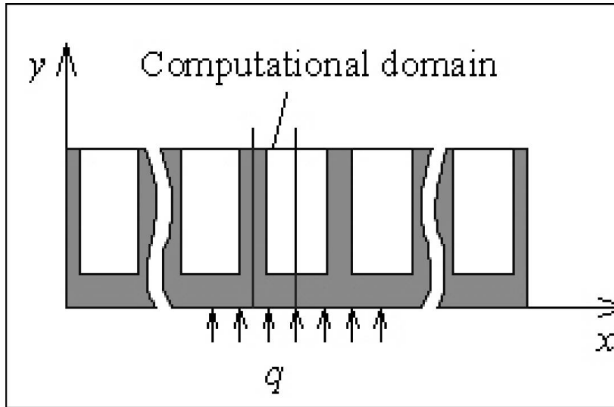
In the third section, the Tuckerman's geometries were solved by the unique Reynolds of 150. As performing a numerical method for the whole micro tubes heat sink is hard; a certain computational domain is considered (Fig. 6.2).

To prevent the various boundary condition effects, the computational domain is taken at the center of the heat sink to have the quoted uniform heat flux in Table 6.1. This is because there is very little spreading of heat towards the heat sinks. There is also some geometrical symmetry, which simplifies the computation. So only a semi channel and semi silicon substrate will be considered and the results will be the same for the other half. The whole substrate is made of silicon with thermal conductivity (k) of 148 (W/m. K). At the top of the channel $y = H_2$, there is a Pyrex plate to make an adiabatic condition (its thermal conductivity is two orders lower than silicon). There are two different boundary conditions at the bottom.

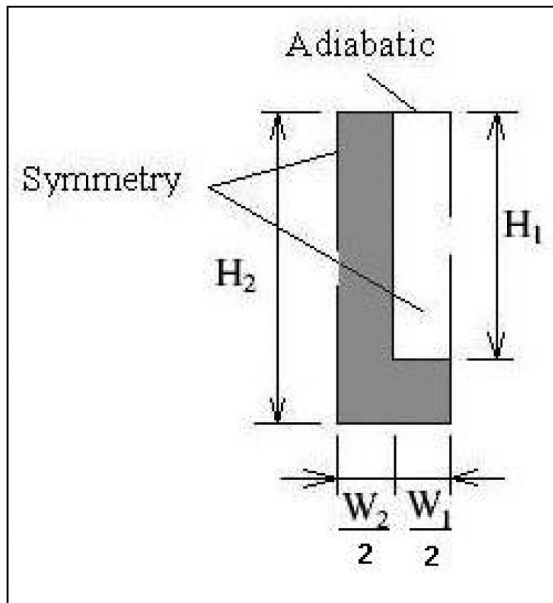
TABLE 6.1 Four Different Cases of Micro Channels

| | Case | | | | |
|-----------------------------------|-------|------|-----|-----|-----|
| | 0 | 1 | 2 | 3 | 4 |
| $L(\text{cm})$ | 2 | 2 | 1.4 | 1.4 | 1.4 |
| $W_1(\mu\text{m})$ | 64 | 64 | 56 | 55 | 50 |
| $W_2(\mu\text{m})$ | 36 | 36 | 44 | 45 | 50 |
| $H_1(\mu\text{m})$ | 280 | 280 | 320 | 287 | 302 |
| $H_2(\mu\text{m})$ | 489 | 489 | 533 | 430 | 458 |
| $\dot{Q}(\text{cm}^3 / \text{s})$ | 1.277 | 1.86 | 4.7 | 6.5 | 8.6 |
| $q(\text{W}/\text{cm}^2)$ | 34.6 | 34.6 | 181 | 277 | 790 |
| Number of channels | 150 | 150 | 200 | 200 | 200 |

For $z < L_h$ a uniform heat flux of q is imposed over the heat sink and the rest is assumed to be adiabatic. Water flows through the channel from the entrance in z direction.



(a)



(b)

FIGURE 6.2 Dimensions and computational domain.

The transverse velocities of the inlet are assumed to be zero. The axial velocity is considered to be evenly distributed through the whole channel. The velocities at the top and bottom of tubes are zero.

Several simplifying assumptions are incorporated before establishing the governing equations for the fluid flow and heat transfer in a unit cell:

1. Steady fluid flow and heat transfer;
2. Incompressible fluid;
3. Laminar flow;
4. Negligible radiative heat transfer; and
5. Constant solid and fluid properties;

In the last assumption the solid and liquid properties are assumed to be constant because of the small variations within the temperature range tested.

Based on the above assumptions, the governing differential equations and Nomenclatures used to describe the fluid flow and heat transfer in a unit cell are expressed as A = flow area, T = Temperature, c_p = Specific heat, T_{in} = inlet temperature, Dh = hydraulic diameter, T_{max} = maximum temperature, EDL = Electric Double Layer, w = velocity (z direction), H_1 = channel height, W_1 = channel width, H_2 = total height, W_2 = substrate width, k = thermal conductivity, L = heat sink length, Φ = viscous dissipation terms in energy equation, Lh = heated length, p = pressure, μ = viscosity, P = wetted perimeter, ρ = density, q = heat flux Subscripts, Q = total average volumetric flow rate, R = thermal resistance, in = inlet, Re = Reynolds number, max = maximum.

Continuity Equation

$$\frac{\partial w}{\partial z} = 0 \quad (1)$$

Momentum Equation

$$\rho \frac{\partial(w_i w_j)}{\partial z_j} = -\frac{\partial p}{\partial z_i} + \mu \frac{\partial}{\partial z_j} \left(\frac{\partial w_i}{\partial z_j} + \frac{\partial w_j}{\partial z_i} \right) - \frac{2}{3} \mu \frac{\partial}{\partial z_i} \left(\frac{\partial w_k}{\partial z_k} \right) \quad (2)$$

Energy Equation

$$\rho c_p \frac{\partial w_j T}{\partial z_j} = k \frac{\partial^2 T}{\partial x_j^2} + \mu \Phi \quad (3)$$

where

$$\Phi = 2 \left[\left(\frac{\partial u}{\partial x} \right)^2 + \left(\frac{\partial v}{\partial y} \right)^2 + \left(\frac{\partial w}{\partial z} \right)^2 \right] + \left(\frac{\partial u}{\partial y} + \frac{\partial v}{\partial x} \right)^2 + \left(\frac{\partial u}{\partial z} + \frac{\partial w}{\partial x} \right)^2 + \left(\frac{\partial v}{\partial z} + \frac{\partial w}{\partial y} \right)^2 \quad (4)$$

The finite volume method (FVM) is used to solve the continuity, momentum, and energy equations. A very brief description of the method used is given here.

In this method the domain is divided into a number of control volumes such that there is one control volume surrounding each grid point. The grid point is located in the center of a control volume. The governing equations are integrated over the individual control volumes to construct algebraic equations for the discrete dependent variables such as velocities, pressure, and temperature. The discretization equation then expresses the conservation principle for a finite control volume just as the partial differential equation expresses it for an infinitesimal control volume. In the present study, a solution is deemed converged when the mass imbalance in the continuity equation is less than 10^{-6} .

As the thermal specifications and flow characteristics are of the great importance in design of micro channel heat sinks, the results are concentrated in these fields.

For solving the equations several grid structures were used. The grid density of $120 \times 40 \times 20$ in z , y , and x directions is considered to be appropriate.

The thermal resistance is calculated as follows:

$$R(z) = \frac{T_{\max}(z) - T_{\text{in}}}{q} \quad (5)$$

In Eq. (5), $R(z)$, $T_{\max}(z)$, T_{in} and q the thermal resistance at $z(\text{cm})$ from the entrance, the inlet water temperature and the heat flux at the heating area.

In addition to thermal resistance, the Reynolds number is calculated as:

$$\text{Re} \equiv \frac{\rho w_{\text{ave}} D_h}{\mu} \quad (6)$$

where

$$D_h \equiv \frac{4A}{P} = \frac{2H_1W_1}{H_1 + W_1} \tag{7}$$

6.3 RESULTS

First, the temperature distribution, thermal resistances, and pressure drops based on the numerical results are demonstrated. Then the numerical results are compared with Tuckerman’s experiments data.

6.3.1 TEMPERATURE DISTRIBUTION AND THERMAL RESISTANCE

The temperature distributions at four x - y cross sections along the channel are shown in Fig. 6.3 for Case 0. The four sections, $z = 1, 3, 6, 9$ mm are all in the heated area. As all heat exchangers, isotherms are closest at the entrance of the channels. This means that heat transfer rate is the highest at the entrance and it decreases along the channel.

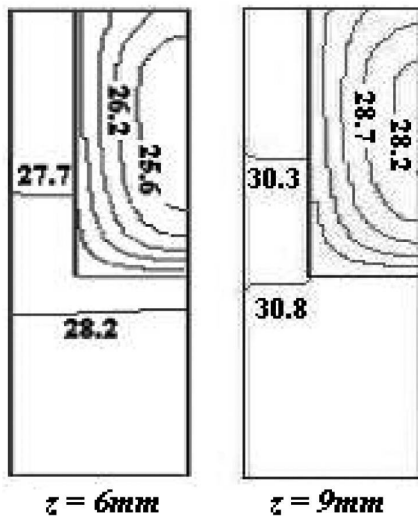


FIGURE 6.3 Temperature distribution along the tube for Case 0.

The thermal resistance along the tube is shown in Fig. 6.4 for cases 0 and 1. It can be seen that the thermal resistance has increased by increasing the z value and attained the maximum value at $z = 9$ mm. It is consistent with Tuckerman's experiments. It may be seen that the thermal resistance increased linearly through the channel except the entry region and near its peak. The sharper slopes in the experimental data of Fig. 6.4(a) and the numerical prediction in Fig. 6.4(b) are evidently due to the entrance region effects. So the flow may be considered thermally fully developed with a proper precision. The maximum thermal resistance is occurred in $z = 9$ mm, which is consistent with Tuckerman's experiments. For the other Cases the results are given in Table 6.2. The numerical values of resistances are predicted well.

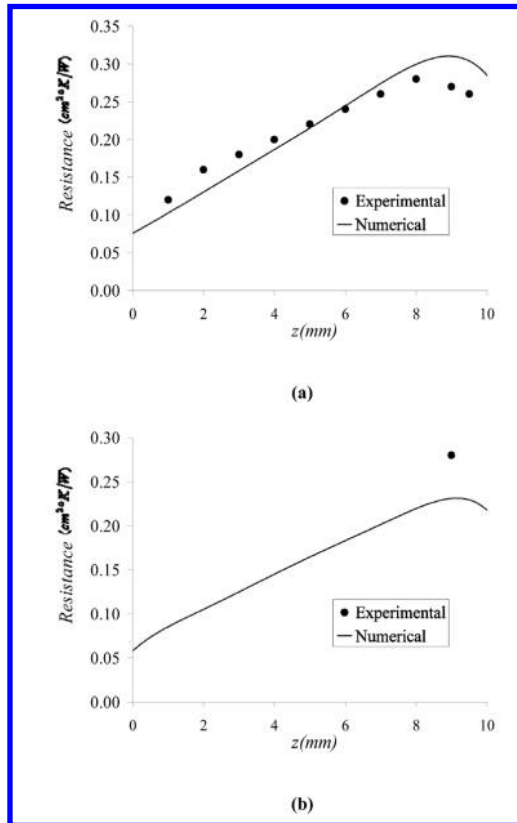


FIGURE 6.4. Numerical and experimental thermal resistances for: (a) Case 0, and (b) Case 1.

TABLE 6.2 Thermal Resistance Comparison

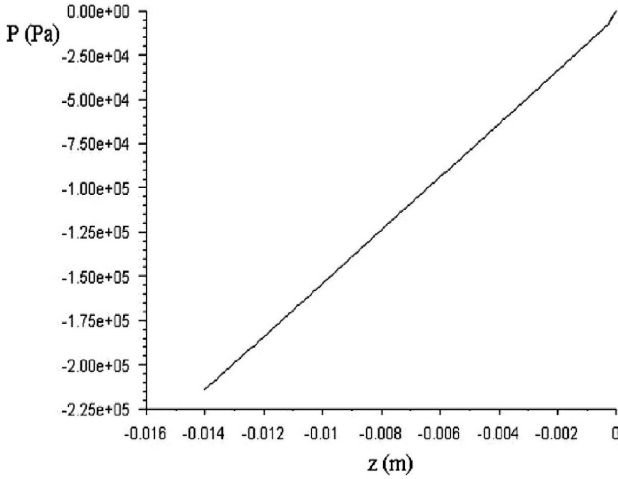
| Case | Re | R (cm ² K/W) | | Error (%) |
|------|------|-------------------------|-----------|-----------|
| | | Experimental | Numerical | |
| 0 | 34.6 | 0.277 | 0.253 | 5.8 |
| 1 | 34.6 | 0.280 | 0.246 | 12.1 |
| 2 | 181 | 0.110 | 0.116 | 5.0 |
| 3 | 277 | 0.113 | 0.101 | 8.1 |
| 4 | 790 | 0.090 | 0.086 | 3.94 |

6.3.2. PRESSURE DROP

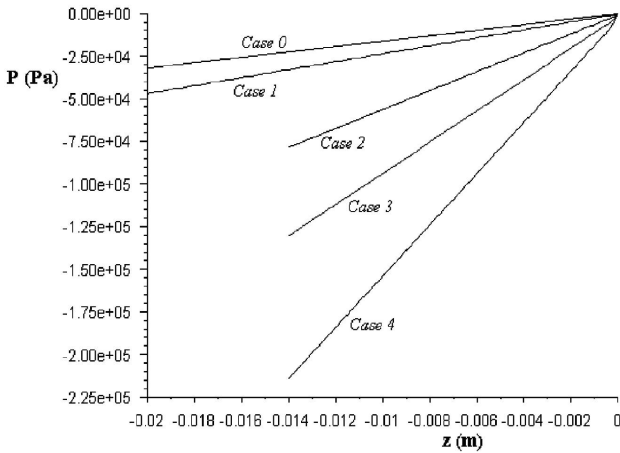
Pressure drop is linear along the channel. Figure 6.5(a) shows the pressure drop for Case 4. The pressure drop increases by increasing the inlet velocity. The slope of the pressure line in the entrance of the channel is maximum. This is due to the entry region effects. The velocity field will be fully developed after a small distance from the entrance. So the assumption of fully developed flow is acceptable. Figure 6.5(b) shows the pressure drop for all five cases. These amounts are tabulated in Table 6.3.

TABLE 6.3 Pressure Drop in Five Cases

| <i>Case</i> | <i>Pressure Drop (bar)</i> |
|-------------|----------------------------|
| 0 | 0.322 |
| 1 | 0.469 |
| 2 | 0.784 |
| 3 | 1.302 |
| 4 | 2.137 |



(a)



(b)

FIGURE 6.5 Pressure drop, (a) Case 4, (b) all cases.

The effects of velocity on the temperature rise and pressure drop in micro tubes are displayed in Figs. 6.6 and 6.7. The amount of heat dissipation increases by increasing the velocity. But it can be seen that the amount of decrease in temperature falls drastically by increase in velocity.

The following function can predict the temperature rise:

$$(T_{\max} - T_{in}) = 265.67w^{-0.4997} \tag{8}$$

The pressure drop is a linear function of velocity. The amounts of temperature rise and pressure drop are given in Table 6.4.

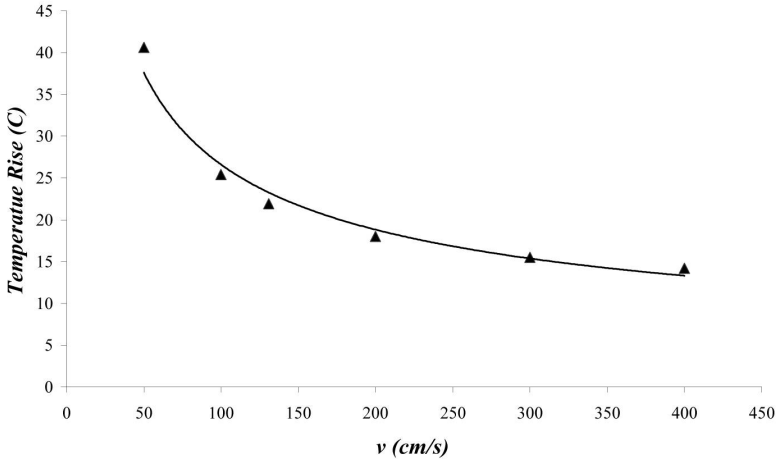


FIGURE 6.6 Temperature rise for different velocities.

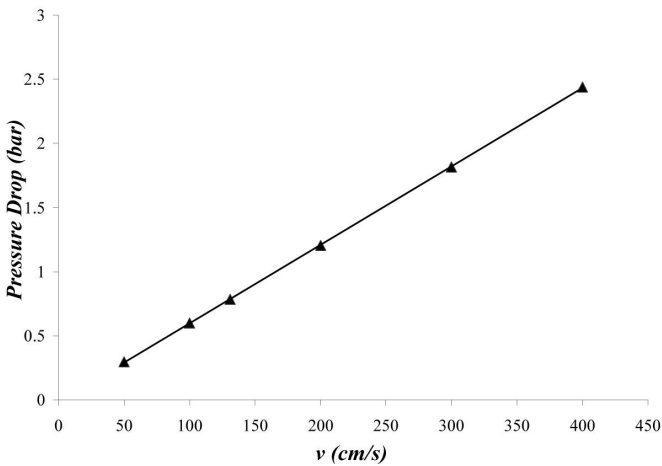


FIGURE 6.7 Pressure drop for different velocities.

TABLE 6.4 Temperature Rise and Pressure Drop for Section 2

| <i>Velocity (cm/s)</i> | <i>Re</i> | <i>Temp. Rise (°C)</i> | <i>Pressure Drop (bar)</i> |
|------------------------|-----------|------------------------|----------------------------|
| 50 | 47 | 40.6 | 0.298 |
| 100 | 95 | 25.4 | 0.598 |
| 131 | 124 | 21.9 | 0.784 |
| 200 | 190 | 18.0 | 1.206 |
| 300 | 285 | 15.5 | 1.817 |
| 400 | 380 | 14.2 | 2.439 |

Aspect ratio is an important factor in micro tube design. In this section the inlet heat flux of 181 (W/cm²) imposed over the heat sinks and the hydraulic diameter changes between 85.8 and 104.2. Figure 6.8 shows the maximum temperature of each case. It may be seen that with an identical heat flux the heat dissipation of the largest aspect ratio is the lowest. But this case has the minimum pressure drop too (Fig. 6.9). By increasing the amount of aspect ratio the ability of heat dissipation increases [28–104].

The amounts of temperature rise and temperature rise of all geometries are given in Table 6.5.

TABLE 6.5 Temperature Rise and Pressure Drop for Section 3

| <i>Case</i> | <i>Aspect Ratio</i> | <i>Hydraulic Diameter (μm)</i> | <i>Velocity (m/s)</i> | <i>Temp. Rise (°C)</i> | <i>Pressure Drop (bar)</i> |
|-------------|---------------------|--------------------------------|-----------------------|------------------------|----------------------------|
| 1 | 4.375 | 104.19 | 1.447 | 27.84 | 0.98 |
| 2 | 5.714 | 95.32 | 1.58 | 19.97 | 0.95 |
| 3 | 5.218 | 92.31 | 1.633 | 20.76 | 1.03 |
| 4 | 6.040 | 85.80 | 1.76 | 20.35 | 1.31 |

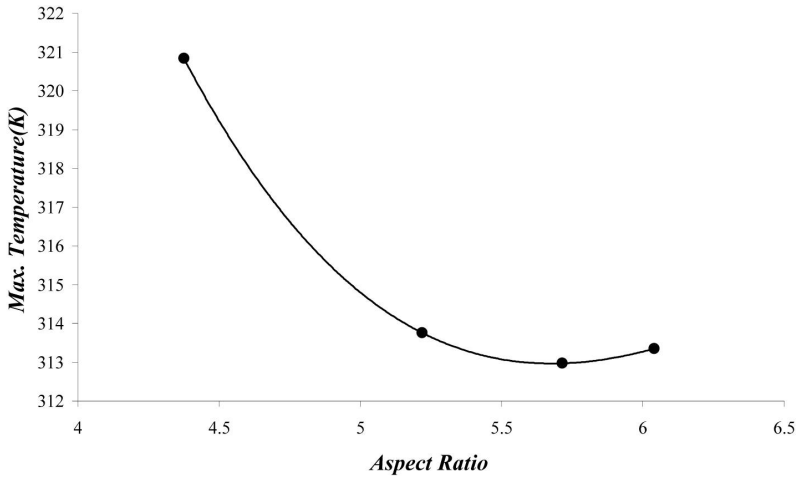


FIGURE 6.8 Temperature with respect to aspect ratio.

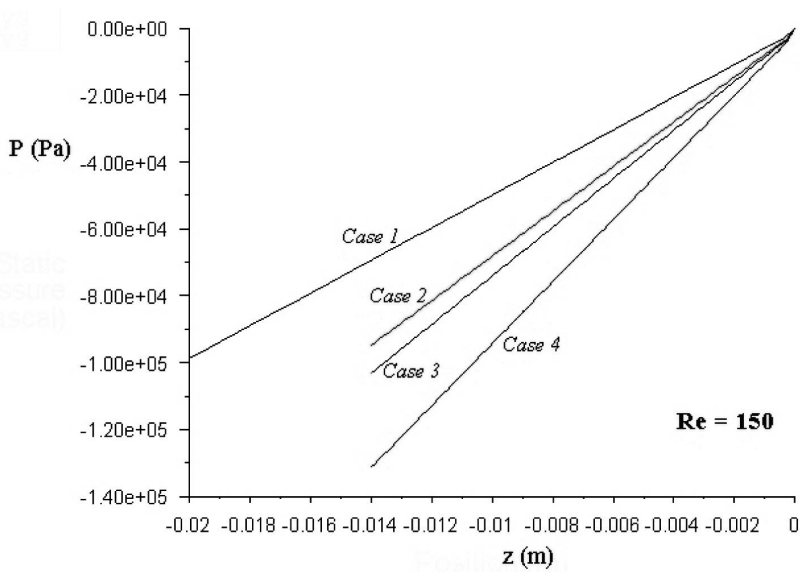


FIGURE 6.9 Pressure drops relating geometry in constant Reynolds of 150.

6.4 CONCLUSION

The third geometry has the minimum temperature rise. The temperature rise of second and fourth geometries are approximately alike. But the pressure drop of these two cases has a noticeable difference. The pressure drop increases with increase in aspect ratio.

KEYWORDS

- **Computational domain**
- **Micro channels**
- **Pressure drop**
- **Temperature rise**
- **Thermal resistance**

REFERENCES

1. Adams, T. M., Abdel-Khalik, S. I., Jeter, S. M., & Qureshi, Z. H. (1998). AN Experimental investigation of Single-Phase Forced Convection in Micro channels, *Int. J. Heat Mass Transfer*, *41*, 851–857.
2. Allievi, L. (1982). “General Theory of Pressure Variation in Pipes,” *Ann. D. Ing.*, 166–171.
3. Apoloniusz Kodura, & Katarzyna Weinerowska (2005). Some Aspects of Physical and Numerical Modeling of Water Hammer in Pipelines,” 126–132.
4. Anuchina, N. N., Volkov, V. I., Gordeychuk, V. A., Eskov, N. S., Ilyutina, O. S., & Kozzyrev, O. M. (2004). “Numerical Simulations of Rayleigh Taylor & Richtmyer Meshkov, instability using Mah-3 code,” *J. Comput., Appl. Math*, *168*, 11.
5. Bergeron, L. (1961). “Water Hammer in Hydraulics and Wave Surge in Electricity,” John Wiley and Sons, Inc., N.Y., 102–109.
6. Bergant Anton (1980). Discrete Vapour Cavity Model with Improved Timing of Opening and Collapse of Cavities, 1–11.
7. Bracco, A., Mc Williams, J. C., Murante, G., Provenzale, A., & Weiss, J. B. (2000). “Revisiting Freely Decaying Two-Dimensional Turbulence at Millennial Resolution,” *Phys., Fluids*, *12(11)*, 2931–2941.
8. Brunone, B., Karney, B. W., Mecarelli, M., & Ferrante, M. (2000). “Velocity Profiles and unsteady pipe friction in Transient Flow,” *Journal of Water Resources Planning and Management, ASCE*, *126(4)*, July, 236–244.

9. Cabot, W. H., Cook, A. W., Miller, L., Laney, D. E., Miller, M. C., & Childs, H. R. (2005). "Large Eddy Simulations of Rayleigh-Taylor Instability," *Phys. Fluids*, September, *17*, 91–106.
10. Cabot, W. (2006). University of California, Lawrence Livermore National Laboratory, Livermore, CA, *Physics of Fluids*, 94–550.
11. Chaudhry, M. H. (1979). "Applied Hydraulic Transients," Van Nostrand Reinhold Co., N.Y., 1322–1324.
12. Chaudhry, M. H., & Yevjevich, V. (1981). "Closed Conduit Flow," Water Resources Publication, USA, 255–278.
13. Chaudhry, M. H. (1987). "Applied Hydraulic Transient," Van Nostrand Reinhold, New York, USA, 165–167.
14. Clark, T. T. (2003). "A Numerical Study of the Statistics of a Two-Dimensional Rayleigh-Taylor Mixing Layer," *Phys., Fluids* *15*, 2413p.
15. Cook, A. W., Cabot, W., & Miller, L. (2004). "The mixing transition in Rayleigh-Taylor instability" *J. Fluid, Mech.*, *511*, 333p.
16. Choi, S. B., Barren, R. R., & Warrington, R. O. (1991). *Fluid Flow and Heat Transfer in Microtubes*, ASME DSC, *40*, 89–93.
17. Dimonte, G., Youngs, D., Dimits, A., Weber, S., & Marinak, M. (2004). "A Comparative Study of the Rayleigh-Taylor Instability using High-Resolution Three-Dimensional Numerical Simulations, The Alpha Group Collaboration," *Phys., Fluids* *16*, 1668.
18. Dimotakis, E. (2000). "The mixing transition in Turbulence" *J. Fluid, Mech.*, *409*, 69.
19. Elansari, A. S., Silva, W., & Chaudhry, M. H. (1994). "Numerical and Experimental Investigations of Transients Pipe flow" *Journal of Hydraulic Research*, *32*, 689.
20. Filion, Y., & Karney, B. W. (2002). "A Numerical Exploration of Transient Decay Mechanisms in Water Distribution Systems," Proceedings of the ASCE Environmental Water Resources Institute Conference, American Society of Civil Engineers, Roanoke, Virginia, 30.
21. Fok, A. (1978). "Design Charts for Air Chamber on Pump Pipelines," *J. Hyd. Div., ASCE*, Sept., 15–74.
22. Fok, A., Ashamalla, A., & Aldworth, G. (1978). "Considerations in Optimizing Air Chamber for Pumping Plants," Symposium on Fluid Transients and Acoustics in the Power Industry, San Francisco, USA, Dec., 112–114.
23. Fok, A. (1980). "Design Charts for Surge Tanks on Pump Discharge Lines," BHRA 3rd Int. Conference on Pressure Surges, Bedford, England, Mar., 23–34.
24. Fok, A. (1982). "Water Hammer and Its Protection in Pumping Systems," Hydro Technical Conference, CSCE, Edmonton, May, 45–55.
25. Fok, A. (1987). "A Contribution to the Analysis of Energy Losses in Transient Pipe Flow," PhD Thesis, University of Ottawa, 176–182.
26. Fox, J. A. (1977). "Hydraulic Analysis of Unsteady Flow in Pipe Network," Wiley, N.Y., 78–89.
27. Fedorov, A. G., & Viskanta, R. (2000). Three-dimensional Conjugate Heat Transfer into Microchannel Heat Sink for Electronic Packaging, *Int. J. Heat Mass Transfer*, *43*, 399–415.

28. Hamam, M. A., & Mc Corquodale, J. A. (1982). "Transient Conditions in the Transition from Gravity to Surcharged Sewer Flow," *Canadian, J. Civil Eng., Canada*, Sep., 65–98.
29. Harms, T. M., Kazmierczak, M. J., Cerner, F. M., Holke, A., Henderson, H. T., Pilchowski, H. T., & Baker, K. (1997). Experimental Investigation of Heat Transfer and Pressure Drop through Deep Micro channels in a (100) Silicon Substrate, in: *Proceedings of the ASME. Heat Transfer Division, HTD, 351*, 347–357.
30. Holland, F. A., & Bragg, R. (1995). *Fluid Flow for Chemical Engineers*, Edward Arnold Publishers, London, 1–3.
31. George, E., & Glimm, J. (2005). "Self-Similarity of Rayleigh-Taylor Mixing Rates," *Phys., Fluids, 17*, 054101, 1–3.
32. Goncharov, V. N. (2002). "Analytical Models of nonlinear, single-mode, Classical Rayleigh-Taylor instability at Arbitrary Atwood Numbers," *Phys., Rev. Letters, 88*, 134502, 10–15.
33. Ishii, M. (1975). *Thermo-Fluid Dynamic Theory of Two-Phase Flow*, Collection de, Liles, D. R. & Reed, W. H. "A Sern-Implicit Method for Two-Phase Fluid la Direction des Etudes et Recherché d'Electricite de France, 22 Dynamics," *Journal of Computational Physics 26*, Paris, 390–407.
34. JaimeSuárez, A. (2005). "Generalized Water Hammer Algorithm for Piping Systems with Unsteady Friction," 72–77.
35. Jaeger, C. (1977). "Fluid Transients in Hydro-Electric Engineering Practice," Blackie and Son Ltd, 87–88.
36. Joukowski, N. (1904). Paper to Polytechnic Soc., Moscow Spring of 1898, English Translation by Miss Simin, O., *Proc. AWWA*, 57–58.
37. Kodura, A., & Weinerowska, K. (2005). The Influence of the Local Pipeline Leak on Water Hammer Properties, Materials of the II Polish Congress of Environmental Engineering, Lublin, 125–133.
38. Kane, J., Arnett, D., Remington, B. A., Glendinning, S. G., & Baz'an, G. (2000). "Two-Dimensional Versus Three-Dimensional Supernova Hydrodynamic Instability Growth," *J. Astrophys., 528*–989.
39. Karassik, I. J. (2001). "Pump Handbook Third Edition," McGraw-Hill, 19–22.
40. Koelle, E., Jr. Luvizotto E., & Andrade, J. P. G. (1996). "Personality Investigation of Hydraulic Networks using MOC Method of Characteristics" *Proceedings of the 7th International Conference on Pressure Surges and Fluid Transients*, Harrogate Durham, United Kingdom, 1–8.
41. Kerr, S. L. (1949). "Minimizing Service Interruptions due to Transmission Line Failures Discussion," *Journal of the American Water Works Association, 41, 634*, July, 266–268.
42. Kerr, S. L. (1951). "Water Hammer Control," *Journal of the American Water Works Association, 43*, December, 985–999.
43. Kraichnan, R. H., & Montgomery, D. (1967). "Two-Dimensional Turbulence," *Rep. Prog., Phys., 43*, 547, 1417–1423.
44. Leon Arturo, S. (2007). "An Efficient Second-Order Accurate Shock-Capturing Scheme for Modeling One and Two-Phase Water Hammer Flows," PhD Thesis, March 29, 4–44.

45. Lee, T. S., & Pejovic, S. (1996). Air Influence on Similarity of Hydraulic Transients and Vibrations, *ASME J. Fluid Eng.*, *118(4)*, 706–709.
46. Li, J., & McCorquodale, A. (1999). “Modeling Mixed Flow in Storm Sewers,” *Journal of Hydraulic Engineering*, ASCE, *125(11)*, 1170–1180.
47. Mala, G., Li, D., & Dale, J. D. (1997). Heat Transfer and Fluid Flow in Micro channels, *J. Heat Transfer*, *40*, 3079–3088.
48. Miller, L., Cabot, W. H., & Cook, A. W. (2005). “Which way is up? A Fluid Dynamics Riddle,” *Phys., Fluids*, *17*, 091110, 1–26.
49. Minnaert, M. (1933). On Musical Air Bubbles and the Sounds of Running Water, *Phil. Mag.*, *16(7)*, 235–248.
50. Moeng, C. H., McWilliams, J. C., Rotunno, R., Sullivan, P., & Weil, J. (2004). “Investigating 2D Modeling of Atmospheric Convection in the PBL,” *J. Atm., Sci.* *61*, 889–903.
51. Moody, L. F. (1944). “Friction Factors for Pipe Flow,” *Trans. ASME*, *66*, 671–684.
52. Nagiyev, F. B. (1993). Dynamics, Heat and Mass Transfer of Vapor-Gas Bubbles in a Two-Component Liquid, Turkey-Azerbaijan petrol semin., Ankara, Turkey, 32–40.
53. Nagiyev, F. B. (1995). The Method of Creation Effective Coolness Liquids, Third Baku international Congress, Baku, Azerbaijan Republic, 19–22.
54. Neshan, H. (1985). Water Hammer, Pumps Iran Co. Tehran, Iran, 1–60.
55. Nigmatulin, R. I., Khabeev, N. S., & Nagiyev, F. B. (1981). Dynamics, Heat and Mass transfer of Vapor-Gas Bubbles in a Liquid, *Int. J. Heat Mass Transfer*, *24(N6)*, Printed in Great Britain, 1033–1044.
56. Oron, D., Arazi, L., Kartoon, D., Rikanati, A., Alon, U., & Shvarts, D. (2001). “Dimensionality Dependence of the Rayleigh-Taylor & Richtmyer-Meshkov instability, late-time scaling laws,” *Phys., Plasmas*, *8*, 2883.
57. Parmakian, J. (1957). “Water hammer Design Criteria,” *Journal of Power Div., ASCE*, Sept., 456–460.
58. Parmakian, J. (1963). “Water hammer Analysis,” Dover Publications, Inc., New York, New York, 51–58.
59. Perry, R. H., Green, D. W., & Maloney, J. O. (1997). *Perry’s Chemical Engineers Handbook*, 7th Edition, McGraw-Hill, New York, 1–61.
60. Peng, X. F., & Peterson, G. P. (1996). Convective Heat Transfer and Flow Friction for Water Flow in Microchannel Structure, *Int. J. Heat Mass Transfer*, *36*, 2599–2608.
61. Pickford, J. (1969). “Analysis of Surge,” MacMillan, London, 153–156.
62. *Pipeline Design for Water and Wastewater*, American Society of Civil Engineers, (1975), New York, 54.
63. Qu, W., Mala, G. M., & Li, D. (1993). Heat Transfer for Water Flow in Trapezoidal Silicon Micro channels, 399–404.
64. Quick, R. S. (1933). “Comparison and Limitations of Various Water hammer Theories,” *J. Hyd. Div., ASME*, May, 43–45.
65. Rayleigh, (1917). On the Pressure developed in a Liquid during the collapse of a Spherical Cavity, *Philos., Mag. Ser. 6*, *34(N200)*, 94–98.
66. Ramaprabhu, P., & Andrews, M. J. (2004). “Experimental Investigation of Rayleigh-Taylor mixing at small Atwood numbers” *J. Fluid Mech.*, *502*, 233.
67. Rich, G. R. (1963). “Hydraulic Transients,” Dover, USA, 148–154.

68. Savic, D. A., & Walters, G. A. (1995). "Genetic Algorithms Techniques for Calibrating Network Models," Report No. 95/12, Centre for Systems and Control Engineering, 137–146.
69. Savic, D. A., & Walters, G. A. (1995). Genetic algorithms Techniques for Calibrating Network Models, University of Exeter, Exeter, United Kingdom, 41–77.
70. Shvarts, D., Oron, D., Kartoon, D., Rikanati, A., & Sadot, O. (2000). "Scaling Laws of nonlinear Rayleigh-Taylor and Richtmyer-Meshkov instabilities in two and three dimensions," *C. R. Acad. Sci. Paris IV*, 719, 312.
71. Sharp, B. (1981). "Water Hammer Problems and Solutions," Edward Arnold Ltd, London, 43–55.
72. Skousen, (1998). "Valve Handbook," McGraw Hill, New York, Hammer Theory and Practice, 687–721.
73. Song, C. C. et al. (1983). "Transient Mixed-Flow Models for Storm Sewers," *J. Hyd. Div.*, Nov., 109, 458–530.
74. Stephenson, D. (1984). "Pipe Flow Analysis," Elsevier, 19, S.A., 670–788.
75. Streeter, V. L., & Lai, C. (1962). "Water hammer Analysis Including Fluid Friction," *Journal of Hydraulics Division, ASCE*, 88, 79.
76. Streeter, V. L., & Wylie, E. B. (1979). "Fluid Mechanics," McGraw-Hill Ltd., USA, 492–505.
77. Streeter, V. L., & Wylie, E. B. (1981). "Fluid Mechanics," McGraw-Hill Ltd., USA, 398–420.
78. Tijsseling, "Alan, E. Vardy, (1993). Time Scales and FSI in Unsteady Liquid-Filled Pipe Flow," 5–12.
79. Tuckerman, D. B., & Pease, R. F. W. (1981). High Performance Heat Sinking for VLSI, *IEEE Electron device letter, DEL-2*, 126–129.
80. Tennekes, H., & Lumley, J. L. (1972). *A First Course in Turbulence*, the MIT Press, 410–466.
81. Thorley, A. R. D. (1991). "Fluid Transients in Pipeline Systems," D. and, L. George, Herts, England, 231–242.
82. Tullis, J. P. (1971). "Control of Flow in Closed Conduits," Fort Collins, Colorado, 315–340.
83. Tuckerman, D. B. (1984). *Heat transfer Microstructures for Integrated Circuits*, Ph.D. Thesis, Stanford University, 10–120.
84. Vallentine, H. R. (1965). "Rigid Water Column Theory for Uniform Gate Closure," *J. Hyd. Div. ASCE*, July, 55–243.
85. Waddell, J. T., Niederhaus, C. E., & Jacobs, J. W. (2001). "Experimental Study of Rayleigh-Taylor instability, Low Atwood number Liquid Systems with Single-Mode Initial Perturbations," *Phys., Fluids*, 13, 1263–1273.
86. Watters, G. Z. (1984). "Modern Analysis and Control of Unsteady Flow in Pipelines," *Ann Arbor Sci.*, 2nd Ed., 1098–1104.
87. Walski, T. M., & Lutes, T. L. (1994). "Hydraulic Transients Cause Low-Pressure Problems," *Journal of the American Water Works Association*, 75(2), 58–160, Weber, S. V., Dimonte, G., & Marinak, M. M. (2003). "Arbitrary Lagrange-Eulerian code simulations of turbulent Rayleigh-Taylor instability in two and three dimensions," *Laser and Particle Beams*, 21, 455.

88. Wood, D. J., Dorsch, R. G., & Lightener, C. (1966). "Wave-Plan Analysis of Unsteady Flow in Closed Conduits," *Journal of Hydraulics Division, ASCE*, 92, 83–110.
89. Wood, D. J., & Jones, S. E. (1973). "Water hammer Charts for various types of Valves," *Journal of the Hydraulics Division, Proceedings of the American Society of Civil Engineers*, January, 167–178.
90. Wood, F. M. (1970). "History of Water Hammers," *Civil Engineering Research Report #65*, Queens University, Canada, 66–70.
91. Wu, Z. Y., & Simpson, A. R. (2001). Competent Genetic Evolutionary Optimization of water Distribution Systems, *J. Comput. Civ. Eng.*, 15(2), 89–101.
92. Wylie, E. B., & Talpin, L. B. (1983). Matched impedance to Control Fluid Transients, *Trans., ASME*, 105 (2), 219–224.
93. Wylie, E. B., & Streeter, V. L. (1993). *Fluid Transients in system*, Prentice-Hall, Englewood Cliffs, New Jersey, 4.
94. Wylie, E. B., & Streeter, V. L. (1983). *Fluid Transients*, Feb Press, Ann Arbor, MI, 1982, corrected copy, 158.
95. Wu, Y., & Little, W. A. (1983). Measurement of Friction Factor for Flow of Gases in Very Fine Channels Used for Micro Miniature, Joule Thompson refrigerators, *Cryogenics* 24(8), 273–277.
96. Xu, B., Ooi, K. T., Mavriplis, C., & Zaghoul, M. E. (2002). Viscous Dissipation Effects for Liquid Flow in Micro Channels, *Microsystems*, 53–57.
97. Young, Y. N., Tufo, H., Dubey, A., & Rosner, R. (2001). "On the Miscible Rayleigh-Taylor Instability Two and Three Dimensions," *J. Fluid Mech.*, 447, 377, 2003–2500.
98. Wood, D. J., Dorsch, R. G., & Lightener, C. (1966). "Wave-Plan Analysis of Unsteady Flow in Closed Conduits," *Journal of Hydraulics Division, ASCE*, 92, 83–110.
99. Wylie, E. B., & Streeter, V. L. (1993). *Fluid transients in system*, Prentice-Hall, Englewood Cliffs, New Jersey, 4.
100. Brunone, B., Karney, B. W., Mecarelli, M., & Ferrante, M. (2000). "Velocity Profiles and unsteady pipe friction in Transient Flow," *Journal of Water Resources Planning and Management, ASCE*, 126(4), July, 236–244.
101. Koelle, E., Jr. Luvizotto, E., & Andrade, J. P. G. (1996). "Personality Investigation of Hydraulic Networks using MOC Method of Characteristics" *Proceedings of the 7th International Conference on Pressure Surges and Fluid Transients*, Harrogate Durham, United Kingdom, 1–8.
102. Filion, Y., & Karney, B. W. (2002). "A Numerical Exploration of Transient Decay Mechanisms in Water Distribution Systems," *Proceedings of the ASCE Environmental Water Resources Institute Conference, American Society of Civil Engineers*, Roanoke, Virginia, 30.
103. Hamam, M. A., & Mc Corquodale, J. A. (1982). "Transient Conditions in the Transition from Gravity to Surcharged Sewer Flow," *Canadian, J. Civil Eng.*, Canada, Sep., 65–98.
104. Savic, D. A., & Walters, G. A. (1995). "Genetic Algorithms Techniques for Calibrating Network Models," *Report No. 95/12*, Centre for Systems and Control Engineering, 137–146.

CHAPTER 7

COMPUTATIONAL MODEL FOR HEAT FLOW PROCESS

CONTENTS

| | | |
|-----|----------------------------|-----|
| 7.1 | Introduction..... | 160 |
| 7.2 | Materials and Methods..... | 162 |
| 7.3 | Results..... | 172 |
| 7.4 | Conclusions..... | 179 |
| | Keywords | 179 |
| | References..... | 179 |

7.1 INTRODUCTION

When faced with a drying problem on an industrial scale, many factors have to be taken into account in selecting the most suitable type of dryer to install and the problem requires to be analyzed from several standpoints. Even an initial analysis of the possibilities must be backed up by pilot-scale tests unless previous experience has indicated the type most likely to be suitable. The accent today, due to high labor costs, is on continuously operating unit equipment, to what extent possible automatically controlled. In any event, the selection of a suitable dryer should be made in two stages, a preliminary selection based on the general nature of the problem and the textile material to be handled, followed by a final selection based on pilot-scale tests or previous experience combined with economic considerations.

A leather industry involves a crucial energy-intensive drying stage at the end of the process to remove moisture left from dye setting. Determining drying characteristics for leather, such as temperature levels, transition times, total drying times, and evaporation rates, is vitally important so as to optimize the drying stage. Meanwhile, a textile material undergoes some physical and chemical changes that can affect the final leather quality [1–11].

In considering a drying problem, it is important to establish at the earliest stage, the final or residual moisture content of the textile material, which can be accepted. This is important in many hygroscopic materials and if dried below certain moisture content they will absorb or “regain” moisture from the surrounding atmosphere depending upon its moisture and humidity. The material will establish a condition in equilibrium with this atmosphere and the moisture content of the material under this condition is termed the equilibrium moisture content. Equilibrium moisture content is not greatly affected at the lower end of the atmospheric scale but as this temperature increases the equilibrium moisture content figure decreases, which explains why materials can in fact be dried in the presence of superheated moisture vapor. Meanwhile, drying medium temperatures and humidities assume considerable importance in the operation of direct dryers [12–21].

It should be noted that two processes occur simultaneously during the thermal process of drying a wet leather material, namely, heat transfer in order to raise temperature of the wet leather and to evaporate its moisture

content together with mass transfer of moisture to the surface of the textile material and its evaporation from the surface to the surrounding atmosphere which, in convection dryers, is the drying medium. The quantity of air required to remove the moisture as liberated, as distinct from the quantity of air which will release the required amount of heat through a drop in its temperature in the course of drying, however, has to be determined from the known capacity of air to pick up moisture at a given temperature in relation to its initial content of moisture. For most practical purposes, moisture is in the form of water vapor but the same principles apply, with different values and humidity charts, for other volatile components [22–31].

Thermal Drying consumes from 9–25% of national industrial energy consumption in the developed countries. In order to reduce net energy consumption in the drying operation there are attractive alternatives for drying of heat sensitive materials. Leather industry involves a crucial energy-intensive drying stage to remove the moisture left. Synthetic leather drying is the removal of the organic solvent and water. Determining drying characteristics for leathers is vitally important so as to optimize the drying stage. This chapter describes a way to determine the drying characteristics of leather with analytical method developed for this purpose. The model presented, is based on fundamental heat and mass transfer equations. Altering air velocity varies drying conditions. The work indicates closest agreement with the theoretical model. The results from the parametric study provide a better understanding of the drying mechanisms and may lead to a series of recommendations for drying optimization. Among the many processes that are performed in the leather industry, drying has an essential role: by this means, leathers can acquire their final texture, consistency and flexibility. However, some of the unit operations involved in leather industry, especially the drying process is still based on empiricism and tradition, with very little use of scientific principles. Widespread methods of leather drying all over the world are mostly convective methods requiring a lot of energy. Specific heat energy consumption increases, especially in the last period of the drying process, when the moisture content of the leather approaches the value at which the product is storable. However, optimizing the drying process using mathematical analysis of temperature and moisture distribution in the material can reduce energy consumption in a convective dryer. Thus, development of a suitable mathematical

model to predict the accurate performance of the dryer is important for energy conservation in the drying process [32–40].

The manufacturing of new-generation synthetic leathers involves the extraction of the filling polymer from the polymer-matrix system with an organic solvent and the removal of the solvent from the highly porous material. In this chapter, a mathematical model of synthetic leather drying for removing the organic solvent is proposed. The model proposed adequately describes the real processes. To improve the accuracy of calculated moisture distributions a velocity correction factor (VCF) introduced into the calculations. The VCF reflects the fact that some of the air flowing through the bed does not participate very effectively in drying, since it is channeled into low-density areas of the inhomogeneous bed. This chapter discusses the results of experiments to test the deductions that increased rates of drying and better agreement between predicted and experimental moisture distributions in the drying bed can be obtained by using higher air velocities.

This chapter focuses on reviewing convective heat and mass transfer equations in the industrial leather drying process with particular reference to VCF [41–51].

7.2 MATERIALS AND METHODS

The theoretical model (the Eqs. (1)–(42)) proposed in this model is based on fundamental equations to describe the simultaneous heat and mass transfer in porous media. It is possible to assume the existence of a thermodynamic quasi equilibrium state, where the temperatures of gaseous, liquid and solid phases are equal, that is,

$$T_s = T_L = T_G = T \quad (1)$$

LIQUID MASS BALANCE:

$$\frac{\partial(\varepsilon_L \rho_L)}{\partial t} + \nabla(\rho_L \bar{u}_L) + \dot{m} = 0 \quad (2)$$

WATER VAPOR MASS BALANCE:

$$\frac{\partial[(\varepsilon - \varepsilon_L)X_V \rho_G]}{\partial t} + \nabla(X_V \rho_G \bar{u}_G + \bar{J}_V) - \dot{m} = 0 \quad (3)$$

$$\bar{J}_V = -\rho_G(\varepsilon - \varepsilon_L)D_{EFF} \nabla X_V \quad (4)$$

AIR MASS BALANCE:

$$\frac{\partial((\varepsilon - \varepsilon_L)X_A \rho_G)}{\partial t} + \nabla(X_A \rho_G \bar{u}_G - \bar{J}_V) = 0 \quad (5)$$

LIQUID MOMENTUM EQUATION (DARCY'S LAW):

$$\bar{u}_L = -\left(\frac{\alpha_G}{\mu_G}\right) \nabla(P_G) \quad (6)$$

THERMAL BALANCE:

The thermal balance is governed by Eq. (7).

$$\frac{\partial\left\{\left[\rho_S C_{p_S} + (\varepsilon - \varepsilon_L)\rho_G(X_V C_{p_V} + X_A C_{p_A}) + \varepsilon_L \rho_L C_{p_L}\right]T\right\}}{\partial t} - \nabla(k_E \nabla T) + \nabla\left[\left(\rho_L \bar{u}_L C_{p_L} + \rho_G \bar{u}_G(X_V C_{p_V} + X_A C_{p_A})\right)T\right] + (\varepsilon - \varepsilon_L)\frac{\partial P_G}{\partial t} + \dot{m}\Delta H_V = 0 \quad (7)$$

THERMODYNAMIC EQUILIBRIUM-VAPOR MASS FRACTION:

In order to attain thermal equilibrium between the liquid and vapor phase, the vapor mass fraction should be such that the partial pressure of the

vapor (P'_v) should be equal to its saturation pressure (P_{vs}) at temperature of the mixture. Therefore, thermodynamic relations can obtain the concentration of vapor in the air/vapor mixture inside the pores. According to Dalton's Law of Additive Pressure applied to the air/vapor mixture, one can show that:

$$\rho_G = \rho_v + \rho_A \quad (8)$$

$$X_v = \frac{\rho_v}{\rho_G} \quad (9)$$

$$\rho_v = \frac{P'}{R_v T} \quad (10)$$

$$\rho_A = \frac{(P_G - P'_v)}{R_A T} \quad (11)$$

Combining Eqs. (8)–(11), one can obtain:

$$X_v = \frac{1}{1 + \left(\frac{P_G R_v}{P'_v R_A} \right) - \left(\frac{R_v}{R_A} \right)} \quad (12)$$

MASS RATE OF EVAPORATION:

The mass rate of evaporation was obtained in two different ways, as follows:

First of all, the mass rate of evaporation m was expressed explicitly by taking it from the water vapor mass balance (the Eq. (2)), since vapor concentration is given by Eq. (12).

$$\dot{m} = \frac{\partial [(\varepsilon - \varepsilon_L) X_v \rho_G]}{\partial t} + \nabla \cdot (X_v \rho_G \bar{u}_G + \bar{J}_v) \quad (13)$$

Secondly, an equation to compute the mass rate of evaporation can be derived with a combination of the liquid mass balance (the Eq. (1)) with a first-order-Arrhenius type equation. From the general kinetic equation:

$$\frac{\partial \alpha}{\partial t} = -kf(\alpha) \quad (14)$$

$$k = A \exp\left(-\frac{E}{RT_{SUR}}\right) \quad (15)$$

$$\alpha = 1 - \frac{\varepsilon_L(t)}{\varepsilon_0} \quad (16)$$

DRYING KINETICS MECHANISM COUPLING:

Using thermodynamic relations, according to Amagat's law of additive volumes, under the same absolute pressure,

$$m_A = \frac{V_A P_G}{R_A T} \quad (17)$$

$$m_A = \frac{V_A P_G}{R_A T} \quad (18)$$

$$m_T = m_V + m_A \quad (19)$$

$$m_T = m_V + m_A \quad (20)$$

$$V_G = V_V + V_A \quad (21)$$

$$V_G = (\varepsilon - \varepsilon_L) V_S \quad (22)$$

Solving the set of algebraic (the Eqs. (17)–(22)), one can obtain the vapor-air mixture density:

$$\rho_G = \frac{(m_V + m_A)}{V_G} \quad (23)$$

$$\rho_A = \frac{m_A}{V_G} \quad (24)$$

$$\rho_A = \frac{m_A}{V_G} \quad (25)$$

EQUIVALENT THERMAL CONDUCTIVITY:

It is necessary to determine the equivalent value of the thermal conductivity of the material as a whole, since no phase separation was considered in the overall energy equation. The equation we can propose now which may be used to achieve the equivalent thermal conductivity of materials K_E , composed of a continued medium with a uniform disperse phase. It is expressed as follows in Eq. (26).

$$K_E = \left[\frac{k_S + \varepsilon_L k_L \left(\frac{3k_S}{2k_S + k_L} \right) + k_G (\varepsilon - \varepsilon_L) \left(\frac{3k_S}{2k_S + k_G} \right)}{1 + \varepsilon_L \left(\frac{3k_S}{2k_S + k_L} \right) + (\varepsilon - \varepsilon_L) \left(\frac{3k_S}{2k_S + k_G} \right)} \right] \quad (26)$$

$$k_G = X_V k_V + X_A k_A \quad (27)$$

EFFECTIVE DIFFUSION COEFFICIENT EQUATION:

The binary bulk diffusivity D_{AV} of air-water vapor mixture is given by:

$$D_{AV} = (2.20)(10^{-5}) \left(\frac{P_{ATM}}{P_G} \right) \left(\frac{T_{REF}}{273.15} \right)^{1.75} \quad (28)$$

Factor α_F can be used to account for closed pores resulting from different nature of the solid, which would increase gas outflow resistance, so the equation of effective diffusion coefficient D_{EFF} for fiber drying is:

$$D_{EFF} = \alpha_F D_{AV} \quad (29)$$

The convective heat transfer coefficient can be expressed as:

$$h = Nu_{\delta} \left(\frac{k}{\delta} \right) \quad (30)$$

The convective mass transfer coefficient is:

$$h_M = \left(\frac{h}{C_{PG}} \right) \left(\frac{Pr}{Sc} \right)^{2/3} \quad (31)$$

$$Pr = \frac{C_{PG} \mu_G}{k_G} \quad (32)$$

$$Sc = \frac{\mu_G}{\rho_G D_{AV}} \quad (33)$$

The deriving force determining the rate of mass transfer inside the fiber is the difference between the relative humidities of the air in the pores and the fiber. The rate of moisture exchange is assumed to be proportional to the relative humidity difference in this study.

The heat transfer coefficient between external air and fibers surface can be obtained by: $h = Nu_{\delta} \left(\frac{k}{\delta} \right)$.

The mass transfer coefficient was calculated using the analogy between heat transfer and mass transfer as $h_M = \left(\frac{h}{C_{PG}} \right) \left(\frac{Pr}{Sc} \right)^{2/3}$. The convective heat and mass transfer coefficients at the surface are important parameters in drying processes; they are functions of velocity and physical properties of the drying medium.

Describing kinetic model of the moisture transfer during drying as follows:

$$-\frac{dX}{dt} = k(X - X_e) \quad (34)$$

Where, X is the material moisture content (dry basis) during drying (kg water/kg dry solids), X_e is the equilibrium moisture content of dehydrated material (kg water/kg dry solids), k is the drying rate (min^{-1}), and t is the time of drying (min). The drying rate is determined as the slope of the

falling rate-drying curve. At zero time, the moisture content (dry basis) of the dry material X (kg water/kg dry solids) is equal to X_i , and Eq. (34) is integrated to give the following expression:

$$X = X_e - (X_e - X_i)e^{-kt} \quad (35)$$

Using above equation Moisture Ratio can be defined as follows:

$$\frac{X - X_e}{X_i - X_e} = e^{-kt} \quad (36)$$

This is the Lewis's formula introduced in 1921. But using experimental data of leather drying, there was an error in curve fitting of e^{-at} .

The experimental moisture content data were non-dimensionlized using the equation:

$$MR = \frac{X - X_e}{X_i - X_e} \quad (37)$$

where MR is the moisture ratio. For the analysis it was assumed that the equilibrium moisture content, X_e , was equal to zero.

Selected drying models, detailed in Table 7.1, were fitted to the drying curves (MR versus time), and the equation parameters determined using nonlinear least squares regression analysis, as shown in Table 7.2.

TABLE 7.1 Drying Models Fitted to Experimental Data

| Model | Mathematical Expression |
|--|--------------------------------|
| Lewis (1921) | $MR = \exp(-at)$ |
| Page (1949) | $MR = \exp(-at^b)$ |
| Henderson and Pabis (1961) | $MR = a \exp(-bt)$ |
| Quadratic function | $MR = a + bt + ct^2$ |
| Logarithmic (Yaldiz and Eterkin, 2001) | $MR = a \exp(-bt) + c$ |
| 3rd. Degree Polynomial | $MR = a + bt + ct^2 + dt^3$ |

TABLE 7.1 (Continued)

| Model | Mathematical Expression |
|-------------------|---|
| Rational function | $MR = \frac{a + bt}{1 + ct + dt^2}$ |
| Gaussian model | $MR = a \exp\left(\frac{-(t-b)^2}{2c^2}\right)$ |
| Present model | $MR = a \exp(-bt^c) + dt^2 + et + f$ |

TABLE 7.2 Estimated Values of Coefficients and Statistical Analysis for the Drying Models

| Model | Constants | T = 50 | T = 65 | T = 80 |
|--------------------|-----------|--------------|--------------|-------------|
| Lewis | a | 0.08498756 | 0.1842355 | 0.29379817 |
| | S | 0.0551863 | 0.0739872 | 0.0874382 |
| | r | 0.9828561 | 0.9717071 | 0.9587434 |
| Page | a | 0.033576322 | 0.076535988 | 0.14847589 |
| | b | 1.3586728 | 1.4803604 | 1.5155253 |
| | S | 0.0145866 | 0.0242914 | 0.0548030 |
| | r | 0.9988528 | 0.9972042 | 0.9856112 |
| Henderson | a | 1.1581161 | 1.2871764 | 1.4922171 |
| | b | 0.098218605 | 0.23327801 | 0.42348755 |
| | S | 0.0336756 | 0.0305064 | 0.0186881 |
| | r | 0.9938704 | 0.9955870 | 0.9983375 |
| Logarithmic | a | 1.246574 | 1.3051319 | 1.5060514 |
| | b | 0.069812589 | 0.1847816 | 0.43995186 |
| | c | -0.15769402 | -0.093918118 | 0.011449769 |
| | S | 0.0091395 | 0.0117237 | 0.0188223 |
| | r | 0.9995659 | 0.9993995 | 0.9985010 |
| Quadratic function | a | 1.0441166 | 1.1058544 | 1.1259588 |
| | b | -0.068310663 | -0.16107942 | -0.25732004 |
| | c | 0.0011451149 | 0.0059365371 | 0.014678241 |
| | S | 0.0093261 | 0.0208566 | 0.0673518 |

TABLE 7.2 (Continued)

| Model | Constants | T= 50 | T= 65 | T= 80 |
|-------------------------------|-----------|------------------|------------------|------------------|
| 3rd. Degree Polynomial | r | 0.9995480 | 0.9980984 | 0.9806334 |
| | a | 1.065983 | 1.1670135 | 1.3629748 |
| | b | -0.076140508 | -0.20070291 | -0.45309695 |
| | c | 0.0017663191 | 0.011932525 | 0.053746805 |
| | d | -1.335923e-005 | -0.0002498328 | -0.0021704758 |
| Rational function | S | 0.0061268 | 0.0122273 | 0.0320439 |
| | r | 0.9998122 | 0.9994013 | 0.9961941 |
| | a | 1.0578859 | 1.192437 | 1.9302135 |
| | b | -0.034944627 | -0.083776453 | -0.16891461 |
| | c | 0.03197939 | 0.11153663 | 0.72602847 |
| Gaussian model | d | 0.0020339684 | 0.01062793 | 0.040207428 |
| | S | 0.0074582 | 0.0128250 | 0.0105552 |
| | r | 0.9997216 | 0.9993413 | 0.9995877 |
| | a | 1.6081505 | 2.3960741 | 268.28939 |
| | b | -14.535231 | -9.3358707 | -27.36335 |
| Present model | c | 15.612089 | 7.7188252 | 8.4574493 |
| | S | 0.0104355 | 0.0158495 | 0.0251066 |
| | r | 0.9994340 | 0.9989023 | 0.9973314 |
| | a | 0.77015136 | 2.2899114 | 4.2572457 |
| | b | 0.073835826 | 0.58912095 | 1.4688178 |
| | c | 0.85093985 | 0.21252159 | 0.39672164 |
| | d | 0.00068710356 | 0.0035759092 | 0.0019698297 |
| | e | -0.037543605 | -0.094581302 | -0.03351435 |
| | f | 0.3191907 | -0.18402789 | 0.04912732 |
| | S | 0.0061386 | 0.0066831 | 0.0092957 |
| | r | 0.9998259 | 0.9998537 | 0.9997716 |

The experimental results for the drying of leather are given in Fig. 7.7. Fitting curves for two sample models (Lewis model and present model) and temperature of 80 °C are given in Figs. 7.8 and 7.9. Two criteria were adopted to evaluate the goodness of fit of each model, the Correlation Coefficient (r) and the Standard Error (S). The standard error of the estimate is defined as follows:

$$S = \sqrt{\frac{\sum_{i=1}^{n_{points}} (MR_{exp,i} - MR_{pred,i})^2}{n_{points} - n_{param}}} \tag{38}$$

where $MR_{exp,i}$ is the measured value at point i , and $MR_{pred,i}$ is the predicted value at that point, and n_{param} is the number of parameters in the particular model (so that the denominator is the number of degrees of freedom).

To explain the meaning of correlation coefficient, we must define some terms used as follow:

$$S_t = \sum_{i=1}^{n_{points}} (\bar{y} - MR_{exp,i})^2 \tag{39}$$

Where, the average of the data points (\bar{y}) is simply given by

$$\bar{y} = \frac{1}{n_{points}} \sum_{i=1}^{n_{points}} MR_{exp,i} \tag{40}$$

The quantity S_t considers the spread around a constant line (the mean) as opposed to the spread around the regression model. This is the uncertainty of the dependent variable prior to regression. We also define the deviation from the fitting curve as:

$$S_r = \sum_{i=1}^{n_{points}} (MR_{exp,i} - MR_{pred,i})^2 \tag{41}$$

Note the similarity of this expression to the standard error of the estimate given above; this quantity likewise measures the spread of the points around the fitting function. In view of the above, the improvement (or error reduction) due to describing the data in terms of a regression model can be quantified by subtracting the two quantities [52–78]. Because the

magnitude of the quantity is dependent on the scale of the data, this difference is normalized to yield

$$r = \sqrt{\frac{S_t - S_r}{S_t}} \quad (42)$$

where, r is defined as the correlation coefficient. As the regression model better describes the data, the correlation coefficient will approach unity. For a perfect fit, the standard error of the estimate will approach $S = 0$ and the correlation coefficient will approach $r = 1$.

The standard error and correlation coefficient values of all models are given in Figs. 7.10 and 7.11.

7.3 RESULTS

Synthetic leathers are materials with much varied physical properties (Figs. 7.1–7.11). As a consequence, even though a lot of research of simulation of drying of porous media has been carried out, the complete validation of these models are very difficult. The drying mechanisms might strongly influence by parameters such as permeability and effective diffusion coefficients. The unknown effective diffusion coefficient of vapor for fibers under different temperatures may be determined by adjustment of the model's theoretical alpha correction factor and experimental data. The mathematical model can be used to predict the effects of many parameters on the temperature variation of the fibers. These parameters include the operation conditions of the dryer, such as the initial moisture content of the fibers, heat, and mass transfer coefficients, drying air moisture content, and dryer air temperature. From Figs. 7.1–7.6, it can be observed that the shapes of the experimental and calculated curves are somewhat different. It can be seen that as the actual air velocity used in this experiment increases, the value of VCF necessary to achieve reasonable correspondence between calculation and experiment becomes closer to unity; that is, a smaller correction to air velocity is required in the calculations as the actual air velocity increases. This appears to confirm the fact that the loss in drying efficiency caused by bed in homogeneity tends to be reduced as air velocity increases. Figure 7.7 shows a typical heat distribution during convective drying. Table 7.3 relates the VCF to the values of air velocity actually used in the experiments. It is evident from the table that the results

show a steady improvement in agreement between experiment and calculation (as indicated by increase in VCF) for air velocities up to 1.59 m/s, above which to be no further improvement with increased flow.

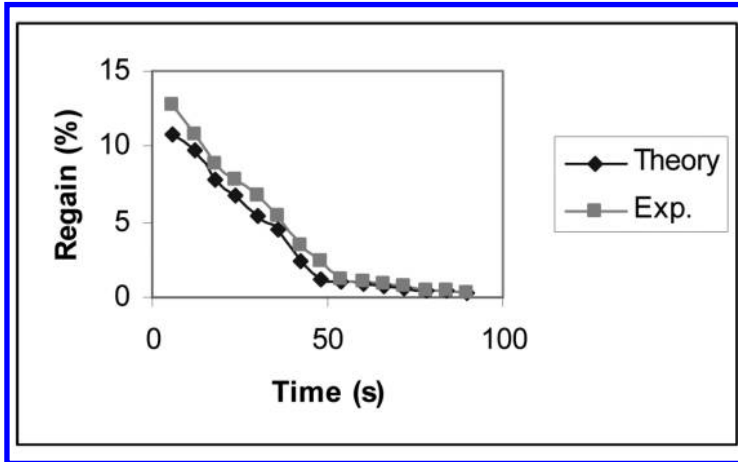


FIGURE 7.1 Comparison of the theoretical and experimental Distribution at air velocity of 0.75 m/s and VCF = 0.39.

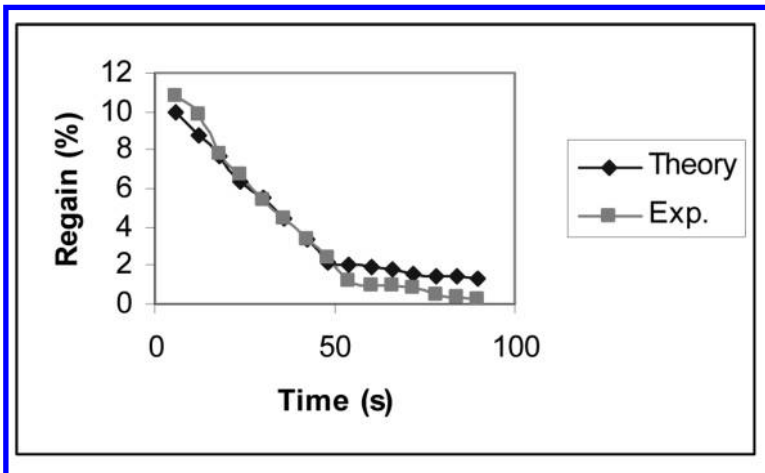


FIGURE 7.2 Comparison of the theoretical and experimental Distribution at air velocity of 0.89 m/s and VCF = 0.44.

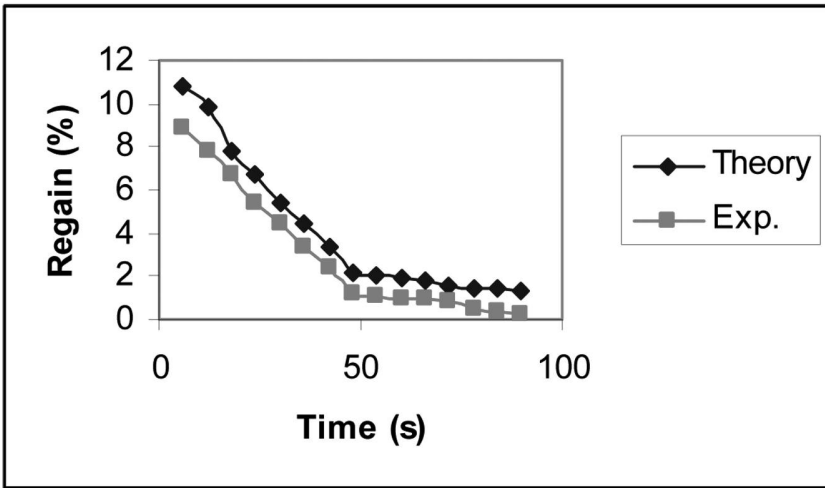


FIGURE 7.3 Comparison of the theoretical and experimental Distribution at air velocity of 0.95 m/s and VCF = 0.47.

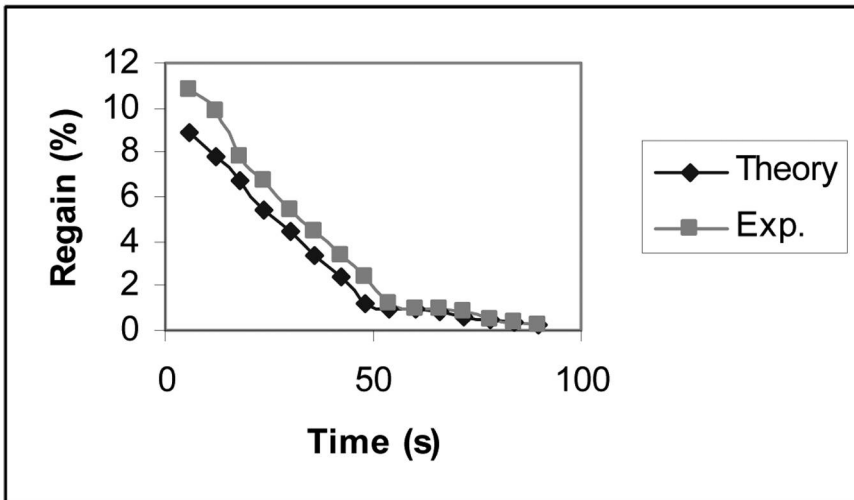


FIGURE 7.4 Comparison of the theoretical and experimental Distribution at air velocity of 1.59 m/s and VCF = 0.62.

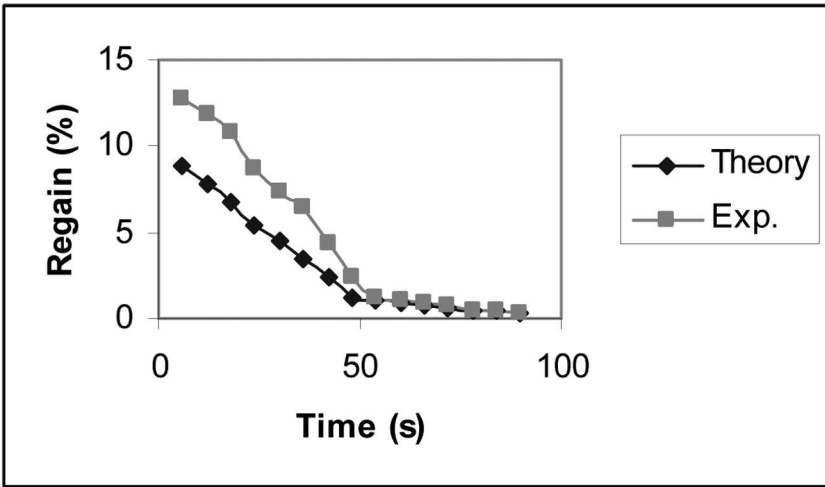


FIGURE 7.5 Comparison of the theoretical and experimental Distribution at air velocity of 2.10 m/s and VCF = 0.62.

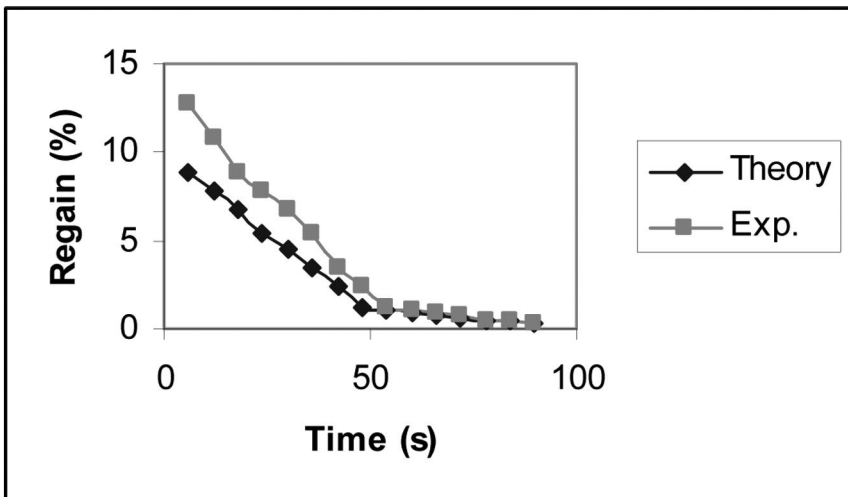


FIGURE 7.6 Comparison of the theoretical and experimental Distribution at air velocity of 2.59 m/s and VCF = 0.61.

TABLE 7.3 Variation of VCF with Air Velocity

| | | | | | | |
|-------------------|------|------|------|------|------|------|
| Air velocity, m/s | 0.75 | 0.89 | 0.95 | 1.59 | 2.10 | 2.59 |
| VCF used | 0.39 | 0.44 | 0.47 | 0.62 | 0.62 | 0.61 |

In this work, the analytical model has been applied to several drying experiments. The results of the experiments and corresponding calculated distributions are shown in Figs. 7.7–7.11. It is apparent from the curves that the calculated distribution is in reasonable agreement with the corresponding experimental one. In view of the above, it can be clearly observed that the shapes of experimental and calculated curves are somewhat similar.

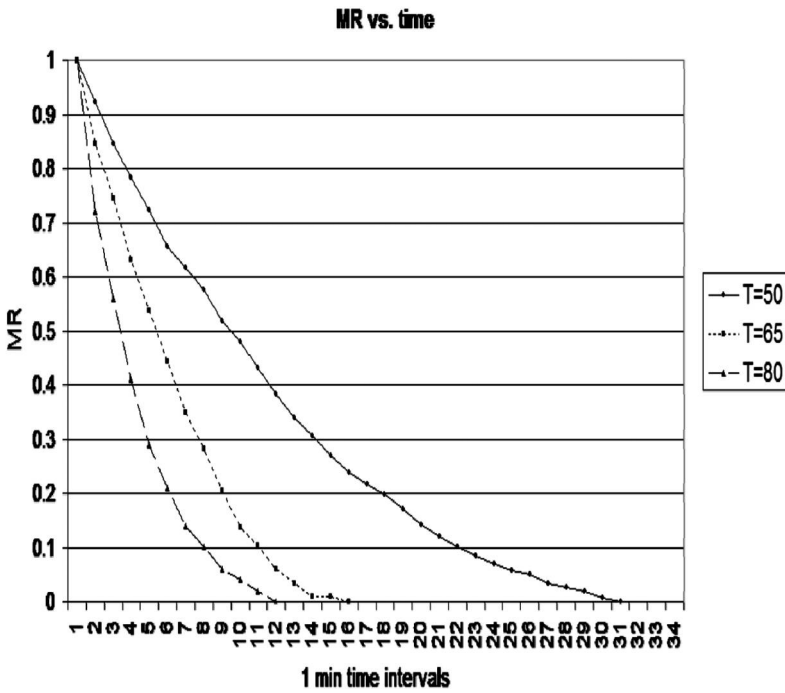


FIGURE 7.7 Moisture Ratio vs. time.

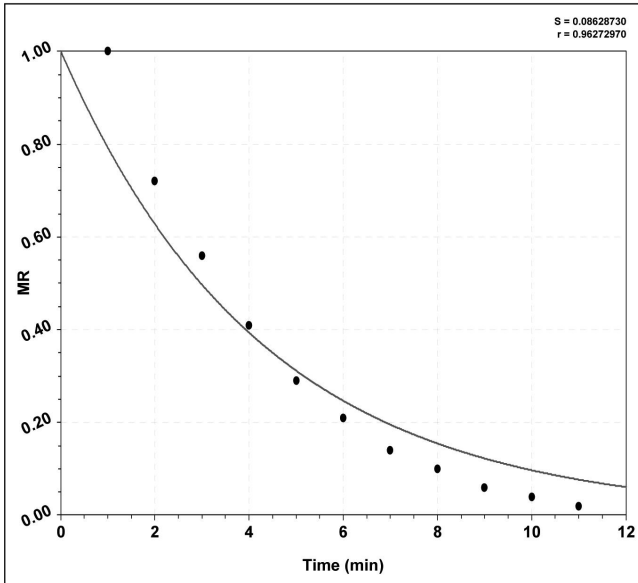


FIGURE 7.8 Lewis model.

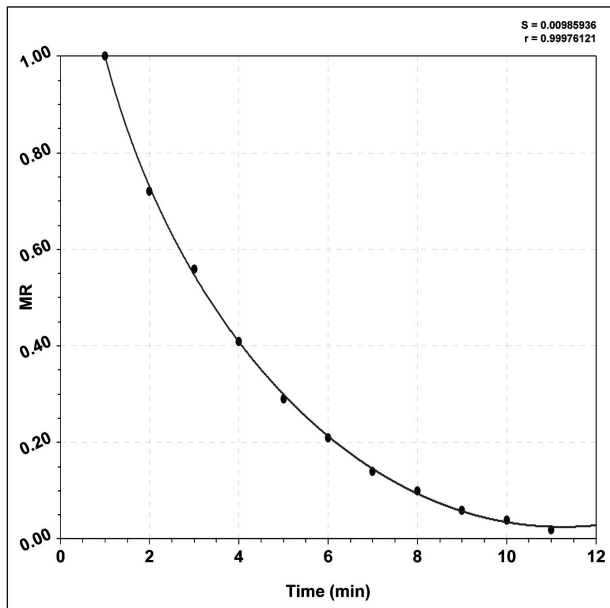


FIGURE 7.9 Present model.

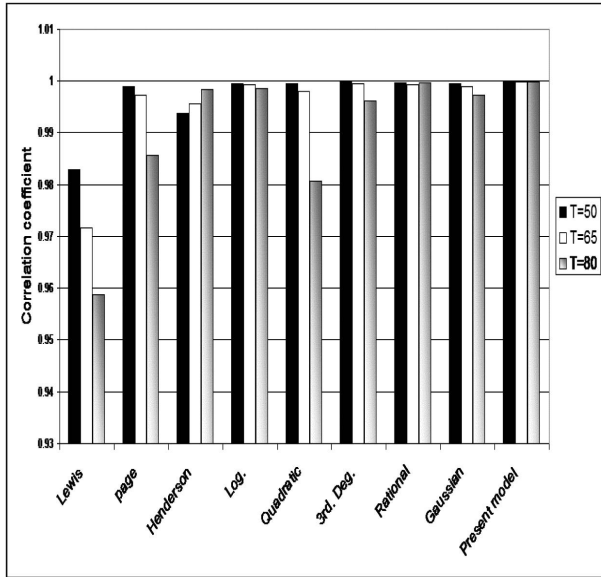


FIGURE 7.10 Correlation coefficient of all models.

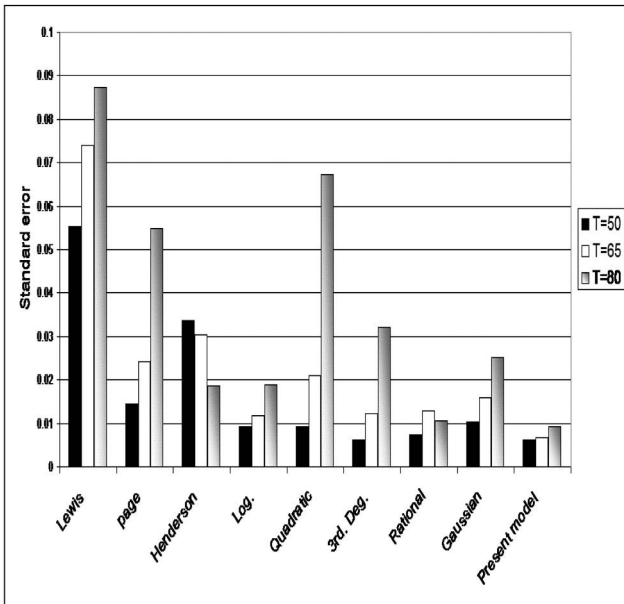


FIGURE 7.11 Standard error of all models.

7.4 CONCLUSIONS

In the model presented in this chapter, a simple method of predicting moisture distributions leads to prediction of drying times more rapid than those measured in experiments. From this point of view, the drying reveals many aspects which are not normally observed or measured and which may be of value in some application.

The derivation of the drying curves is an example. It is clear from the experiments over a range of air velocities that it is not possible to make accurate predictions and have the experimental curves coincide at all points with the predicted distributions simply by introducing a VCF into the calculations. This suggests that a close agreement between calculated and experimental curves over the entire drying period could be obtained by using a large value of VCF in the initial stages of drying and progressively decreasing it as drying proceeds.

KEYWORDS

- **Drying process**
- **Pilot-scale**
- **Statistical analysis**
- **Textile material**
- **Vapor concentration**
- **Vapor mass balance**

REFERENCES

1. Harms, T. M., Kazmierczak, M. J., Cerner, F. M., Holke A., Henderson, H. T., Pilchowski, H. T., & Baker, K. (1997). Experimental Investigation of Heat Transfer and Pressure Drop through Deep Micro channels in a (100) Silicon Substrate, in: Proceedings of the ASME. Heat Transfer Division, HTD, 351, 347–357.
2. Holland, F. A., & Bragg, R. (1995). Fluid Flow for Chemical Engineers, Edward Arnold Publishers, London, 1–3.
3. George, E., & Glimm, J. (2005). “Self-similarity of Rayleigh-Taylor Mixing Rates,” Phys., Fluids, 17, 054101, 1–3.

4. Goncharov, V. N. (2002). "Analytical Model of Nonlinear, Single-Mode, Classical Rayleigh-Taylor Instability at Arbitrary Atwood Numbers," *Phys. Rev. Letters*, *88*, 134502, 10–15.
5. Ishii, M. (1975). Thermo-Fluid Dynamic Theory of Two-Phase Flow, Collection de Liles, D. R., & Reed, W. H. "A Sern-Implicit Method for Two-Phase Fluid la Direction des Etudes et Recherché d' Electricite de France, *22*, Dynamics," *Journal of Computational Physics*, *26*, Paris, 390–407.
6. Chen, C. S., & Johnson, W. H. (1969). Kinetics of Moisture Movement in Hygroscopic Materials, In: *Theoretical Considerations of Drying Phenomenon*, Trans. ASAE, *12*, 109–113.
7. Barnes, J., & Holcombe, B. (1996). Moisture Sorption and Transport in Clothing during Wear, *Textile Res. J.* *66*(12), 777–786.
8. Chen, P., & Pei, D. (1988). A Mathematical Models of Drying process *Int. J. Heat Mass Transfer*, *31*(12), 2517–2562.
9. Davis, A., & James, D. (1996). Slow Flow Through a Model Fibrous Porous Medium, *Int. J. Multiphase Flow* *22*, 969–989.
10. Jirsak, O., Gok, T., Ozipek, B., & Pau, N. (1998). Comparing Dynamic and Static Methods for Measuring Thermal Conductive Properties of Textiles, *Textile Res. J.* *68*(1), 47–56.
11. Kaviany, M. (1991). "Principles of Heat Transfer in Porous Media," Springer, New York.
12. Jackson, J., & James, D. (1986). The Permeability of Fibrous Porous Media, *Can. J. Chem. Eng.* *64*, 364–374.
13. Dietl, C., George, O. P., & Bansal, N. K. (1995). Modeling of Diffusion in Capillary Porous Materials During the Drying Process, *Drying Technol.*, *13*(1&2), 267–293.
14. Ea, J. Y. (1988). Water Vapour Transfer in Breathable Fabrics for Clothing, PhD thesis, University of Leeds.
15. Haghi, A. K. (2004). Moisture Permeation of Clothing, *JTAC*, *76*, 1035–1055.
16. Haghi, A. K. (2003). Thermal Analysis of Drying Process *JTAC*, *74*, 827–842.
17. Haghi, A. K. (2000). Some Aspects of Microwave Drying, *The Annals of Stefan cel Mare University*, Year VII, (14), 22–25.
18. Haghi, A. K. (2000). A Thermal Imaging Technique for Measuring Transient Temperature Field an Experimental Approach, *The Annals of Stefan cel Mare University*, Year VI, (12), 73–76.
19. Haghi, A. K. (2001). Experimental Investigations on Drying of Porous Media using Infrared Radiation, *Acta Polytechnica*, *41*(1), 55–57.
20. Haghi, A. K. (2001). A Mathematical Model of the Drying Process, *Acta Polytechnica*, *41*(3) 20–23.
21. Haghi, A. K. (2001). Simultaneous Moisture and Heat Transfer in Porous System, *Journal of Computational and Applied Mechanics*, *2*(2), 195–204.
22. Haghi, A. K. (2002). A Detailed Study on Moisture Sorption of Hygroscopic Fiber, *Journal of Theoretical and Applied Mechanics*, *32*(2), 47–62.
23. Dietl, C., George, O. P., & Bansal, N. K. (1995). Modeling of Diffusion in Capillary Porous Materials During the Drying Process, *Drying Technol.*, *13*(1&2), 267–293.
24. Ea, J. Y. (1988). Water Vapour Transfer in Breathable Fabrics for Clothing, PhD thesis, University of Leeds,

25. Flory, P. J. (1969). *Statistical Mechanics of Chain Molecules*, Interscience Pub., New York.
26. Walski, T. M., & Lutes, T. L. (1994). "Hydraulic Transients Cause Low-Pressure Problems," *Journal of the American Water Works Association*, 75(2), 58.
27. Nigmatulin, R. I., Khabeev, N. S., & Nagiyev, F. B. (1981). Dynamics, Heat and Mass Transfer of Vapor-Gas Bubbles in a Liquid, *Int. J. Heat Mass Transfer*, 24(N6), Printed in Great Britain, 1033–1044.
28. Oron, D., Arazi, L., Kartoon, D., Rikanati, A., Alon, U., & Shvarts, D. (2001). "Dimensionality dependence of the Rayleigh-Taylor & Richtmyer Meshkov instability, late-time scaling laws," *Phys., Plasmas*, 8, 2883p.
29. Parmakian, J. (1957). "Water hammer Design Criteria," *J. Power Div., ASCE*, Sept., 456–460.
30. Parmakian, J. (1963). "Water Hammer Analysis," Dover Publications, Inc., New York, New York, 51–58.
31. Perry, R. H., Green, D. W., & Maloney, J. O. (1997). *Perry's Chemical Engineers Handbook*, 7th Edition, McGraw-Hill, New York, 1–61.
32. Peng, X. F., & Peterson, G. P. (1996). Convective Heat Transfer and Flow Friction for Water Flow in Microchannel Structure, *Int. J. Heat Mass Transfer*, 36, 2599–2608.
33. Pickford, J. (1969). "Analysis of Surge," MacMillan, London, 153–156.
34. *Pipeline Design for Water and Wastewater*, American Society of Civil Engineers (1975), New York, 54p.
35. Qu, W., Mala, G. M., & Li, D. (1993). Heat Transfer for Water Flow in Trapezoidal Silicon Micro channels, 399–404.
36. Quick, R. S. (1933). "Comparison and Limitations of Various Water hammer Theories," *J. Hyd. Div., ASME*, May, 43–45.
37. Rayleigh, (1917). On the Pressure developed in a Liquid during the Collapse of a Spherical Cavity, *Philos. Mag., Ser. 6*, 34(N200), 94–98.
38. Ramaprabhu, P., & Andrews, M. J. (2004). "Experimental Investigation of Rayleigh-Taylor mixing at small Atwood numbers" *J. Fluid Mech.*, 502, 233.
39. Rich, G. R. (1963). "Hydraulic Transients," Dover, USA, 148–154.
40. Savic, D. A., & Walters, G. A. (1995). "Genetic Algorithms Techniques for Calibrating Network Models," Report No. 95/12, Centre for Systems and Control Engineering, 137–146.
41. Savic, D. A., & Walters, G. A. (1995). *Genetic Algorithms Techniques for Calibrating Network Models*, University of Exeter, Exeter, United Kingdom, 41–77.
42. Shvarts, D., Oron, D., Kartoon, D., Rikanati, A., & Sadot, O. (2000). "Scaling Laws of nonlinear Rayleigh-Taylor & Richtmyer-Meshkov instabilities in Two and Three Dimensions," *C. R. Acad., Sci., Paris IV*, 719, 312p.
43. Sharp, B. (1981). "Water Hammer Problems and Solutions," Edward Arnold Ltd., London, 43–55.
44. Skousen, P. (1998). "Valve Handbook," McGraw Hill, New York, Hammer Theory and Practice, 687–721.
45. Song C. C. et al. (1983). "Transient Mixed-Flow Models for Storm Sewers," *J. Hyd. Div., Nov.*, 109, 458–530.
46. Stephenson, D. (1984). "Pipe Flow Analysis," Elsevier, 19, S.A., 670–788.

47. Streeter, V. L., & Lai, C. (1962). "Water hammer Analysis Including Fluid Friction," *Journal of Hydraulics Division, ASCE*, 88, 79p.
48. Streeter, V. L., & Wylie, E. B. (1979). "Fluid Mechanics," McGraw-Hill Ltd., USA, 492–505.
49. Streeter, V. L., & Wylie, E. B. (1981). "Fluid Mechanics," McGraw-Hill Ltd., USA, 398–420.
50. Tijsseling, "Alan, E. Vardy, (1993). Time Scales and FSI in Unsteady Liquid-Filled Pipe Flow," 5–12.
51. Tuckerman, D. B., & Pease, R. F. W. (1981). High Performance Heat Sinking for VLSI, *IEEE Electron device letter, DEL-2*, 126–129.
52. Tennekes, H., & Lumley, J. L. (1972). *A First Course in Turbulence*, the MIT Press, 410–466.
53. Thorley, A. R. D. (1991). "Fluid Transients in Pipeline Systems," D. & L. George, Herts, England, 231–242.
54. Tullis, J. P. (1971). "Control of Flow in Closed Conduits," Fort Collins, Colorado, 315–340.
55. Tuckerman, D. B. (1984). *Heat Transfer Microstructures for Integrated Circuits*, PhD. Thesis, Stanford University, 10–120.
56. Vallentine, H. R. (1965). "Rigid Water Column Theory for Uniform Gate Closure," *J. Hyd. Div. ASCE*, July, 55–243.
57. Waddell, J. T., Niederhaus, C. E., & Jacobs, J. W. (2001). "Experimental study of Rayleigh-Taylor instability: Low Atwood number Liquid Systems with Single-Mode Initial Perturbations," *Phys., Fluids*, 13, 1263–1273.
58. Watters, G. Z., (1984). "Modern Analysis and Control of Unsteady Flow in Pipelines," *Ann Arbor Sci.*, 2nd Ed., 1098–1104.
59. Walski, T. M., & Lutes, T. L. (1994). "Hydraulic Transients Cause Low-Pressure Problems," *Journal of the American Water Works Association*, 75(2), 58.
60. Weber, S. V., Dimonte, G., & Marinak, M. M. (2003). "Arbitrary Lagrange-Eulerian code simulations of Turbulent Rayleigh-Taylor instability in two and three dimensions," *Laser and Particle Beams*, 21, 455p.
61. Wood, D. J., Dorsch, R. G., & Lightener, C. (1966). "Wave-Plan Analysis of Unsteady Flow in Closed Conduits," *Journal of Hydraulics Division, ASCE*, 92, 83–110.
62. Wood, D. J., & Jones, S. E. (1973). "Water Hammer Charts for Various Types of Valves," *Journal of the Hydraulics Division, Proceedings of the American Society of Civil Engineers*, January, 167–178.
63. Wood, F. M. (1970). "History of Water Hammers," *Civil Engineering Research Report #65*, Queens University, Canada, 66–70.
64. Wu, Z. Y., & Simpson, A. R. (2001). Competent Genetic-Evolutionary Optimization of Water Distribution Systems, *J. Comput., Civ. Eng.*, 15(2), 89–101.
65. Wylie, E. B., & Talpin, L. B. (1983). Matched Impedance to controls fluid transients, *Trans., ASME*, 105(2), 219–224.
66. Wylie, E. B., & Streeter, V. L. (1993). *Fluid Transients in system* Prentice-Hall, Englewood Cliffs, New Jersey, 4.
67. Wylie, E. B., & Streeter, V. L. (1982), *Fluid Transients*, Feb Press, Ann Arbor, MI, Corrected Copy, 1983, 158p.

68. Wu, P. Y., & Little, W. A. (1983). Measurement of Friction Factor for Flow of Gases in Very Fine Channels used For Micro Miniature, Joule Thompson Refrigerators, *Cryogenics*, 24(8), 273–277.
69. Xu, B., Ooi, K. T., Mavriplis, C., & Zaghoul, M. E. (2002). Viscous Dissipation Effects for Liquid Flow in Micro channels, *Microsystems*, 53–57.
70. Young, Y. N., Tufo, H., Dubey, A., & Rosner, R. (2001). “On the Miscible Rayleigh-Taylor Instability Two and Three Dimensions,” *J. Fluid Mech.*, 447, 377, 2003–2500.
71. Wood, D. J., Dorsch, R. G., & Lightener, C. (1966). “Wave-Plan Analysis of Unsteady Flow in Closed Conduits,” *Journal of Hydraulics Division, ASCE*, 92, 83–110.
72. Wylie, E. B., & Streeter, V. L. (1993). *Fluid Transients in System* Prentice Hall Engle Wood Cliffs, New Jersey, 4p.
73. Brunone, B., Karney, B. W., Mecarelli, M., & Ferrante, M. (2000). “Velocity Profiles and Unsteady Pipe Friction in Transient Flow,” *Journal of Water Resources Planning and Management, ASCE*, 126(4), July, 236–244.
74. Koelle, E., Jr. Luvizotto, E., & Andrade, J. P. G. (1996). “Personality Investigation of Hydraulic Networks using MOC-Method of Characteristics” *Proceedings of the 7th International Conference on Pressure Surges and Fluid Transients, Harrogate Durham, United Kingdom*, 1–8.
75. Fillion, Y., & Karney, B. W. (2002). “A Numerical Exploration of Transient Decay Mechanisms in Water Distribution Systems,” *Proceedings of the ASCE Environmental Water Resources Institute Conference, American Society of Civil Engineers, Roanoke, Virginia*, 30.
76. Hamam, M. A., & McCorquodale, J. A. (1982). “Transient Conditions in the Transition from Gravity to Surcharged Sewer Flow,” *Canadian J. Civil Eng., Canada, Sep.*, 65–98.
77. Savic, D. A., & Walters, G. A. (1995). “Genetic Algorithms Techniques for Calibrating Network Models,” *Report No. 95/12, Centre for Systems and Control Engineering*, 137–146.
78. Till Mathis Wagner, (2004). A very short introduction to the Finite Element Method, *Technical University of Munich, JASS 2004, St Petersburg, May 4*.

CHAPTER 8

SIMULATION OF THERMAL PROCESS

CONTENTS

| | | |
|-----|---|-----|
| 8.1 | Introduction..... | 186 |
| 8.2 | Materials and Methods..... | 188 |
| 8.3 | Results and Discussion | 200 |
| 8.4 | Non-Homogeneous Material and Heat Flow | 201 |
| 8.5 | Computer Models for Heat Flow in Non-Homogeneous Material..... | 202 |
| 8.6 | Heat Flow During Drying Process..... | 203 |
| 8.7 | Conclusion | 224 |
| | Keywords | 225 |
| | References..... | 226 |

8.1 INTRODUCTION

Many factors have to be taken into account in selecting the most suitable type of dryer to install and the problem requires to be analyzed from several standpoints. Even an initial analysis of the possibilities must be backed up by pilot-scale tests unless previous experience has indicated the type most likely to be suitable. The accent today, due to high labor costs is on continuously operating unit equipment, to what extent possible automatically controlled. In any event, the selection of a suitable dryer should be made in two stages, a preliminary selection based on the general nature of the problem and the textile material to be handled, followed by a final selection based on pilot-scale tests or previous experience combined with economic considerations.

A leather industry involves a crucial energy-intensive drying stage at the end of the process to remove moisture left from dye setting. Determining drying characteristics for leather, such as temperature levels, transition times, total drying times, and evaporation rates, is vitally important so as to optimize the drying stage. Meanwhile, a textile material undergoes some physical and chemical changes that can affect the final leather quality [1–11].

In considering a drying problem, it is important to establish at the earliest stage, the final or residual moisture content of the textile material, which can be accepted. This is important in many hygroscopic materials and if dried below certain moisture content they will absorb or “regain” moisture from the surrounding atmosphere depending upon its moisture and humidity. The material will establish a condition in equilibrium with this atmosphere and the moisture content of the material under this condition is termed the equilibrium moisture content. Equilibrium moisture content is not greatly affected at the lower end of the atmospheric scale but as this temperature increases the equilibrium moisture content figure decreases, which explains why materials can in fact be dried in the presence of superheated moisture vapor. Meanwhile, drying medium temperatures and humidities assume considerable importance in the operation of direct dryers [12–21].

It should be noted that two processes occur simultaneously during the thermal process of drying a wet leather material, namely, heat transfer in order to raise temperature of the wet leather and to evaporate its moisture content together with mass transfer of moisture to the surface of the textile

material and its evaporation from the surface to the surrounding atmosphere which, in convection dryers, is the drying medium. The quantity of air required to remove the moisture as liberated, as distinct from the quantity of air which will release the required amount of heat through a drop in its temperature in the course of drying, however, has to be determined from the known capacity of air to pick up moisture at a given temperature in relation to its initial content of moisture. For most practical purposes, moisture is in the form of water vapor but the same principles apply, with different values and humidity charts, for other volatile components [22–31].

Thermal drying consumes from 9–25% of national industrial energy consumption in the developed countries. In order to reduce net energy consumption in the drying operation there are attractive alternatives for drying of heat sensitive materials. Leather industry involves a crucial energy-intensive drying stage to remove the moisture left. Synthetic leather drying is the removal of the organic solvent and water. Determining drying characteristics for leathers is vitally important so as to optimize the drying stage. This book describes a way to determine the drying characteristics of leather with analytical method developed for this purpose. The model presented, is based on fundamental heat and mass transfer equations. Altering air velocity varies drying conditions. The work indicates closest agreement with the theoretical model. The results from the parametric study provide a better understanding of the drying mechanisms and may lead to a series of recommendations for drying optimization. Among the many processes that are performed in the leather industry, drying has an essential role: by this means, leathers can acquire their final texture, consistency and flexibility. However, some of the unit operations involved in leather industry, especially the drying process, is still based on empiricism and tradition, with very little use of scientific principles. Widespread methods of leather drying all over the world are mostly convective methods requiring a lot of energy. Specific heat energy consumption increases, especially in the last period of the drying process, when the moisture content of the leather approaches the value at which the product is storable. However, optimizing the drying process using mathematical analysis of temperature and moisture distribution in the material can reduce energy consumption in a convective dryer. Thus, development of a suitable mathematical model to predict the accurate performance of the dryer is important for energy conservation in the drying process [31–40].

The manufacturing of new-generation synthetic leathers involves the extraction of the filling polymer from the polymer-matrix system with an organic solvent and the removal of the solvent from the highly porous material. In this paper, a mathematical model of synthetic leather drying for removing the organic solvent is proposed. The model proposed adequately describes the real processes. To improve the accuracy of calculated moisture distributions a velocity correction factor (VCF) introduced into the calculations. The VCF reflects the fact that some of the air flowing through the bed does not participate very effectively in drying, since it is channeled into low-density areas of the inhomogeneous bed. This chapter discusses the results of experiments to test the deductions that increased rates of drying and better agreement between predicted and experimental moisture distributions in the drying bed can be obtained by using higher air velocities. Thus, this chapter focuses on reviewing convective heat and mass transfer equations in the industrial leather drying process with particular reference to VCF [41–50].

8.2 MATERIALS AND METHODS

The theoretical model [1–42] proposed in this model is based on fundamental equations to describe the simultaneous heat and mass transfer in porous media. It is possible to assume the existence of a thermodynamic quasi equilibrium state, where the temperatures of gaseous, liquid and solid phases are equal (Figs. 8.1–8.11).

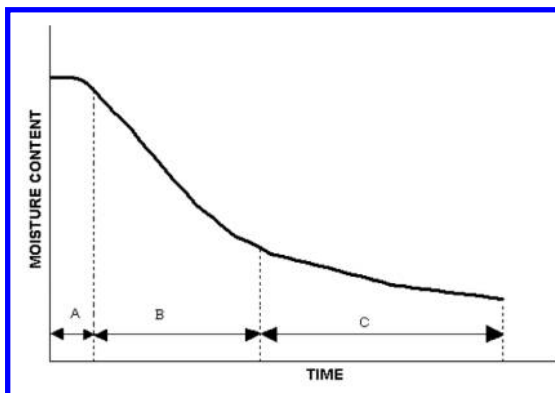


FIGURE 8.1 Drying characteristic of Porous media: (a) Constant rate region; (b) first falling rate region; (c) second falling rate region.

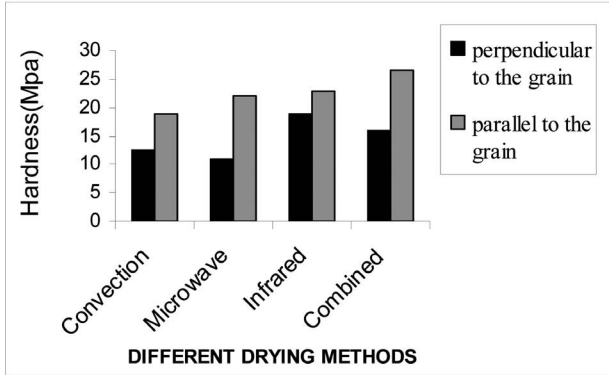


FIGURE 8.2 Brinell hardness for Guilan spruce.

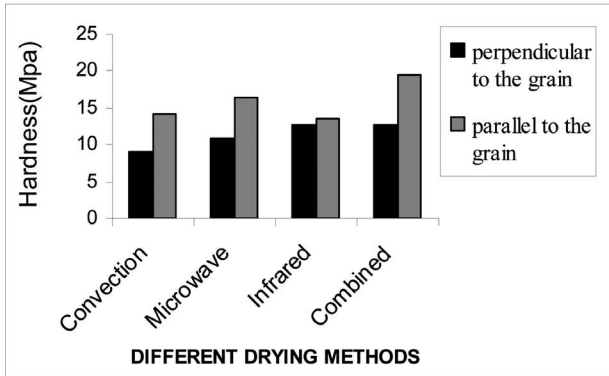


FIGURE 8.3 Brinell hardness for Pine.

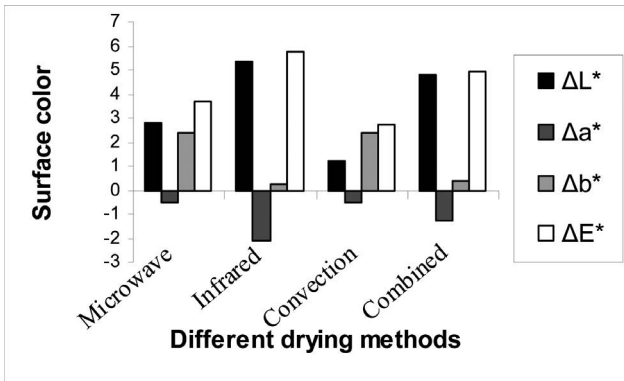


FIGURE 8.4 Surface color of Pine.

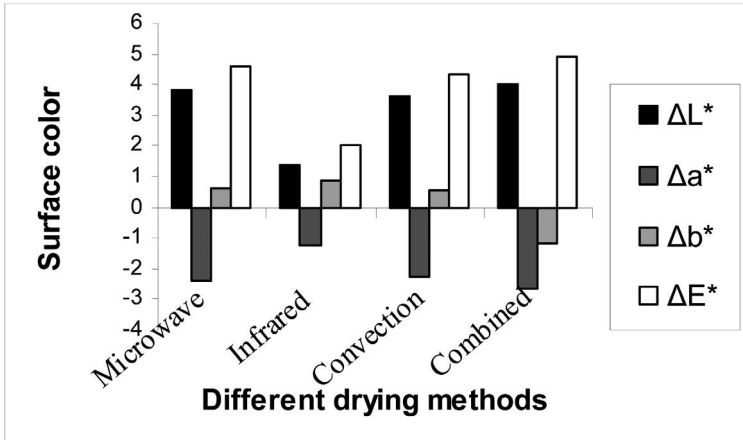


FIGURE 8.5 Surface color.

$$\text{That is, } T_s = T_L = T_G = T, \tag{1}$$

Liquid Mass Balance:

$$\frac{\partial(\epsilon_L \rho_L)}{\partial t} + \nabla(\rho_L \bar{u}_L) + \dot{m} = 0, \tag{2}$$

Water Vapor Mass Balance:

$$\frac{\partial[(\epsilon - \epsilon_L) X_V \rho_G]}{\partial t} + \nabla(X_V \rho_G \bar{u}_G + \bar{J}_V) - \dot{m} = 0, \tag{3}$$

$$\bar{J}_V = -\rho_G (\epsilon - \epsilon_L) D_{EFF} \nabla X_V, \tag{4}$$

Air Mass Balance:

$$\frac{\partial((\epsilon - \epsilon_L) X_A \rho_G)}{\partial t} + \nabla(X_A \rho_G \bar{u}_G - \bar{J}_V) = 0, \tag{5}$$

Liquid Momentum Equation (Darcy’s Law):

$$\bar{u}_L = - \left(\frac{\alpha_G}{\mu_G} \right) \nabla(P_G), \tag{6}$$

Thermal Balance:

The thermal balance is governed by Eq. (8.7).

$$\frac{\partial \left\{ \rho_s C_{\rho_s} + (\varepsilon - \varepsilon_L) \rho_G (X_V C_{\rho_V} + X_A C_{\rho_A}) + \varepsilon_L \rho_L C_{\rho_L} \right\} T}{\partial t} - \nabla (k_E \nabla T) + \nabla \left[(\rho_L \bar{u}_L C_{\rho_L} + \rho_G \bar{u}_G (X_V C_{\rho_V} + X_A C_{\rho_A})) T \right] + (\varepsilon - \varepsilon_L) \frac{\partial P_G}{\partial t} + \dot{m} \Delta H_V = 0, \quad (7)$$

Thermodynamic Equilibrium-Vapor mass Fraction:

In order to attain thermal equilibrium between the liquid and vapor phase, the vapor mass fraction should be such that the partial pressure of the vapor (P'_V) should be equal to its saturation pressure (P_{VS}) at temperature of the mixture. Therefore, thermodynamic relations can obtain the concentration of vapor in the air/vapor mixture inside the pores. According to Dalton’s Law of Additive Pressure applied to the air/vapor mixture, one can show that:

$$\rho_G = \rho_V + \rho_A \quad (8)$$

$$X_V = \frac{\rho_V}{\rho_G}, \quad (9)$$

$$\rho_V = \frac{P'}{R_V T}, \quad (10)$$

$$\rho_A = \frac{(P_G - P'_V)}{R_A T}, \quad (11)$$

Combining Eqs. (8)–(11), one can obtain:

$$X_V = \frac{1}{1 + \left(\frac{P_G R_V}{P'_V R_A} \right) - \left(\frac{R_V}{R_A} \right)}, \quad (12)$$

Mass Rate of Evaporation:

The mass rate of evaporation was obtained in two different ways, as follows:

First of all, the mass rate of evaporation \dot{m} was expressed explicitly by taking it from the water vapor mass balance (2), since vapor concentration is given by Eq. (12).

$$\dot{m} = \frac{\partial[(\varepsilon - \varepsilon_L)X_V \rho_G]}{\partial t} + \nabla(X_V \rho_G \bar{u}_G + \bar{J}_V), \quad (13)$$

Secondly, an equation to compute the mass rate of evaporation can be derived with a combination of the liquid mass balance (1) with a first-order-Arrhenius type equation. From the general kinetic equation:

$$\frac{\partial \alpha}{\partial t} = -kf(\alpha), \quad (14)$$

$$k = A \exp\left(-\frac{E}{RT_{SUR}}\right), \quad (15)$$

$$\alpha = 1 - \frac{\varepsilon_L(t)}{\varepsilon_0}, \quad (16)$$

Drying Kinetics Mechanism Coupling:

Using thermodynamic relations, according to Amagat's law of additive volumes, under the same absolute pressure,

$$m_V = \frac{V_V P_G}{R_V T} \quad (17)$$

$$m_A = \frac{V_A P_G}{R_A T}, \quad (18)$$

$$m_V = X_V m_T, \quad (19)$$

$$m_T = m_V + m_A \quad (20)$$

$$V_G = V_V + V_A, \quad (21)$$

$$V_G = (\varepsilon - \varepsilon_L)V_S, \quad (22)$$

Solving the set of algebraic equations (17)–(22), one can obtain the vapor-air mixture density:

$$\rho_G = \frac{(m_V + m_A)}{V_G}, \quad (23)$$

$$\rho_V = \frac{m_V}{V_G}, \quad (24)$$

$$\rho_A = \frac{m_A}{V_G}, \quad (25)$$

Equivalent Thermal Conductivity:

It is necessary to determine the equivalent value of the thermal conductivity of the material as a whole, since no phase separation was considered in the overall energy equation. The equation we can propose now which may be used to achieve the equivalent thermal conductivity of materials K_E , composed of a continued medium with a uniform disperse phase. It is expressed as follows in Eq. (26).

$$K_E = \left[\frac{k_S + \varepsilon_L k_L \left(\frac{3k_S}{2k_S + k_L} \right) + k_G (\varepsilon - \varepsilon_L) \left(\frac{3k_S}{2k_S + k_G} \right)}{1 + \varepsilon_L \left(\frac{3k_S}{2k_S + k_L} \right) + (\varepsilon - \varepsilon_L) \left(\frac{3k_S}{2k_S + k_G} \right)} \right], \quad (26)$$

$$k_G = X_V k_V + X_A k_A, \quad (27)$$

Effective Diffusion Coefficient Equation:

The binary bulk diffusivity D_{AV} of air-water vapor mixture is given by:

$$D_{AV} = (2.20)(10^{-5}) \left(\frac{P_{ATM}}{P_G} \right) \left(\frac{T_{REF}}{273.15} \right)^{1.75}, \quad (28)$$

Factor α_F can be used to account for closed pores resulting from different nature of the solid, which would increase gas outflow resistance, so the equation of effective diffusion coefficient D_{EFF} for fiber drying is:

$$D_{EFF} = \alpha_F D_{AV} , \quad (29)$$

The convective heat transfer coefficient can be expressed as:

$$h = Nu_{\delta} \left(\frac{k}{\delta} \right) , \quad (30)$$

The convective mass transfer coefficient is:

$$h_M = \left(\frac{h}{C_{PG}} \right) \left(\frac{Pr}{Sc} \right)^{2/3} , \quad (31)$$

$$Pr = \frac{C_{PG} \mu_G}{k_G} , \quad (32)$$

$$Sc = \frac{\mu_G}{\rho_G D_{AV}} , \quad (33)$$

The driving force determining the rate of mass transfer inside the fiber is the difference between the relative humidities of the air in the pores and the fiber. The rate of moisture exchange is assumed to be proportional to the relative humidity difference in this study.

The heat transfer coefficient between external air and fibers surface can be obtained by: $h = Nu_{\delta} \left(\frac{k}{\delta} \right)$.

The mass transfer coefficient was calculated using the analogy between heat transfer and mass transfer as $h_M = \left(\frac{h}{C_{PG}} \right) \left(\frac{Pr}{Sc} \right)^{2/3}$. The convective heat and mass transfer coefficients at the surface are important parameters in drying processes; they are functions of velocity and physical properties of the drying medium.

Describing kinetic model of the moisture transfer during drying as follows:

$$-\frac{dX}{dt} = k(X - X_e), \quad (34)$$

where, X is the material moisture content (dry basis) during drying (kg water/kg dry solids), X_e is the equilibrium moisture content of dehydrated material (kg water/kg dry solids), k is the drying rate (min^{-1}), and t is the time of drying (min). The drying rate is determined as the slope of the falling rate-drying curve. At zero time, the moisture content (dry basis) of the dry material X (kg water/kg dry solids) is equal to X_i , and Eq. (34) is integrated to give the following expression:

$$X = X_e - (X_e - X_i)e^{-kt}, \quad (35)$$

Using above equation Moisture Ratio can be defined as follows:

$$\frac{X - X_e}{X_i - X_e} = e^{-kt}, \quad (36)$$

This is the Lewis's formula introduced in 1921. But by using experimental data of leather drying it seemed that there was a error in curve fitting of e^{-at} .

The experimental moisture content data were non-dimensionlized using the equation:

$$MR = \frac{X - X_e}{X_i - X_e}, \quad (37)$$

where MR is the moisture ratio. For the analysis it was assumed that the equilibrium moisture content, X_e , was equal to zero.

Selected drying models, detailed in Tables 8.1–8.3, were fitted to the drying curves (MR versus time), and the equation parameters determined using nonlinear least squares regression analysis, as shown in Table 8.2.

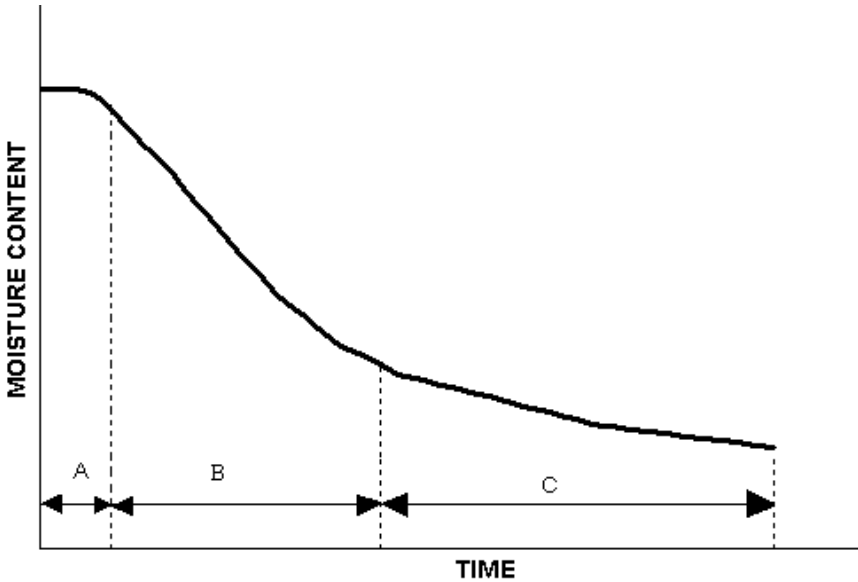


FIGURE 8.6 Drying characteristic of porous media: (a) constant rate region; (b) first falling rate region; (c) second falling rate region.

The experimental results for the drying of leather are given in Fig. 8.7. Fitting curves for two sample models (Lewis model and present model) and temperature of 80 °C are given in Figs. 8.8 and 8.9. Two criteria were adopted to evaluate the goodness of fit of each model, the Correlation Coefficient (r) and the Standard Error (S). The standard error of the estimate is defined as follows:

$$S = \sqrt{\frac{\sum_{i=1}^{n_{points}} (MR_{exp,i} - MR_{Pred,i})^2}{n_{points} - n_{param}}}, \quad (38)$$

where $MR_{exp,i}$ is the measured value at point i , and $MR_{Pred,i}$ is the predicted value at that point, and n_{param} is the number of parameters in the particular model (so that the denominator is the number of degrees of freedom).

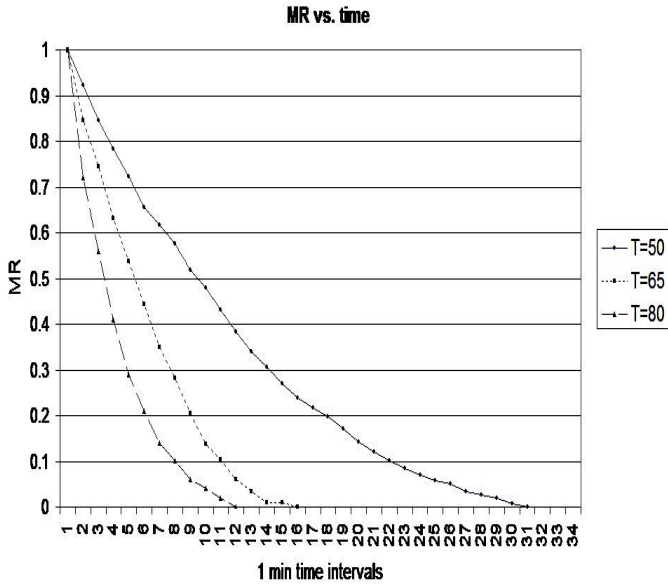


FIGURE 8.7 Moisture ratio vs. time.

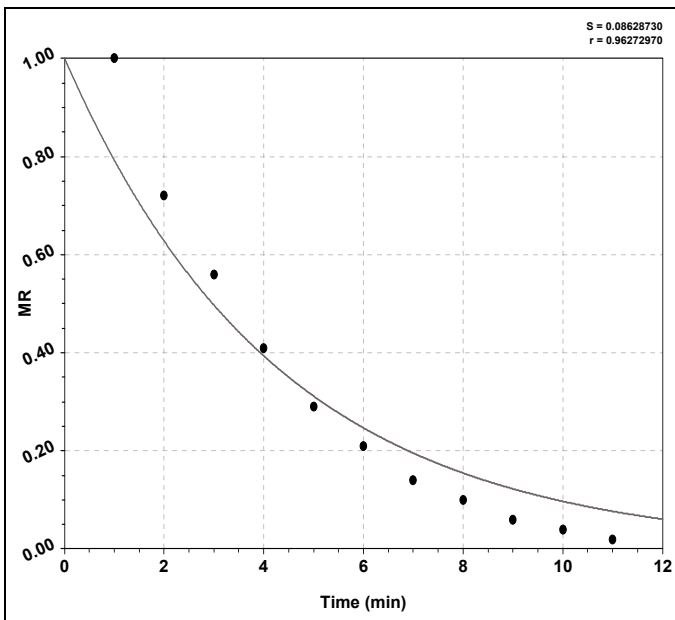


FIGURE 8.8 Lewis model.

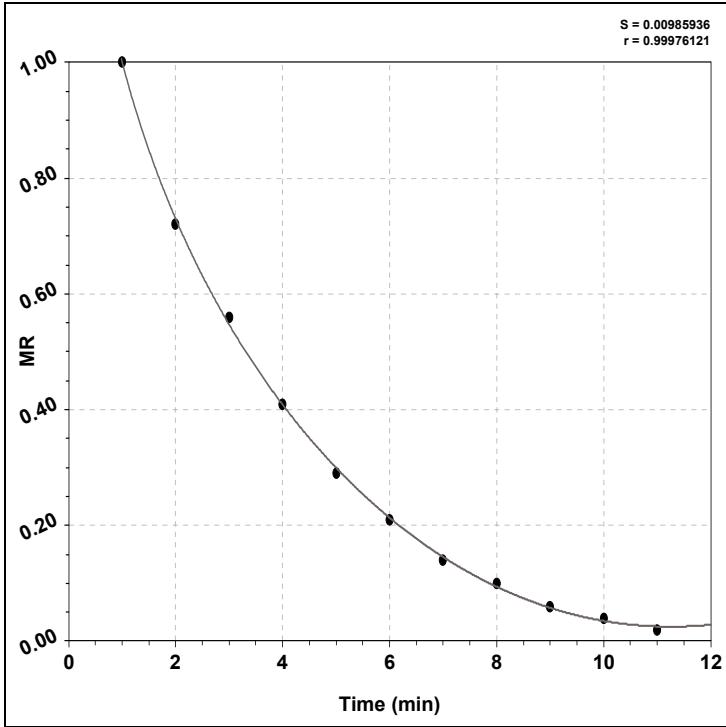


FIGURE 8.9 Present model.

To explain the meaning of correlation coefficient, we must define some terms used as follow:

$$S_t = \sum_{i=1}^{n_{points}} (\bar{y} - MR_{exp,i})^2, \quad (39)$$

where, the average of the data points (\bar{y}) is simply given by

$$\bar{y} = \frac{1}{n_{points}} \sum_{i=1}^{n_{points}} MR_{exp,i}, \quad (40)$$

The quantity S_t considers the spread around a constant line (the mean) as opposed to the spread around the regression model. This is the uncertainty of the dependent variable prior to regression. We also define the deviation from the fitting curve as:

$$S_r = \sum_{i=1}^{n_{points}} (MR_{exp,i} - MR_{pred,i})^2, \tag{41}$$

Note, the similarity of this expression to the standard error of the estimate given above; this quantity likewise measures the spread of the points around the fitting function. In view of the above, the improvement (or error reduction) due to describing the data in terms of a regression model can be quantified by subtracting the two quantities [51–108]. Because the magnitude of the quantity is dependent on the scale of the data, this difference is normalized to yield,

$$r = \sqrt{\frac{S_t - S_r}{S_t}} \tag{42}$$

where r is defined as the correlation coefficient. As the regression model better describes the data, the correlation coefficient will approach unity. For a perfect fit, the standard error of the estimate will approach $S = 0$ and the correlation coefficient will approach $r = 1$.

The standard error and correlation coefficient values of all models are given in Figs. 8.10 and 8.11.

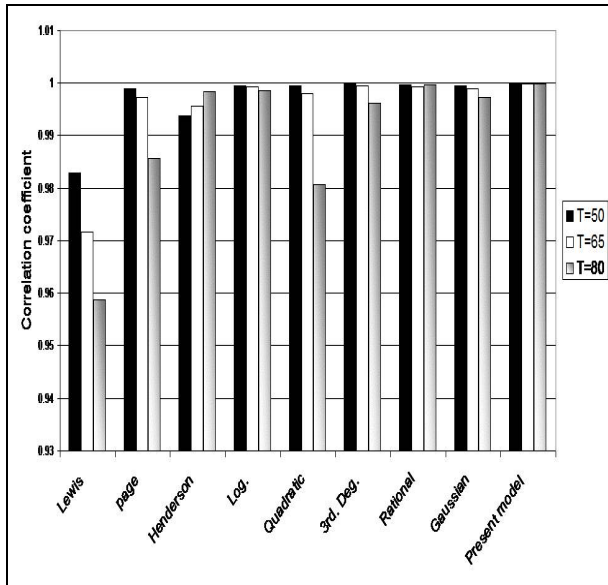


FIGURE 8.10 Correlation coefficient of all models.

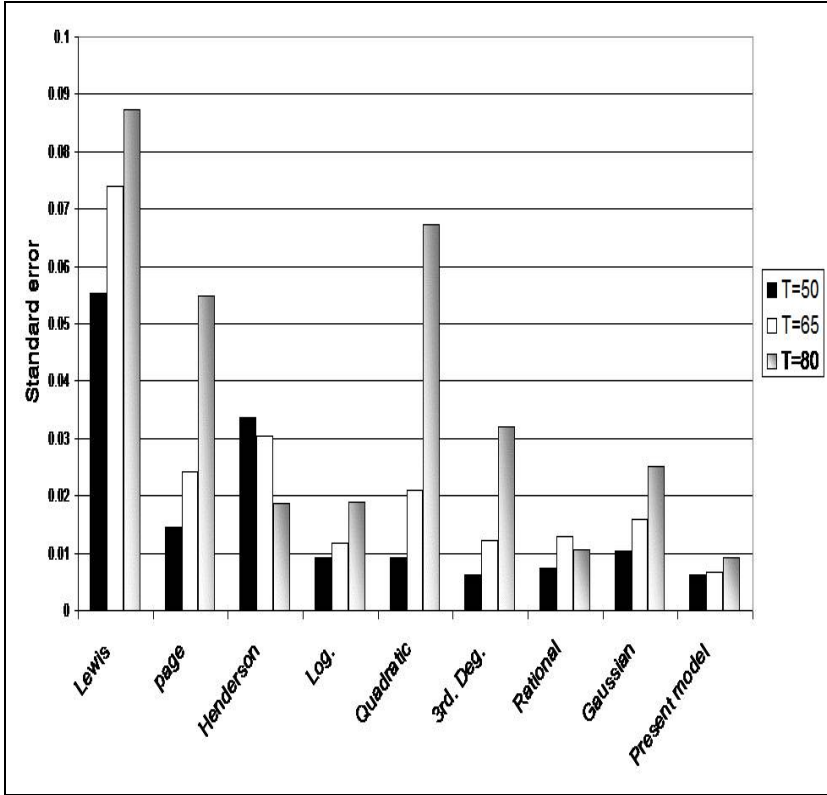


FIGURE 8.11 Standard error of all models.

8.3 RESULTS AND DISCUSSION

Synthetic leathers are materials with much varied physical properties. As a consequence, even though a lot of research of simulation of drying of porous media has been carried out, the complete validation of these models are very difficult. The drying mechanisms might strongly influence by parameters such as permeability and effective diffusion coefficients. The unknown effective diffusion coefficient of vapor for fibers under different temperatures may be determined by adjustment of the model's theoretical alpha correction factor and experimental data. The mathematical model can be used to predict the effects of many parameters on the temperature

variation of the fibers. These parameters include the operation conditions of the dryer, such as the initial moisture content of the fibers, heat and mass transfer coefficients, drying air moisture content, and dryer air temperature. From Figs. 8.1–8.6, it can be observed that the shapes of the experimental and calculated curves are somewhat different.

It can be seen that as the actual air velocity used in this experiment increases, the value of VCF necessary to achieve reasonable correspondence between calculation and experiment becomes closer to unity; that is, a smaller correction to air velocity is required in the calculations as the actual air velocity increases. This appears to confirm the fact that the loss in drying efficiency caused by bed inhomogeneity tends to be reduced as air velocity increases. Figure 8.7 shows a typical heat distribution during convective drying. Table 8.3 relates the VCF to the values of air velocity actually used in the experiments. It is evident from the table that the results show a steady improvement in agreement between experiment and calculation (as indicated by increase in VCF) for air velocities up to 1.59 m/s, above which to be no further improvement with increased flow.

In this chapter, the analytical model has been applied to several drying experiments. The results of the experiments and corresponding calculated distributions are shown in Figs. 8.7–8.11. It is apparent from the curves that the calculated distribution is in reasonable agreement with the corresponding experimental one. In view of the above, it can be clearly observed that the shapes of experimental and calculated curves are somewhat similar.

8.4 NON-HOMOGENEOUS MATERIAL AND HEAT FLOW

Wood is a hygroscopic, porous, anisotropic and nonhomogeneous material (Figs. 8.12–8.16). After log sawing, the lumber contains liquid water in fiber cavities (capillary water) and bound water inside the fiber wall (hygroscopic water). Porosity refers to volume fraction of void space. This void space can be actual space filled with air or space filled with both water and air. Capillary-porous materials are sometimes defined as those having pore diameter less than 10^{-7} m. Capillary porous materials (Tables 8.4–8.6) were defined as those having a clearly recognizable pore space. In capillary porous material, transport of water is a more complex phenomena. In addition to molecular diffusion, water transport can be due to

vapor diffusion, surface diffusion, Knudsen diffusion, capillary flow, and purely hydrodynamic flow. In hygroscopic materials, there is large amount of physically bound water and the material often shrinks during heating.

8.5 COMPUTER MODELS FOR HEAT FLOW IN NON-HOMOGENEOUS MATERIAL

In hygroscopic materials there is a level of moisture saturation below which the internal vapor pressure is a function of saturation and temperature. These relationships are called equilibrium moisture isotherms. Above this moisture saturation, the vapor pressure is a function of temperature only (as expressed by the Clapeyron equation) and is independent of the moisture level. Thus, above certain moisture level, all materials behave non-hygroscopic.

Green wood contains a lot of water. In the outer parts of the stem, in the sapwood, spruce and pine have average moisture content of about 130%, and in the inner parts, in the heartwood, the average moisture content is about 35%. Wood drying is the art of getting rid of that surplus water under controlled forms. It will dry to an equilibrium moisture content of 8–16% fluid content when left in air which improves its stability, reduces its weight for transport, prepares it for chemical treatment or painting and improves its mechanical strength.

Water in wood is found in the cell cavities and cell walls. All void spaces in wood can be filled with liquid water called free water. Free water is held by adhesion and surface tension forces. Water in the cell walls is called bound water. Bound water is held by forces at the molecular level. Water molecules attach themselves to sites on the cellulose chain molecules. It is an intimate part of the cell wall but does not alter the chemical properties of wood. Hydrogen bonding is the predominant fixing mechanism. If wood is allowed to dry, the first water to be removed is free water. No bound water is evaporated until all free water has been removed. During removal of water, molecular energy is expended. Energy requirement for vaporization of bound water is higher than free water. Moisture content at which only the cell walls are completely saturated (all bound water) but no free water exists in all lumens is called the fiber saturation point (F.S.P.). Typically the F.S.P. of wood is within the range of 20–40% moisture content depending on temperature and wood species. Water in

wood normally moves from high to low zones of moisture content. The surface of the wood must be drier than the interior if moisture is to be removed. Drying can be divided into two phases: movement of water from the interior to the surface of the wood, and removal of water from the surface. Water moves through the interior of the wood as a liquid or water vapor through various air passageways in the cellular structure of wood and through the cell walls.

Drying is a process of simultaneous heat and moisture transfer with a transient nature. The evolution process of the temperature and moisture with time must be predicted and actively controlled in order to ensure an effective and efficient drying operation. Lumber drying can be understood as the balance between heat transfer from air flow to wood surface and water transport from the wood surface to the air flow. Reduction in drying time and energy consumption offers the wood industries a great potential for economic benefit. In hygroscopic porous material like wood, mathematical models describing moisture and heat movements may be used to facilitate experimental testing and to explain the physical mechanisms underlying such mass transfer processes. The process of wood drying can be interpreted as simultaneous heat and moisture transfer with local thermodynamic equilibrium at each point within the timber. Drying of wood is in its nature an unsteady-state non-isothermal diffusion of heat and moisture, where temperature gradients may counteract with the moisture gradient.

8.6 HEAT FLOW DURING DRYING PROCESS

First stage: When both surface and core MC are greater than the F.S.P. Moisture movement is by capillary flow. Drying rate is evaporation controlled.

Second stage: When surface MC is less than the FSP and core MC is greater than the F.S.P. Drying is by capillary flow in the core and by bound water diffusion near the surface as fiber saturation line recedes into wood, resistance to drying increases. Drying rate is controlled by bound water diffusion.

Third stage: When both surface and core MC are less than the F.S.P. Drying is entirely by diffusion. As the MC gradient between surface and core becomes less, resistance to drying increases and drying rate decreases.

Capillary pressure is a driving force in convective wood drying at mild conditions. The temperature is higher outside than inside. The moisture profile during convective drying is in the opposite direction, namely, the drier part is toward the exposed surface of wood. This opposite pattern of moisture and temperature profiles lead to the concept of the wet front that separates the outer area, where the water is bound to the cell wall, from the inner area, where free water exists in liquid and vapor form. A wet front that moves slowly from the surface toward the center of a board during convective drying leads to subsequent enhancement of the capillary transportation. Capillary transportation can then be justified due to the moisture gradients developed around that area. When the drying conditions are mild, the drying period is longer so the relative portion of the total moisture removal, due to the capillary phenomena, is high, and it seems that this is the most important mass transfer mechanism.

Credible data on the bound water diffusion coefficient in wood and the boundary condition for the interface between moist air and wood surface are very important for accurate description of timber drying as well as for the proper design and use of products, structures and buildings made of wood already dried below the fiber saturation point. During the last century, two groups of methods for measuring the bound water diffusion coefficient in wood were developed. The first one, traditionally called the cup method, uses data from the steady-state experiments of bound water transfer and is based on Fick's First law of diffusion. Unfortunately, the method is not valid for the bound water diffusion coefficient determination in wood because it cannot satisfy the requirements of the boundary condition of the first kind and the constant value of the diffusion coefficient. The second group of methods is based on the unsteady-state experiments and Fick's Second law of diffusion. The common name of this group is the sorption method and it was developed to overcome the disadvantages of the cup technique.

In solving the diffusion equations (the Eqs. (43)–(100)) for moisture variations in wood, some authors have assumed that the diffusion coefficient depends strongly on moisture content, while others have taken the diffusion coefficient as constant. It has been reported that the diffusion coefficient is influenced by the drying temperature, density and moisture content of timber. The diffusion coefficient of water in cellophane and wood substance was shown to increase with temperature in proportion to the increase in vapor pressure of water. It is also observed that the diffu-

sion coefficient decreased with increasing wood density. Other factors affecting the diffusion coefficient that are yet to be quantified are the species (specific gravity) and the growth ring orientation. Literature has suggested that the ratios of radial and tangential diffusion coefficients vary for different tree species. The radial diffusion coefficient of New Zealand *Pinus radiata* has been estimated to be approximately 1.4 times the tangential diffusion coefficient. It is observed that for northern red oak, the diffusion coefficient is a function of moisture content only. It increases dramatically at low moisture content and tends to level off as the fiber saturation point is approached.

In a one-dimensional formulation with moisture moving in the direction normal to a specimen of a slice of wood of thickness $2a$, the diffusion equation can be written as:

$$\frac{\partial(MC)}{\partial t} = \frac{\partial}{\partial X} \left(D \frac{\partial(MC)}{\partial X} \right) (0 < X < a, t > 0), \quad (43)$$

where MC is moisture content, t is time, D is diffusion coefficient, and X is space coordinate measured from the center of the specimen.

The moisture content influences on the coefficient D only if the moisture content is below the fiber saturation point (F.S.P.) (typically 20%–30% for softwoods):

$$D(u) = \begin{cases} f_D(u) & , u < u_{fsp} \\ f_D(u_{fsp}) & , u \geq u_{fsp} \end{cases}, \quad (44)$$

where u_{fsp} denotes the F.S.P. and $f_D(u)$ is a function which expresses diffusion coefficient in moisture content, temperature and may be some other parameters of ambient air climate. The expression of $f_D(u)$ depends on variety of wood.

It was assumed that the diffusion coefficient bellow F.S.P. can be represented by:

$$f_D(u) = A.e^{\frac{5280}{T} \cdot \frac{B.u}{100}}, \quad (45)$$

where T is the temperature in Kelvin, u is percent moisture content, A and B can be experimentally determined.

The regression equation of diffusion coefficient of *Pinus radiata* timber using the dry bulb temperature and the density is:

$$D(10^{-9}) = 1.89 + 0.127 \times T_{DB} - 0.00213 \times \rho_S \quad (R^2 = 0.499), \quad (46)$$

The regression equations of diffusion coefficients below of Masson's pine during high temperature drying are:

$$D = 0.0046MC^2 + 0.1753MC + 4.2850 \quad (R^2 = 0.9391), \quad (47)$$

TANGENTIAL DIFFUSION

$$D = 0.0092MC^2 + 0.3065MC + 4.9243 \quad (R^2 = 0.9284), \quad (48)$$

RADIAL DIFFUSION

The transverse diffusion coefficient D can be expressed by the porosity of wood ν , the transverse bound water diffusion coefficient D_{bt} of wood and the vapor diffusion coefficient D_v in the lumens:

$$D = \frac{\sqrt{\nu}D_{bt}D_v}{(1-\nu)(\sqrt{\nu}D_{bt} + (1-\sqrt{\nu})D_v)}, \quad (49)$$

The vapor diffusion coefficient D_v in the lumens can be expressed as:

$$D_v = \frac{M_w D_a P_s}{SG_d \rho_w R T_k} \cdot \frac{d\phi}{du}, \quad (50)$$

where M_w (kg/kmol) is the molecular weight of water.

$$D_a = \frac{9.2 \cdot 10^{-9} T_k^{2.5}}{(T_k + 245.18)}, \quad (51)$$

is the inter diffusion coefficient of vapor in air,

$$SG_d = \frac{1.54}{(1 + 1.54u)}, \quad (52)$$

where SG_d is the nominal specific gravity of wood substance at the given bound water content. $\rho_w = 103 \text{ kg/m}^3$ is the density of water, $R = 8314.3 \text{ kmol}$, K is the gas constant, T_k is the Kelvin temperature, Ψ is the relative humidity (%/100), and P_{sat} is saturated vapor pressure given by:

$$P_{\text{sat}} = 3390 \exp(-1.74 + 0.0759T_C - 0.000424T_C^2 + 2.44 \cdot 10^{-6} T_C^3), \quad (53)$$

The derivative of air relative humidity Ψ with respect to moisture content MC is given as:

$$MC = \frac{18}{w} \left(\frac{k_1 k_2 \Psi}{1 + k_1 k_2 \Psi} + \frac{k_2 \Psi}{1 - k_2 \Psi} \right), \quad (54)$$

where:

$$k_1 = 4.737 + 0.04773T_C - 0.00050012T_C^2, \quad (55)$$

$$k_2 = 0.7059 + 0.001695T_C + -0.000005638T_C^2, \quad (56)$$

$$W = 223.4 + .6942T_C + 0.01853T_C^2, \quad (57)$$

The diffusion coefficient D_{bt} of bound water in cell walls is defined according to the Arrhenius equation as:

$$D_{bt} = 7 \cdot 10^{-6} \exp(-E_b / RT_k), \quad (58)$$

where:

$$E_b = (40.195 - 71.179Mc + 291Mc^2 - 669.92Mc^3) \cdot 10^6, \quad (59)$$

where E_b is the activation energy.

The porosity of wood is expressed as:

$$v = 1 - SG(0.667 + Mc), \quad (60)$$

where specific gravity of wood SG at the given moisture content u is defined as:

$$SG = \frac{\rho_s}{\rho_w(1 + Mc)} = \frac{\rho_0}{\rho_w + 0.883\rho_0 Mc}, \quad (61)$$

where ρ_s is density of wood, ρ_0 is density of oven-dry wood (density of wood that has been dried in a ventilated oven at approximately 104 °C until there is no additional loss in weight).

Wood thermal conductivity (K_{wood}) is the ratio of the heat flux to the temperature gradient through a wood sample. Wood has a relatively low thermal conductivity due to its porous structure, and cell wall properties. The density, moisture content, and temperature dependence of thermal conductivity of wood and wood-based composites were demonstrated by several researchers. The transverse thermal conductivity can be expressed as:

$$K_{wood} = [SG \times (4.8 + 0.09 \times MC) + 0.57] \times 10^{-4} \frac{cal}{cm \cdot Cs} \quad (62)$$

When moisture content of wood is below 40%.

$$K_{wood} = [SG \times (4.8 + 0.125 \times MC) + 0.57] \times 10^{-4} \frac{cal}{cm \cdot Cs} \quad (63)$$

When moisture content of wood is above 40%.

The specific gravity and moisture content dependence of the solid wood thermal conductivity in the transverse (radial and tangential) direction is given by:

$$K_T = SG(K_{cw} + K_w \cdot Mc) + K_a v, \quad (64)$$

where: SG = specific gravity of wood; K_{cw} = conductivity of cell wall substance (0.217 J/m/s/K); K_w = conductivity of water (0.4 J/m/s/K); K_a = conductivity of air (0.024 J/m/s/K); Mc = moisture content of wood (fraction); n = porosity of wood.

The thermal conductivity of wood is affected by a number of basic factors: density, moisture content, extractive content, grain direction, structural irregularities such as checks and knots, fibril angle, and temperature. Thermal conductivity increases as density, moisture content, temperature, or extractive content of the wood increases. Thermal conductivity is nearly the same in the radial and tangential directions with respect to the growth rings.

The longitudinal thermal conductivity of solid wood is approximately 2.5 times higher than the transverse conductivity:

$$K_L = 2.5K_T \quad (65)$$

For moisture content levels below 25%, approximate thermal conductivity K across the grain can be calculated with a linear equation of the form:

$$K_{wood} = G(B + CM) + A \quad (66)$$

where SG is specific gravity based on oven dry weight and volume at a given moisture content MC (%) and A , B , and C are constants.

For specific gravity >0.3 , temperatures around 24 °C, and moisture content values $<25\%$, $A = 0.01864$, $B = 0.1941$, and $C = 0.004064$ (with k in W/(mK)). It was derived from measurements made by several researchers on a variety of species.

During the early stages of drying the material consists of so much water that liquid surfaces exist and drying proceeds at a constant rate. Constant drying rates are achieved when surface free water is maintained and the only resistance to mass transfer is external to the wood. The liquid water moves by capillary forces to the surface in same proportion of moisture evaporation. Moisture movement across the lumber will depend on the wood permeability and the drying rate itself is controlled by external conditions in this period. Energy received by the surface increase temperature in this region, and the heat transfer to the inner part of lumber starts. Since the moisture source for the surface is internal moisture, constant drying

rates can only be maintained if there is sufficient moisture transport to keep the surface moisture content above the F.S.P. If this level is not maintained then some of the resistance to mass transfer becomes internal and neither the drying rate nor the surface temperature remains constant and drying proceeds to the falling rate period. As the lumber dries, the liquid water or wet line recedes into wood and the internal moisture movement involves the liquid flow and diffusion of water vapor and hygroscopic water. The effect of internal resistance on the drying rate increases. In the last phase (second falling rate period) there is no more liquid water in the lumber, and the drying rate is controlled only by internal resistance (material characteristics) until an equilibrium moisture content is reached.

A typical drying curve showing three stages of drying characteristic is illustrated in Fig. 8.1.

Pang et al. proposed that the three drying periods (constant rate, first falling rate and second falling rate) based on simulated drying of veneer be expressed by the following equations:

$$-\frac{d(MC)}{dt} = j_0 \text{ For } MC > M_{cr1}, \quad (67)$$

$$-\frac{d(MC)}{dt} = A + B * MC \text{ For } M_{cr1} > MC > M_{cr2}, \quad (68)$$

$$-\frac{d(MC)}{dt} = \frac{A + B * M_{cr2}}{M_{cr2} - M_e} * (MC - M_e) \text{ For } MC < M_{cr2}, \quad (69)$$

where, j_0 is constant drying rate, M_{cr1} is the first critical moisture content, M_{cr2} is the second critical moisture content, constants A and B also vary with wood thickness, wood density, and drying conditions.

Moisture content of wood is defined as the weight of water in wood expressed as a fraction, usually a percentage, of the weight of oven dry wood. Moisture exists in wood as bound water within the cell wall, capillary water in liquid form and water vapor in gas form in the voids of wood. Capillary water bulk flow refers to the flow of liquid through the interconnected voids and over the surface of a solid due to molecular attraction between the liquid and the solid. Moisture content varies widely between species and within species of wood. It varies particularly between heart-

wood and sapwood. The amount of moisture in the cell wall may decrease as a result of extractive deposition when a tree undergoes change from sapwood to heartwood. The butt logs of trees may contain more water than the top logs. Variability of moisture content exists even within individual boards cut from the same tree. Green wood is often defined as freshly sawn wood in which the cell walls are completely saturated with water. Usually green wood contains additional water in the lumens. Moisture content at which both the cell lumens and cell walls are completely saturated with water is the maximum moisture content. An average green moisture content value taken from the Wood Handbook (Forest Products Society, 1999) of southern yellow pine (loblolly) is 33 and 110% for heartwood and sapwood, respectively. Sweet gum is 79% and 137% while yellow-poplar is 83% and 106% for heartwood and sapwood, respectively.

Permeability refers to the capability of a solid substance to allow the passage of gases or liquids under pressure. Permeability assumes the mass movement of molecules in which the pressure or driving force may be supplied by such sources as mechanically applied pressure, vacuum, thermal expansion, gravity, or surface tension. Under this condition, the permeability of wood is the dominant factor controlling moisture movement.

Fluid movement in wood is a very important process in wood products industries. An understanding of wood permeability is essential for determining lumber drying schedules for treating lumber and for producing high-quality wood products. The flow of gas inside the wood particle is limited due to the fact that wood consists of a large number of clustered small pores. The pore walls act as barriers largely preventing convective flow between adjacent pores. The wood annular rings also act as barriers for flow in the radial direction which makes flow in the axial direction more favorable and giving a lower permeability in the radial direction than in the axial direction where the axial flow is regarded as flow parallel to the wood fiber grains and the radial flow as flow perpendicular to the wood grains. The permeability in the wood cylinder is therefore an important parameter for the velocity field in the wood. The dry wood radial permeability is 10,000 times lower than the dry wood axial permeability. The chemical composition of the wood/char structure also affects the permeability, where the permeability in char is in order of 1000 times larger than for wood.

Longitudinal flow becomes important, particularly in specimens having a low ratio of length to diameter, because of the high ratio of longi-

tudinal to transverse permeability. Longitudinal permeability was found to be dependent upon specimen length in the flow direction, that is, the decrease of specimen length appears result in greater permeability in less permeable species.

The effect of drying conditions on gas permeability and preservative treatability was assessed on western hemlock lumber. Although there were no differences in gas permeability between lumber dried at conventional and high temperatures, there were differences in preservative penetration. High temperature drying significantly reduced drying time, but did not appear to affect permeability or shell-to-core MC differences compared with drying at conventional temperature. Pits have a major influence on softwood permeability. Across pits can be impeded by aspiration or occlusion by deposition extractives on the membrane. Drying conditions can significantly affect pit condition, sometimes inducing aspiration that blocks both air and fluid flow. Pressure treatment is presumed to enhance preservative uptake and flow across pits, but the exact impact of pit condition (i.e., open or aspirated) is unknown. Drying conditions may also alter the state of materials deposited on pits, thereby altering the effects of pressure and perhaps the nature of preservative wood interactions. The latter effect may be especially important, since changes in wood chemistry could affect the rates of preservative fixation, which could produce more rapid preservative deposition on pit membranes that would slow further fluid ingress. The longitudinal permeability of the outer heartwood of each species also was determined to evaluate the effect of growth rate on the decrease in longitudinal permeability following sapwood conversion to heartwood. Faster diameter growth produced higher longitudinal permeability in the sapwood of yellow-poplar, but not in the sapwood of northern red oak or black walnut. Growth rate had no effect on either vessel lumen area percentage or decrease in longitudinal permeability in newly formed heartwood for all three species. Table 8.1 represents typical values for gas permeability. Values are given in orders of magnitude.

Darcy's law for liquid flow:

$$k = \frac{\text{flux}}{\text{gradient}} = \frac{V / (t \times A)}{\Delta P / L} = \frac{V \times L}{t \times A \times \Delta P}, \quad (70)$$

where: k = Permeability [cm^3 (liquid)/ (cm atm sec)]; V = Volume of liquid flowing through the specimen (cm^3); t = Time of flow (sec); A = Cross-sectional area of the specimen perpendicular to the direction of flow (cm^2); DP = Pressure difference between ends of the specimen (atm); L = Length of specimen parallel to the direction of flow (cm).

Darcy's law for gaseous flow:

$$K_g = \frac{V \times L \times P}{t \times A \times \Delta P \times \bar{P}}, \quad (71)$$

where: K_g = Superficial gas permeability [cm^3 (gas)/(cm atm sec)]; V = Volume of gas flowing through the specimen (cm^3 (gas)); P = Pressure at which V is measured (atm); t = Time of flow (sec); A = Cross-sectional area of the specimen perpendicular to the direction of flow (cm^2); DP = Pressure difference between ends of the specimen (atm); L = Length of specimen parallel to the direction of flow (cm); \bar{P} = Average pressure across the specimen (atm).

TABLE 8.1 Typical Values for Gas Permeability

| Type of sample | Longitudinal gas permeability [cm^3 (gas)/ (cm at sec)] |
|---|---|
| Red oak (R = 150 micrometers) | 10,000 |
| Basswood (R = 20 micrometers) | 1000 |
| Maple, Pine sapwood, Coast Douglas-fir sapwood | 100 |
| Yellow-poplar sapwood, Spruce sapwood, Cedar sapwood | 10 |
| Coast Douglas-fir heartwood | 1 |
| White oak heartwood, Beech heartwood | 0.1 |
| Yellow-poplar heartwood, Cedar heartwood, Inland Douglasfir heartwood | 0.01 |
| Transverse Permeabilities (In approx. same species order as longitudinal) | 0.001–0.0001 |

To simulate the heat and mass transport in drying, conservation equations for general non-hygroscopic porous media have been developed by Whitaker based on averaging procedures of all of the variables. These equations were further employed and modified for wood drying. Mass conservation equations for the three phases of moisture in local form are summarized in equations.

Water vapor:

$$\frac{\partial}{\partial t}(\phi_g \rho_v) = -\text{div}(\rho_v V_v) + \dot{m}_{wv} + \dot{m}_{bv}, \quad (72)$$

Bound water:

$$\frac{\partial}{\partial t}(\phi_s \rho_b) = -\text{div}(\rho_b V_b) + \dot{m}_{bv} + \dot{m}_{wb}, \quad (73)$$

Free water:

$$\frac{\partial}{\partial t}(\phi_w \rho_w) = -\text{div}(\rho_w V_w) - \dot{m}_{wv} - \dot{m}_{wb}, \quad (74)$$

where the velocity of the transported quantity is denoted by V_i , r_i is the density, and \dot{m}_{ij} denotes the transition from phases i and j . From here on, the subscripts w , b , v , and s refer, respectively, to free water, bound water, water vapor, and the solid skeleton of wood. Denoting the total volume by V and the volume of the phase i by V_i , the volumetric fraction of this phase is:

$$\phi_i = \frac{V_i}{V}, \quad (75)$$

with the geometrical constraint:

$$\phi_g + \phi_s + \phi_w = 1, \quad (76)$$

Darcy's law, by using relative permeabilities, provides expressions for the free liquid and gas phase velocities as follows:

$$V_l = -\frac{K_l K_{rl}}{\mu_l} \nabla P_l, \quad (77)$$

and

$$V_v = -\frac{K_v K_{rv}}{\mu_v} \nabla P_v, \quad (78)$$

where K is the intrinsic permeability (m^2), K_r is the relative permeability, P is the pressure (Pa), and μ is the viscosity (Pa.s).

The heat flux (q) and the moisture flux (N_v) are estimated by:

$$q = h(T_G - T_{surf}), \quad (79)$$

$$N_v = \psi K_0 (Y_{surf} - Y_G) = \beta (p_G^v - p_{atm}^v), \quad (80)$$

where T_{surf} , Y_{surf} and p_s^v are, respectively, the wood temperature, the air humidity and the vapor partial pressure at the wood surface and, T_G , Y_G and p_G are the corresponding parameters in the air stream. The heat-transfer coefficient is represented by h . The mass-transfer coefficient is β when vapor partial pressure difference is taken as driving force and is k_0 when humidity difference is taken as the driving force with ψ being the humidity factor. The mass-transfer coefficient related to humidity difference is a function of distance along the airflow direction from the inlet side. The heat-transfer coefficient is correlated to the mass-transfer coefficient, as shown by and can be calculated from it. The humidity coefficient ϕ has been found to vary from 0.70 to 0.76, depending on the drying schedules and board thickness.

For the moisture mass transfer and balance, the moisture loss from wood equals the moisture gain by the hot air, and the moisture transfer rate from the board is described by mass transfer coefficient multiplied by driving force (humidity difference, for example). These considerations yield:

$$-\frac{\partial}{\partial \tau} [MC \cdot \rho_s \cdot (1 - \varepsilon)] = G \cdot \frac{\partial Y}{\partial X} = \begin{cases} -\psi K_0 \cdot a \cdot (Y_{surf} - Y_G) & \text{(condensation)} \\ \psi K_0 \cdot a \cdot f \cdot (Y_{sat} - Y_G) & \text{(evaporation)} \end{cases}, \quad (81)$$

where MC is the wood moisture content, r_s is the wood basic density, ϵ is the void fraction in the lumber stack, a is the exposed area per unit volume of the stack and G is the dry air mass flow rate. In order to solve the above equations, the relative drying rate (f) needs to be defined which is a function of moisture content.

For the heat transfer and balance, the energy loss from the hot air equals the heat gain by the moist wood. The convective heat transfer is described by product of heat transfer coefficient and the temperature difference between the hot air and the wood surface. The resultant relationships are as follows:

$$\frac{\partial T_{wood}}{\partial \tau} = \frac{(1 + \alpha_R - \alpha_{LS})}{\rho_s \cdot (1 - \epsilon) \cdot C_{Pwood}} \cdot \left[h.a.(T_G - T_{wood}) - G \cdot \Delta H_{wv} \cdot \frac{\partial Y_G}{\partial X} \right]$$

$$\frac{\partial T_G}{\partial X} = \frac{\left(h.a + G.C_{Pv} \frac{\partial Y_G}{\partial Z} \right) \cdot (T_G - T_{wood})}{G \cdot (C_{Pv} + Y_G \cdot C_{Pv})} \quad , \quad (82)$$

In the above equations, T_{wood} is the wood temperature, α_R and α_{LS} are coefficients to reflect effects of heat radiation and heat loss, C_{Pwood} is the specific heat of wood, and ΔH_{wv} is the water evaporation. These equations have been solved to determine the changes of air temperature and wood temperature along the airflow direction and with time.

The energy rate balance (kW) of a drying air adjacent to the wood throughout the wood board can be represented as follows:

$$\frac{1}{2} V_a \rho_a \cdot c_{p_a,mt} \frac{dT_a}{dt} = \frac{1}{2} v A_{cs} c_{p_a,mt} (T_{a,in} - T_{a,ex}) + \dot{Q}_{evap} - \dot{Q}_{conv} \quad , \quad (83)$$

Where \dot{Q}_{evap} and \dot{Q}_{conv} (kW) are the evaporation and convection heat transfer rates between the drying air and wood, which can be calculated as follows:

$$\dot{Q}_{evap} = r \dot{m}_{wv,s} A_{surf} \quad , \quad (84)$$

$$\dot{Q}_{conv} = hA(T_a - T_{SO}) \quad , \quad (85)$$

The specific water vapor mass flow rate ($\dot{m}_{wv,surf}$)(kg/m² s) to the drying air can be calculated as follows:

$$\dot{m}_{wv,surf} = \frac{h_D}{R_{wv}T_{SO}}(P_{wv,surf} - P_{wv,a}), \quad (86)$$

The vapor pressure on the wood surface can be determined from the sorption isotherms of wood. The mass transfer coefficient (h_D) (m/s) can be calculated from the convection heat transfer coefficient (h) (kW/m² K) as follows:

$$h_D = h \frac{1}{\rho_{a,mt} c p_{a,mt} L e^{0.58}} / \left(1 - \frac{\rho_{wv,m}}{P} \right), \quad (87)$$

Water transfer in wood involves liquid free water and water vapor flow while MC of lumber is above the F.S.P.

According to Darcy's law the liquid free water flux is in proportion to pressure gradient and permeability. So Darcy's law for liquid free water may be written as:

$$J_f = \frac{K_l \rho_l}{\mu_l} \cdot \frac{\partial P_c}{\partial \chi} \quad (88)$$

where: J_f = liquid free water flow flux, kg/m²·s; K_l = specific permeability of liquid water, m³(vapor)/m; ρ_l = density of liquid water, kg/m³; μ_l = viscosity of liquid water, p_a·s; p_c = capillary pressure, p_a; χ = water transfer distance, m; $\partial p_c / \partial \chi$ = capillary pressure gradient, p_a/m.

The water vapor flow flux is also proportional to pressure gradient and permeability as follows:

$$J_{vf} = \frac{K_v \rho_v}{\mu_v} \cdot \frac{\partial P_v}{\partial \chi} \quad (89)$$

where: J_{vf} = water vapor flow flux, kg/m²·s; K_v = specific permeability of water vapor, m³(vapor)/m; ρ_v, μ_v = density and viscosity of water vapor respectively, kg/m³ and p_a·s; $\partial p_v / \partial \chi$ = vapor partial pressure gradient, p_a/m.

Therefore, the water transfer equation above F.S.P. during high temperature drying can be written as:

$$\rho_s \frac{\partial(MC)}{\partial t} = \frac{\partial}{\partial x} (J_f + J_{vf}), \quad (90)$$

where: ρ_s = basic density of wood, kg/m³; MC = moisture content of wood, %; t = time, s; $\partial(MC)/\partial t$ = the rate of moisture content change, %/s; x = water transfer distance, m.

Water transfer in wood below F.S.P. involves bound water diffusion and water vapor diffusion. The bound water diffusion in lumber usually is unsteady diffusion; the diffusion equation follows Fick's second law as follows:

$$\frac{\partial(MC)}{\partial t} = \frac{\partial}{\partial x} \left(D_b \frac{\partial(MC)}{\partial x} \right), \quad (91)$$

where D_b is bound water diffusion coefficient, m²/s, $\partial(MC)/\partial x$ is MC gradient of lumber, %/m.

The bound water diffusion flux J_b can be expressed as:

$$J_b = D_b \rho_s \frac{\partial(MC)}{\partial x}, \quad (92)$$

where: ρ_s is basic density of wood, kg/m³. The water vapor diffusion equation is similar to bound water diffusion equation as follows:

$$\frac{\partial(MC)}{\partial t} = \frac{\partial}{\partial x} \left(D_v \frac{\partial(MC)}{\partial x} \right), \quad (93)$$

where D_v is water vapor diffusion coefficient, m²/s. The water vapor diffusion flux can be expressed as:

$$J_v = D_v \rho_s \frac{\partial(MC)}{\partial x}, \quad (94)$$

Therefore, the water transfer equation below F.S.P. during high temperature drying can be expressed as:

$$\rho_s \frac{\partial(MC)}{\partial t} = \frac{\partial}{\partial x}(J_b + J_V), \quad (95)$$

Two types of wood samples (namely; spruce and pine) were selected for drying investigation. Natural defects such as knots, checks, splits, etc., which would reduce strength of wood are avoided. All wood samples were dried to a moisture content of approximately 30%. The effect of drying temperature and drying modes on the surface roughness, hardness and color development of wood samples are evaluated.

The average roughness is the area between the roughness profile and its mean line, or the integral of the absolute value of the roughness profile height over the evaluation length:

$$R_a = \frac{1}{L} \int_0^L |r(x)| dx \quad (96)$$

When evaluated from digital data, the integral is normally approximated by a trapezoidal rule:

$$R_a = \frac{1}{N} \sum_{n=1}^N |r_n|, \quad (97)$$

The root-mean-square (RMS) average roughness of a surface is calculated from another integral of the roughness profile:

$$R_q = \sqrt{\frac{1}{L} \int_0^L r^2(x) dx}, \quad (98)$$

The digital equivalent normally used is:

$$R_q = \sqrt{\frac{1}{N} \sum_{n=1}^N r_n^2}, \quad (99)$$

R_z (ISO) is a parameter that averages the height of the five highest peaks plus the depth of the five deepest valleys over the evaluation length. These parameters, which are characterized by ISO 4287, were employed to evaluate influence of drying methods on the surface roughness of the samples.

We investigated the influence of drying temperatures on the surface roughness characteristics of veneer samples as well. The results showed that the effect of drying temperatures used in practice is not remarkable on surface roughness of the sliced veneer and maximum drying temperature (130 °C) applied to sliced veneers did not affect significantly surface roughness of the veneers. Veneer sheets were classified into four groups and dried at 20, 110, 150, and 180 °C. According to the results, the smoothest surfaces were obtained for 20° C drying temperature while the highest values of surface roughness were obtained for 180 °C. Because some surface checks may develop in the oven-drying process. It was also found in a study that the surface roughness values of beech veneers dried at 110 °C was higher than that of dried at 20 °C.

In another experimental study, veneer sheets were oven-dried in a veneer dryer at 110 °C (normal drying temperature) and 180 °C (high drying temperature) after peeling process. The surfaces of some veneers were then exposed at indoor laboratory conditions to obtain inactive wood surfaces for glue bonds, and some veneers were treated with borax, boric acid and ammonium acetate solutions. After these treatments, surface roughness measurements were made on veneer surfaces. Alder veneers were found to be smoother than beech veneers. It was concluded that the values mean roughness profile (R_a) decreased slightly or no clear changes were obtained in R_a values after the natural inactivation process. However, little increases were obtained for surface roughness parameters, no clear changes were found especially for beech veneers.

The changes created by weathering on impregnated wood with several different wood preservatives were investigated. The study was performed on the accelerated weathering test cycle, using UV irradiation and water spray in order to simulate natural weathering. Wood samples were treated with ammonium copper quat (ACQ 1900 and ACQ 2200), chromated copper arsenate (CCA), Tanalith E 3491 and Wolmanit CX-8 in accelerated weathering experiment. The changes on the surface of the weathered sam-

ples were characterized by roughness measurements on the samples with 0, 200, 400 and 600 h of total weathering. Generally the surface values of alder wood treated with copper-containing preservatives decreased with over the irradiation time except for treated Wolmanit CX-82% when comparing values. Surface values of pine treated samples generally increased with increasing irradiation time except for ACQ-1900 groups.

Because the stylus of detector was so sensitive first each sample was smoothened with emery paper then measurement test was performed before and after drying. The Mitutoyo Surface roughness tester SJ-201P instrument was employed for surface roughness measurements. Cut-off length was 2.5 mm, sampling length was 12.5 mm and detector tip radius was 5 μ m in the surface roughness measurements. Tables 8.2 and 8.3 displays the changes in surface roughness parameters (R_a , R_z and R_q) of the Pine and Guilan spruce at varying drying methods. In both cases the surface roughness becomes higher during microwave and infrared heating while surface smoothness of both pine and Guilan spruce increased during convection and combined drying. However, the roughness of wood is a complex phenomenon because wood is an anisotropic and heterogeneous material. Several factors such as anatomical differences, growing characteristics, machining properties of wood, pretreatments (e.g., steaming, drying etc.) applied to wood before machining should be considered for the evaluation of the surface roughness of wood.

TABLE 8.2 Surface Roughness (μ m) for Pine

| Drying methods | Drying conditions | R_a | R_z | R_q |
|----------------|-------------------|-------|-------|-------|
| Microwave | Before drying | 4.52 | 24.68 | 5.39 |
| | After drying | 5.46 | 30.21 | 6.62 |
| Infrared | Before drying | 4.42 | 25.52 | 5.43 |
| | After drying | 4.87 | 26.55 | 5.69 |
| Convection | Before drying | 4.66 | 26.87 | 5.86 |
| | After drying | 4.08 | 24.64 | 5.12 |
| Combined | Before drying | 5.23 | 32.59 | 6.42 |
| | After drying | 3.41 | 21.7 | 4.27 |

TABLE 8.3 Surface Roughness (μm) for Guilan Spruce

| Drying methods | Drying conditions | R_a | R_z | R_q |
|----------------|-------------------|-------|-------|-------|
| Microwave | Before drying | 6.44 | 34.18 | 7.85 |
| | After drying | 7.77 | 44.3 | 9.82 |
| Infrared | Before drying | 4.92 | 30.61 | 6.30 |
| | After drying | 6.42 | 38.93 | 8.17 |
| Convection | Before drying | 4.97 | 32.41 | 6.5 |
| | After drying | 4.78 | 32.27 | 6.34 |
| Combined | Before drying | 10.41 | 59.5 | 13.37 |
| | After drying | 9.11 | 54.31 | 11.5 |

Hardness represents the resistance of wood to indentation and marring. In order to measure the hardness of wood samples, the Brinell hardness method was applied. In this method a steel hemisphere of diameter 10 mm was forced into the surface under test. The Brinell method measures the diameter of the mark caused by the steel ball in the specimens. The specimens were loaded parallel and perpendicular to the direction of wood grains. After applying the force the steel ball was kept on the surface for about 30 seconds. In both type of samples the hardness measured in longitudinal direction is reported to be higher than tangential. The amount of fibers and its stiffness carrying the load are expected to be lower when the load direction is angled to the grain. Results showed that hardness of wood increased in combined drying. The hardness of wood is proportional to its density. The hardness of wood varies, depending on the position of the measurement. Latewood is harder than early wood and the lower part of a stem is harder than the upper part. Increase in moisture content decreases the hardness of wood. It was observed the effect of different drying temperatures during air circulation drying. The result indicates no significant influence of temperature on hardness; still the specimens dried at higher temperature gave a hard and brittle impression. It was also investigated whether wood hardness is affected by temperature level during microwave drying and whether the response is different from that of conventionally dried wood. It was concluded that there is a significant difference in wood hardness parallel to the grain between methods when drying progresses to

relatively lower level of moisture content, that is, wood hardness becomes higher during microwave drying. Variables such as density and moisture content have a greater influence on wood hardness than does the drying method or the drying temperature.

Color development of wood surfaces can be measured by using optical devices such as spectrophotometers. With optical measurement methods, the uniformity of color can be objectively evaluated and presented as L^* , a^* and b^* coordinates named by CIEL*a*b* color space values. Measurements were made both on fresh and dried boards and always from the freshly planted surface. Three measurements in each sample board were made avoiding knots and other defects and averaged to one recording. The spectrum of reflected light in the visible region (400–750 nm) was measured and transformed to the CIEL*a*b* color scale using a 10° standard observer and D65 standard illuminant.

These color space values were used to calculate the total color change (ΔE^*) applied to samples according to the following equations:

$$\begin{aligned}\Delta L^* &= L_f^* - L_i^* \\ \Delta a^* &= a_f^* - a_i^* \\ \Delta b^* &= b_f^* - b_i^* \\ \Delta E^* &= \sqrt{(\Delta L^*)^2 + (\Delta a^*)^2 + (\Delta b^*)^2},\end{aligned}\quad (100)$$

where, f and i are subscripts after and before drying, respectively.

In this three-dimensional coordinates, L^* axis represents non-chromatic changes in lightness from an L^* value of 0 (black) to an L^* value of 100 (white), $+a^*$ represents red, $-a^*$ represents green, $+b^*$ represents yellow and $-b^*$ represents blue.

As can be seen from Figs. 8.4 and 8.5, color space values of both pine and Guilan spruce changed after drying.

Results shows that Δa^* generally decreased but Δb^* increased for both pine and spruce wood samples except during combined heating. The lightness values ΔL^* increased during drying. The L^* of wood species such as tropical woods, which originally have dark color increases by exposure to light. This is due to the special species and climate condition of pines wood. Positive values of Δb^* indicate an increment of yellow color and negative values an increase of blue color. Negative values of Δa^* indicate a tendency of wood surface to greenish. A low ΔE^* corresponds to a

low color change or a stable color. The biggest changes in color appeared in ΔE^* values of pine samples during infrared drying while for spruce it was reversed. Due to differences in composition of wood components, the color of fresh, untreated wood varies between different species, between different trees of the same species and even within a tree. Within a species wood color can vary due to the genetic factors and environmental conditions. In discoloration, chemical reactions take place in wood, changing the number and type of chromophores.

Discolorations caused by the drying process are those that actually occur during drying and are mainly caused by non-microbial factors. Many environmental factors such as solar radiation, moisture and temperature cause weathering or oxidative degradation of wooden products during their normal use; these ambient phenomena can eventually change the chemical, physical, optical and mechanical properties of wood surfaces.

A number of studies have been conducted that have attempted to find a solution to kiln brown stain, the majority of them being pretreatment processes. Biological treatment, compression rolling, sap displacement and chemical inhibitors have all been used as pretreatments.

In all cases these processes were successful in reducing or eliminating stain but were not considered economically viable. Vacuum drying and modified schedules have been tried as modified drying processes with only limited success. Within industry various schedules have been developed, though these are generally kept secret and it is difficult to gauge their success. Generally it seems that industry has adopted a post drying process involving the mechanical removal of the kiln brown stain layer [51–52].

8.7 CONCLUSION

Microwave processing of materials is a relatively new technology that provides new approaches to improve the physical properties of materials. Microwave drying generate heat from within the grains by rapid movement of polar molecules causing molecular friction and help in faster and more uniform heating than does conventional heating. If wood is exposed to an electromagnetic field with such high frequency as is characteristic for microwaves, the water molecules, which are dipoles, begin to turn at the same frequency as the electromagnetic field. Wood is a complex composite material, which consists mainly of cellulose (40–45%), hemi-

celluloses (20–30%) and lignin (20–30%). These polymers are also polar molecules, and therefore even they are likely to be affected by the electromagnetic field. This could possibly cause degradation in terms wood hardness. For spruce the average of hardness is shown to be much higher than pine. From the experimental results it can be observed that in combined microwave dryer, the hardness was relatively improved in comparison to the other drying methods. Microwave and infrared drying can increase wood surface roughness while the smoothness of wood increases during convection and combined drying. The effect varies with the wood species. Thus this work suggests keeping the core temperature below the critical value until the wood has dried below fiber saturation as one way of ensuring that the dried wood is acceptably bright and light in color. In the model presented in this paper, a simple method of predicting moisture distributions leads to prediction of drying times more rapid than those measured in experiments. From this point of view, the drying reveals many aspects which are not normally observed or measured and which may be of value in some application.

The derivation of the drying curves is an example. It is clear from the experiments over a range of air velocities that it is not possible to make accurate predictions and have the experimental curves coincide at all points with the predicted distributions simply by introducing a VCF into the calculations. This suggest that a close agreement between calculated and experimental curves over the entire drying period could be obtained by using a large value of VCF in the initial stages of drying and progressively decreasing it as drying proceeds.

KEYWORDS

- **Conservation equations**
- **Method of characteristics**
- **Microwave**
- **Moisture distributions**
- **Spectrophotometers**

REFERENCES

1. Incropera, F. P., & Dewitt, D. P. (1985). *Fundamentals of Heat and Mass Transfer*, second Ed., Wiley, New York.
2. Ghali, K., Jones, B., & Tracy, E. (1995). Modeling Heat and Mass Transfer in Fabrics, *Int. J. Heat Mass Transfer*, *38(1)*, 13–21.
3. Flory, P. J. (1969). *Statistical Mechanics of Chain Molecules*, Inter science Pub. NY.
4. Hadley, G. R. (1984). Numerical Modeling of the Drying of Porous Materials, in, *Proceedings of the Fourth International Drying Symposium*, *1*, 151–158.
5. Hong, K., Hollies, N. R. S., & Spivak, S. M. (1988). Dynamic Moisture Vapour Transfer through Textiles, Part I: Clothing Hygrometry and the Influence of Fiber Type, *Textile Res. J.* *58(12)*, 697–706.
6. Chen, C. S., & Johnson, W. H. (1969). Kinetics of Moisture Movement in Hygroscopic Materials, In *Theoretical Considerations of Drying Phenomenon*, *Trans. ASAE.*, *12*, 109–113.
7. Barnes, J., & Holcombe, B. (1996). Moisture Sorption and Transport in Clothing during Wear, *Textile Res. J.* *66(12)*, 777–786.
8. Chen, P., & Pei, D. (1988). A Mathematical Models of Drying Process *Int.*, *J. Heat Mass Transfer*, *31(12)*, 2517–2562.
9. Davis, A., & James, D. (1996). Slow Flow through a Model Fibrous Porous Medium, *Int. J. Multiphase Flow*, *22*, 969–989.
10. Jirsak, O., Gok, T., Ozipek, B., & Pau, N. (1998). Comparing Dynamic and Static Methods for Measuring Thermal Conductive Properties of Textiles, *Textile Res. J.*, *68(1)*, 47–56.
11. Kaviany, M. (1991). “Principles of Heat transfer in Porous Media,” Springer, New York.
12. Jackson, J., & James, D. (1986). The Permeability of Fibrous Porous Media, *Can. J. Chem. Eng.* *64*, 364–374.
13. Dietl, C., George, O. P., Bansal, N. K. (1995). Modeling of Diffusion in Capillary Porous Materials During the Drying Process, *Drying Technol.*, *13 (1&2)*, 267–293.
14. Ea, J. Y. (1988). *Water Vapor Transfer in Breathable Fabrics for Clothing*, PhD thesis, University of Leeds.
15. Haghi, A. K. (2004). Moisture Permeation of Clothing, *JTAC*, *76*, 1035–1055.
16. Haghi, A. K. (2003). Thermal Analysis of Drying Process *JTAC*, *74*, 827–842.
17. Haghi, A. K. (2000). Some Aspects of Microwave Drying, *The Annals of Stefan Cel Mare University*, Year VII, *(14)*, 22–25.
18. Haghi, A. K. (2000). A Thermal Imaging Technique for Measuring Transient Temperature Field An Experimental Approach, *The Annals of Stefan Cel Mare University*, Year VI, *(12)*, 73–76.
19. Haghi, A. K. (2001). Experimental Investigations on Drying of Porous Media using Infrared Radiation, *Acta Polytechnica*, *41(1)*, 55–57.
20. Haghi, A. K. (2001). A Mathematical Model of the Drying Process, *Acta Polytechnica*, *41(3)*, 20–23.
21. Haghi, A. K. (2001). Simultaneous Moisture and Heat Transfer in Porous System, *Journal of Computational and Applied Mechanics*, *2(2)*, 195–204.

22. Hagi, A. K. (2002). A Detailed Study on Moisture Sorption of Hygroscopic Fiber, *Journal of Theoretical and Applied Mechanics*, 32(2), 47–62.
23. Dietl, C., George, O. P., & Bansal, N. K. (1995). Modeling of Diffusion in Capillary Porous Materials During the Drying Process, *Drying Technol.*, 13(1&2), 267–293.
24. Ea, J. Y. (1988). Water Vapour Transfer in Breathable Fabrics for Clothing, PhD thesis, University of Leeds.
25. Flory, P. J. (1969). *Statistical Mechanics of Chain Molecules*, Inter science Pub. NY.
26. Nigmatulin, R. I., Khabeev, N. S., & Nagiyev, F. B. (1981). Dynamics, Heat and Mass Transfer of Vapor-Gas Bubbles in a Liquid, *Int. J. Heat Mass Transfer*, 24(N6), Printed in Great Britain, 1033–1044.
27. Vargaftik, N. B. (1972). *Handbook of Thermo-Physical Properties of Gases and Liquids*, Oxford: Pergamon Press, 98.
28. Laman, B. F. (1988). *Hydro Pumps and Installation*, 278.
29. Nagiyev, F. B., & Kadyrov, B. A. (1986). Heat Transfer and the Dynamics of Vapor Bubbles in a Liquid Binary Solution, *DAN Azerbaijani SSR*, (4), 10–13.
30. Alyshev, V. M. (2003). *Hydraulic Calculations of Open Channels on your PC*, Part 1 Tutorial Moscow: MSUE, 185.
31. Streeter, V. L., & Wylie, E. B. (1979). “Fluid Mechanics,” McGraw-Hill Ltd., USA, 492–505.
32. Sharp, B. (1981). “Water Hammer Problems and Solutions,” Edward Arnold Ltd, London, 43–55.
33. Skousen, P. (1998). “Valve Handbook,” McGraw Hill, New York, Hammer Theory and Practice, 687–721.
34. Shaking, N. I. (1988). Water Hammer to Breaks the Continuity of the Flows in Pressure Conduits Pumping Stations, Dis., on Kharkov, 225.
35. Tijsseling, “Alan, E. Vardy, (1993). Time Scales and FSI in Unsteady Liquid-Filled Pipe Flow,” 5–12.
36. Wu, P. Y., & Little, W. A. (1983). Measurement of Friction Factor for Flow of Gases in Very Fine Channels used For Micro Miniature, Joule Thompson Refrigerators, *Cryogenics*, 24(8), 273–277.
37. Song, C. C. et al. (1983). “Transient Mixed-Flow Models for Storm Sewers,” *J. Hyd. Div.*, Nov., 109, 458–530.
38. Stephenson, D. (1984). “Pipe Flow Analysis,” Elsevier, 19, S.A., 670–788.
39. Chaudhry, M. H. (1979). “Applied Hydraulic Transients,” Van Nostrand Reinhold Co., N.Y., 1322–1324.
40. Chaudhry, M. H., & Yevjevich, V. (1981). “Closed Conduit Flow,” *Water Resources Publication*, USA, 255–278.
41. Chaudhry, M. H. (1987). “Applied Hydraulic Transients,” Van Nostrand Reinhold, New York, USA, 165–167.
42. Kerr, S. L. (1949). “Minimizing Service Interruptions due to Transmission Line Failures, Discussion,” *Journal of the American Water Works Association*, 41, 634, July, 266–268.
43. Kerr, S. L. (1951). “Water Hammer Control,” *Journal of the American Water works Association*, 43, December, 985–999.
44. Apoloniusz Kodura, & Katarzyna Weinerowska (2005). “Some Aspects of Physical and Numerical Modeling of Water Hammer in Pipelines,” 126–132.

45. Anuchina, N. N., Volkov, V. I., Gordeychuk, V. A., Es'kov, N. S., Ilyutina, O. S., & Kozyrev, O. M. (2004). "Numerical Simulations of Rayleigh"—Taylor & Richtmyer-Meshkov, instability using Mah-3 code, *J. Comput. Appl. Maths*, *168*, 11.
46. Fox, J. A. (1977). "Hydraulic Analysis of Unsteady Flow in Pipe Network," Wiley, N. Y., 78–89.
47. Karassik, I. J. (2001). "Pump Handbook," Third Edition, McGraw-Hill, 19–22.
48. Fok, A. (1978). "Design Charts for Air Chamber on Pump Pipelines," *J. Hyd. Div., ASCE*, Sept., 15–74.
49. Fok, A., Ashamalla, A., & Aldworth, G. (1978). "Considerations in Optimizing Air Chamber for Pumping Plants," Symposium on Fluid Transients and Acoustics in the Power Industry, San Francisco, USA, Dec., 112–114.
50. Fok, A. (1980). "Design Charts for Surge Tanks on Pump Discharge Lines," BHRA 3rd Int. Conference on Pressure Surges, Bedford, England, Mar., 23–34.
51. Stark, N. (1999). *Forest Prod J.*, *49(6)*, 39.
52. Fok, A. (1982). "Water Hammer and its Protection in Pumping Systems," Hydro Technical Conference, CSCE, Edmonton, May, 45–55.
53. Fok, A. (1987). "A Contribution to the Analysis of Energy Losses in Transient Pipe Flow," PhD Thesis, University of Ottawa, 176–182.

INDEX

A

Acceleration factor, 56
Acceleration of gravity, 34
Acoustic field, 61
ADI technique, 96
Adiabatic index, 65
Air mass balance, 163
Algebraic equation system, 2
Amagat's law of additive volumes, 165, 192
Ammonium copper quat, 125, 220
Angular frequency, 37
Ansatz function, 6, 7
Aqueous solution, 16, 61, 62, 63, 64, 65, 66, 67
 ethylene glycol, 61
Arrhenius equation, 112, 207

B

Beech heartwood, 118, 213
Biological treatment, 131, 224
Bound water diffusion, 107, 108, 109, 111, 119, 123, 202, 203, 204, 206, 214, 218
Boundary condition at interface of, 94
 fluid, 94
 solid, 94
Bouyancy coefficient of, 84
 concentration, 84
 temperature, 84
Brinell hardness for pine, 128, 189
Brinell hardness method, 127, 222
Bubble binary solution, 69
Bubble dynamics, 56
Bubble flow, 50
Bubble of water solutions, 61
 ethanol, 61
 methanol, 61
 toluene monotonic, 61

Bubbles, 50, 53, 54, 55, 59, 60, 61, 62, 63, 68

C

Capillary effects, 77
Capillary porous materials, 106, 201
Capillary pressure, 108, 204
Capillary transportation, 108, 204
Capillary water bulk flow, 116, 210
Cedar heartwood, 118, 213
Characteristic equation, 21, 42
Chromated copper arsenate, 125, 220
Chromophores type, 130
Clapeyron equation, 106, 202
Clausius-Clapeyron relation, 60
Clean water, 63, 67
Combined drying, 126, 127, 131, 221, 222, 225
Commercial codes, 5
Computational domain, 141, 142, 152
Computational fluid dynamics, 16
Conservation equations, 3, 119, 214, 225
Conservation laws, 3, 99
Continuity equation, 8, 17, 19
Continuity of concentration, 95
Continuity of temperature, 94
Control volumes, 5, 144
Convective dryer, 161, 187
Convective mass transfer coefficient, 167, 194
Coupled heat and liquid moisture transport, 77
Critical moisture content, 79

D

Dalton's Law of Additive Pressure, 164, 191
Darcy's law, 118, 119, 122, 190, 212, 213, 214, 217

Darcy's law for liquid flow, 118, 212
 Darcy's law for liquid free water, 122, 217
 Darcy-Weisbach friction factor, 25
 Deep pool filled with water, 34
 Direct numerical simulation, 6, 7, 8
 Discolorations, 130, 224
 Discrete locations, 2
 Discretization errors, 3
 Discretization process, 3
 Discretize Navier-Stokes equation, 8
 Dispersed fluid, 24, 43
 Dispersive properties of media, 39
 Douglas-fir heartwood, 118, 213
 Drying conditions, 117, 126, 127, 212, 221, 222
 Drying curve, 86, 90, 97
 forced convection model, 92
 mixed model
 Drying kinetics mechanism coupling, 165, 192
 Drying process, 77, 79, 83, 98, 99, 125, 130, 131, 161, 162, 187, 188, 220, 224

E

Effect of buoyancy forces on streamlines, 91
 Effect of diffusion inhibition, 67
 Effective diffusion coefficient equation, 166
 Effects of transients, 54
 hydraulic transients, 54
 steam pump cavitations, 54
 Elastic system, 4
 Electromagnetic energy transmission, 77
 Electromagnetic field, 131, 132, 224, 225
 Elliptic equations, 7
 Enthalpy of evaporation, 84
 Equilibrium moisture content, 160, 186
 Equivalent thermal conductivity, 166, 193
 Ethyl alcohol, 60, 62, 65, 67, 68
 Ethylene glycol, 60, 61, 62, 63, 64, 65, 66, 67, 68
 Euler equation, 18, 35, 36

Eulerian model, 4, 9, 132
 for water, 9

F

Falling drying rate period, 79
 Far stream boundary condition (upper boundary), 95
 Fiber saturation point, 107, 109, 110, 202, 204, 205
 Fiber wall, 106, 201
 hygroscopic water, 106
 Fick's law, 109, 123, 204
 first law of diffusion, 109
 second law of diffusion, 109, 123, 204
 Finite differences, 2
 Finite element method, 2, 5, 82, 83
 partial differential equations, 5
 Finite volume, 2, 83, 96
 Finite volume method, 3, 5, 99, 140, 144
 commercial codes, 5
 CFX, 5
 Flow3D, 5
 Fluent, 5
 Phoenix, 5
 conservation (transport) equation, 5
 control volumes, 5
 First derivatives, 38
 forces of friction, 38
 First law of thermodynamics, 3
 First-order-Arrhenius type equation, 164
 Fitting curves for two sample models, 171, 196
 Lewis model, 171
 present model, 171
 Flow properties, 81
 laminar, 81
 turbulent, 81
 Flow3D, 5
 Fluctuations, 41, 42, 55, 56, 67
 Fluid concentration, 96
 Fluid motion modeling, 16
 Fluid movement in wood, 116, 211
 Fluid particle, 3, 80
 first law of thermodynamics, 3

Newton's second law, 3
 Fluid thermal conductivity, 84
 Free surface, 35, 36
 Free undammed oscillations, 42
 Free water, 107, 119, 202, 214
 FV solver, 138

G

Gas constant, 58
 Gas-liquid mixture, 52
 Gas-phase liquid components, 60
 Gaussian model, 169, 170
 Global regulation of steam pressure, 55
 Governing equations for solid, 93
 Grash number, 82
 Green wood, 106, 116, 202, 211
 Grid dependency, 96
 Guilan spruce, 129, 189, 221, 223

H

Heat and Mass Transfer, 67
 Heat balance, 95
 Heat transfer coefficients, 81
 air, 81
 water, 81
 Heterogeneous model, 9
 High transient flows, 54
 deterioration of joints, 54
 leakage, 54
 shut off valve, 54
 Homogeneity of parameters, 57
 Hydraulic simulation model, 3
 Hydraulic system, 43
 Hydraulic transients, 54
 Hydraulic transition, 55, 69
 Hydrogen bonding, 107, 202
 Hydro-machines phenomenon, 9
 Hydrophobic fibers, 79
 Hygroscopic porous material, 107, 203
 Hyperbolic, 7

I

Ideal fluid, 43
 Incompressible fluid, 16, 34, 43
 Industrial leather drying process, 162

Infrared drying, 130, 131, 224, 225
 Inlet boundary condition, 95
 Iso-thermal diffusion coefficient of
 porous body, 84
 liquid phase, 84
 vapor phase, 84
 Iteration errors, 3

J

Joukowski formula, 4

K

Knudsen diffusion, 106, 202

L

Lagrangian and Eulerian model, 3
 Lagrangian approach, 24
 Laplace rule, 26
 Large Eddy Simulation, 6, 9
 Lax Equivalence theorem, 3
 Leakage, 54, 55
 Leather industry, 160, 161, 186, 187
 Leather quality, 160, 186
 Level of hydraulic pressure, 55
 Lewis model, 171, 177, 196, 197
 Lewis's formula, 168, 195
 Liquid layers, 7
 turbulence, 7
 counter flows, 7
 Liquid mass balance, 162, 164, 192
 Liquid momentum equation, 163
 Darcy's law, 163
 Liquid recirculation zone, 52
 vena contraction, 52
 Liquid surface, 34, 35, 37
 Log sawing, 106, 201
 Low-pressure drops, 65
 super-cooling of the liquid, 65
 super-heating of the liquid, 65

M

Mass transfer mechanism, 108, 204
 Masson's pine, 110, 206
 Mathematical model, 2, 3, 162, 172,
 187, 188, 200

Method of characteristics, 3, 20, 21, 69, 225

Microwave drying, 131, 224

Microwave processing of materials, 131, 224

Modeling errors, 3

Modes of moisture transport by, 79

- capillary forces, 79
- due to pressure gradient, 79
- effusion (Knudsen-type diffusion), 79
- liquid diffusion, 79
- osmotic pressure, 79
- thermo diffusion, 79
- vapor diffusion, 79

Moisture distributions, 225

Moisture transported in porous media, during drying through, 79

- capillary flow of unbound water, 79
- movement of bound water, 79
- vapor transfer, 79

Momentum equation, 4, 8, 17, 94

- 2D Navier-Stokes, 94

Moody diagram, 25

N

Navier-Stoke's approach, 138

Navier-Stokes equations, 4, 8, 9, 83

New Zealand Pinus radiata, 109, 205

New-generation synthetic leathers, 162, 188

Newton second law, 3, 17

Newton's law of cooling, 80

Newtonian fluid, 16

No bound water, 107, 202

No slip condition, 94

Non-isothermal diffusion coefficient of porous body, 84

- in liquid phase, 84
- in vapor phase, 84

Numerical grid, 2

Numerical method, 2, 141

- mathematical model, 2

Nusselt number, 82, 139

Nusselt parameter, 56, 58, 59, 69

O

Oscillatory motion, 9

Outflow boundary condition, 95

P

Parabolic, 7

Partial differential equations, 2, 4, 5, 38, 82

Phase velocity, 37, 39, 41, 42

Phoenics, 5

Pilot-scale, 179

Pilotscale tests, 160

Pinus radiata timber, 206

Pipe wall, 43

Poisson-Boltzmann equation, 139

Polar molecules, 131, 224, 225

Porosity of wood, 112, 113, 208, 209

Porous body thermal conductivity, 84

Porous media, 76, 78, 79, 82, 115, 119, 162, 172, 188, 196, 200, 214

Prandtl number, 81

Present model, 169, 170, 177, 198

Pressure drop, 25, 61, 138, 140, 147, 148, 149, 150, 152

Pressure wave, 4, 7, 55

Problem model, 84

Propagation velocity of waves on water, 34

Q

Quadratic function, 168, 169

R

Radial diffusion, 109, 205, 206

Radiation, 77

- form of electromagnetic energy transmission, 77

Radius of the bubble, 65

Rate of phase transformations, 61, 68

Rational function, 169, 170

Rayleigh equation, 56

Refractive index, 38

Regression analysis, 4, 168, 195

Resonance, 55

Restoring force, 34
 Reynolds number, 16, 81, 83, 97, 98, 99,
 138, 139, 140, 143, 144
 magnitude, 16
 Reynolds-Averaged Navier-Stokes, 6, 9
 Ritz method, 7
 Root-mean-square, 124, 219
 Rupture, 54, 55

S

Sapwood, 106, 116, 117, 118, 202, 211,
 212, 213
 Saturation pressure, 58, 164, 191
 Sherwood parameter, 59
 Short waves, 34
 restoring force, 34
 Shut off valve, 54
 SIMPLE algorithm, 96
 Single-phase (pure liquid) transient
 equations, 4
 Snapshot laboratory set up, 51
 sonic velocity, 16
 southern yellow pine, 116, 211
 loblolly, 116
 Species flux balance, 95
 Spectrophotometers, 128, 223, 225
 Speed of propagation, 7
 Stages of drying, 108, 114, 179, 209,
 210, 225
 first stage, 108
 second stage, 108
 third stage, 108
 Statistical analysis, 179
 Structured grid, 2
 Sub grid-scale (SGS) models, 9
 Superheated solution, 65, 67
 Surge wave, 3, 9, 10
 Sweet gum, 116, 211
 Synthetic leather drying, 161, 187
 Synthetic leathers, 172, 200
 System of linear homogeneous alge-
 braic, 42
 Systematic errors, 3
 Discretization errors, 3
 Iteration errors, 3
 Modeling errors, 3

T

Tanalith E 3491, 125, 220
 Tangential diffusion, 109, 205, 206
 Tangential diffusion coefficients, 109,
 205
 Telegraph equation, 38, 39
 for electric waves in a conductive
 line, 38
 Temperature rise, 148, 149, 150, 152
 Textile material, 160, 161, 179, 186
 That Eulerian based computational
 model, 9
 Theoretical model, 161, 162, 187, 188
 Theory of oscillations, 39
 Thermal balance, 163, 191
 Thermal diffusivity of fluid, 59
 Thermal drying, 161, 187
 Thermal equilibrium, 163, 191
 Thermal resistance, 139, 143, 144, 145,
 146, 152
 Thermodynamic quasi equilibrium state,
 162, 188
 Thermodynamic relations, 164, 165,
 191, 192
 Three dimensional heat transfer charac-
 teristics, 138
 Three modes of heat flow in porous
 media, 77
 conduction, 77
 convection, 77
 radiation, 77
 Timber, 82, 107, 109, 110, 203, 204
 Transfer of heat in porous media, 76
 Transient theory, 4
 Transverse velocities, 143
 Trapezoidal rule, 124, 219
 Tuckerman's experiments, 145, 146
 data, 145
 Turbulent flows, 6, 8
 Direct Numerical Simulation, 6
 Large Eddy Simulation, 6
 Reynolds-Averaged Navier-Stokes, 6
 Two phases flow, 50
 Two-dimensional model, 82, 83
 Two-fluid systems, 50

- air, 50
- liquid, 50
- Two-phase fluids, 50
 - liquid, 50
 - vapor, 50
- Types of flows, 51
- Types of grids, 2
 - block-structured grid, 2
 - structured grid, 2
 - unstructured grid, 2

U

- Unstructured grid, 2

V

- Vapor bubble, 56, 58, 60, 61, 66, 68, 69
 - binary solution, 61
- Vapor concentration, 94, 179
- Vapor density, 65
- Vapor mass balance, 179
- Vapor mass fraction, 163, 191
- Vapor-liquid flow, 52, 53
- Vapors cavitations, 54
- Variational principle, 6
- Velocity correction factor, 162, 188
- Velocity phase of the harmonic wave, 37
- Vena contraction, 52, 69
- Vibration, 55
 - acceleration factor, 56
 - fluctuations, 55
 - leakage, 55
 - rapid changes, 55
 - resonance, 55
 - rupture, 55
- Void space, 77, 106, 201
- Volume concentration, 50

W

- Water hammer, 7, 24
- Water column separation, 54

- collapse of cavitations bubbles, 54
- excess of atmospheric pressure, 54
- local high points, 54
- vapors cavitations, 54
- Water in wood, 107, 202
 - cell cavities, 107
 - cell walls, 107
- Water transmission, 10
- Water vapor mass balance, 163, 164, 191
- Wave characteristic method, 4
- Wave number, 37, 38, 39
- Wavelength, 34, 35, 36, 37, 41
- Whitaker procedures, 119
- White oak heartwood, 118, 213
- Wolmanit CX-8, 125, 220
- Wood, 13, 106, 112, 116, 131, 201, 202, 208, 211, 220, 224
 - Wood annular rings, 116, 211
 - Wood grains, 116, 127, 211, 222
 - Wood permeability, 114, 116, 209, 211
 - Wood samples, 124, 125, 127, 130, 219, 222, 223
 - ammonium copper quat, 125
 - chromated copper arsenate, 125
 - pine, 124
 - spruce, 124
 - Tanalith E 3491, 125
 - Wolmanit CX-8, 125
- Wood species, 107, 131, 202, 223, 225

Y

- Yellow-poplar, 116, 211, 212
- Yellow-poplar heartwood, 118, 213

Z

- Zhukousky formula, 23